vol. 4, no. 6

June , 1958

THE SOVIET JOURNAL OF

ATOMIC ENERGY

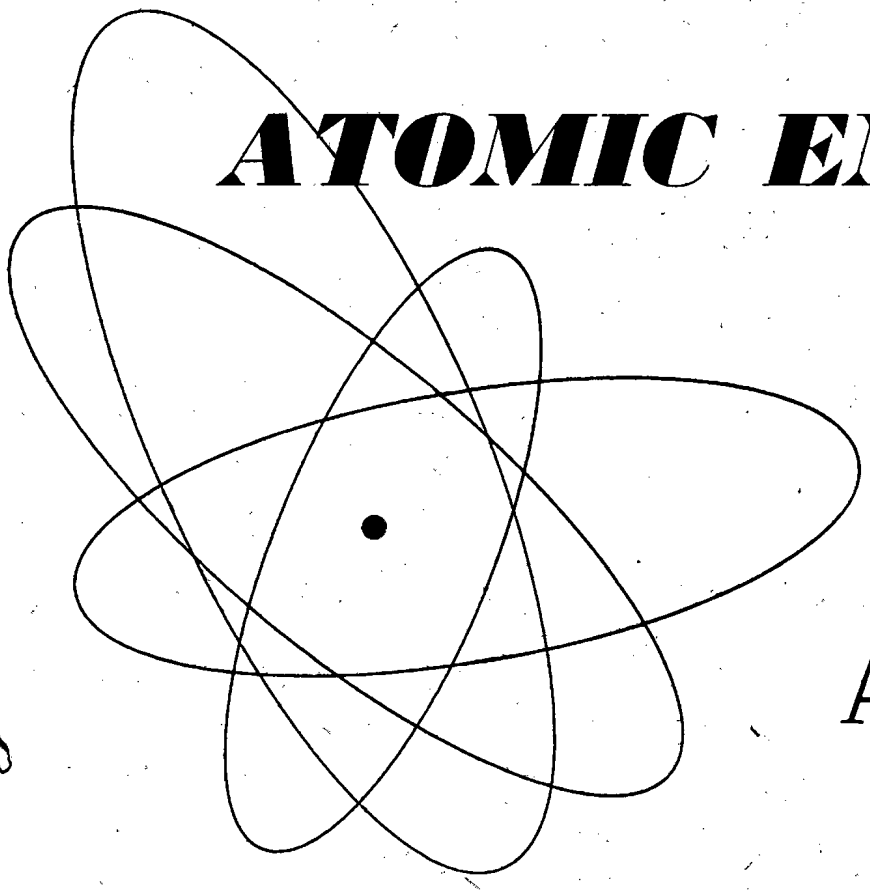

Атомная энергия

TRANSLATED FROM RUSSIAN

CONSULTANTS BUREAU, INC.

recent Russian research

—in complete English translation

A New Method in the Theory of SUPERCONDUCTIVITY

BY *N. N. BOGOLIUBOV*
V. V. TOLMACHEV
AND D. V. SHIRKOV

IN THIS unprecedented *complete* solution to the perplexing problem of constructing a microscopic theory of superconductivity, the authors explain their new method—*a result of the research of N. N. Bogoliubov and V. V. Tolmachev*—based on a physical and mathematical analogy with superfluidity.

Here they give *calculations for the energy of the superconducting ground state using Fröhlich's Hamiltonian, as well as of the one-fermion and collective elementary excited states;* they provide a detailed analysis of *the role of the Coulomb interaction between the electrons in the theory of superconductivity;* and demonstrate how *a system of fermions is treated with a fourth-order interaction Hamiltonian and establish the criterion for its superconductivity* — all of which is indicated in greater detail in the complete table of contents shown to the right.

cloth bound • 130 pages • $5.75

Complete Table of Contents

CB translations by bilingual scientists include all diagrammatic, photographic and tabular material integral with the text.

CONSULTANTS BUREAU, INC.

227 WEST 17TH STREET, NEW YORK 11, N. Y.

vol. 4, no. 6

June , 1958

THE SOVIET JOURNAL OF

ATOMIC ENERGY

ATOMNAIA ENERGIIA

A publication of the Academy of Sciences of the USSR

Annual Subscription *$75.00*
Single Issue *20.00*

Year and issue of first translation:
volume 1, number 1 january 1956

TRANSLATED FROM RUSSIAN

Printed in the United States

SOVIET JOURNAL OF ATOMIC ENERGY

Volume 4, Number 6 June 1956

CONTENTS

CONTENTS (continued)

THE INVESTIGATION OF THE TRANSITIONAL ACCELERATION STAGE IN A SYNCHROTRON WITH A BETATRON INITIAL STAGE

I. S. Danilkin and V. E. Pisarev

This paper is devoted to an application of the theory of the transition stage (the process of transition from betatron to synchrotron acceleration) to the FIAN 250 Mev synchrotron for the case when the accelerating field is established adiabatically. From the experiments and calculations that have been carried out it is possible to judge the correctness of the theory as applied to accelerators of this type. Some characteristics of the electron beam during the betatron stage, for example, the electron energy distribution, have been obtained from the experimental data.

It is also shown that it is possible to use the dependence of the accelerated-particle beam intensity on the amplitude of the accelerating potential to determine the voltage amplitude at the resonant cavity.

By the transition stage in synchrotrons with an initial betatron stage we usually mean the combination of processes associated with the capture of the electron beam into the synchrotron acceleration conditions after a preliminary acceleration during the betatron stage. Because of the relative simplicity of the theory of the transition stage it is possible, as will be shown below, to verify the correctness of the theory itself, to analyze the experimental features of this acceleration stage, and to determine a number of characteristics of the particle beam captured into the synchrotron stage.

The present paper is devoted to an analysis of experiments on the transition stage of synchrotron operation. The experimental part of the work was carried out during 1951-1952 at the FIAN 250 Mev synchrotron [1]. A detailed description of this accelerator is given in [2].

The Theoretical Investigation of the Transition Stage

The theory which was used in carrying out the calculations has been developed in a series of papers [3-5]* and therefore here we will only present the main arguments and the results obtained.

As is known [3, 4], the phase motion of a particle after the accelerating electric field is switched on is described by the equation:

$$\frac{d}{dt}\frac{E_s}{\omega_s^2 K}\frac{d\varphi}{dt} - \frac{eV(t)}{2\pi}\cos\varphi = -\frac{ev_s}{2\pi}, \qquad (1)$$

where φ is the phase angle of the electron, E_s and ω_s are the total energy and angular velocity of rotation of an equilibrium electron, V(t) is the amplitude of the accelerating electric field, ev_s the average fractional increment of the electron energy during one revolution, and $K = 1 + \frac{n}{1-n}\frac{1}{\beta^2}$ (n is the exponent describing

* Reference [5] deals with the experimental verification of the theory presented in [4]. It must be pointed out, however, that this work differs completely from our own in scope, aims, and experimental conditions.

the rate of fall of the field, β is the ratio of the particle velocity to that of light c).

V(t), the amplitude of the accelerating field, is usually a function which increases monotonically from zero, such that for $t - t_0 > \tau$, $V(t) \approx V_m$ = constant. The time t is measured from the instant when the value of the magnetic field intensity passes through zero (the start of the betatron acceleration cycle), t_0 denotes the instant when the accelerating field is switched on, while τ is the time interval during which it is established.

Taking into account that usually in the interval τ, $E_s \approx$ constant, we obtain by integrating (1):

$$\left.\begin{aligned} \dot{\varphi}^2 &= \dot{\varphi}_0^2 - 2kv_s(\varphi - \varphi_0) + 2kV(\sin\varphi - \overline{\sin\varphi}), \\ \overline{\sin\varphi} &= \frac{1}{V}\int_0^V \sin\varphi\, dV, \quad k = \frac{e\omega_s^2 K}{2\pi E_s}. \end{aligned}\right\} \tag{2}$$

Thus, instead of the integration constant $G(\varphi_0, \dot{\varphi}_0) = \dot{\varphi}_0^2 + 2kv_s\varphi_0 - 2kV\sin\varphi_0$, which determines the phase trajectory for the case V = constant, we have for V = V(t)

$$G(\varphi_0, \dot{\varphi}_0, t) = \dot{\varphi}_0^2 + 2kv_s\varphi_0 - 2kV(t)\,\overline{\sin\varphi}. \tag{3}$$

Comparing (2) with the equation of the curve which determines the boundary of the region of stability:

$$\left.\begin{aligned} \varphi^2 &= 2kV(t)[\sin\varphi + \sin\varphi_s - (\varphi + \varphi_s)\cos\varphi_s], \\ \cos\varphi_s &= \frac{v_s}{V}, \end{aligned}\right\} \tag{4}$$

we find the condition governing the capture of particles into the region of stability at time t:

$$\left.\begin{aligned} G(\varphi_0 - 2\pi n, \dot{\varphi}_0, t) &\leqslant 2kV(t)[\sin\varphi_s - \varphi_s\cos\varphi_s], \\ n &= 0, \pm 1, \pm 2\ldots, \\ -\varphi_s &\leqslant \varphi_0 \leqslant 2\pi - \varphi_s. \end{aligned}\right\} \tag{5}$$

The calculation of $\overline{\sin\varphi}$ for the general case is very difficult. Only two limiting cases are exceptions.

In the first case, when the accelerating field is established very rapidly, the variation of φ during the time τ is negligibly small. Then $\overline{\sin\varphi} \approx \sin\varphi_0$ and Condition (5) reduces to the usual result: for capture it is necessary that

$$\dot{\varphi}_0^2 \leqslant 2kV[\sin\varphi_s + \sin\varphi_0 - (\varphi_0 + \varphi_s)\cos\varphi_s]. \tag{6}$$

In the second case, when the accelerating field is established adiabatically, the variation of φ during the time τ is large and $\overline{\sin\varphi} \approx 0$. Then, in the first approximation, during the time interval t ($t_0 < t < t_0 + \tau$) those particles will be captured for which the following condition is satisfied:

$$\left.\begin{aligned} &|\dot{\varphi}_0^2 + 2kv_s(\varphi_0 - 2\pi n)| \leqslant \\ &\leqslant 2kV[\sin\varphi_s - \varphi_s\cos\varphi_s]. \end{aligned}\right\} \tag{7}$$

In determining the range of values of φ in which capture occurs we neglect the oscillating term in Equation (1), i.e., we assume that *

$$2\pi n \approx \varphi_0 + \dot{\varphi}_0\Delta t - \frac{kv_s(\Delta t)^2}{2} \qquad (\Delta t = t - t_0),$$

and obtain

$$|\dot{\varphi}_0 - kv_s\Delta t| \leqslant \sqrt{2kV(\sin\varphi_s - \varphi_s\cos\varphi_s}. \tag{7a}$$

* This equation is correct only for sufficiently large values of n; however, in the case considered this condition is automatically satisfied because V(t) is established adiabatically.

In synchrotrons with a betatron initial stage, the variation of the phase velocity $kv_s\Delta t$, governed by the contraction of central beam orbit up to the instant of capture, is usually small* and therefore (7a) reduces to the condition

$$|\dot{\varphi}_0| \leqslant \sqrt{2kV}. \tag{7b}$$

The range of applicability of Equation (7b) is determined by the inequalities

$$2\frac{V}{v_s} \gg \Delta t \sqrt{2kV} \gg 0{,}5. \tag{8}$$

Relation (7b) is one of the basic computational equations which can be used for investigating the transition stage in a synchrotron with a betatron initial stage of acceleration. It gives the initial conditions for the particles that will be captured into the region of phase stability and transferred to the synchrotron stage of acceleration at the moment when the accelerating field is fully established.

Another factor which must be taken into account in the investigation of the transition stage is the contraction of the region of phase stability (a possible loss of particles) as the result of saturation of the betatron core which leads to a decrease of the induced emf and an increase in v_s. Since this process is slow, its influence on the transition stage can be allowed for with the help of the adiabatic invariants [3-4]. The calculation of the saturation effects can be reduced to the requirement that the amplitude of the accelerating field V_m has to be increased by comparison with the value given by Relation (7b).

The Experimental Features of the Transition Stage

The important parameters of the synchrotron used in the experiments are given below.

The final energy of the electrons $E_f = 250$ Mev, the radius of the equilibrium orbit $R_s = 82.5$ cm, the maximum field at the orbit $H_m = 10{,}550$ oerst, current frequency in the magnet $f = 50$ cps, field strength of the supplementary magnetization system $H = 4500$ oerst, the maximum energy in the betatron stage $E_{f\beta} = 4$ Mev, the energy of injection into the betatron stage $E_i = 60$-70 kev, and the time during which the accelerating field is established $\tau \approx 10$ μsec.

The relations, required for an investigation of the transition stage, between the magnetic field H, the energy E_s, and the equilibrium potential v_s of the accelerating slit and the time t have been obtained from special experiments and are given in Fig. 1.

Let us show that in our case the amplitude of the accelerating field is established adiabatically and that Relation (7b) is satisfied. If $E_s \approx 4$ Mev ($\beta = 1$), $V_m = 1000$ v, $K = 1/(1-n) \approx 2.5$ ($n \approx 0.6$), $\omega_s = c/R_s \approx$ $\approx 3.6 \cdot 10^8$ rad/sec, then the parameter $\Delta t \sqrt{2kV} \approx 50$. Taking from Fig. 1 the value of v_s, we find that the Inequalities (8) governing the applicability of Relation (7b) are in fact satisfied.

In the course of the experiments the following relations which describe the transition stage of the accelerator were obtained: the function $J(V_m)$ giving the dependence of the hard γ-radiation emission (or the beam intensity of the accelerated particles) on the amplitude of the accelerating field (Fig. 2) and the function $J(t_0)$ giving the dependence of the hard γ-radiation emission on the time at which the accelerating field is switched on (Fig. 3).

The function $J(V_m)$ has the following simple meaning: as the amplitude V_m of the accelerating field increases, the size of the region of phase stability increases and correspondingly the beam intensity of the accelerated particles increases. $J(v_{s,\max}) = 0$, where $v_{s,\max}$ is the maximum value of v_s during an acceleration cycle. For a known value of $v_{s,\max}$ the extreme left-hand point on the curve $J(V_m)$ can be used for finding the scale along the V_m-axis, thus making it possible to use a simple indirect method in a number of cases for solving the difficult problem of determining the effective amplitude V_m of the resonant-cavity accelerating potential. The calculation of the quantity $v_s(t)$, required for the determination of $v_{s,\max}$, is very simple when the accelerator characteristics are known.

* When the accelerating field is switched on in such equipment, the betatron condition is also satisfied and acceleration occurs at the expense of the induced emf.

The second point on the function $J(V_m)$ which is of interest to us is the point $V_m = V_m^*$, starting from which all the captured particles remain in the synchrotron stage. This point corresponds to the time t^* when $v_s(t^*) = v_{s,\max}$.

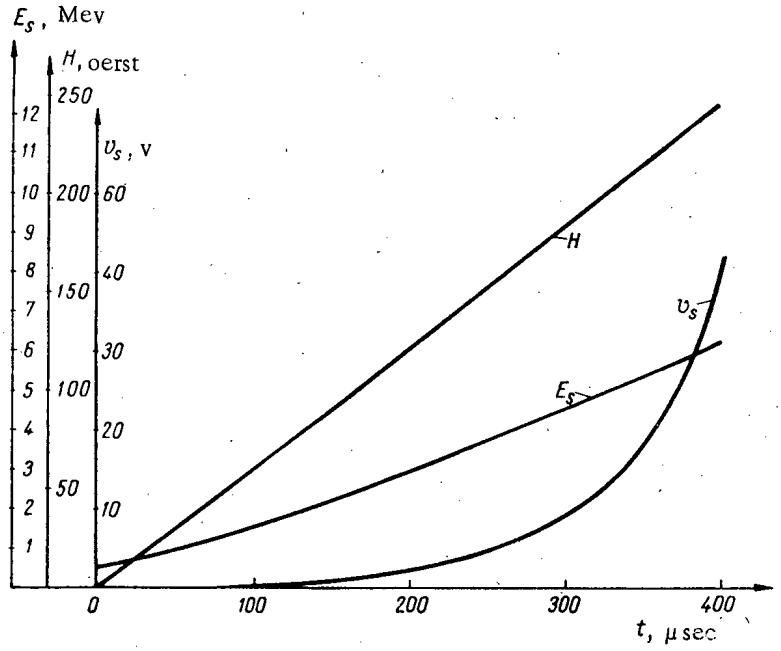

Fig. 1. The magnetic field H, the total energy of the electrons E_s, and the equilibrium potential difference v_s as a function of the time t measured from the start of the acceleration cycle from a 250 Mev synchrotron.

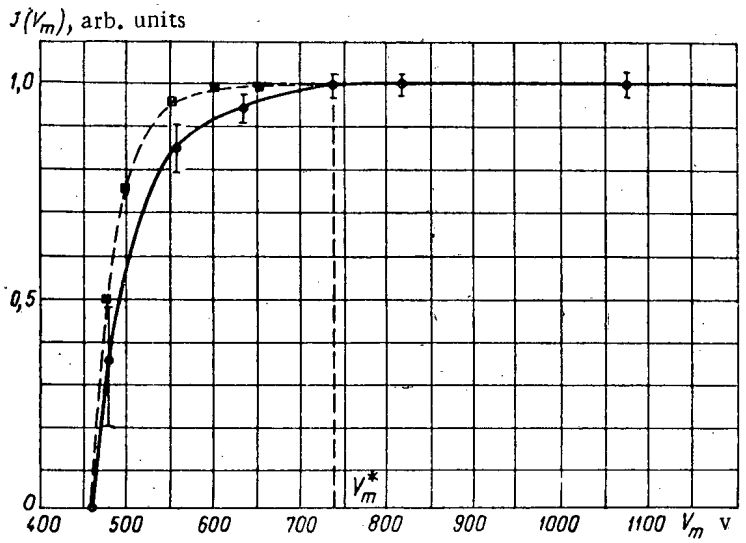

Fig. 2. J, the intensity of the hard γ-radiation, as a function of the amplitude V_m of the accelerating field.
—●— experimental curve, -- ■ --- theoretical curve.
(V_m^* is the minimum value of the amplitude necessary to preserve practically all of the captured electrons during the acceleration process).

Knowing the value of V_m^* from Equation (4) we can determine the $\dot{\varphi}$ distribution for the particles or, using the relation

$$\rho = \frac{\dot{\varphi} R_s}{\omega_s K \beta^2 (1-n)},$$

where $\rho = R - R_s$ is the deviation of the instantaneous equilibrium orbit of radius R from the synchrotron orbit, we can find the radial dimensions of the beam of accelerated electrons at the instant when v_s has its maximum value. Using the adiabatic invariants to transform the beam dimensions from the instant t to the time $t = t_0 + \tau$ (keeping $V_m = V_m^*$) and then taking into account the change of the amplitude from V_m^* to the value of the accelerating field amplitude at the end of the capture $V_1 (t = t_1)$, we can determine the dimensions of the beam at the instant when the edge electrons are captured into the region of phase stability (4). From Relation (7b), we can find the dimensions of the beam at the moment t_0 when the accelerating field is switched on (see Table).

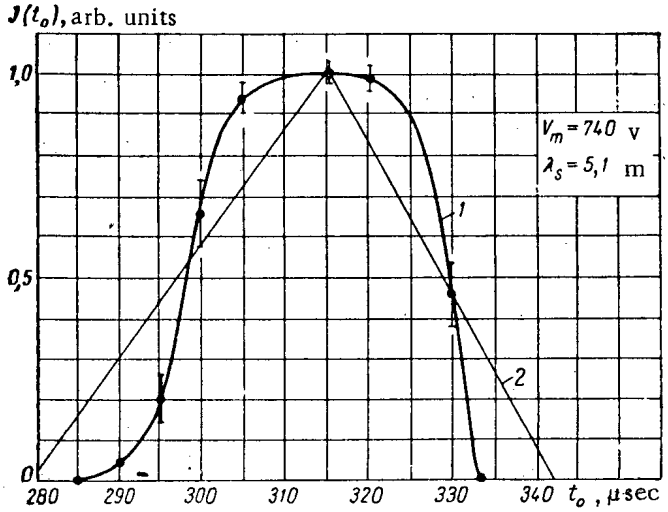

Fig. 3. The intensity J of the hard γ-radiation as a function of t_0, the time at which the accelerating field is switched on. 1) Experimental curve; 2) the function a(t) corresponding to $J(t_0)$ for a uniform distribution of electrons over the equilibrium orbits (λ_s is the wavelength of the high-frequency generator).

TABLE

The Results of the Conversion of the Accelerated-Electron Frequency Spread from the Time t^* ($v_s = v_{s,max}$) to the Time t_0 when the Accelerating Field is Switched on and the Time t_1 when the Electron Capture is Complete

Time t, μsec	$t^* = 700$	t_1	$t_0 = 315$
Other parameters	$v_{s,max} = 464$ v, $V_m^* = 740$ v, $E_s = 19.48$ Mev	$V_1 = 156$ v, $E_s = 4.94$ Mev	$V_m = 0$, $E_s = 4.86$ Mev
$\dot{\varphi}_{0s}/\omega_s$	$0.366 \cdot 10^{-2}$	$0.709 \cdot 10^{-2}$	$0.501 \cdot 10^{-2}$
The radial size of the beam ΔR, cm	0.302	0.585	0.413

The function $J(t_0)$. It is obvious that the dimensions of the beam along ρ or $\dot{\varphi}$, calculated by the above method, represent essentially the region of the initial conditions $\dot{\varphi}_{0S}$ or ρ_{0S} for which electrons can be accelerated without losses during the synchrotron stage. These regions of initial conditions can be calculated in a completely analogous manner for other values of the switching-on time t_0 or of the amplitude V_m. Thus, for a fixed value of V_m, we can plot in the plane (ω, t) the strip bounded by $\omega_S \pm \dot{\varphi}_{0S}(t)$ (see Fig. 4) whose width for a given $t = t_0$ will represent the region of angular frequencies (or the radii of the instantaneous equilibrium orbits $R = R_S + \rho$) corresponding to those particles that will be accelerated during the synchrotron stage when the accelerating equipment is switched on at time t_0. Let us investigate in the same plane (ω, t) the region occupied at different times by the beam of electrons accelerated during the betatron stage. The angular frequency of a particle moving along an orbit of radius R_β at the end of the betatron acceleration stage will be

$$\omega_\beta(t) = \frac{c\beta(t)}{R_\beta} = \frac{c\beta(t)}{R_S - \Delta R(t)} \approx \frac{c\beta(t)}{R_S}\left[1 + \frac{\Delta R}{R_S}\right], \tag{9}$$

where $\Delta R(t)$ is the contraction of the betatron-orbit radius due to the saturation of the core and the breakdown of the "2:1 betatron condition" in the region $R_\beta \approx R_S$. After calculating

$$\Delta R(t) = -\int_{t'}^{t} \dot{R}\,dt = \int_{t'}^{t} \frac{cev_S(t)\,dt}{2\pi E_S(t)\,\beta(1-n)}, \tag{10}$$

where t' is the time corresponding to the start of the saturation (for $t > t'$, $v_S > 0$) and putting

$$\delta(t) = \frac{ec}{2\pi R_S(1-n)} \int_{t'}^{t} \frac{v_S(t)}{E_S(t)}\,dt, \tag{11}$$

we can write Expression (9) in its final form:

$$\omega_\beta \approx \omega_S[\beta(t) + \delta(t)]. \tag{12}$$

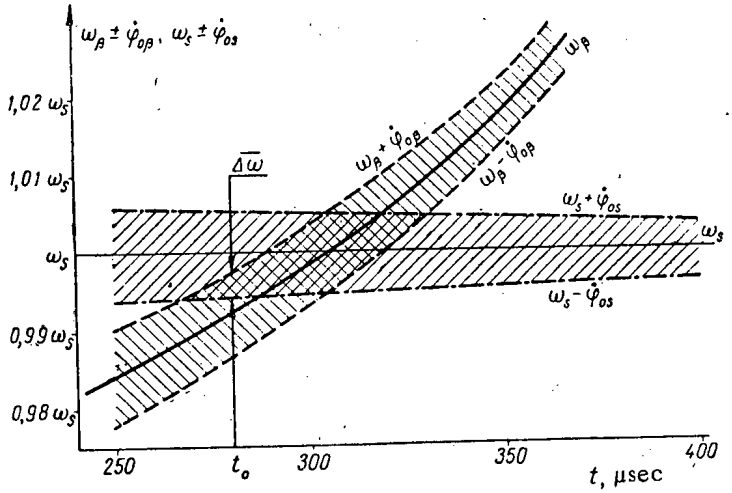

Fig. 4. The variation of the equilibrium angular frequency of the captured electrons ω_β and the synchrotron frequency ω_S with time during the transition stage.
The curves $\omega_\beta \pm \dot{\varphi}_{0\beta}$ and $\omega_S \pm \dot{\varphi}_{0S}$ give the frequency spread in the betatron beam being captured and the allowed frequency spread.

The frequency region occupied by the electron beam as a function of time is bounded in Fig. 4 by the curves $\omega_\beta(t) \pm \dot{\varphi}_{0\beta}(t)$.

It is obvious that a partial or complete capture of electrons into the synchrotron stage of acceleration is possible only for that interval of switching-on time where the frequency region $\omega_\beta \pm \dot{\varphi}_{0\beta}$ occupied by the betatron beam at the time $t = t_0$ when the accelerating field is switched on, overlaps partially or completely the region of the allowed initial conditions $\omega_s \pm \dot{\varphi}_{0s}$. Introducing the function $\Psi(F)$, the distribution of electrons across the radial width of the beam $\rho = F\Delta R$, where ΔR is the total radial width of the beam, while for definiteness ρ is measured from the inner edge of the electron beam, we find that

$$J(t_0) = \int_0^{a(t_0)} \Psi[F(\xi)] \frac{dF}{d\xi} d\xi. \tag{13}$$

Here $a(t) = \frac{\overline{\Delta\omega}(t)}{2\dot{\varphi}_{0\beta}(t)}$ [$\overline{\Delta\omega}(t)$] is the frequency interval which corresponds, for a chosen t, to the common ordinate in the intersecting regions bounded by the curves $\omega_s \pm \dot{\varphi}_{0s}$ and $\omega_\beta \pm \dot{\varphi}_{0\beta}$ (Fig. 4)] and the variable of integration is $\xi = \frac{\Delta\omega}{2\dot{\varphi}_{0\beta}(t)}$ ($\Delta\omega$ is measured from the lower end of the interval $\overline{\Delta\omega}$).

The function a(t) calculated for our equipment (Fig. 3) represents the function $J(t_0)$ for the case when the electrons are distributed uniformly along the radius [$\Psi(F)$ = constant]. The two end points of the function describing the beam intensity of the accelerated particles are determined by the obvious relations

$$\omega_\beta(t) + \dot{\varphi}_{0\beta}(t) = \omega_s - \dot{\varphi}_{0s}(t),$$
$$\omega_\beta(t) - \dot{\varphi}_{0\beta}(t) = \omega_s + \dot{\varphi}_{0s}(t)$$

and are independent of the form of the distribution function $\Psi(F)$.

The Distribution of the Instantaneous Equilibrium Orbits of the Electrons During the Betatron Acceleration Stage. Comparison of the Experimental Results and the Theory of the Transition Stage

From Expression (13), which gives the beam intensity of the accelerated particles as a function of the time at which the accelerating field is switched on, we can easily calculate the distribution of the radii of the instantaneous equilibrium orbits $\Psi(F)$ for the electrons in the betatron beam. In fact, from (13) it follows that

$$\Psi(\bar{F}) = \frac{dJ[t_0(\bar{F})]}{d\bar{F}} = \frac{dJ}{dt_0}\frac{dt_0}{d\bar{F}}, \tag{14}$$

where $\bar{F}$ is the value of F corresponding to $\overline{\Delta\omega}$. Since in our case $\beta \approx 1$ and consequently $\frac{\Delta\omega}{\omega} \approx -\frac{\Delta R}{R}$, then approximately $\bar{F} = a$. Therefore, in order to determine $\frac{dt_0}{d\bar{F}}$ we can use directly the curve a(t) given in Fig. 3. The quantity $\frac{dJ(t_0)}{dt_0}$ is found by differentiating the function $J(t_0)$, given in the same figure.

The function $\Psi(F)$ calculated in this way is shown in Fig. 5.

Finally, converting with the help of the well-known relation

$$\Delta R(t) = \Delta R(t_0)\frac{H(t_0)}{H(t)}$$

the radial dimensions of the betatron beam to the start of the betatron acceleration stage, we find that at the instant of injection $\Delta R_i = 7$ cm. Comparing this value with the dimensions of the working region of the chamber (6.25 cm) we conclude that in the equipment investigated the capture into the betatron acceleration stage takes place over a wide range of positions of the instantaneous equilibrium orbits in the space between the chamber center and the injector and target and that capture is predominantly into the central orbits (the distribution function $\Psi(F)$ is independent of the time if the loss of particles during the acceleration stage is neglected).

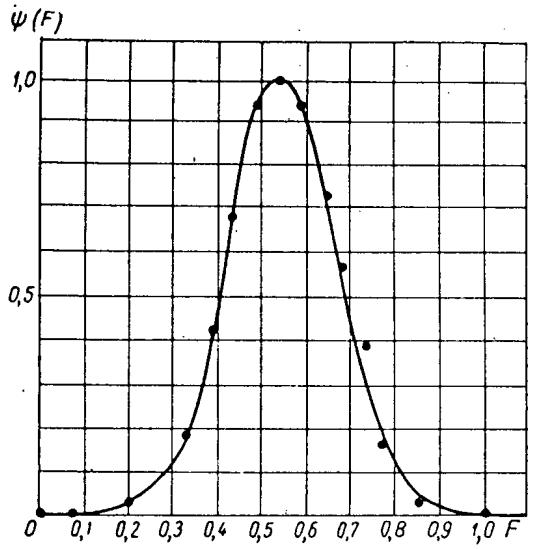

Fig. 5. The distribution function of the electron equilibrium orbits at the beginning of capture into the synchrotron acceleration stage.

In order to verify the correctness of the distribution of the instantaneous equilibrium orbits that was obtained, the functions $J(t_0)$ and $J(V)$, the beam intensity of the accelerated particles as a function of the accelerating electric-field amplitude, were calculated for other values of the equipment parameters; the function $J(V)$ is also dependent on $\Psi(F)$:

$$J(V) = \int_0^{\bar{F}(V)} \Psi(F)\, dF,$$

where $\bar{F}(V)$ can be easily found with the help of the adiabatic invariants and the capture Condition (7b) in a way which is completely analogous to the method used above.

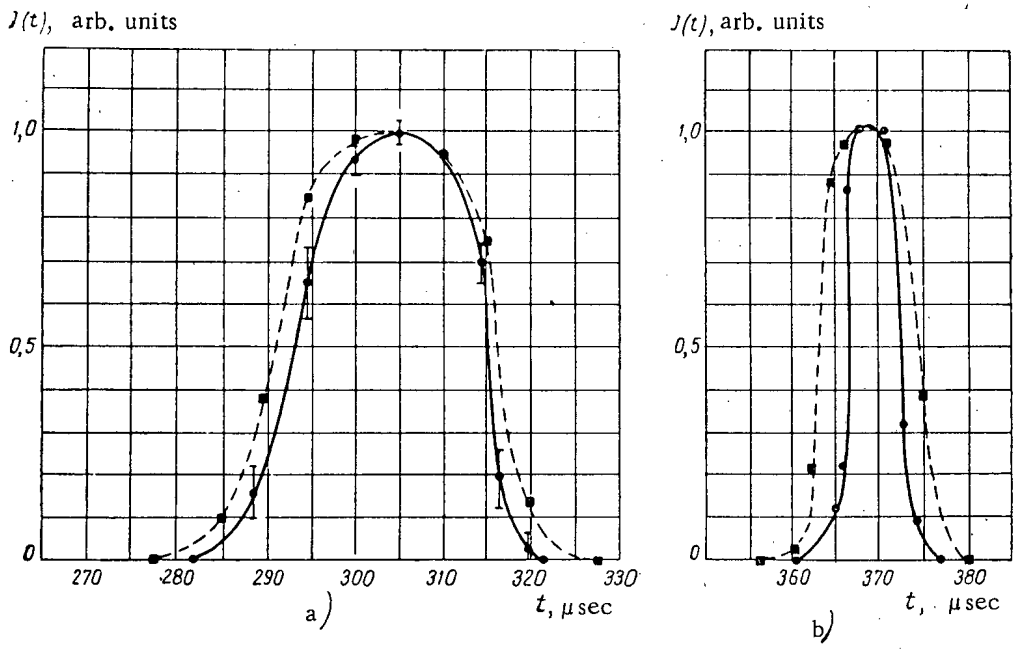

Fig. 6. Comparison of the calculated and experimental functions $J(t)$ for two operating conditions of the accelerator. a) $V_m = 681$ v, $\lambda_s = 5.1$ m; b) $V_m \approx 680$ v, $\lambda_s = 4.94$ m; - - ■ - -) calculated curves; —●—) experimental curves.

The results of the calculations of the functions $J(t_0)$ and $J(V)$ on the basis of the distribution function $\Psi(F)$ (Fig. 5) and the experimentally determined curves are given in Fig. 6. The agreement between the experimental and the theoretical curves is very satisfactory.

Further, an indirect confirmation of the theory of the transition stage is the agreement of the limiting points on the initial function $J(t_0)$ (Fig. 3), since the dimensions of the betatron beam determining this coincidence were found from independent experiments which correspond to the function $J(V_m)$ (Fig. 2).

SUMMARY

The calculations and experiments that have been carried out lead to the conclusion that the theory of the transition stage for synchrotrons with a betatron initial stage is sufficiently adequate when the accelerating field is established adiabatically [Relation (7b)]. Using the theory of the transition stage, we are able to develop the methods for the indirect investigation of the betatron stage, to obtain a number of functions [$\Psi(F)$, ΔR] characterizing the capture of the electron beam, and on the basis of the experimental data obtained to study some of the features of the capture of particles into the betatron stage of acceleration.

In addition to this, the investigation of the transition stage leads to a deeper understanding of the operation of the accelerator and makes it possible for us to determine some of its parameters (for example, the effective amplitude of the resonant-cavity electric field) when the determination of these parameters by another method is associated with difficulties of some kind.

The authors express their gratitude to M. S. Rabinovich for his advice on numerous occasions and for fruitful discussions.

LITERATURE CITED

[1] V. E. Pisarev, Thesis [In Russian] (FIAN SSSR, 1954).

[2] A. Ia. Beliak, V. I. Veksler, V. N. Kanunnikov, P. A. Cherenkov, and B. N. Iablokov, Supplement No. 4 to J. Atomic Energy (USSR) (1957), p. 57. *

[3] M. S. Rabinovich, Thesis [In Russian] (FIAN SSSR, 1948).

[4] T. R. Kaiser, Proc. Phys. Soc. 63A, 52 (1950).

[5] T. R. Kaiser and J. L. Tuck, Proc. Phys. Soc. 63A, 67 (1950).

Received September 27, 1957

* Original Russian pagination. See C. B. Translation.

EFFECTIVE BOUNDARY CONDITIONS IN THE THEORY OF NEUTRON DIFFUSION

(Survey)

G. A. Bat' and D. F. Zaretskii

In this review, a method of determining effective boundary conditions (EBC) is described which guarantees the asymptotic agreement of the solution of the neutron diffusion equation with the solution of the corresponding kinetic equation. For monoenergetic neutrons, the EBC are considered for plane and cylindrical surfaces of "black" and "gray" bodies. Results are given for the EBC for the case of cylinders of arbitrary section.

The authors discuss the simplest problem in the determination of EBC for neutrons that are slowed-down in a medium with heavy atoms and with an energy-independent cross section. The review gives also results obtained by various authors in the USSR and in other countries.

INTRODUCTION

In the great majority of cases, the critical dimensions of nuclear reactors are determined by solving a system of spatial differential equations (diffusion equations) for the neutron density. Thereby, it is necessary that boundary conditions be given on the surface of the control-rod system guaranteeing the absorption of neutrons of various energies. However, in the neighborhood of bodies which strongly absorb neutrons, the conditions of applicability of the diffusion equations are violated. The diffusion equations may be "adjusted" by introducing boundary conditions which have the property that in a region far from the absorbing surfaces, the solution of the diffusion equation agrees with the exact solution.

The boundary conditions for the neutron density guaranteeing agreement in the asymptotic region of the solution of the diffusion equation with the solution of the kinetic equation are ordinarily called effective boundary conditions (EBC).

In order to find the EBC, it is necessary to consider either the kinetic equation for the neutron distribution function with respect to space, flight directions and energies or the integral equation for the neutron density, the zeroth moment of the distribution function.

Let us observe that the application of the diffusion equation to strongly absorbing media requires the introduction not only of EBC but also of effective diffusion coefficients and effective neutron sources [1].

We shall limit consideration to the case of greatest practical interest of rods in weakly absorbing media. The effective diffusion coefficient will be written in the form $D = \frac{1}{3}$, taking the velocity and mean free path of the neutrons to be equal to unity.

A body will be called "black" or "gray" depending on whether it completely or partially absorbs the neutrons incident on its surface. Ordinarily the EBC are given in the form of a logarithmic derivative of the asymptotic neutron density n^{as} at the surface S of the absorbing rod:

$$\frac{1}{\lambda} = \left.\frac{d \ln n^{as}(\mathbf{r})}{d\nu}\right|_s,$$

where ν is the direction of the outward normal to the surface of the absorber. Another widely used form of the EBC is the prescription of a surface upon which $n^{as}(\mathbf{r})$ vanishes. There are then introduced, for example, an effective rod radius r_{eff} and an extrapolation length z_0 for the case of a plane boundary between the medium and the vacuum.

The usual conditions for the absorbing rods in reactors are such that the density of neutron sources may be assumed to be uniform. However, the problem of determining the EBC is often facilitated if one assumes that there are no sources in the medium but that a neutron current is given at infinity. From the work of Le Caine [2] concerning the density of neutrons near the plane boundary of a half-infinite medium and vacuum, it follows that the value of z_0 for the case of a uniform distribution of sources differs only slightly from that for the case of a neutron current incident from infinity. Therefore, we may assume that for our conditions the choice of the source distribution does not influence the EBC.

We present below a review of various methods of determining the EBC along with the results obtained by these methods. In the majority of cases, the further development of the ideas involved and of the nature of the calculational methods is possible, but is very cumbersome.

The generality and effectiveness of the methods developed make them an important part of the theory of kinetic equations.

Monoenergetic Neutrons

1. The simplest determination of the EBC is for the case of an infinitely thin black rod (filamentary sink) in a medium with a uniform distribution of sources. Such a sink does not violate the isotropy of the neutron current, and the correct boundary condition

$$\lambda = \lambda_0 = 4/3 \tag{1}$$

is obtained by comparing the unidirectional kinetic and diffusion currents at the rod:

$$\frac{n}{4} = D\frac{dn}{dr}.$$

2. The other limiting case of a plane dividing boundary between the medium and vacuum is considerably more complicated and has been considered by two methods.

Exact (analytical) method of Wiener-Hopf [3]. The starting point is the Boltzmann equation for the neutron distribution function with respect to space ($\underline{z}$) and direction of flight (Ω) in sourceless media:

$$\Omega\nabla f(z, \Omega) + f(z, \Omega) = \Sigma_s \int_{\Omega} F(\Omega', \Omega) f(z, \Omega') \frac{d\Omega'}{4\pi}, \tag{2}$$

where $f(z, \Omega)dzd\Omega$ is the number of neutrons in an element of volume in the neighborhood of a point $\underline{z}$ for velocities in an element of solid angle $d\Omega$, and $F(\Omega', \Omega)$ is the scattering indicatrix (the probability that the neutron changes the direction of its velocity from Ω' to Ω as a result of collision). For the case of isotropic (in the laboratory system) scattering, $F(\Omega', \Omega) = 1$ and Equation (2) has the form

$$\mu\frac{\partial f(z, \mu)}{\partial z} + f(z, \mu) = \frac{\Sigma_s}{2} n(z), \tag{3}$$

where μ is the cosine of the angle between the direction of flight of the neutrons and the normal to the surface of the dividing plane, $n(z)$ is the neutron density ("zeroth moment" of the distribution function):

$$n(z) = \int_{-1}^{+1} f(z, \mu)\, d\mu. \tag{4}$$

Taking the Laplace transform of (3) and using the notation

$$\Phi(s, \mu) = \int_0^{\infty} e^{-sz} f(z, \mu)\, dz,$$

$$\Phi_0(s) = \int_0^\infty e^{-sz} n(z)\, dz,$$

we obtain

$$\Phi(s, \mu) = \frac{\Sigma_s \Phi_0(s)/2 + \mu f(0, \mu)}{1 + s\mu}. \tag{5}$$

Integrating (5) with respect to μ between the limits -1 and $+1$, we find that*

$$\Phi_0(s)\left(1 - \Sigma_s \frac{\operatorname{arc\,th} s}{s}\right) = \int_{-1}^{0} \frac{\mu f(0, \mu)}{1 + s\mu} d\mu. \tag{6}$$

The basis of the method of Wiener-Hopf is the fact that Equation (6), with the help of a theorem of Liouville [4], can be brought to the form

$$\Phi_0(s) \frac{\varkappa^2 - s^2}{\chi(s)} = \text{const}, \tag{7}$$

where $\chi(s)$ is a known regular function, $\pm \kappa$ are the principal roots of the equation

$$\Sigma_s \frac{\operatorname{arc\,th} \varkappa}{\varkappa} = 1. \tag{8}$$

The inverse Laplace transform reduces to the calculation of residues at the points $s = \pm \kappa$.

We obtain as a result that in a region far from the boundary

$$n^{as}(z) \approx \operatorname{sh} \varkappa (z + z_0), \tag{9}$$

where the extrapolation length z_0 is determined by the expression [2]

$$z_0(\Sigma_s) = \frac{\Sigma_s}{2\varkappa} \int_0^1 \frac{[1 - \mu^2(1 - \Sigma_s)] \operatorname{arc\,th}(\varkappa\mu)}{(1 - \mu^2)\left\{[1 - \Sigma_s \mu \operatorname{arc\,th} \mu]^2 + \left[\frac{\pi \Sigma_s}{2}\right]^2\right\}} d\mu. \tag{10}$$

For

$$\Sigma_s \to 0$$
$$z_0(\Sigma_s) \approx 1/\Sigma_s + (\ln \Sigma_s)/2 - (\ln 2)/2 + (\Sigma_s \ln 2)/2, \tag{11}$$
$$z_0(1) = 0{,}7104\ldots$$

Variational Method [2, 5]. The kinetic Equation (3) with boundary conditions may be reduced to the integral equations of Peierls for the neutron density (this equation may also be obtained directly from physical considerations):

$$n(z) = \frac{\Sigma_s}{2} \int_0^\infty n(z') E_1(|z - z'|)\, dz', \tag{12}$$

where

$$E_1(x) = \int_1^\infty \frac{e^{-xt}}{t} dt. \tag{13}$$

The basis of the variational method is the fact that for an inhomogeneous integral equation with a symmetric kernel [$K(z, z') = K(z', z)$] with

* 'th' ≡ 'tanh', 'sh' ≡ 'sinh'; 'ch' ≡ 'cosh'; 'tg' ≡ 'tan' – Publisher.

$$q(z) = \int q(z')\, K(z, z')\, dz' + h(z) \tag{14}$$

the functional

$$F(q) = \frac{\int q(z) \left[q(z) - \int q(z')\, K(z, z')\, dz' \right] dz}{\left[\int h(z)\, q(z)\, dz \right]^2} \tag{15}$$

has a minimum and equals $\left[\int h(z)\, q(z)\, dz \right]^{-1}$, when q(z) is a solution of Equation (14).

In order to reduce (12) to the form (14), Le Caine used the two expressions

$$n(z) = k_1 \left[\operatorname{sh} \varkappa (z + z_0) + q_1(z) \right] \tag{16}$$

and

$$n(z) = k_1 \left[e^{\varkappa z} + q_2(z) \right] \frac{e^{\varkappa z_0}}{2}. \tag{17}$$

The simplest trial function $\overline{q_2}(z) = e^{-\varkappa z}$ in (17) yields

$$z_0 = -\frac{1}{2\varkappa} \ln \left\{ \frac{\left[\frac{1}{1+\varkappa} - \frac{1}{\varkappa} \ln (1+\varkappa) \right]^2 - \frac{1}{4\varkappa^2} \ln^2 (1-\varkappa^2)}{\frac{1}{\varkappa} \left(\frac{1}{1-\varkappa^2} - \frac{1}{\Sigma_s} \right) \ln (1-\varkappa^2)} \right\}. \tag{18}$$

TABLE 1
Values of $\Sigma_s z_0$

Σ_s \ Formula for z_0	Formula (10)	Formula (24) of [2]	Formula (18)	Formula (19)*
1,0	0,7104	0,7104	0,7083	0,7104
0,9	0,7106	0,7106	0,7095	0,7091
0,8	0,7113	0,7113	0,7105	0,7091
0,7	0,7127	0,7127	0,7121	0,7140
0,6	0,7154	0,7154	0,7150	0,7318
0,5	0,721	0,7204	0,7202	0,7792
0,4	0,730	0,7300	0,7298	—
0,3	0,749	0,7484	0,7484	—
0,2	0,785	0,7847	0,7848	—
0,1	0,850	0,8539	0,8538	—
0,0	1,0	1,000	1,000	—

* Values of $\Sigma_s z_0^*$.

The results of the calculation of z_0 according to Formulas (10), (18), as well as Formula (24) of [2], which was obtained by using a more complicated trial function $\overline{q_1}(z)$, are given in Table 1. Note that down to $\Sigma_s \approx \Sigma_c$, $z_0 = 0.71/\Sigma_s$ with good accuracy.

In the last column of the table are entered the extrapolation lengths for the case of a uniform distribution of sources:

$$z_0^* = z_0 + \frac{1}{\varkappa} \ln \frac{\Sigma_s}{1-\Sigma_s} \sqrt{\frac{(1-\Sigma_s)(\varkappa^2 - 1 + \Sigma_s)}{2(1-\varkappa^2)}}. \tag{19}$$

It is evident from the table that z_0^* begins to differ appreciably from z_0 only when $\Sigma_s = 0.5 = \Sigma_c$.

3. Of primary importance for the calculation of the efficiency of reactor regulators are the EBC at the surface of a black, circular cylinder. We describe below the basic methods of solution of this problem.

Equilibrium method. On the basis of neutron equilibrium, A. Brudno (1951) found EBC for a black cylinder of arbitrary radius r_0 located in a nonabsorbing medium with isotropic scattering for the case of a current incident from infinity. This method is very simple and guarantees sufficient accuracy.

The normal component of the kinetic current at the point $\mathbf{r}$ is given by the expression

$$P(\mathbf{r}) = \iiint_V n(\mathbf{r}') \frac{e^{-R}}{4\pi R^2} \cos\varphi\, dV, \tag{20}$$

where R is the distance between the points $\mathbf{r}$ and $\mathbf{r}'$, φ is the angle between R and $\mathbf{r}$ and the integration is carried out over the region V not "screened" by the rod (that is, the largest region such that a straight line between the point $\mathbf{r}$ and any point $\mathbf{r}'$ of the region does not touch the rod).

The neutron density may be determined from the Peierls equation

$$n(\mathbf{r}) = \int\int\int_V n(\mathbf{r}') \frac{e^{-R}}{4\pi R^2} dV. \tag{21}$$

At a great distance from the rod, the density is given by the expression

$$n^{as}(r) = \lambda + r_0 \ln \frac{r}{r_0}. \tag{22}$$

In the asymptotic region, the current through an arbitrary surface coincides with the diffusion current: $P(\infty) = \frac{1}{3}$.

Since, by hypothesis, the medium is nonabsorbing, this same current passes through an arbitrary surface surrounding the rod. In particular, $P(r_0) = \frac{1}{3}$.

We may also approximate $P(r_0)$ by substituting (22) into the right-hand side of Expression (20). We then obtain λ as a function of r_0:

$$\lambda(r_0) = \frac{4}{3} - r_0 R(r_0), \tag{23}$$

where

$$R(r_0) = \frac{2}{\pi}\int_0^\infty [K_1(x) - K_i(x)]\, x\, \rho\left(\frac{x}{r_0}\right) dx,$$

$$\rho(t) = -1 + \frac{\pi}{2} t + \left(\frac{1}{t} - t\right) \operatorname{arctg} t + \ln(1+t^2),$$

$$K_i(x) = \int_x^\infty K_0(y)\, dy$$

(K_0 and K_1 are MacDonald functions).

From (23) it follows that $\lambda(r_0) \equiv \lambda_0 = 4/3$ for $r_0 \to 0$ and $\lambda(r_0) = 2/3$ for $r_0 \to \infty$. The last value differs somewhat from the exact value $\lambda(\infty) = z_0 = 0.7104$. The error in the determination of $\lambda(r_0)$ for thick rods may be diminished by using the interpolation formula

$$\lambda^*(r_0) = \lambda(r_0) + \frac{0{,}7104 - \frac{2}{3}}{\frac{4}{3} - \frac{2}{3}} \left[\frac{4}{3} - \lambda(r_0)\right]. \tag{24}$$

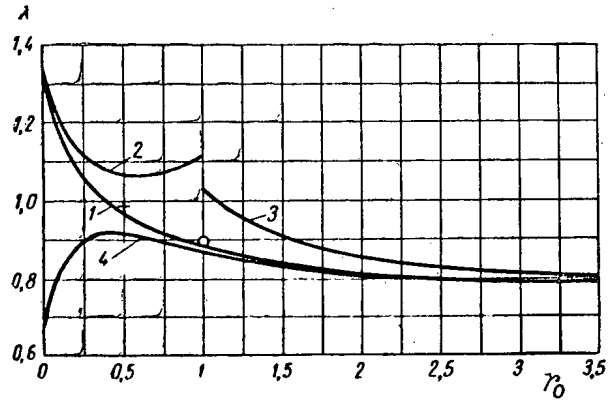

Fig. 1. EBC for black cylinders. 1) Equilibrium method; 2) expansion for small r_0; 3) expansion for large r_0; 4) P_3 approximation of variational method; O) numerical solution.

The result of the calculation is given in Fig. 1.

Numerical solution. In 1951, S. Sobolev, A. Brudno, M. Lavrova, G. Mukhina, and V. Khodakov by means of a direct numerical solution established the reference point value $\lambda(1) = 0.889 \pm 1\%$. A grid method of solution was used. The agreement of the above-mentioned results of Brudno with the exact numerical solution is completely satisfactory.

Variational method [6]. As in the case of the direct numerical solution, the variational method gives extremely reliable results. Just as in the problem of the half-space, the Peierls equation leads to the inhomogeneous equation

$$n(r) = 1 + q(r), \tag{25}$$

where $q(r) \underset{r\to\infty}{\longrightarrow} b \ln r$, and the functional form (15) is used. The condition of the conservation in a nonabsorbing medium of the current through an arbitrary surface surrounding the rod leads to the integral relation

$$b = -3\int_{r_0}^{\infty} q(r)\, h(r)\, r\, dr - 3\int_{r_0}^{\infty} rh(r)\, dr. \tag{26}$$

The choice of a trial function in the form $\overline{q}(r) = b \ln r$ permits one to find rather easily the quantity $\int_{r_0}^{\infty} q(r)\, h(r)\, r\, dr$, and therefore also the quantity $\underline{b}$ which is connected with the boundary condition by the relation

$$\lambda(r_0) = \frac{1 + b \ln r_0}{b/r_0}. \tag{27}$$

The variational method gives extremely small errors. For example, λ equals $\frac{17}{24}$ for $r_0 \to \infty$ [5] and 0.99 for $r_0 = 0.5$.

Method of spherical harmonics. As far as we know, the method of spherical harmonics for obtaining EBC on the surface of a black rod was first used by Galanin in 1947. Results of calculations with this method are given also in an article of Davison [7].

The kinetic equation of the type of Formula (2) is expanded in Legendre polynomials and leads to an infinite system of differential equations with respect to the angular moments $f_n(r)$ of the distribution function $f(r, \Omega)$. This system is "truncated" by assuming that starting with a certain $\underline{n}$ all $f_n(r) = 0$. If we assume that all moments beginning with the second are zero, then we obtain the P_1 approximation (diffusion approximation); if all moments are zero beginning with the fourth, we have the P_3 approximation, and so forth.

We see from Fig. 1 that for thin rods ($r_0 < 1$), the method of spherical harmonics leads to appreciable error ($\frac{2}{3}$ instead of $\frac{4}{3}$ for $r_0 \to 0$). The poor convergence of the method for small r_0 is connected with the fact that the neutron density is approximated to the asymptotic density not at the distance $1/\Sigma_s$ but at the smaller distance r_0. This leads to such a large rate of change of the neutron density in the neighborhood of the rod that the density may no longer be described by only a few of the moments $f_n(r)$.

Solution of the Peierls equation for large and small r_0 [7]. The Peierls equation for a black cylinder in a nonabsorbing, isotropically scattering medium may be written in the form

$$n(r) = \int_{r_0}^{\infty} r' n(r')\, K(r, r', r_0)\, dr' \quad (r \geqslant r_0), \tag{28}$$

where

$$K(r, r', r_0) = \frac{2}{\pi} \int_{|r-r'|}^{(r^2-r_0^2)^{1/2}+(r'^2-r_0^2)^{1/2}} \frac{K_1(\rho)\, d\rho}{\{\rho^2 - (r-r')^2\}^{1/2}\{(r+r')^2 - \rho^2\}^{1/2}}, \tag{29}$$

ρ is the distance between the points $\mathbf{r}$ and $\mathbf{r}'$ in the plane $z = 0$,

$$\rho^2 = r^2 + r'^2 - 2rr' \cos\vartheta.$$

In order to determine EBC for $r_0 \ll 1$, Kushnerik utilized the fact that even for $r_0 \approx 1$ the contribution from the "screened" region to the neutron density is small. Therefore, the Peierls equation may be written as if the integration were extended over the entire volume and the effect of "screening" divided off into free terms. For this purpose, the neutron density is defined for $r < r_0$ by the expression

$$n(r) = \int_{r_0}^{\infty} r' n(r') K(r, r', 0)\, dr' \tag{30}$$

and represented as a series

$$n(r) = n_0(r) + n_1(r) + \ldots + n_m(r) + \ldots, \tag{31}$$

where $n_m(r)$ is determined by the system of equations:

$$\left.\begin{aligned} n_0(r) &= \int_0^{\infty} r' n_0(r') K(r, r', 0)\, dr', \\ n_m(r) &= \int_0^{\infty} r' n_m(r') K(r, r', 0)\, dr' + f_m(r), \\ & \qquad m \geqslant 1 \end{aligned}\right\} \tag{32}$$

The free terms $f_m(r)$ are calculated recursively:

$$\begin{aligned} f_m(r) = s(r - r_0) \int_{r_0}^{\infty} r' n_{m-1}(r') \{K(r, r', r_0) - \\ - K(r, r', 0)\}\, dr' - \\ - \int_0^{r_0} r' n_{m-1}(r') K(r, r', 0)\, dr', \end{aligned} \tag{33}$$

where

$$s(r - r_0) = \begin{cases} 1 & \text{for } r > r_0, \\ 0 & \text{for } r < r_0. \end{cases}$$

The neutron density is normalized by

$$\lambda [r/r_0 n'(r)]_{r \to \infty} = 1. \tag{34}$$

If we take $n_0(r) \equiv 1$ and $n_m^{as}(r) = B_m(r_0) \ln r/r_0$, we obtain

$$\lambda = r_0 \Big/ \sum_{m=1}^{\infty} B_m(r_0). \tag{35}$$

The solutions of Equations (32) are given by the formulas

$$\begin{aligned} n_m(r) = \int\int\int n_0(R) f_m(\sqrt{x_0^2 + y_0^2})\, dx_0\, dy_0\, dz_0 + \\ + f_m(r), \quad m \geqslant 1, \end{aligned} \tag{36}$$

$$B_m(r_0) = -3 \int_0^{\infty} r' f_m(r')\, dr',$$

where R is the distance between the points (x, y, z) and (x_0, y_0, z_0); $n_0(R)$ is the neutron density due to a single point source in an infinite medium at a distance R from the source.

If we limit ourselves to terms with $m \leq 2$, then

$$\lambda = 4/3 + (1 - 16/3\pi^2)\, r_0 \ln r_0 - 0{,}2164 r_0 + 0\,(r_0^2 \ln^2 r_0). \tag{37}$$

Davison brought Equation (28) to a form suitable for $r_0 \gg 1$. For this purpose he expanded

$$\{(r+r')^2 - \rho^2\}^{-1/2} \equiv \left(2\sqrt{rr'}\cos\frac{\vartheta}{2}\right)^{-1}$$

in a series in powers of $\{\rho^2 - (r-r')^2\}/4rr' \equiv \sin^2\frac{\vartheta}{2}$ and assumed that

$$r = r_0 + x, \quad r' = r_0 + y, \quad r^{1/2} n(r) = c' q(x), \tag{38}$$

where c' is a certain constant. Thereby, Equation (28) takes the form

$$\begin{aligned} q(x) = \frac{1}{2}\int_0^\infty q(y)\,dy \sum_{n=0}^{\infty} \frac{|P_{2n}(0)|}{[4(r_0+x)(r_0+y)]^n} \times \\ \times \{F_n(|x-y|) - \widetilde{F}_n[|x-y|,\ (2r_0x+x^2)^{1/2} + \\ + (2r_0y+y^2)^{1/2}]\}, \end{aligned} \tag{39}$$

where P_{2n} are Legendre polynomials and the functions F_n and $\widetilde{F}_n$ are defined by the equations

$$\left.\begin{aligned} \widetilde{F}_n(h,k) = \frac{2}{\pi}\int_h^\infty K_i(\rho)\,[\rho^2 - h^2]^{n-1/2}\,d\rho, \\ (k \geqslant h \geqslant 0), \\ F_n(h) = \widetilde{F}_n(h,h),\ F_0(h) = E_1(h), \\ F_n(h) = (2n-1)\int_h^\infty t F_{n-1}(t)\,dt. \end{aligned}\right\} \tag{40}$$

Expanding $[(r_0 + x)(r_0 + y)]^{-n}$ in powers of r_0^{-1}, we find easily that

$$q(x) = \hat{L}_1 q + \hat{L}_2 q + \hat{L}_3 q + \ldots, \tag{41}$$

where

$$\hat{L}_1 q \equiv \frac{1}{2}\int_0^\infty E_1(|x-y|)\,q\,dy,$$

$$\begin{aligned} \hat{L}_2 q \equiv \frac{1}{2}\int_0^\infty \left\{\frac{|P_2(0)|}{4r_0^2} F_1(|x-y|) - \right. \\ - \widetilde{F}_0[|x-y|,\ (2r_0x+x^2)^{1/2} + \\ \left. + (2r_0y+y^2)^{1/2}]\right\} q\,dy, \end{aligned}$$

$$\hat{L}_3 q \equiv -\frac{1}{2}\int_0^\infty (x+y)\frac{|P_2(0)|}{4r_0^3} F_1(|x-y|)\,q\,dy.$$

Equation (41) is solved by a perturbation method. The function q(x) is represented in the form

$$q(x) = q_0(x) + q_2(x) + q_3(x) + \ldots, \tag{42}$$

where $q_i(x)$ is determined by the equations

$$\begin{gathered} q_0(x) = \hat{L}_1 q_0, \quad q_2(x) = L_1 q_2 + \hat{L} q_0, \\ q_3(x) = \hat{L}_1 q_3 + \hat{L}_2 q_2 + L_1 q_0. \end{gathered} \tag{43}$$

For a suitable choice of the normalization constant,

$$\lambda = \sum_{m=0}^{\infty} \Big\{ \sum_{n=0}^{\infty} \tilde{q}_n(\infty) \Big\}^{m+1} \Big/ (2r_0)^m, \tag{44}$$

where $q_n(x)$ are functions describing the deviation of the $\tilde{q}_n(x)$ from their asymptotic values:

$$\begin{aligned} \tilde{q}_0(x) &= q_0(x) - x, \\ \tilde{q}_2(x) &= q_2(x) + \frac{x^3 + 3x^2 \tilde{q}_0(\infty)}{24 r_0^2}, \\ \tilde{q}_3(x) &= q_3(x) - \frac{x^4 + 2x^3 q_0(\infty)}{24 r_0^3}, \text{ etc.} \end{aligned} \tag{45}$$

For $\tilde{q}_2(x)$, $\tilde{q}_3(x)$, etc, we obtain equations of the Milne type with right-hand side

$$\begin{aligned} \tilde{q}_2(x) &= \frac{1}{2} \int_0^{\infty} \tilde{q}_2(y) E_1(|x-y|)\, dy + f_2(q_0), \\ \tilde{q}_3(x) &= \frac{1}{2} \int_0^{\infty} \tilde{q}_3(y) E_1(|x-y|)\, dy + f_3(q_0, q_2), \text{ etc.}, \end{aligned} \tag{46}$$

from which it follows that

$$\tilde{q}_n(\infty) = 3 \int_0^{\infty} q_0(x) f_n(x)\, dx. \tag{47}$$

Calculation gives the following results for $\lambda(r_0)$ for $r_0 \gg 1$:

$$\begin{aligned} \lambda(r_0) &= 0{,}7104 + 0{,}2524 r_0^{-1} + 0{,}0949 r_0^{-2} - \\ &- \frac{5}{64} r_0^{-3} \ln r_0 - 0{,}01634 r_0^{-3} + 0(r_0^{-4} \ln^2 r_0). \end{aligned} \tag{48}$$

4. In the case of black rods of arbitrary section, the problem of determining the exact EBC is, from a practical point of view, insoluble.

Hurwitz and Roe [8] have given the following approximate method of solution for this problem. Let us consider a rod located in a medium with a rate of generation of thermal neutrons that is uniform with respect to volume. The absorbing power of the rod may be described by a quantity called the "absorption cross section," which is defined as the ratio of the current absorbed per unit length of the rod to the number of thermal neutrons that are generated per unit volume per unit time. Particularly simple and instructive results are obtained for the limiting case when the diffusion length L is greater than the scattering length and also greater than the characteristic dimensions of the rod section. In this case, elementary diffusion theory yields the following expression for the neutron density:

$$n^{as}(r) = c_1 \left\{ \ln \frac{r}{r_{eff}} + \sum_{n=1}^{\infty} \frac{a_n}{r^n} \cos(n\varphi + \delta_n) \right\}, \tag{49}$$

where a_n, δ_n, and r_{eff} are determined by the form of the rod section. For distances much larger than the characteristic dimensions of the rod, the last term may be neglected. Then it turns out that r_{eff} is equal to the radius of a circular cylinder with the same absorption cross section C as the actual rod:

$$C = 2\pi r_{eff} L \frac{K_1 (r_{eff}/L)}{K_0 (r_{eff}/L)}. \tag{50}$$

We give below values of r_{eff} calculated by elementary diffusion theory for rods of various sectional forms.

Shape of section:	Effective radius:
Line segment of length 2a	$\frac{a}{2}$
Symmetric cross with ray length a	$\frac{a\sqrt{2}}{2}$
Ellipse with semiaxes a and b	$\frac{a+b}{2}$

Values of r_{eff} for rectangular rods are given in Table 2.

TABLE 2

Effective Radii of Rods With Rectangular Section

$\frac{b}{a}$	0,00	0,0432	0,2219	0,3968	0,5850	0,6418	0,8030	1,00
$\frac{r_{eff}}{a}$	0,25	0,2732	0,3439	0,4038	0,4401	0,4820	0,5314	0,5902

If the kinetic effect is taken into account, then we obtain in place of Formula (50) the following formula:

$$C = 2\pi r_{eff} L \Big/ \left\{ \frac{K_0 (r_{eff}/L)}{K_1 (r_{eff}/L)} + \frac{\lambda (r_{eff})}{L} \right\}. \tag{51}$$

The introduction of a kinetic correction is, of course, meaningful only when the characteristic dimensions of the section are less than unity. In the opposite limiting case when L is much smaller than the characteristic dimensions of the rod section, we have the following expression for C:

$$C = L \{P + L \sum_i D(\Phi_{0i})\}, \tag{52}$$

where P is the perimeter of the rod section, $D(\Phi_{0i})$ is a correction to the perimeter due to the presence of an edge, Φ_{0i} is the exterior angle of the i-th edge. These corrections are listed in Table 3.

TABLE 3

Values of Edge Correction for Various Exterior Angles Φ_0

Φ_0	2π	$\frac{3\pi}{2}$	π	$\frac{\pi}{2}$	$\pi/3$
$D(\Phi_0)$	1	$\frac{4}{3\pi}\left(\frac{4\pi}{3\sqrt{3}} - 1\right)$	0	$-4/\pi$	$-4/\sqrt{3}$

For intermediate values of L, the problem of determining C may be solved by a variational method. The resulting formulas are extremely unwieldy.

5. The determination of the EBC for gray rods is a problem of great practical interest. This problem may be solved only by approximate methods. One such method is a variational method similar to the one described above for black rods. In [6] this method is used to discuss the case of rods for which the mean capture length is comparable with the rod diameter and scattering may be neglected. However, the formulas obtained are too cumbersome to be suitable for a practical calculation.

The matter is simpler for the limiting case of thin rods. For $r_0 \ll 1$ we may find the relation between b_{gray} and b_{black} from simple physical considerations (b is the constant entering into Formula (27) for λ):

$$b_{gray} = b_{black} \frac{16 r_0^2}{\pi l^2} \int_0^1 \sqrt{1-x^2}\, x \left[K_1\left(\frac{2r_0 x}{l}\right) - K_i\left(\frac{2r_0 x}{l}\right)\right] dx, \tag{53}$$

where l is the full mean free path for neutrons in the rod.

A comparison of the values of λ obtained with Formulas (27) and (53) with the more exact values given by the variational method shows that Formula (53) may be used for $r_0 \leqslant 0.5$. The resulting error is never more than a few percent. Values of λ are given in Table 4. If $r_0 > 0.5$, the use of Formula (53) leads to appreciable error. Therefore, it is necessary in this case to use a more exact method, for example, the variational method.

For $r_0 > 1$, the P_3 approximation of the method of spherical harmonics also gives small errors. Indeed, even for black rods, for which the convergence of the P_n approximation is slower than for gray rods, $\lambda(1)$ in the P_3 approximation is 0.867 (the numerical solution of S. Sobolev et al gives $\lambda(1) = 0.889$). Royston [9] has carried out a calculation for the P_3 approximation. The results are shown in Fig. 2.

TABLE 4

Values of $\lambda_{gray}(r_0, l)$

r_0 / r_0/l	0,1	0,2	0,3	0,4	0,5
2	1,31	1,23	1,16	1,11	1,06
3/2	1,39	1,31	1,24	1,18	1,13
1	1,57	1,49	1,41	1,35	1,29
2/3	1,89	1,81	1,73	1,66	1,58
1/2	2,22	2,15	2,06	1,99	1,89
1/4	3,66	3,60	3,48	3,36	3,20

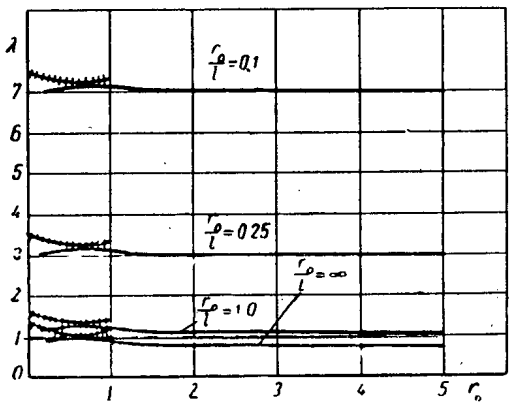

Fig. 2. EBC for gray cylinders. Continuous curves — P_3 approximation; cross-hatched curve — expansion for small r_0.

In the region $0.5 < r_0 < 1$, λ may be found from the data of Fig. 2 and Table 4 by interpolation.

6. The exact EBC for gray bodies may be obtained only in the limiting case of two half-spaces. This case was discussed in 1952 by D. Zaretskii with the Wiener-Hopf method mentioned in section 2. The following formula is obtained, relating z_0 to the macroscopic cross sections of the media, Σ_s:

$$z_0(\Sigma_c^{(1)}, \Sigma_c^{(2)}) = \frac{1}{2\varkappa^{(1)}} \ln \left| \frac{\Sigma_s^{(1)}}{\Sigma_c^{(2)} - \Sigma_c^{(1)}} \right| + \frac{1}{\pi} \int_0^\infty \frac{\ln\left[1 - \Sigma_s^{(2)} \frac{\operatorname{arc\,tg} z}{z}\right]}{z^2 + (\varkappa^{(1)})^2} dz + z_0(\Sigma_c^{(1)}), \tag{54}$$

$$\Sigma_s^{(1)} + \Sigma_c^{(1)} = 1, \quad \Sigma_s^{(2)} + \Sigma_c^{(2)} = 1,$$

where $z_0(\Sigma_c^{(1)})$ is the extrapolation length for the Milne problem; the index (1) denotes the medium for which the current at infinity is given. For $\Sigma_c^{(1)} > \Sigma_c^{(2)}$ the quantity that vanishes at $z_0(\Sigma_c^{(1)}, \Sigma_c^{(2)})$ is not the asymptotic neutron density but the gradient of the density $n_0^{as}(z)$ in medium (1). This is connected with the fact that for $\Sigma_c^{(1)} > \Sigma_c^{(2)}$ $n_0^{(1)as} \approx \operatorname{ch} x^{(1)}(z + z_0)$, but not $\operatorname{sh} x^{(1)}(z + z_0)$.

In Table 5 are given values of the extrapolation length calculated with the use of Formula (54).

TABLE 5

Extrapolation Lengths for Two Half-Spaces.

$\Sigma_c^{(2)}$ \ $\Sigma_c^{(1)}$	0,0	0,1	0,2	0,3	0,4	0,5	0,6	0,7	0,8	0,9
0	—	0,015	0,045	0,095	0,169	0,297	0,725	1,008	2,171	6,380
0,1	1,882	—	1,368	0,973	0,869	0,903	1,084	1,531	2,682	6,884
0,2	1,368	1,782	—	1,587	1,422	1,212	1,347	1,768	2,906	7,097
0,3	1,144	1,373	1,774	—	1,760	1,529	1,596	1,982	3,099	7,277
0,4	1,012	1,176	1,413	1,822	—	1,976	1,882	2,205	3,288	7,445
0,5	0,923	1,054	1,230	1,487	1,925	—	2,299	2,473	3,497	7,622
0,6	0,859	0,971	1,166	1,314	1,606	2,103	—	2,878	3,756	7,821
0,7	0,809	0,909	1,035	1,204	1,439	1,793	2,407	—	4,151	8,073
0,8	0,770	0,860	0,975	1,125	1,328	1,628	2,099	2,970	—	8,465
0,9	0,737	0,822	0,927	1,065	1,247	1,519	1,934	2,662	4,234	—
1,0	0,710	0,790	0,889	1,018	1,192	1,441	1,825	2,495	3,924	8,539

In all the cases considered above, it has been assumed that the neutron scattering is isotropic in the laboratory system of coordinates. In the case of greatest interest of weak absorption in the diffusing medium, the anisotropy may be taken into account adequately by increasing the extrapolation length by the factor

$$1/(1 - \overline{\cos\theta})$$

where $\overline{\cos\theta}$ is the average cosine of the scattering angle. For media with arbitrarily strong absorption, the solution for the problem of two half-spaces is known [10] but numerical results have not been obtained.

A certain amount of information concerning EBC including the case of anisotropic scattering is contained in the handbook [1] (pages 147 and following, pages 271 and following) with references to unpublished work.*

In conclusion, we remark that for thick rods, an effective radius may be introduced, at which the asymptotic neutron density vanishes:

$$r_{\text{eff}} = r_0 e^{-z_0/r_0} \tag{55}$$

(z_0 is found with the help of Formula (54)).

Problems That Take into Account the Neutron Spectrum

If the neutron absorption in the rod is important not only for the thermal region but also in the slowing-down process, it is possible to obtain exact EBC only in relatively simple limiting cases. Thus, for heavy retarders with isotropic scattering and an energy independent of Σ_s, the problem with the slowing-down process may be reduced to the monoenergetic problem with absorption. In the work of D. Zaretskii (1951) for the region $u \equiv \frac{1}{\xi} \ln \frac{E_0}{E} \gg 1$

* In the Russian edition of the handbook, Table 44 is incorrectly reproduced. [The page references here are to the Russian edition — Publisher.]

(ξ is the average logarithmic energy loss) an expansion is used which corresponds to the age theory approximation for the slowing-down process:

$$\psi(u', \mathbf{r}) \approx \psi(u, \mathbf{r}) + (u' - u)\frac{\partial \psi(u, \mathbf{r})}{\partial u}. \tag{56}$$

This expansion is substituted into an equation of the Peierls type for the distribution of neutrons from a monoenergetic source $\delta(E - E_0) f(\mathbf{r})$:

$$\begin{aligned} \psi(E, \mathbf{r}) &= \frac{1}{4\pi(1-\varepsilon)} \int d\mathbf{r} \int_{E}^{E/\varepsilon} \psi(E', \mathbf{r}') \frac{e^{-|\mathbf{r}-\mathbf{r}'|}}{|\mathbf{r}-\mathbf{r}'|^2} \times \\ &\times \frac{dE'}{E'} + \frac{\delta(E - E_0)}{4\pi} \int d\mathbf{r}' f(\mathbf{r}') \frac{e^{-|\mathbf{r}'-\mathbf{r}|}}{|\mathbf{r}-\mathbf{r}'|^2}, \\ \psi &\equiv nv\Sigma_s, \quad \varepsilon = \left(\frac{M-1}{M+1}\right)^2, \quad \Sigma_s = \text{const}. \end{aligned} \tag{57}$$

For the function $\varphi(u, \mathbf{r}) = \xi\psi(u, \mathbf{r})$ we obtain the equation

$$\begin{aligned} \varphi(u, \mathbf{r}) &= \frac{1}{4\pi} \int \varphi(u, \mathbf{r}') \frac{e^{-|\mathbf{r}-\mathbf{r}'|}}{|\mathbf{r}-\mathbf{r}'|^2} d\mathbf{r}' - \\ &- \frac{1}{4\pi} \int \frac{\partial \varphi(u, \mathbf{r}')}{\partial u} \frac{e^{-|\mathbf{r}-\mathbf{r}'|}}{|\mathbf{r}-\mathbf{r}'|^2} d\mathbf{r}' + \\ &+ \frac{\delta(u)}{4\pi} \int f(r') \frac{e^{-|\mathbf{r}-\mathbf{r}'|}}{|\mathbf{r}-\mathbf{r}'|^2} d\mathbf{r}'. \end{aligned} \tag{58}$$

If we take the Laplace transform with respect to u, it is not difficult to see that the equation for the Laplace transform $F(\eta, \mathbf{r})$ is equivalent to the Peierls equation for monoenergetic neutrons in a medium with absorption. The parameter of the Laplace transform plays the part of the macroscopic absorption cross section.

$$\begin{aligned} F(\eta, \mathbf{r}) &= \frac{1-\eta}{4\pi} \int F(\eta, \mathbf{r}') \frac{e^{-|\mathbf{r}-\mathbf{r}'|}}{|\mathbf{r}-\mathbf{r}'|^2} d\mathbf{r}' + \\ &+ \frac{1}{4\pi} \int f(\mathbf{r}') \frac{e^{-|\mathbf{r}-\mathbf{r}'|}}{|\mathbf{r}-\mathbf{r}'|^2} d\mathbf{r}'. \end{aligned} \tag{59}$$

The determination of the EBC in the region of large slowing-down ($u \gg 1$) requires the knowledge of the expansion of $F(\eta, \mathbf{r})$ for small "absorptions" η. For the geometry of a plane, such an expansion may be found exactly. In cases of spherical or cylindrical symmetry, it is necessary to use an approximate method (for example, the variational method). However, it may be shown that under the assumptions that have been made, independently of the geometry, the EBC for neutrons that are slowing down coincide with the EBC for monoenergetic neutrons in a medium with weak absorption.

In the case of variable $\Sigma_s(u)$, the problem of taking into account the effect of the slowing-down process in the determination of the EBC has not yet been solved. We mention only the following considerations. Ordinarily, for reactor calculations a multiple group method is used in which a system of one-velocity equations is considered. If in the equation for the i-th group, the term making this equation inhomogeneous (due to sources) does not change too rapidly in the neighborhood of the rod, then the results of section 2 may be used. A smooth change of the source density means that this change must be small over the distance where the neutron density differs from its asymptotic value. Thus, the use of the monoenergetic EBC for each group is justified, at any rate, for thin rods ($r_0 \ll 1$).

LITERATURE CITED

[1] U. S. Atomic Energy Reactor Handbook, Vol. 1, Physics of nuclear reactors (Foreign Literature Press, 1956), p. 145 [Russian translation].

[2] J. Le Caine, Canad. J. Res. A 28, 3, 242 (1950).

[3] E. Titchmarsh, Introduction to the Theory of Fourier Integrals (State Technical Press, 1948), p. 429 [Russian translation].

[4] M. A. Lavrent'ev and B. V. Shabat, Methods in the Theory of Functions of a Complex Variable, (State Technical Press, 1951), p. 58.*

[5] R. E. Marshak, Phys. Rev. 71, 688 (1947).

[6] D. F. Zaretskii, Reactor Construction and Theory of Reactors, (Report of the Soviet Delegation to the International Conference for Peaceful Uses of Atomic Energy) (Academy of Sciences, USSR, 1955), p. 279.

[7] B. Davison, Proc. Phys. Soc. A 64, 9, 881 (1951).

[8] H. Hurwitz and C. M. Roe, J. Nucl. Energy 2, 2, 85 (1955).

[9] R. Royston, Nucl. Energy 1, 3, 194 (1955).

[10] G. A. Bat' and D. F. Zaretskii, Reactor construction and theory of reactors, (Report of the Soviet Delegation to the International Conference for Peaceful Uses of Atomic Energy) (Academy of Sciences, USSR, 1955), p. 294.

Received October 4, 1957

* In Russian.

RESONANCE ABSORPTION OF NEUTRONS IN AN INFINITE HOMOGENEOUS MEDIUM

G. I. Marchuk and F. F. Mikhailus

The problem of the slowing down of neutrons in an infinite homogeneous medium with strong resonance absorption and uniformly distributed neutron sources is investigated in this paper.

The solution of the adjoint equation represents the probability that a neutron of energy E escapes resonance absorption during the process of slowing down to a certain asymptotic energy. The solution of the main and the adjoint problems makes it possible for us to apply a perturbation method to take into account the influence on the resonance integral of the Doppler broadening of the resonance level.

The methods developed have been applied to the calculation of the collision density and the resonance integrals for the first level of U^{238} ($E_0 = 6.7$ ev) in pure uranium and in uranium oxide UO_2.

1. Approximate Representation of the Scattering Function

In an infinite homogeneous medium with monoenergetic neutron sources and elastic scattering, isotropic in the center of mass, the collision density is given by the following integral equation:

$$\varphi(u) = \int_0^{u_{as}} g(u, u')\, A(u')\, \varphi(u')\, du' + \delta(u), \tag{1}$$

where $g(u, u') = \sum_i g_i(u, u') \frac{A_i(u')}{A(u')}$, the "scattering kernel," is the probability that after scattering the lethargy of a neutron changes from u' to u; $g_i(u, u')$ is the probability that after a scatter from a nucleus of mass M_i the lethargy of a neutron changes from u' to u:

$$g_i(u, u') = \begin{cases} \frac{1}{1-\alpha_i} e^{-(u-u')}, & u - q_i < u' < u, \\ 0, & u' > u,\ u' < u - q_i, \end{cases} \tag{1a}$$

$A_i(u) = \frac{\sigma_s^{(i)}(u)}{\sigma(u)}$ is the ratio of the scattering to the total cross section; $q_i = -\ln \alpha_i$ is the maximum change in the lethargy due to scattering from nuclei of mass M_i;

$$\alpha_i = \left(\frac{M_i - 1}{M_i + 1}\right)^2;$$

and u_{as} is a value of the lethargy which is very much larger than the lethargy of the resonance being investigated.

The problems of the neutron-energy distribution in an infinite medium which lead to Equation (1) were first investigated by Placzek [1]. He obtained a solution in the case of a single-component moderator and of a mixture with constant absorption. Further, on the assumption that in the interval of maximum change of the lethargy the variation of the absorption cross section is small, Placzek derived an expression for the asymptotic distribution of the collision density.

In the case of resonance absorption, Placzek's results are not applicable if the level width exceeds q_i.

Methods of investigating Equation (1) when the absorption cross section is not constant have been partially described in [2]. The principles of these methods are the following.

The scattering kernel (1a) in Equation (1) is determined over the interval $u - q < u' < u$ and is discontinuous at the boundaries of this interval. The scattering kernel is replaced by a function which is continuous over the whole range of variation of u' $(0 < u' < u)$ and is such that the normalization and the values of one or two moments of this function must be the same as the values of these quantities for the exact scattering kernel. Such kernels are usually called "synthetic kernels."

In the case of a single-component moderator the synthetic kernels have the form

$$\tilde{g}(u, u') = \xi\delta'(u-u') + \delta(u-u') \tag{2}$$

"Fermi kernel",

$$\tilde{g}(u, u') = \begin{cases} \frac{1}{\xi} e^{-\frac{u-u'}{\xi}}, & u \geqslant u', \\ 0, & u < u' \end{cases} \tag{3}$$

"Wigner kernel",

$$\tilde{g}(u, u') = \begin{cases} \frac{1}{\varepsilon 2\xi} e^{-\frac{u-u'}{\varepsilon\xi}} + \left(1 - \frac{1}{\varepsilon}\right)\delta(u-u'), \\ u' \leqslant u, \\ 0, \quad u' > u \end{cases} \tag{4}$$

"Greuling-Goertzel kernel",

where

$$\xi = 1 - \frac{\alpha}{1-\alpha} q \tag{5}$$

(ξ is the average lethargy change in one act of scattering),

$$\varepsilon = \frac{\overline{(u-u')^2}}{2\xi^2}, \tag{6}$$

$\overline{(u-u')^2}$ is the mean square change of the lethargy due to the scattering.

For all three of the synthetic kernels the normalization is the same and coincides with the exact one; the mean changes of the lethargy also coincide with the exact values. In fact, the exact scattering kernel is normalized to unity and the mean lethargy change has the following form:

$$\xi = \int_{u'}^{\infty} g(u, u')(u-u')\,du.$$

In the case of the synthetic kernels these quantities have the form

$$\int_{u'}^{\infty} (u-u')\left[\xi\delta'(u-u') + \delta(u-u')\right] du' = \xi$$

for the Fermi kernel,

$$\frac{1}{\xi}\int_{u'}^{\infty}(u-u')\,e^{-\frac{u-u'}{\xi}}\,du'=\xi$$

for the Wigner kernel,

$$\frac{1}{\varepsilon^2\xi}\int_{u'}^{\infty}(u-u')\left[e^{-\frac{u-u'}{\varepsilon\xi}}+\left(1-\frac{1}{\varepsilon}\right)\delta(u-u')\right]du'=\xi$$

for the Greuling-Goertzel kernel.

Let us now investigate the mean square change of the lethargy for the exact scattering kernel:

$$\overline{(u-u')^2}=\frac{1}{1-\alpha}\int_0^q x^2e^{-x}\,dx.$$

Taking into account Expression (5), we get

$$\overline{(u-u')^2}=2\xi-q(1-\xi). \tag{7}$$

Using (4), we obtain for the Greuling-Goertzel kernel:

$$\overline{(u-u')^2}=2\xi^2\varepsilon. \tag{8}$$

If we choose ϵ in accordance with Expression (6), then the mean square change of the lethargy for the Greuling-Goertzel kernel will be the same as the corresponding exact value.

From Relations (6) and (7) it follows that the quantity ϵ in the case of the Greuling-Goertzel kernel has the form

$$\varepsilon=\frac{2\xi-q(1-\xi)}{2\xi^2}. \tag{6a}$$

All of the above conditions for obtaining synthetic kernels remain unaltered in the case of a moderator consisting of a mixture of elements if we take the approximate kernel $\tilde{g}(u, u')$ to be the quantity

$$\tilde{g}(u,u')=\frac{1}{A(u')}\sum_i\tilde{g}_i(u,u')\,A_i(u'), \tag{9}$$

where $\tilde{g}_i(u, u')$ are the synthetic kernels for scattering from nuclei of mass M_i. Then the mean change and the mean square change of the lethargy will be averaged over the components of the mixture:

$$\bar{\xi}=\frac{1}{A(u')}\sum_i\xi_i\,A_i(u'), \tag{9a}$$

$$\int_{u'}^{\infty}\tilde{g}(u,u')(u-u')^2\,du=\frac{1}{A(u')}\sum_i\overline{(u-u')_i^2}\,A_i(u'),$$

where ξ_i is the mean square change of the lethargy due to scattering from nuclei of mass M_i and $\overline{(u-u')_i^2}$ is the mean square change of the lethargy due to scattering from nuclei of mass M_i.

Replacing in Equation (1) the exact scattering kernel by the synthetic, we obtain a new equation which for a single-component moderator has the following solution:

$$\varphi(u)=\frac{1}{\xi\{A(u)+\varepsilon[1-A(u)]\}}\times$$
$$\times\,e^{-\frac{1}{\xi}\int_0^u\frac{1-A'(u')}{A(u')+\varepsilon[1-A(u')]}\,du'}. \tag{10}$$

We get the Fermi approximation for $\epsilon = 0$, the Wigner approximation for $\epsilon = 1$. ϵ for the Greuling-Goertzel approximation is given by Expression (6a).

If absorption is absent, Equation (10) gives the exact asymptotic expression for the collision density. It must be pointed out that in the Wigner and Greuling-Goertzel approximations the solution given by (10) will be exact in the case of hydrogen.

In the case of strong resonance absorption in a pure substance or in a mixture it is not clear, without further investigations, how satisfactory the method of synthetic kernels is. Therefore, numerical methods of solving Equation (1) are of interest.

2. The Derivation of the Conjugate Equation for the Slowing Down of Neutrons

We will investigate in the case of a moderator with resonance absorption the behavior of the collision density, averaged over space and angles, determined by Equation (1). The energy dependence of the cross sections is given by the Breit-Wigner Formula; the total cross section takes into account the interference between potential and resonance scattering. We assume that the width of the resonance level is considerably greater than the maximum possible energy loss resulting from the scattering, but the ratio of the scattering to the total cross section cannot be considered as constant in the region of the maximum energy losses. We also assume that the level under investigation is so far removed from other neighboring levels that it may be considered to be isolated.

If the medium consists only of nuclei having such a resonance level, then the quantity $A(u)$ appearing in Equation (1) can be written in the form

$$A(u) = \frac{\sigma_{sp} + \frac{\sigma_{sr0}}{1+x^2} + \sigma_{int}\frac{x}{1+x^2}}{\sigma_{sp} + \frac{\sigma_{sr0}}{1+x^2} + \frac{\sigma_{ar0}}{1+x^2}\sqrt{\frac{E_0}{E}} + \sigma_{int}\frac{x}{1+x^2}}. \tag{11}$$

Here $x = \frac{E_0 - E}{\Gamma/2}$ (E_0 is the resonance energy, Γ is the total half-width), σ_{sr0} is the resonance-scattering cross section at energy E_0, σ_{sp} is the potential-scattering cross section, σ_{ar0} is the resonance-absorption cross section at energy E_0, and σ_{int} is the cross section for the interference between the resonance and potential scattering.

If there are light nuclei in the medium without resonance levels in the energy range considered ($E < 1$ kev), then for $A(u)$ we have

$$A_1(u) = \frac{\sigma_{sp}^{(1)} + \frac{\sigma_{sr0}}{1+x^2} + \sigma_{int}\frac{x}{1+x^2}}{\sigma_{sp} + \frac{\sigma_{sr0}}{1+x^2} + \frac{\sigma_{ar0}}{1+x^2}\sqrt{\frac{E_0}{E}} + \sigma_{int}\frac{x}{1+x^2}}, \tag{12}$$

$$A_i(u) = \frac{\sigma_{sp}^{(i)}}{\sigma_{sp} + \frac{\sigma_{sr0}}{1+x^2} + \frac{\sigma_{ar0}}{1+x^2}\sqrt{\frac{E_0}{E}} + \sigma_{int}\frac{x}{1+x^2}}. \tag{13}$$

Here $A_1(u)$ refers to nuclei with resonance properties, $A_i(u)$ to nuclei without resonance levels, and $\sigma_{sp} = \sum_i \sigma_{sp}^{(i)}$ is the total potential-scattering cross section for the mixture.

Let us formulate the problem of slowing down in an infinite medium in the following terms: we have to find a certain functional ν which is determined by the equation system

$$\begin{cases} \varphi(u) = \int_0^{u_{as}} g(u, u') A(u') \varphi(u')\, du' + \delta(u), \\ 1 = \nu \int_0^{u_{as}} G(u_{as}, u') A(u') \varphi(u')\, du'. \end{cases} \tag{14}$$

Here

$$G(u, u') = \int_{u}^{\infty} g(u'', u')\, du'' \tag{14a}$$

is the slowing-down kernel, i.e., the probability that a neutron of lethargy u' has after scattering a lethargy greater than u. The functional ν is related to the resonance integral by the expression

$$J = \ln \nu. \tag{15}$$

Further, there exists a relation between ν and the asymptotic expression for the slowing-down density:

$$q(u_{as}) = 1/\nu. \tag{15a}$$

Let us introduce the function $\psi(u) = \varphi(u) + \delta(u)$. Then the System (14) can be written in the following form:

$$\begin{cases} \psi(u) = \int_{0}^{u_{as}} g(u, u')\, A(u')\, \psi(u')\, du' + \\ \qquad\qquad + g(u, 0)\, A(0), \\ 1 = \nu \int_{0}^{u_{as}} G(u_{as}, u')\, A(u')\, \psi(u')\, du'. \end{cases} \tag{16}$$

Next, let us consider the set of vector functions $\Psi = \begin{pmatrix} \psi(u) \\ \psi_0 \end{pmatrix}$ (ψ_0 is a constant). With the help of these functions we can write System (16) in an abbreviated form as follows:

$$\Psi = L\Psi. \tag{17}$$

Here L is the matrix operator

$$\begin{pmatrix} g(u, u')\, A(u'), & g(u, 0)\, A(0) \\ \nu G(u_{as}, u'), & 0 \end{pmatrix} \tag{17a}$$

Let us indicate some of the functional properties of the vector-function set Ψ and of the operator L:

1. The elements of the set $\{\Psi\}$ form a Hilbert space. Let us define addition and multiplication by a number for it in the same way as for matrices. Scalar multiplication we define in the following way:

$$(\Psi, \Phi) = (\psi(u), \varphi(u)) + \psi_0 \varphi_0 = \\ = \int_{0}^{u_{as}} \psi(u')\, \varphi(u')\, du' + \psi_0 \varphi_0. \tag{18}$$

All of the axioms of linearity are then satisfied and the vector-function set has the property of completeness.

2. The operator L is completely continuous. In fact, since the elements of the matrix (17a) are quadratically integrable and the components of the vector Ψ are continuous, complete continuity holds for each component L_{ij} of the operator L. Consequently, the whole operator L is completely continuous.

Let us construct the adjoint operator. The condition of adjointness is

$$(\Phi, L\Psi) = (L^*\Phi, \Psi) \tag{19}$$

for arbitrary Φ and Ψ belonging to the Hilbert Space. In our case

$$(\Phi, L\Psi) = \int_0^{u_{as}} \varphi(u) \int_0^{u_{as}} g(u, u') A(u') \psi(u') du' du + A(0) \int_0^{u_{as}} g(u, 0) \varphi(u) du +$$
$$+ \nu \int_0^{u_{as}} G(u_{as}, u') A(u') \psi(u') du'.$$

Changing the order of integration in the first integral, we get

$$(\Phi, L\Psi) = \int_0^{u_{as}} A(u) \psi(u) du \int_0^{u_{as}} g(u', u) \varphi(u') du' +$$
$$+ A(0) \int_0^{u_{as}} \varphi(u') g(u', 0) du' +$$
$$+ \nu \int_0^{u_{as}} G(u_{as}, u') A(u') \psi(u') du'.$$

On the other hand, from the definition of scalar multiplication we can write

$$(\Phi, L\Psi) =$$
$$= \begin{pmatrix} A(u) \int_0^{u_{as}} g(u', u) \varphi(u') du' + \nu G(u_{as}, u) A(u) \\ A(0) \int_0^{u_{as}} \varphi(u') g(u', 0) du' \end{pmatrix} \times$$
$$\times \begin{pmatrix} \Psi(u') \\ 1 \end{pmatrix} \equiv (M\Phi, \Psi).$$

From Equation (19) it follows that M = L* and $\Phi = \Psi^*$; in addition

$$\Psi^* = \begin{pmatrix} \frac{1}{\nu} \varphi(u) \\ 1 \end{pmatrix}.$$

The equation for $\psi^*(u)$ can be written in the form

$$\begin{cases} \psi^*(u) = A(u) \int_0^{u_{as}} \psi^*(u') g(u', u) du' + \\ \qquad + G(u_{as}, u) A(u), \\ 1 = \nu A(0) \int_0^{u_{as}} \psi^*(u') g(u', 0), \end{cases} \tag{20}$$

where

$$g(u', u) = \begin{cases} \frac{1}{1-\alpha} e^{-(u'-u)}, & u < u' < u+q, \\ 0, & u > u', \ u' > u+q, \end{cases}$$

$$G(u', u) = \begin{cases} \frac{e^{-(u'-u)} - \alpha}{1-\alpha}, & u < u' < u+q, \\ 0, & u' < u, \\ 1, & u' > u+q. \end{cases}$$

Equation (20) has the following abbreviated form:

$$\Psi^* = L^* \Psi^*, \tag{20a}$$

where L* is the matrix operator

$$\begin{pmatrix} A(u)\, g(u', u), & \nu G(u_{as}, u)\, A(u) \\ A(0)\, g(u', 0), & 0 \end{pmatrix}. \tag{20b}$$

From (17a) and (20b) it can be seen that the operator L is not self-adjoint. It should be noted, however, that the eigenvalues of the basic and the adjoint operators coincide (for example, see [3]).

If $u_{as} \gg u$, then the first of Equations (20) will have the following form:

$$\psi^*(u) = A(u) \int_0^{u_{as}} \psi^*(u')\, g(u', u)\, du'. \tag{20c}$$

The equation determining the probability for a neutron of lethargy u to escape resonance absorption during the process of slowing down to thermal energy has an analogous form. This equation was first obtained by Zel'dovich and Khariton [4].

3. Numerical Method for the Solution of the Slowing-Down Equation

Let us proceed to find the collision density $\psi(u)$. With this in mind, we will use Equation (16) with the function A(u) given by Relations (11) and (12). Since the neutrons from the source have an energy considerably greater than the resonance energy, the asymptotic value of the collision density will be established in the vicinity of E_0.

If we note that in this energy region absorption is still small, we can use Equation (10), obtained with the help of the "Greuling-Goertzel approximation" to obtain $\psi(u)$ for $u_1 \leq u \leq u_0$, where u_0 is determined from the inequality $A(u_0) \ll 1$ and u_1 is the lethargy corresponding to the energy of the source. Thus, for all values of the lethargy u, we find the function $\psi(u)$ from the equations for the one-component moderator:

$$\psi(u) = \frac{1}{1-\alpha} \int_{u-q}^{u} e^{-(u-u')} A(u')\, \psi(u')\, du',$$

$$\text{if } u_0 \leq u \leq u_{as},$$

$$\psi(u) = \frac{1}{\xi} \{A(u) + \varepsilon [1 - A(u)]\}^{-1} \times$$

$$\times e^{-\frac{1}{\xi} \int_{u_{source}}^{u} \frac{1-A(u')}{A(u')+\varepsilon[1-A(u')]}\, du'}, \tag{21}$$

$$\text{if } u_{source} \leq u \leq u_0.$$

For slowing down in a mixture:

$$\psi(u) = \frac{1}{1-\alpha_1} \int_{u-q_1}^{u} e^{-(u-u')} A_1(u')\, \psi(u')\, du' +$$

$$+ \frac{1}{1-\alpha_2} \int_{u-q_2}^{u_{as}} e^{-(u-u')} A_2(u')\, \psi(u')\, du', \tag{22}$$

$$\text{if } u_0 \leq u \leq u_{as},$$

$$\psi(u) = \frac{1}{\bar{\xi}} \{A(u) + \bar{\varepsilon}[1 - A(u)]\}^{-1} \times$$

$$\times e^{-\frac{1}{\bar{\xi}} \int_{u_{source}}^{u} \frac{1 - A(u')}{A(u') + \varepsilon [1 - A(u')]} du'},$$

$$\text{if } u_{source} \leq u \leq u_0,$$

where $\bar{\xi}$ and $\bar{\epsilon}$ are averages over the components of the mixture and $A(u) = A_1(u) + A_2(u)$.

For the solution of the first of Equations (21) we will use the following numerical method. Let us introduce the function $\varphi(u) = \psi(u) e^u$ and rewrite the integral with the help of a quadrature formula having equal steps $\underline{h}$:

$$\varphi_n = \beta \sum_{i=n-k}^{n} A_i \varphi_i + \delta_n,$$

where $\varphi_i = \varphi(ih)$, $A_i = A(ih)$, $k = \frac{q}{h}$, δ_n is the quadrature error, $\beta = \frac{\mu h}{1 - \alpha}$, and μh is the coefficient in the quadrature formula.

For φ_n we obtain the computational formula

$$\varphi_n = \frac{\beta \sum_{i=n-k}^{n-1} A_i \tilde{\varphi}_i}{1 - \beta A_n} + \Delta_n \tag{23}$$

($\varphi_n \equiv \tilde{\varphi}_k + \Delta_n$, Δ_n is the error in the value of φ_n), using which we are able to calculate $\varphi(u)$ for any values of $\underline{u}$ from the known values of φ_i ($i = n - k, n - k + 1, \ldots, n - 1$).

Similarly, for the case of slowing down in a mixture we obtain from (22)

$$\varphi_n = \frac{\beta_1 \sum_{i=n-h_1}^{n-1} A_{1i} \tilde{\varphi}_i + \beta_2 \sum_{i=n-h_2}^{n-1} A_{2i} \tilde{\varphi}_i}{1 - \beta_1 A_{1n} - \beta_2 A_{2n}} + \Delta_n. \tag{24}$$

If q_2 is not an integral multiple of $\underline{h}$, then a correction factor should be introduced on the right-hand side of (24) to take into account the integral over the region $q_2 - k_2 h$.

4. Numerical Method for the Solution of the Adjoint Equation

We now proceed to the solution of the adjoint equation.

From the first equation of System (20), using a method analogous to that used for the solution of the basic problem, let us find numerically the adjoint collision density of neutrons.

For the case of a one-component medium, Equation (20) will have the form

$$\psi^*(u) = \frac{A(u)}{1 - \alpha} \int_{u}^{u_{as}} \psi^*(u') e^{-(u' - u)} du' +$$

$$+ A(u) \frac{e^{-(u'_{as} - u)}}{1 - \alpha}, \tag{25}$$

$$\text{if } u_{as} - q < u < u_{as}.$$

Next, let us introduce the function $\varphi^*(u) = \frac{\psi^*(u)}{A(u)} e^{-u}$. Then Equation (25) will take the form

$$\varphi^*(u) = \frac{1}{1 - \alpha} \int_{u}^{u_{as}} \varphi^*(u') A(u') du' + \frac{e^{-u_{as}} - \alpha e^{-u}}{1 - \alpha}.$$

The solution of this equation is found with the help of differentiation. It is easy to show that in the interval $u_{as} - q < u < u_{as}$ the solution has the following form:

$$\psi^*(u) = A(u)\, e^{u}\left[e^{\frac{1}{1-\alpha}\int_{u}^{u_{as}} A(u')du'} - \right.$$
$$\left. - \frac{\alpha}{1-\alpha}\int_{u}^{u_{as}} e^{\frac{1}{1-\alpha}\int_{u}^{u'} A(u'')du'' - u'}\, du' \right]. \tag{26}$$

For values of $\psi^*(u)$ outside this interval, $\varphi^*(u)$ is calculated with the help of quadrature formulas (see above):

$$\varphi_n^* = \frac{\beta \sum_{i=n+1}^{n+k} A_i \varphi_i^*}{1-\beta A_n} + \Delta_n. \tag{27}$$

For slowing down in a two-component mixture the first equation of System (20) can be written as

$$\varphi^*(u) = \frac{A_1(u)}{1-\alpha_1}\int_{u}^{u_{as}} \varphi^*(u')\, du' + \frac{A_2(u)}{1-\alpha_2}\int_{u}^{u_{as}} \varphi^*(u')du' +$$
$$+ e^{-u_{as}}\left[\frac{A_1(u)}{1-\alpha_1} + \frac{A_2(u)}{1-\alpha_2}\right] +$$
$$+ e^{-u}\left[\frac{\alpha_1 A_1(u)}{1-\alpha_1} + \frac{\alpha_2 A_2(u)}{1-\alpha_2}\right] \tag{28}$$

for $u_{as} - q < u < u_{as}$ (q is the smallest of the numbers q_1 and q_2). Here $\varphi^*(u) = \psi^*(u)\, e^{-u}$. Introducing a new function $\vartheta^*(u) = \frac{\varphi^*(u) - F(u)}{P(u)}$, where

$$P(u) = \frac{A_1(u)}{1-\alpha_1} + \frac{A_2(u)}{1-\alpha_2},$$
$$F(u) = e^{-u_a} P(u) + e^{-u}\left[\frac{\alpha_1 A_1(u)}{1-\alpha_1} + \frac{\alpha_2 A_2(u)}{1-\alpha_2}\right],$$

and differentiating the equation obtained, we can write the adjoint collision density for the interval $u_{as} - q < u < u_{as}$ in the following form:

$$\psi^*(u) = P(u)\, e^{\int_{u}^{u_{as}} P(u')du'} \times$$
$$\times \int_{u}^{u_{as}} F(u')\, e^{-\int_{u'}^{u_{as}} P(u'')du''}\, du' + F(u). \tag{29}$$

From this equation $\varphi^*(u)$ can be calculated for the interval

$$u_{as} - q_2 < u < u_{as} - q_1.$$

For these values of the lethargy the equation can be written as follows:

$$\varphi^*(u) = \frac{A_1(u)}{1-\alpha_1}\int_{u}^{u+q} \varphi^*(u')\, du' + \tag{30}$$
$$+ \frac{A_2(u)}{1-\alpha_2}\int_{u}^{u_{as}} \varphi^*(u')\, du' + A_2(u)\,\frac{e^{-u_{as}} - ae^{-u}}{1-\alpha_2}.$$

Applying to this equation the method of numerical integration described above, we get

$$\varphi^*(u_n) = \frac{\beta_1 A_1(u_n) \sum_{i=n+1}^{n+k_1} \varphi^*(u_i) + \beta_2 A_2(u_n) \sum_{i=n+1}^{m} \varphi_i^* + A_2(u_n) \frac{e^{-u_{as}} - \alpha_2 e^{-u_n}}{1-\alpha_2}}{1-\beta_1 A_1(u_n) - \beta_2 A_2(u_n)}. \tag{31}$$

Here $m = \frac{u_{as}}{q_1/k_1}$, $k_1 = \frac{q_1}{h}$, $\beta_1 = \frac{\mu h}{1-\alpha_1}$ and $\beta_2 = \frac{\mu h}{1-\alpha_2}$ are the coefficients of the quadrature formula used to calculate the integrals

$$\int_u^{u_{as}} \varphi^*(u')\,du', \quad \int_u^{u+q_1} \varphi^*(u')\,du'. \tag{32}$$

When the values of u lie in the range $u_{as} - q_1 < u < u_{as} - q_2$, the last term in the numerator becomes equal to zero and further calculations are carried out with the formula

$$\varphi^*(u_n) = \frac{\beta_1 A_1(u_n) \sum_{i=n+1}^{n+k_1} \varphi^*(u_i) + \beta_2 A_2(u_n) \sum_{i=n+1}^{n+k_2} \varphi^*(u_n) + Q_n}{1-\beta_1 A_1(u_n) - \beta_2 A_2(u_n)}. \tag{33}$$

Here k_2 is the integral part of the quantity $\frac{q_2}{q_1/k_1}$ and Q_n is the value of the Integrals (32) over the region

$$u_n + k_2 \frac{q_1}{k_1} < u < u_n + q_2.$$

Thus, the adjoint collision density is calculated in both cases up to a lethargy u_0 for which $A(u_0)$ approaches unity. In order to find the adjoint collision density for the range of lethargy $u_{source} < u < u_0$, we can use the method of synthetic kernels. The exact kernels of the adjoint equations differ from the kernels of the basic equations by a transposition of the variables u and u'. It is clear that the condition for the equality of moments relative to the quantity $|u - u'|$ will lead to a similar difference between the basic and adjoint synthetic kernels.

Keeping this remark in mind, let us write down the equation for the function $\Psi^*(u)$ with the synthetic Greuling-Goertzel kernel:

$$\psi^*(u) = \frac{A(u)}{\xi\varepsilon^2} \int_u^{u_{as}} e^{-\frac{u'-u}{\xi\varepsilon}} \psi^*(u)\,du' + A(u)\left(1 - \frac{1}{\varepsilon}\right)\psi^*(u), \tag{34}$$

where $\frac{1}{\xi\varepsilon^2} e^{-\frac{u'-u}{\xi\varepsilon}} + \left(1 - \frac{1}{\varepsilon}\right)\delta(u-u')$ is the transposed Greuling-Goertzel kernel. This equation has the following solution:

$$\psi^*(u) = \frac{A(u)}{A(u_{as})} \frac{A(u_{as}) + \varepsilon[1 - A(u_{as})]}{A(u) + \varepsilon[1 - A(u)]} \times \times \Psi^*(u_{as})\, e^{-\frac{1}{\xi} \int_u^{u_{as}} \frac{1 - A(u')}{A(u') + \varepsilon[1 - A(u')]} du'} \tag{35}$$

As was shown above, in the case of a mixture this solution is the same as Expression (35) if ξ and ϵ are taken to be averages over the components of the mixture and $A(u) = A_1(u) + A_2(u)$.

Thus, Equations (29), (31), (33), and (35) give the adjoint collision density for the whole of the range of lethargy variation. Knowing it, we are able to calculate the functional ν and to compare it with the functional obtained from the basic equations.

5. Results of Calculation

With the help of the method developed in Sections 3 and 4, the collision density and the resonance escape probability (adjoint collision density) were calculated for the first resonance level of U^{238} ($E_0 = 6.7$ ev) in an infinite medium of pure uranium and of uranium dioxide UO_2.

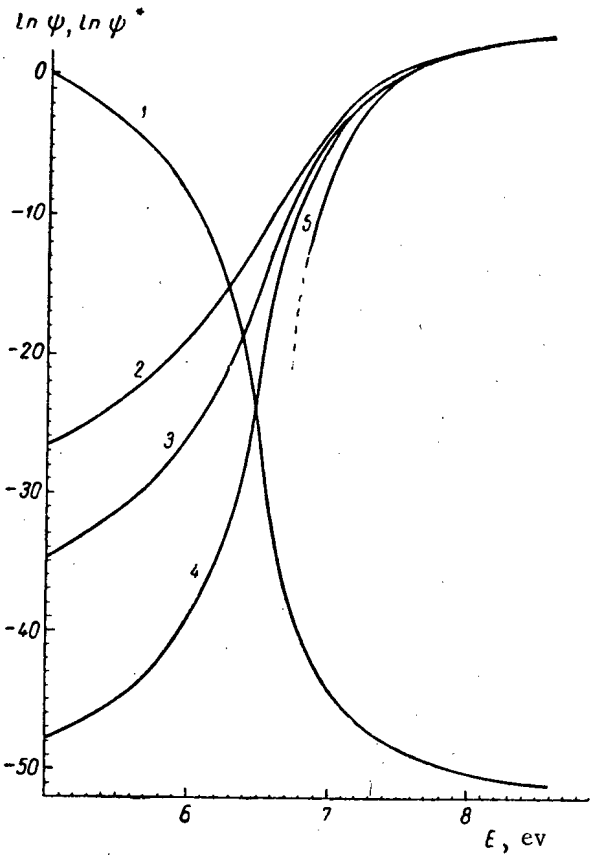

Fig. 1. The collision density for slowing down in U^{238}. 1) Exact solution of the adjoint equation (ψ^*); 2) Wigner approximation; 3) Greuling-Goertzel approximation; 4) exact solution of the basic equation; 5) Fermi approximation.

In Expressions (11) and (12), the constants for this level were taken as follows: $\Gamma = 0.0255$ ev, $\sigma_{sr0} + \sigma_{ar0} = 2.330 \cdot 10^4$ barn, $\sigma_{sr0} = 1.386 \cdot 10^3$ barn, $\sigma_{sp}^{u} = 8.3$ barn, $\sigma_{sp} = 15.9$ barn, and $\sigma_{int} = 212.88$ barn.

The results of the solution of the basic and the adjoint problem are given in Figs. 1, 2, and 3. The collision density and the resonance escape probability calculated from the method of synthetic kernels are also given in these figures.

Using these functions, we can calculate the functional ν which is related to the resonance integral by the Relation (15). The results obtained are given in Table 1.

In the case of slowing down in pure uranium a check was kept on the error by dividing the step in the quadrature formula, as halving the step in the quadrature formula changes $q(u_{as})$ by no more than 2%. In the case of slowing down in the mixture, the check was made from the neutron balance.

The comparison of the results shows that of all the synthetic kernels studied in Section 1, the Greuling-Goertzel kernel is the best when the width of the "danger zone," i.e., the region where $\frac{1 - A(u)}{A(u)} \gg 1$, is considerably greater than the mean logarithmic energy loss. For slowing down in U^{238} the ratio of these quantities was of the order of 10, for slowing down in UO_2 it was somewhat less than 1. In this case, as was to be expected, the Wigner approximation is preferable.

TABLE 1

The Value of the Resonance Integral ($J = -\ln q(u_{as})$) for the first U^{238} Level for Slowing Down in U^{238} and in UO_2

Substance	From the exact solution of the basic equation	In the Fermi approximation	In the Wigner approximation	In the Greuling-Goertzel approximation	From the exact solution of the adjoint equation
U^{238}	52.59	818	31.3	39.2	52.66
UO_2	3.088	20.04	3.140	5.188	3.084

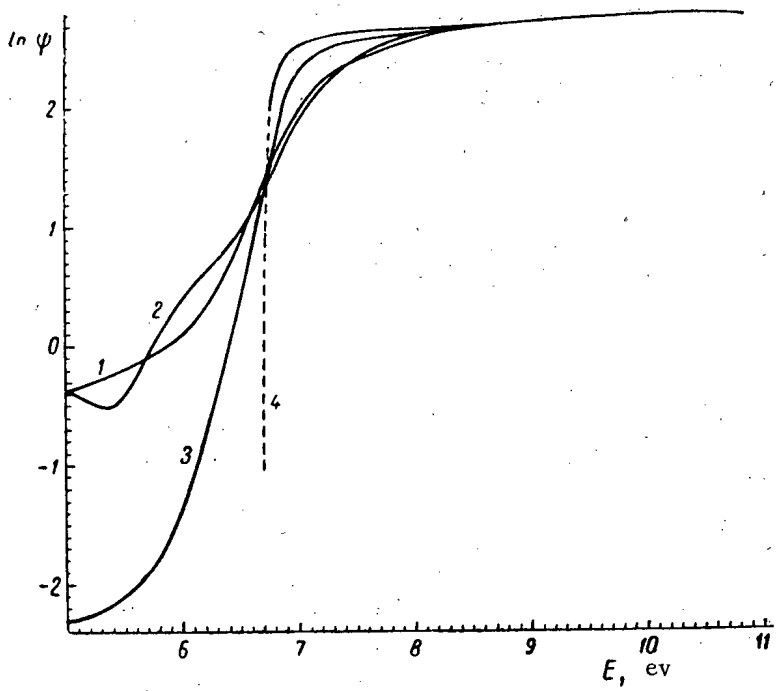

Fig. 2. Collision density for the case of slowing down in UO_2.
1) Wigner approximation; 2) exact solution; 3) Greuling-Goertzel approximation; 4) Fermi approximation.

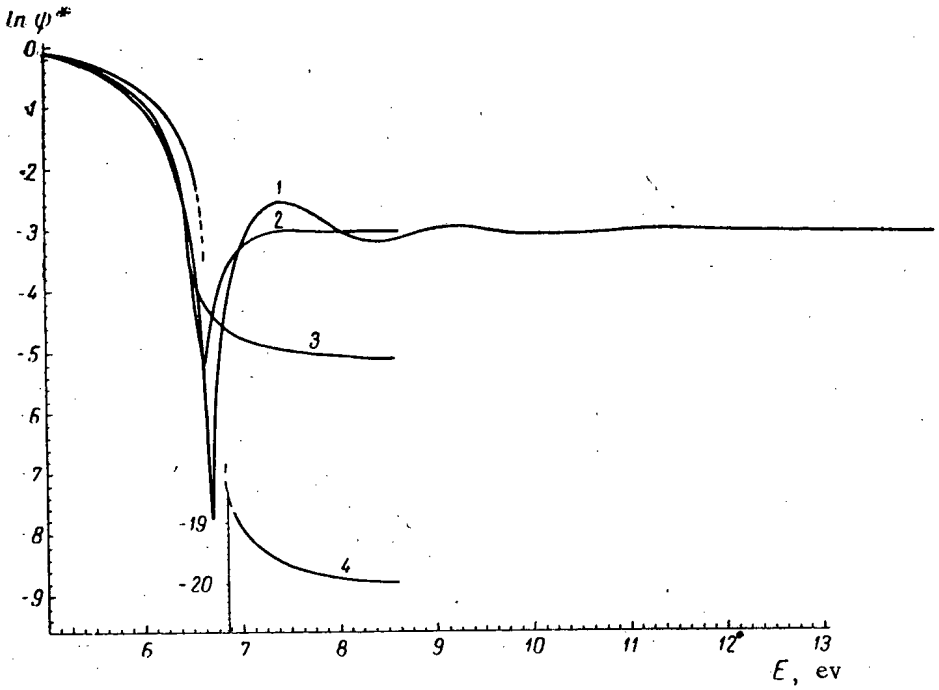

Fig. 3. The function adjoint to the collision density for the case of slowing down in UO_2. 1) Exact solution; 2) Wigner approximation; 3) Greuling-Goertzel approximation; 4) Fermi approximation.

6. The Use of the Perturbation Functional To Take The Doppler Effect Into Account

Let us now proceed to consider the corrections to the resonance integral associated with the distortion of the assumed form of the resonance [see Equations (11) - (13)]. The calculations will be carried out within the framework of perturbation theory.

As is known, in the case of small perturbations the variation of the eigenvalue of the perturbed operator can be approximately written down as

$$\delta\lambda_0 \approx \frac{(f_0^*,\ \hat{\Delta} f_0)}{(f_0^*,\ f_0)}\ . \tag{36}$$

Here $\hat{\Delta}$ is the perturbation operator and f_0, f_0^* are the solutions of the basic and the adjoint equations.

The operator derived in Sections 2 and 3 is a function of the characteristic parameter ν. Using Equation (36), we can construct a functional which describes the variation of the quantity ν and, consequently, of the quantity $q(u_{as})$ which is associated with it. In fact, since $\Psi(u)$ has been determined to within a constant multiplying factor, the unperturbed operator can be written in the following way:

$$L = \begin{pmatrix} g(u, u')\,A(u'), & \nu g(u, 0)\,A(0) \\ G(u_{as}, u')\,A(u'), & 0 \end{pmatrix} \tag{37}$$

Then, the perturbed operator has the form

$$L' = \begin{pmatrix} g'(u, u')\,A'(u'), & (\nu+\delta\nu)\,g'(u, 0)\,A(0) \\ G'(u_{as}, u')\,A'(u'), & 0 \end{pmatrix} \tag{37a}$$

Taking into account the fact that $\delta\lambda = 0$ and using Relations (36) and (15a) for the case of a one-component moderator for which $g(u, u') = g'(u, u')$ and $G(u_{as}, u') = G'(u_{as}, u')$, we obtain for $\delta q(u_{as})$

$$\delta q(u_{as}) = -\Big[\int_0^{u_{as}} \psi^*(u) \int_0^{u_{as}} g(u,u')\Delta(u')\psi(u')du'du + \int_0^{u_{as}} G(u_{as}, u')\,\Delta(u')\,\psi(u')\,du'\Big], \tag{38}$$

where $\Delta(u') = A(u') - A'(u')$. For slowing down in a mixture $\delta q(u_{as})$ has the form

$$\delta q(u_{as}) = -\Big[\int_0^{u_{as}} \psi^*(u) \times \times \int_0^{u_{as}} \sum_i \Delta_i g_i(u, u')\,\psi(u')\,du'\,du + \int_0^{u_{as}} \sum_i G_i(u_{as}, u)\,\Delta_i\psi(u')\,du'\Big], \tag{39}$$

where $\Delta_i(u) = A_i(u) - A_i'(u)$, while $g_i(u, u')$ and $G_i(u, u')$ are given by Equations (1a) and (14a).

Thermal motion of the moderator atoms leads to a change in the energy dependence of both the cross sections of potential and resonance scattering, as well as of the interference between the resonance and potential scattering. To within the limits of experimental error this dependence for the U^{238} levels, as is known, is described by the following expressions:

$$\sigma_{a,D} = \frac{\sigma_{ar0}\xi}{2\sqrt{\pi}} \int_{-\infty}^{\infty} \frac{e^{-\frac{\xi^2}{4}(x-y)^2}}{y^2+1}\, dy,$$

$$\sigma_{s,D} = \frac{\sigma_{sr0}\xi}{2\sqrt{\pi}} \int_{-\infty}^{\infty} \frac{e^{-\frac{\xi^2}{4}(x-y)^2}}{y^2+1}\, dy, \qquad (40)$$

$$\sigma_{int,D} = \frac{\sigma_{int}\xi}{2\sqrt{\pi}} \int_{-\infty}^{\infty} \frac{ye^{-\frac{\xi^2}{4}(x-y)^2}}{y^2+1}\, dy,$$

where $\xi = \frac{\Gamma}{\Delta}$ $\left(\Delta = \sqrt{4EkT\frac{m}{M}}\right)$, and the other symbols are the same as those used in Equations (11) - (13).

Using the expression for the complex probability integral, we can rewrite Expressions (40) as

$$\sigma_{a,D} = \sigma_{ar0}\Psi(\xi, x), \quad \sigma_{srD} = \sigma_{sr0}\Psi(\xi, x), \qquad (40a)$$
$$\sigma_{int,D} = \sigma_{int}\varphi(\xi, x),$$

where

$$\Psi(\xi, x) = \frac{\xi\sqrt{\pi}}{2} U\left(\frac{x\xi}{2}, \frac{\xi}{2}\right),$$

$$\varphi(\xi, x) = \frac{\xi\sqrt{\pi}}{2} V\left(\frac{x\xi}{2}, \frac{\xi}{2}\right),$$

TABLE 2

The Values of the Resonance Integrals Corrected for the Doppler Effect*

Substance	$T=0°$ K ($\xi=\infty$)	$T=419°$ K ($\xi=0,4$)	$T=655°$ K ($\xi=0,32$)
U^{238}	52,59	51,12 (51,04)	50,93 (50,89)
UO_2	3,09	3,28 (3,23)	3,31 (3,26)

* The values of the quantities obtained with the help of the perturbation theory are shown in brackets.

and U and V are the real and imaginary parts of the complex probability integral, respectively.

From Expressions (40), (40a), as well as (11) - (13), we are able to derive a new expression for the resonance integral, taking into account Doppler broadening.

The results of the calculation of the resonance integrals, including a correction for the Doppler effect by the exact method described in Section 3 and with the help of the Functionals (38) and (39), are given in Table 2.

A comparison of the results shows that, in spite of the appreciable change of the quantity $q(u_{as})$ due to the Doppler effect, the use of the Functionals (38) and (39) gives satisfactory results.

In conclusion we express our thanks to V. V. Orlov who took part in the discussion of some of the physical aspects of the present work.

LITERATURE CITED

[1] G. Placzek, Phys. Rev. 69, 9 and 10, 423 (1946).

[2] Materials of the U. S. Atomic Energy Commission, Nuclear Reactors, Vol. 1, Part I, Chapter 3 [Russian Translation], (IL, 1956).

[3] N. I. Akhiezer and I. M. Glazman, The Theory of Linear Operators in Hilbert Space [In Russian] (Goztekhizdat, Moscow-Leningrad, 1950).

[4] Ia. B. Zel'dovich and Iu. B. Khariton, J. Exptl.-Theoret. Phys. (USSR) 10, 29 (1940); A. D. Galanin, Supplement No. 2-3 to J. Atomic Energy (USSR) (1957).*

[5] V. N. Fadeeva and N. M. Terent'ev, Tables of the Probability Integral of a Complex Argument [In Russian], (Goztekhizdat, Moscow-Leningrad, 1954).

Received December 20, 1957

* See C. B. Translation.

MUTUAL SCREENING OF BLOCKS OF RESONANCE NEUTRON ABSORBER IN A "TIGHT" LATTICE

V. V. Orlov

This paper deals with the evaluation of the effect of mutual screening of blocks and layers of resonance absorber which arises when the thickness of the moderator separating the absorber blocks is comparable with or less than the mean free path of neutrons in the moderator. In the calculations it is assumed that the blocks are small and that the absorption cross section is described by the Breit-Wigner formula.

From the calculations carried out for a system of parallel plates it is possible to evaluate the accuracy of the results obtained in [1] and also to obtain an equation for a system which is nearly homogeneous. It is shown that the approximate substitution of an equivalent circular cell for the true cell in a lattice consisting of cylindrical blocks, which is usually justified, in the case of problems of the type considered leads to appreciable errors. In addition, a resonance-absorption formula is obtained in the case of an annular geometry of the absorber.

The theory of the resonance absorption of neutrons by a single small block of absorber has been developed in [2] in which it is assumed that the block is surrounded by an infinite moderator. Often, however, it is necessary to deal with a "tight" lattice of absorbing blocks, situated at distances from each other of the order of the scattering length in the moderator. In this case the resonance-neutron flux at the surface of each block is decreased because of the screening action of neighboring blocks, which leads to a decrease of neutron absorption. The mutual screening effect of blocks has been investigated in [1]. However, as will be shown below, the approximate method used in that paper leads to an overestimate of the screening effect.

We will take the case of thin absorber blocks, so that $d \ll \lambda_s$ (d is the block diameter, λ_s is the mean free path for scattering of neutrons in the block) and consequently base our calculations on the theory developed in [2].

If $\Phi(E)$ neutrons/cm^2 · sec fall normally onto the surface S of a resonance-absorber layer of thickness l, then the number of neutrons absorbed per second is

$$N_a = S \int \Phi(E) \frac{\sigma_a(E)}{\sigma(E)} [1 - e^{-l\rho\sigma(E)}]\, dE, \qquad (1)$$

where ρ is the concentration of absorber atoms in the block, and

$$\sigma(E) = \sigma_{sp} + \sigma_a(E) + \sigma_{sr}(E)$$

[$\sigma_a(E)$ is the resonance-absorption cross section, σ_{sp} is the potential-scattering cross section per nucleus of the absorber, $\sigma_{sr}(E)$ is the resonance-scattering cross section].

For thin blocks $l\rho\sigma_{sp} \ll 1$ and therefore the potential scattering of neutrons in the block can be neglected. In addition, we will assume that resonance scattering "removes" neutrons from the resonance energy interval. Assuming that the shape of the resonance is described by the Breit-Wigner formula

$$\sigma_a(E) \cong \frac{\Gamma_\gamma}{\Gamma_n}\sigma_{sa}(E) = \frac{\sigma_a^0}{1+\frac{4}{\Gamma^2}(E-E_0)^2}, \tag{2}$$

we obtain the number of neutrons absorbed by one resonance as

$$N_a \approx S\Phi(E_0)\frac{\Gamma_\gamma}{2}\int_{-\infty}^{\infty} dx\left[1-e^{-\frac{l\rho\sigma^0}{1+x^2}}\right], \tag{3}$$

where $x = \frac{E-E_0}{\frac{\Gamma}{2}}$, $\sigma^0 = \sigma_a^0 + \sigma_{sr}^0$, and the function $\Phi(E)$ within the resonance region is assumed to be independent of the energy.

Through the substitution $x = \tan\frac{\alpha}{2}$, the Expression (3) can be easily put into the form

$$N_a = S\Phi(E_0)\Gamma_\gamma \pi t e^{-\frac{t}{2}}\left[I_0\left(\frac{t}{2}\right)+I_1\left(\frac{t}{2}\right)\right], \tag{4}$$

where $t = l\rho\sigma^0$, and $I_0(x)$ and $I_1(x)$ are the Bessel functions of an imaginary argument.

If $t \ll 1$ (weak resonance), then it follows from (4) that

$$N_a^0 \approx S\Phi_0\frac{\Gamma_\gamma}{2}\pi l\rho\sigma^0 = E_0\Phi_0 V_{bl}\ \rho J_R, \tag{5}$$

where $V_{bl} = S\,l$ is the volume of the block, and $J_R = \frac{\pi}{2}\frac{\sigma^0\Gamma_\gamma}{E_0}$ is the resonance integral for the absorption.

For $t \gg 1$ (strong resonance), using the asymptotic representation of the Bessel functions, we get

$$N_a \approx S\Phi_0\frac{\Gamma_\gamma}{2}\frac{2}{\sqrt{\pi}}\sqrt{l\rho\sigma^0}. \tag{6}$$

We see that in this case N_a increases only as $\sqrt{l}$, which is the result of the screening of the inner layers of the absorber by the outer. As a characteristic of this self-screening we can introduce the self-screening coefficient

$$k_c = \frac{N_a(l)}{N_a^0(l)} = \frac{2}{\sqrt{\pi}}\frac{1}{\sqrt{l\rho\sigma^0}}. \tag{7}$$

If the neutron beam consecutively traverses resonance-absorber layers of thickness L and l, then

$$N_a(L) \sim \sqrt{L},\ N_a(L+l) \sim \sqrt{L+l},$$

from which

$$N_a(l) \sim \sqrt{l}\left[\sqrt{1+\frac{L}{l}} - \sqrt{\frac{L}{l}}\right]. \tag{8}$$

The mutual screening coefficient $k = \sqrt{1+\frac{L}{l}} - \sqrt{\frac{L}{l}} \leqslant 1$ therefore describes the screening of a layer of thickness l by a layer of thickness L associated with the "disruption" of the resonance-neutron spectrum after the passage through the layer of thickness L. In particular, for $L = l$, $k = \sqrt{2}-1$, for $L = 2l$ $k = \sqrt{3}-\sqrt{2}$, etc.

Let us now consider the case of an absorbing block surrounded by moderator out of which neutrons are falling isotropically on the surface of the block. If the neutron flux is Φ_0 inside the moderator, then the flux incident on

the block is equal to $\frac{\Phi_0}{4}$. In order to obtain the number of absorbed neutrons it is necessary to average Expressions (5) and (6) over all the chords l inside the block:

$$N_a^0 = S\frac{\Phi_0}{4} E_0 \langle l \rangle \rho J_R, \tag{9}$$

$$N_a = S\frac{\Phi_0}{4} E_0 \langle \sqrt{l} \rangle \frac{2}{\sqrt{\pi}} \frac{\sqrt{\rho\sigma^0\Gamma_\gamma^2}}{E_0}. \tag{10}$$

Then

$$k_c = \frac{2}{\sqrt{\pi}} \frac{\langle \sqrt{l} \rangle}{\sqrt{\rho\sigma^0 \langle l \rangle}}. \tag{11}$$

In the case of a tight lattice it is similarly necessary to average Expressions (5) and (6) over all angles.

An important property of the mutual-screening coefficient k in our case is that it is independent of the resonance parameters in the case of strong resonances and depends only on the geometry of the lattice. The present paper is devoted to the calculation of this coefficient for various geometrical conditions.

Knowing the coefficient of mutual screening, we can calculate the resonance escape probability (for the blocked part of the absorption) from the equation

$$-\ln \varphi = \frac{AS \langle \sqrt{l} \rangle}{4\xi\Sigma_s V_m} k, \tag{12}$$

where S is surface area of the block, V_m is the volume of the moderator, ξ is the mean logarithmic energy loss in the moderator, Σ_s is the macroscopic neutron-scattering cross section, and A a constant which characterizes the absorber. For a uranium block, A can be easily found from a comparison of Equation (12) with the equation for a single cylindrical block [3] by setting k = 1.

Resonance Absorption in a Lamellar Lattice

Let us consider a system of parallel infinite resonance-absorber plates of thickness d separated by layers of moderator of thickness D and a macroscopic scattering cross section Σ_S (Fig. 1). We will assume that the flux of neutrons with energies greater than the resonance energy is constant within the lattice. Then, as the result of slowing down, $\Phi_0 \Sigma_S \, dE \, dV$ neutrons with energy in the interval dE will be produced per second in an volume element dV of the moderator; the velocities of these neutrons will be distributed isotropically. Let us consider the neutron flux falling on a surface element of one of these blocks, at an angle θ to the normal.

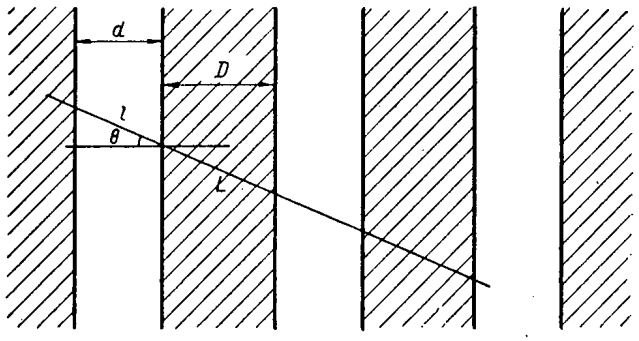

Fig. 1. Lattice consisting of parallel plates.

This flux is compounded from the neutron flux Φ_1 due to neutrons slowed down into the interval dE in the layer of the moderator which lies close to the surface under consideration, the flux Φ_2 which falls on the surface element dS from the next layer, etc.

It is obvious that

$$\Phi_1 \approx 1 - e^{-\Sigma_s L(\theta)},$$

$$\Phi_2 \approx e^{-\Sigma_s L(\theta)} - e^{-2\Sigma_s L(\theta)},$$

$$\Phi_3 \approx e^{-2\Sigma_s L(\theta)} - e^{-3\Sigma_s L(\theta)} \quad \text{etc.},$$

where $L(\theta)$ is the neutron path length in the moderator.

However, the flux Φ_2 before it falls on the surface element dS has already traversed the layer l of the neighboring block and, therefore, is absorbed $(\sqrt{2}-1)$ times less effectively than Φ_1; similarly, flux Φ_3 is absorbed $(\sqrt{3}-\sqrt{2})$ times less effectively than Φ_1, etc. Taking into account that the absorption of neutrons from the flux Φ_1 is $N_a^{(1)} \sim \sqrt{l(\theta)}$, and also that the flux of neutrons falling on dS is proportional to $\cos\theta$ and $d\Omega \sim \sin\theta\, d\theta$, we find that the number of neutrons absorbed from this beam is

$$N_a(\theta)\,d\theta \approx d\theta \sin\theta\cos\theta \sqrt{l(\theta)}\{1-e^{-\Sigma_s L(\theta)}+ \\ +(\sqrt{2}-1)[e^{-\Sigma_s L(\theta)}-e^{-2\Sigma_s L(\theta)}]+\ldots\}. \tag{13}$$

Let us introduce the function

$$L(t)=(1-e^{-t})\sum_{n=0}^{\infty}\left(\sqrt{1+n}-\sqrt{n}\right)e^{-nt}= \\ =(1-e^{-t})(e^{t}-1)\sum_{n=1}^{\infty}\sqrt{n}e^{-nt}. \tag{14}$$

This series, which converges slowly for small t, can be replaced by another converging more rapidly [1]:

$$L(t)=(1-e^{-t})(e^{t}-1)\frac{\sqrt{\pi}}{2}\left\{\frac{1}{t^{3/2}}+\right. \\ +\frac{2}{(2\pi)^{3/2}}\sum_{n=0}^{\infty}(-1)^n\left(\frac{t}{2\pi}\right)^n\prod_{k=1}^{n}\left(1+\frac{1}{2k}\right)\times \\ \left.\times\zeta\left(n+\frac{3}{2}\right)\cos\frac{\pi}{2}\left(n+\frac{3}{2}\right)\right\}= \\ =(1-e^{-t})(e^{t}-1)\left\{\frac{\sqrt{\pi}}{2t^{3/2}}+\right. \\ \left.+\sum_{n=0}^{\infty}\frac{(-1)^n t^n}{n!}\zeta\left(1-n-\frac{3}{2}\right)\right\}^{*} \tag{15}$$

where $\zeta(x)$ is the Rieman function.

For $t \ll 1$, $L(t)\approx\frac{\sqrt{\pi t}}{2}-0{,}208\,t^2$, for $t\to\infty$, $L(t)\approx 1-\sqrt{2}(\sqrt{2}-1)e^{-t}$.

With the help of this function we can write

$$N_a=\int N_a(\theta)\,d\theta\approx \\ \approx\int\sqrt{l(\theta)}\,L[\Sigma_s L(\theta)]\sin\theta\cos\theta\,d\theta. \tag{16}$$

Putting in this expression $l(\theta)=\frac{d}{\cos\theta}$, $L(\theta)=\frac{D}{\cos\theta}$, and taking into account that $L(\infty)=1$, we find the coefficient of mutual screening in the form

* This formula was obtained by T. Kh. Sedel'nikov.

TABLE 1
The Screening Coefficient for a Lamellar Lattice

α	0	0,05	0,1	0,2	0,3	0,4	0,5	0,6	0,7	0,8	0,9	1,0	1,3	1,5	2,0	2,5	3,0	4,0	5,0	8
$k(\alpha)$	0	0,290	0,403	0,546	0,639	0,701	0,742	0,783	0,815	0,843	0,865	0,884	0,925	0,943	0,971	0,985	0,992	0,997	0,999	1
$k_1(\alpha)$	0	0,272	0,373	0,496	0,575	0,631	0,674	0,707	0,734	0,757	0,777	0,791	0,829	0,846	0,878	0,899	0,914	0,934	0,946	1

$$k(\alpha)=\frac{N_a(\alpha)}{N_a(\infty)}=\frac{\int_0^{1/\alpha}\sqrt{\xi}\,L\left(\frac{1}{\xi}\right)d\xi}{\int_0^{1/\alpha}\sqrt{\xi}\,d\xi}=$$

$$=\frac{3\alpha^{3/2}}{2}\int_0^{1/\alpha}\sqrt{\xi}\,L\left(\frac{1}{\xi}\right)d\xi, \qquad (17)$$

where $\alpha = \Sigma_s D$.

The values of the function $k(\alpha)$ are given in Table 1. For a flat layer $\langle l\rangle = 2d$, and

$$\langle\sqrt{l}\rangle=\frac{2\sqrt{2}}{3}\sqrt{2d}=\ 0{,}943\sqrt{\langle l\rangle}.$$

Therefore, the total screening coefficient, taking into account the self-screening of the layer as well as the screening of it by neighboring layers, is $K = k_c \times (d\Sigma^0)\, k(\alpha)$, where according to Equation (11) $k_c = \frac{2\cdot 0.943}{\sqrt{2\pi d\,\Sigma^0}}$. It is interesting to compare the value of K for a heterogeneous lamellar lattice with the screening coefficient for a homogeneous mixture of the same quantities of absorber and moderator. The macroscopic cross sections for a homogeneous mixture are:

$$\Sigma_{s\,\mathrm{hom}}=\Sigma_s\frac{D}{D+d},$$
$$\Sigma^0_{\mathrm{hom}}=\Sigma^0\frac{d}{D+d},$$

where $\Sigma^0=\rho\sigma_0$.

The screening coefficient for a homogeneous mixture is

$$k_{\mathrm{hom}}=\sqrt{\frac{\Sigma_{s\mathrm{hom}}}{\Sigma^0_{\mathrm{hom}}}}=\sqrt{\frac{\Sigma_s}{\Sigma^0}}\sqrt{\frac{D}{d}},$$

from which

$$\frac{K}{k_{\mathrm{hom}}}=\frac{4}{3\sqrt{\pi}}\frac{k(\alpha)}{\sqrt{\alpha}}.$$

Expanding $k(\alpha)$ for small values of α into a power series in α, we find that

$$\frac{K}{k_{\mathrm{hom}}}\approx 1-0{,}705\alpha+0{,}47\alpha^{3/2}. \qquad (18)$$

From this expression we can obtain the error incurred by the homogenization of a tight lattice.

Let us compare the results obtained with the results given in [1]. The screening coefficient found in that paper is

$$k_1(\alpha)=2\alpha F\left(\frac{1}{1+2\alpha}\right),$$

where

$$F(q) = (1-q)\sum_{n=1}^{\infty} \sqrt{n}\, q^n.$$

From a comparison of $k_1(\alpha)$ with the exact values of $k(\alpha)$ (see Table 1) it is seen that the method of averaging taken by the author from [2] is satisfactory only for sufficiently tight lattices, i.e., when there are many layers of absorber in one neutron mean free path. From the table it is seen that for not very tight lattices ($\alpha > 1$) this method overestimates the mutual-screening effect $(1 - k)$ by a factor of 2 or more.

Resonance Absorption in a Circular Cell

The screening coefficient for the slowing down of neutrons in a circular cell (Fig. 2) can be obtained in the same way. Let us consider two cases: a) region I is occupied by the absorber, region II by the moderator (this cell is equivalent to a lattice of cylindrical blocks); b) the absorber is situated in region II, the moderator in region I (such a cell is equivalent to a lattice of absorbing pipes with the moderator placed inside).

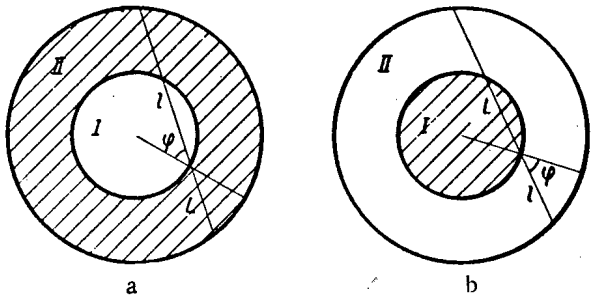

Fig. 2. Circular cell. a) Cell with a cylindrical block; b) cell with an annular block.

Since in a circular cylinder the ray reflected from the boundary does not geometrically differ in any way from the incident ray, we can assume that the resonance neutron, born in the moderator, always moves along the same line in the cell, being reflected from its boundary.

Further calculations are analogous to those for the case of a lamellar lattice.

Case a):

$$l = d\frac{\cos\varphi}{\sin\theta}, \quad L = \frac{\sqrt{D^2 - d^2\sin^2\theta} - d\cos\theta}{2\sin\theta},$$

where φ is the angle between the direction of motion of the neutron and the normal to the surface of the block, θ is the angle between the direction of motion of the neutron and the generatrix of the cylinder, d is the diameter of the block, and D is the diameter of the cell.

Introducing the function

$$F(x) = \frac{\int_0^{\pi/2} \sin^{3/2}\theta\, L\left(\frac{x}{\sin\theta}\right) d\theta}{\int_0^{\pi/2} \sin^{3/2}\theta\, d\theta}$$

and the quantities $\alpha = \Sigma_s D$, $\beta = \frac{d}{D}$, we find that the screening coefficient is

$$k(\alpha, \beta) = \frac{\int_0^{\pi/2} \cos^{3/2}\varphi F\left[\alpha\left(\sqrt{1-\beta^2\sin^2\varphi} - \beta\cos\varphi\right)\right] d\varphi}{\int_0^{\pi/2} \cos^{3/2}\varphi\, d\varphi}; \qquad (19)$$

the values of $k(\alpha, \beta)$ are given in Table 2.

For a cylinder $\langle\sqrt{l}\rangle = \frac{4}{\pi}\sqrt{d}\int_0^{\pi/2} \sin^{3/2}\theta\, d\theta = 0{,}974\sqrt{d}$, and from Equation (12) it is not difficult to find φ.

Case b):

$$l = \frac{\sqrt{D^2 - d^2 \sin^2\varphi} - d\cos\varphi}{\sin\theta},$$

$$L = d\frac{\cos\varphi}{\sin\theta},$$

$$k(\alpha, \beta) = \frac{\int_0^{\pi/2} \sqrt{\sqrt{1-\beta^2\sin^2\varphi} - \beta\cos\varphi}\, F(\alpha\cos\varphi)\cos\varphi\, d\varphi}{\int_0^{\pi/2} \sqrt{\sqrt{1-\beta^2\sin^2\varphi} - \beta\cos\varphi}\cos\varphi\, d\varphi}. \quad (20)$$

For the cell considered

$$\langle\sqrt{l}\rangle = \sqrt{2(D-d)}\, f(\beta),$$

where

$$f(\beta) = \frac{2\sqrt{2}}{\pi}\frac{\int_0^{\pi/2}\cos^{3/2}\varphi\, d\varphi}{\sqrt{1-\beta}} \times \times \int_0^{\pi/2} \sqrt{\sqrt{1-\beta^2\sin^2\varphi} - \beta\cos\varphi}\cos\varphi\, d\varphi. \quad (21)$$

TABLE 2

The Screening Coefficient for a Circular Well with a Cylindrical Absorber

β \ α	0	0,1	0,2	0,3	0,4	0,6	0,8	1,0	1,2	1,5	2,0	2,5	3,0	4,0	∞
0	0	0,317	0,447	0,534	0,596	0,702	0,767	0,821	0,861	0,903	0,944	0,970	0,982	0,987	1
0,1	0	0,302	0,436	0,515	0,577	0,681	0,748	0,800	0,840	0,889	0,935	0,961	0,977	0,986	1
0,2	0	0,285	0,411	0,494	0,556	0,655	0,727	0,776	0,819	0,869	0,920	0,949	0,970	0,983	1
0,4	0	0,243	0,360	0,441	0,502	0,593	0,664	0,720	0,761	0,811	0,875	0,915	0,941	0,973	1
0,6	0	0,188	0,298	0,368	0,426	0,512	0,502	0,628	0,675	0,728	0,795	0,845	0,883	0,930	1
0,8	0	0,102	0,200	0,263	0,305	0,378	0,436	0,483	0,522	0,570	0,641	0,696	0,740	0,804	1
0,9	0	0,049	0,114	0,164	0,205	0,265	0,311	0,350	0,385	0,430	0,490	0,537	0,577	0,646	1
1,0	0	0	0	0	0	0	0	0	0	0	0	0	0	0	

TABLE 3

Values of the Function $f(\beta)$

β	0	0,1	0,2	0,3	0,4	0,6	0,8	0,9	1,0
$f(\beta)$	0,786	0,795	0,803	0,810	0,814	0,843	0,874	0,896	0,943

The values of $f(\beta)$ and $k(\alpha, \beta)$ are given in Tables 3 and 4.

The results obtained in this section show that the substitution of an actual (square, hexagonal, etc.) cell by an equivalent (according to area) circular cell, which is a good approximation in other neutron-diffusion problems, gives a large error in our case, at least for geometrically thin ($\beta \ll 1$) lattices. In fact, it can be

seen from Table 2 that in the limiting case when $\beta = 0$ when we should expect to find $k = 1$, we get $k(\alpha) < 1$. This is the result of the extreme symmetry which is introduced through the substitution of an actual cell by a circular one, since in a circular cell a neutron, once it has penetrated into a block will again move into the block after a reflection from the boundary.

TABLE 4

The Screening Coefficient for a Circular Cell with an Annular Absorber

β \ α	0	0,1	0,2	0,3	0,4	0,6	0,8	1,0	1,5	2,0	2,5	3,0	4,0	∞
0	0	0,280	0,392	0,469	0,531	0,629	0,699	0,784	0,835	0,889	0,922	0,943	0,964	1
0,6	0	0,275	0,388	0,463	0,526	0,622	0,692	0,742	0,820	0,883	0,916	0,938	0,961	1
1,0	0	0,261	0,375	0,442	0,500	0,595	0,663	0,735	0,800	0,856	0,893	0,917	0,945	1

Since in the case of not-very-tight lattices the results of [1] are inapplicable, while the calculation of the mutual screening of blocks in a real lattice (square, hexagonal, etc.) is a very unwieldy computational problem, the following method for calculation may be proposed. Assuming, as in [1], that the screening is determined by the hydraulic diameter $D_h = 4V_m/S$ (V_m is the volume of moderator in the cell) and is independent of the lattice geometry, we can use the function $k(\alpha)$ calculated for the lamellar lattice (Table 1), where $\alpha = \frac{D_h \Sigma_s}{2}$ (since $D_h = 2D$ for a lamellar lattice), as the screening coefficient.

Resonance Absorption in an Absorber with Annular Geometry

In conclusion we will consider the case of an absorber in the form of a cylindrical layer with moderator situated inside and outside of it (Fig. 3). The inner surface of the layer is partially screened.

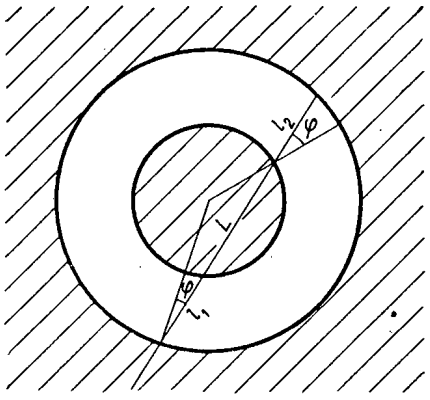

Fig. 3. Absorber with annular geometry.

The fraction of neutrons absorbed from the number of neutrons in the outer moderator which fall on the outer surface of area S_1 is equal to

$$N_a^{(1)} \sim S_1 \langle \sqrt{l_1} \rangle, \tag{22}$$

where l_1 is the path length of the neutrons in the absorber before escape into the moderator.

The neutron flux on the inner surface of the cylindrical layer is compounded from the neutron flux from the moderator inside the tube and the neutron flux from the outer moderator.

This second component has already traversed a distance l_2 in the absorber and is therefore absorbed $\sqrt{2} - 1$ times less effectively. Denoting by $L(\varphi, \theta)$ the neutron path length in the moderator and by $l_2(\varphi, \theta)$ the path length in the absorber, we get

$$N_a^{(2)} \approx S_2 \left\{ \int \sqrt{l_2(\varphi, \theta)} \left(1 - e^{-\Sigma_s L(\varphi, \theta)}\right) \times \right.$$
$$\times \sin^2\theta \cos\varphi \, d\theta \, d\varphi + \left(\sqrt{2} - 1\right) \times$$
$$\left. \times \int \sqrt{l_2(\varphi, \theta)} \, e^{-\Sigma_s L(\varphi, \theta)} \sin^2\theta \cos\varphi \, d\theta \, d\varphi \right\}, \tag{23}$$

where Σ_s is the macroscopic scattering cross section for the inner moderator.

Taking into account that

$$l_1(\varphi, \theta) = \begin{cases} \dfrac{\sqrt{d^2 - D^2 \sin^2\varphi} + d\cos\varphi}{2\sin\theta} & \text{for} \quad \varphi < \arcsin\beta, \\ D\dfrac{\cos\varphi}{\sin\theta} & \text{for} \quad \arcsin\beta < \varphi < \dfrac{\pi}{2}, \end{cases}$$

$$l_2(\varphi, \theta) = \frac{\sqrt{D^2 - d^2\sin^2\varphi} - d\cos\varphi}{2\sin\theta}, \tag{24}$$

we find that

$$\langle\sqrt{l_1}\rangle = \sqrt{D-d}\, f_1(\beta), \tag{25}$$

$$\langle\sqrt{l_2}\rangle = \sqrt{D-d}\, f_2(\beta), \tag{26}$$

where d and D are the inner and outer diameters of the ring, $\beta = \frac{d}{D}$,

$$f_1(\beta) = \frac{2\sqrt{2}}{\pi}\frac{\int_0^{\pi/2}\cos^{3/2}\varphi\, d\varphi}{\sqrt{1-\beta}}\left[\sqrt{2}\int_{\arcsin\beta}^{\pi/2}\cos^{3/2}\varphi\, d\varphi + \right.$$
$$\left. + \beta\int_0^{\pi/2}\sqrt{\sqrt{1-\beta^2\sin^2\varphi} - \beta\cos\varphi}\cos\varphi\, d\varphi\right], \tag{27}$$

and $f_2(\beta) = f(\beta)$ [see Equation (21) and Table 3]. The function $f_1(\beta)$ is given in Table 5.

The coefficient of the screening of the inner surface of the tube is found from Equation (23):

$$k(\alpha, \beta) = \frac{N_a^{(2)}(\alpha)}{N_a^{(2)}(\alpha=\infty)} = 1 - \sqrt{2}\left(\sqrt{2}-1\right)\frac{\int_0^{\pi/2}\sqrt{\sqrt{1-\beta^2\sin^2\varphi} - \beta\cos\varphi}\cos\varphi\, d\varphi \int_0^{\pi/2}\sin^{3/2}\theta e^{-\alpha\frac{\cos\varphi}{\sin\theta}} d\theta}{\int_0^{\pi/2}\sqrt{\sqrt{1-\beta^2\sin^2\varphi} - \beta\cos\varphi}\cos\varphi\, d\varphi \int_0^{\pi/2}\sin^{3/2}\theta\, d\theta}. \tag{28}$$

TABLE 5

Values of the Function $f_1(\beta)$

β	0	0,2	0,4	0,6	0,8	1,0
$f_1(\beta)$	0,974	1,002	1,028	1,027	1,013	0,943

The values of $k(\alpha,\beta)$ are given in Table 6.

Taking into account that $\frac{S_1}{V_m} = \frac{\pi D}{S_m}$ and $\frac{S_2}{V_m} = \frac{\pi d}{S_m}$, we find in accordance with Equation (12) (S_m is the surface area of the moderator in the cell) that

TABLE 6

The Screening Coefficient for an Annular Block

β \ α	0	0,1	0,2	0,4	0,6	0,8	1,0	1,5	2,0	3,0	4,0	∞
0	0,414	0,474	0,523	0,608	0,673	0,728	0,776	0,847	0,896	0,947	0,970	1
0,6	0,414	0,472	0,521	0,604	0,668	0,722	0,769	0,842	0,891	0,942	0,968	1
1,0	0,414	0,468	0,513	0,591	0,651	0,703	0,748	0,818	0,868	0,923	0,951	1

$$-\ln\varphi=\frac{\pi A}{4\xi\Sigma_s S_3}\left[D\sqrt{D-d}\,f_1\left(\frac{d}{D}\right)+d\sqrt{D-d}\,f\left(\frac{d}{D}\right)k\left(d\Sigma_s,\frac{d}{D}\right)\right]. \qquad (29)$$

In conclusion the author thanks G. I. Marchuk and T. Kh. Sedel'nikov for useful discussions and comments.

LITERATURE CITED

[1] Iu. V. Petrov, J. Atomic Energy (USSR) 3, 357 (1957).*

[2] I. I. Gurevich and I. Ia. Pomeranchuk, Reactor Construction and Reactor Theory (Reports of the Soviet Delegation at the International Conferences on the Peaceful Uses of Atomic Energy) [In Russian] (Izd. AN SSSR, Moscow, 1955), p. 220.

[3] M. B. Egiazarov, V. S. Dikarev, and V. G. Madeev, AN SSSR Meeting on the Peaceful Uses of Atomic Energy (Phys.-Math. Sciences Section) [In Russian] (Izd. AN SSSR, 1955), p. 53.

Received November 4, 1957

* Original Russian pagination. See C. B. Translation.

THE ENERGY DISTRIBUTION OF NEUTRONS FROM A PULSED SOURCE IN A MODERATOR WITH A CONSTANT MEAN FREE PATH

M. V. Kazarnovskii

At the present stage in the development of the experimental techniques it is possible to investigate the nonstationary processes occurring in the slowing down and diffusion of neutrons, and therefore a theoretical analysis of these effects is of interest. In the present work an expression is found for the energy distribution of neutrons from a pulsed source in a heavy (mass number M ≫ 1) moderator with a constant mean free path l for energies small by comparison with the initial energy

$$\text{const} \exp\left\{\frac{(1+M)}{2} f_{-1}(z) + f_0(z) + \frac{2}{M+1} f_1(z) + \dots\right\},$$

where $z = \frac{M+1}{vt} l$ (v is the neutron velocity, t is the slowing-down time). Integral representations, analytical expressions near the maximum, asymptotic expansions, and detailed numerical tables are presented for the functions $f_{-1}(z)$, $f_0(z)$, and $f_1(z)$. Numerical evaluations show that these functions are sufficient for a description of the neutron spectrum even in such a light moderator as deuterium. The case of a moderator consisting of a mixture of different kinds of nuclei is investigated. For solving this problem a method is developed for solving integral and integro-differential equations whose kernel K(x, y) is different from zero only for very small values of the quantity $\frac{|x-y|}{|x+y|}$.

INTRODUCTION

The theory of the elastic slowing down of neutrons from a constant-intensity source was investigated in detail during 1945-1950. Considerably less attention has been paid to the investigation of nonstationary elastic slowing down of neutrons (for example, the time dependence of the energy spectrum of neutrons from a pulsed source). This is apparently partially explained by the fact that up to the present the experimental investigation of the nonstationary elastic slowing down of neutrons has been limited by the absence of pulse analyzers with a sufficiently high time-resolving power and by the absence of pulsed neutron sources.

The nonstationary energy distribution of neutrons in hydrogen was obtained by Ornstein and Uhlenbeck [1]. The case of a heavy moderator (mass number M ≫ 1) has been investigated by several authors [2-9]. Olsson [2] derived the distribution function for the case when the mean free path l is proportional to the neutron velocity v. For the considerably more important case of a constant mean free path, Olsson [2] obtains an expansion of the distribution function as a power series in the slowing-down time t. Such an expansion is useful only for the investigation of the initial period of the slowing down. Similarly, in [3] expressions were found for the distribution function in each of the energy intervals $\left(E_0, E_0\left(\frac{M-1}{M+1}\right)^2\right)$ $\left(E_0\left(\frac{M-1}{M+1}\right)^2, E_0\left(\frac{M-1}{M+1}\right)^4\right)$, etc. ($E_0$ is the initial energy of the neutrons). However, these expressions have a very complicated form, even for the first

energy intervals, and cannot be used for the analysis of the neutron-energy distribution for values of the energy that are appreciably different from the initial energy.

The range of energies that are small by comparison with the initial energy (but sufficiently high so that the chemical binding and the thermal motion of atoms can be neglected) has been investigated in [4-9]. Placzek [4] showed that in this case the neutron velocity and the slowing-down time appear in the expression for the distribution function only in the form of a dimensionless combination $x = vt/l$ and obtained the positive moments $\langle x^n \rangle$ of the distribution function. Marshak [5] proposed an approximate function

$$F_0(x) = \text{const} \exp\left[-\left(\frac{b}{x} + x\right)\right] x^{\frac{2}{1-r^2}}, \tag{1}$$

where

$$r = \frac{M-1}{M+1}. \tag{2}$$

High ($n \gg M$) positive moments of this function tend asymptotically to $\langle x^n \rangle$. By choosing the arbitrary constant b so that the maximum of $F_0(x)$ be at the point $x = \langle x \rangle$, Marshak obtained the zero approximation to the distribution function. As a first approximation he proposed the function

$$F_1(x) = \frac{1}{a} x^{1/a} \int_x^\infty dx' (x')^{-1-1/a} F_0(x'), \tag{3}$$

where a is found from the condition that the approximate relation

$$\int_0^\infty dx x^n F_0(x) \approx [1 + a(n+1)] \langle x^n \rangle \tag{4}$$

be satisfied as well as possible.

The function $F_1(x)$ obtained in this way has moments which for M = 9 and M = 15 differ from the exact ones by not more than 5-6%. For M = 2, the agreement is considerably worse and the deviation is as large as 20-25%.*

Dardel [6] has slightly modified the method of selecting the parameters of the function $F_0(x)$ which has appreciably improved the results for M = 2.

It must be pointed out, however, that for very heavy moderators ($M \gtrsim 100$) Marshak's method leads to very unwieldy calculations. Further, in this case the comparison of the exact and approximate moments cannot serve as a reliable criterion for the selection of the approximate function since the neutron spectrum has a relatively narrow maximum (its relative width $\sqrt{\frac{\langle x^2 \rangle - \langle x \rangle^2}{\langle x \rangle^2}}$ is of the order of $M^{-1/2}$). Therefore, the n-th moment $\langle x^n \rangle$ of the distribution function does not differ appreciably from $\langle x \rangle^n$ and is only slightly sensitive to the actual form of the distribution function. The situation is made worse by the fact that the discrepancy between the exact and approximate negative ** moments is considerably greater than the discrepancy between the positive ones.

* For convenience in his calculations, Marshak instead of the true mass M took an approximate mass M' for which the quantity $\frac{2}{1-r^2}$ is a half-integral number. This approximation, correct for large M, can lead to appreciable errors for small M and in particular, as was shown by Dardel [6], for M = 2.

** Expressions for the negative moments of the distribution function were derived by Walen [7] and given in Dardel's paper [6].

The investigation of the neutron-energy distribution in the age approximation shows that the neutron velocities during the slowing down are at each instant of time grouped around a certain average velocity which, in its turn, is uniquely determined by the slowing-down time.* However, it is impossible to obtain the shape of the neutron spectrum in the age approximation. The present paper is devoted to the solution of this problem. In this paper we will assume that the mean free path is independent of the velocity and we will confine ourselves to the region of energy which is small by comparison with the initial energy but which is sufficiently high so that we can neglect the effects of chemical binding and thermal motion of the moderator nuclei. Further, we will neglect neutron capture. In this case, as was stated above, the distribution function depends only on the dimensionless combination of variables vt/l. Some of the results presented here have been summarized in [9].

I

The equation for the nonstationary energy distribution of neutrons in a moderating medium has the form (for example, see [10])

$$\left.\begin{aligned} &\frac{l}{v}\frac{\partial \Psi(u,t)}{\partial t}+\Psi(u,t)= \\ &=\frac{1}{1-\varepsilon}\int\limits_{u-u_M}^{u} e^{-(u-u')}\Psi(u',t)\,du'+ \\ &+\delta(u)\,\delta(t), \\ &u_M=\ln\frac{1}{\varepsilon},\quad \varepsilon=\left(\frac{M-1}{M+1}\right)^2. \end{aligned}\right\} \tag{5}$$

Here $\Psi(u, t)\,dn$ is the number of neutrons in the energy interval $du\,[u = \ln(E_0/E)]$ which have suffered collisions with moderator nuclei during the unit time interval at time t. The function $\Psi(u, t)$ is related to the function $N(u, t)$, the neutron-energy distribution normalized to unity, by the expression

$$\Psi(u,t)=N(u,t)\frac{v}{l}. \tag{6}$$

We will look for a solution of Equation (5) in the form**

$$\Psi(u,t)=\frac{1}{\eta t}n(z),\quad z=\frac{2l}{\eta t v},\quad \eta=\frac{2}{M+1}. \tag{7}$$

The function $n(z)$ determined in this way is dimensionless and has a simple physical meaning: $n(z)\,dz$ is the number of neutrons in the interval dz at the time t. In fact, from Equations (6) and (7) we have that $N(u,t)\,du \equiv n(z)\,dz$.

Substituting (7) into (5), we get after a simple transformation

$$\left.\begin{aligned} &\frac{d}{dz}\{zn(z)\}-\frac{2}{\eta}\frac{n(z)}{z}=-\frac{4}{\eta}\frac{1}{1-\varepsilon}\int\limits_{(1-\eta)z}^{z}\frac{z'}{z^3}n(z')\,dz', \\ &\int\limits_0^\infty n(z)\,dz=1. \end{aligned}\right\} \tag{8}$$

Integrating this equation with respect to z from 0 to z and removing the double integral by an integration by parts, we find

$$n(z)=\frac{1}{\eta}\int\limits_{(1-\eta)z}^{z} n(z')\frac{2}{1-\varepsilon}\left(\frac{z'}{z^3}-\frac{\varepsilon}{z'z}\right)dz'. \tag{9}$$

* In particular, this phenomenon was used for purposes of neutron spectrometry by time of slowing down [8, 9].

** As we will see below, the factor $\frac{2}{\eta}$ in the variable z is chosen so that the maximum of the distribution be at $z = 1$.

The solution of this equation can be obtained by the method described in the Appendix. In fact, Equation (9) is a particular case of Equation (A.1),* where

$$K(z, z', \eta) = \frac{2}{1-\varepsilon}\left(\frac{z'}{z^3} - \frac{\varepsilon}{z'z}\right), \tag{10}$$

and its solution can be given in the form

$$n(z) = \exp\left\{\frac{1}{\eta} f_{-1}(z) + f_0(z) + \eta f_1(z) + \ldots\right\}. \tag{11}$$

Then for the first derivative functions $f_i(z)$ we can find the following system of recurrence equations [see Equation (A.11)]:**

$$\frac{2}{z}\int_0^1 dx\,(1-x)\,e^{-xz\frac{df_{-1}}{dz}} = 1, \tag{12}$$

$$\frac{2}{z}\int_0^1 dx\,(1-x)\,e^{-xz\frac{df_{-1}}{dz}}\left[\frac{x}{2} + \frac{x^2z^2}{2}\frac{d^2f_{-1}}{dz^2} - xz\frac{df_0}{dz}\right] = 0, \tag{13}$$

$$\frac{2}{z}\int_0^1 dx\,(1-x)\,e^{-xz\frac{df_{-1}}{dz}}\left\{\left[\frac{x}{2} + \frac{x^2z^2}{2}\frac{d^2f_{-1}}{dz^2} - xz\frac{df_0}{dz}\right]^2 + 2\left[-\frac{x}{2}(2-3x) - \frac{x^3z^3}{6}\frac{d^3f_{-1}}{dz^3} + \frac{x^2z^2}{2}\frac{d^2f_0}{dz^2} - xz\frac{df_1}{dz}\right]\right\} = 0. \tag{14}$$

Equation (12) is easily solved in parametric form after the substitution

$$z\frac{df_{-1}}{dz} = t,\quad z \equiv z(t),\quad f_{-1}(z) \equiv \varphi_{-1}(t). \tag{15}$$

Then

$$\frac{2}{z}\int_0^1 dx\,(1-x)\,e^{-xt} = 1, \tag{16}$$

i.e.,

$$z = \frac{2}{t^2}(e^{-t} - 1 + t). \tag{17}$$

Next, from Equation (15), we have

$$\frac{d\varphi_{-1}}{dt} = \frac{df_{-1}(z)}{dz}\frac{dz}{dt} = \frac{t}{z}\frac{dz}{dt}, \tag{18}$$

from which

$$\varphi_{-1}(t) = \int_a \frac{t'}{z(t')}\frac{dz(t')}{dt'}\,dt'. \tag{19}$$

* Equations of the Appendix are distinguished by the letter "A".

** The quantities $K_0(z, x)$ and $\alpha_i(z, x)$ appearing in this system according to Equations (10) and (A.10) have the form

$$K_0(z, x) = \frac{2(1-x)}{z},\quad \alpha_1 = \frac{x}{2},\quad \alpha_2 = -\frac{x(2-3x)}{8}.$$

Then, obtaining $\frac{df_0}{dz}$ from (13) and $\frac{df_1}{dz}$ from (14) and integrating them with respect to $\underline{z}$, we get

$$f_0 = \int_b^z \frac{dz'}{\int_{z'}^1 dx\,(1-x)\,xe^{-xt'}} \int_0^1 dx\,(1-x)\,e^{-xt'} \times \times \left[\frac{x}{2} + \frac{x^2z'^2}{2}\frac{d^2f_{-1}}{dz'^2}\right], \tag{20}$$

$$f_1 = \frac{1}{2}\int_c^z \frac{dz'}{\int_{z'}^1 dx\,(1-x)\,xe^{-xt'}} \int_0^1 dx\,(1-x)\,e^{-xt'} \times \times \left\{\left[\frac{x}{2} + \frac{x^2z'^2}{2}\frac{d^2f_{-1}}{dz'^2} - xz'\frac{df_0}{dz'}\right]^2 + + 2\left[-\frac{x}{8}(2-3x) - \frac{x^3z'^3}{6}\frac{d^3f_{-1}}{dz'^3} + \frac{x^2z'^2}{2}\frac{d^2f_0}{dz'^2}\right]\right\}. \tag{21}$$

After simple but awkward transformations, we obtain the following parametric representations for the three functions f_i:

$$\left.\begin{aligned}
&f_{-1}(z) \equiv \varphi_{-1}(t) = \\
&\quad = -\int_0^t \left(2 - t'\frac{1-e^{-t'}}{e^{-t'}-1+t'}\right)dt', \\
&f_0(z) \equiv \varphi_0(t) = \\
&= \frac{1}{2}\int_0^t \left(\frac{6}{t'} + 4 + t'\frac{e^{-t'}-4}{e^{-t'}-1+t'}\right)dt' - \\
&- \frac{1}{2}\ln 3\left(\frac{2}{t} - \frac{1-e^{-t}}{e^{-t}-1+t}\right), \\
&f_1(z) \equiv \varphi_1(t) = \frac{1}{2}\frac{1}{z^2}\frac{dz}{dt}\frac{d^2z}{dt^2}\times \\
&\times\left[\frac{5}{12}\left(z\frac{dt}{dz}-t\right)^2 + \frac{2}{3}t\left(z\frac{dt}{dz}-t\right)\right] + \\
&\quad + \frac{1}{8}\frac{1}{z}\left(\frac{d^2z}{dt^2}\right)^2\frac{dt}{dz}\left[\left(z\frac{dt}{dz}-t\right)^2 + \right. \\
&\quad \left. + \frac{2}{3}\left(z\frac{dt}{dz}\right)^2\right] - \frac{1}{4}\ln z - \\
&- \frac{1}{8}\frac{1}{z}\frac{d^3z}{dt^3}\left(z\frac{dt}{dz}-t\right)^2 - \frac{1}{2z^2}\left(\frac{3}{t}+1\right) - \\
&- \frac{7}{4}\frac{1}{t} - \frac{13}{24}t - \frac{t^2}{12} + \frac{1}{2z}\left(\frac{11}{3} + \frac{13}{2}\frac{1}{t} + t\right) - \\
&- \frac{203}{160} + \frac{1}{2}\int_0^t \left\{\frac{1+t'/6-t'^2/6}{e^{-t'}-1+t'} - \frac{2}{t'^2} - \frac{1}{t'}\right\}dt',
\end{aligned}\right\} \tag{22}$$

where $\underline{z}$ is given by Expression (17). The integration constants are so chosen that for z = 1 (t = 0) $f_{-1} = f_0 = f_1 = 0$. It can be shown that when $\underline{z}$ is close to unity

$$\left.\begin{aligned}
f_{-1}(z) &= -\frac{3}{2}(z-1)^2 + \frac{7}{4}(z-1)^3 - \ldots, \\
f_0(z) &= -\frac{1}{4}(z-1) + \frac{23}{40}(z-1)^2 - \ldots, \\
f_1(z) &= -\frac{87}{320}(z-1) + \ldots,
\end{aligned}\right\} \tag{23}$$

when $z \to 0$

$$\left.\begin{aligned} f_{-1}(z) &= -\frac{2}{z} + \ln\frac{2}{z} + 2{,}135\ldots, \\ f_0(z) &= \frac{3}{2}\ln\frac{2}{z} + 2{,}166\ldots, \\ f_1(z) &= -\frac{1}{4}\ln z + 0{,}166\ldots, \end{aligned}\right\} \qquad (24)$$

and, finally, when $z \to \infty$

$$\left.\begin{aligned} f_{-1}(z) &= -\frac{t^2}{2} + 2|t| - 4{,}482, \\ f_0(z) &= \frac{5}{2}|t| - 3\ln|t| - 3{,}569, \\ f_1(z) &= \frac{t^2}{24} - \frac{3}{8}|t| + 0{,}948\ldots \end{aligned}\right\} \qquad (25)$$

The numerical values of these functions in the intermediate region of z are given in the table.

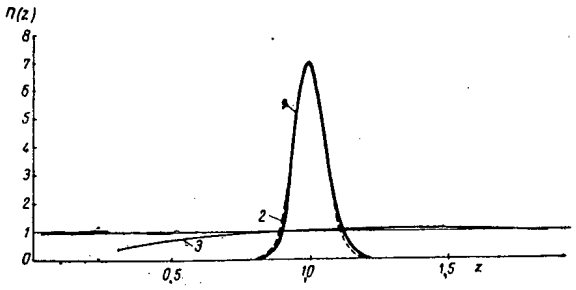

Fig. 1. The distribution function for neutrons in lead (M = 207.4). 1) Calculated from Equation (11); 2) calculated from Equation (26); 3) $e^{-[f_0(z)+\eta f_1(z)]}$.

TABLE
The Function $f_i(z)$

z	$f_{-1}(z)$	$f_0(z)$	$f_1(z)$
0,4555	−1,0805	0,4683	0,258
0,4649	−1,0204	0,4497	—
0,4747	−0,9614	0,4310	0,243
0,4848	−0,9036	0,4124	—
0,4953	−0,8469	0,3939	0,228
0,5063	−0,7914	0,3754	—
0,5176	−0,7372	0,3569	0,213
0,5294	−0,6844	0,3386	—
0,5416	−0,6329	0,3204	0,197
0,5544	−0,5830	0,3023	—
0,5677	−0,5345	0,2844	0,180
0,5815	−0,4877	0,2667	—
0,5959	−0,4425	0,2492	0,163
0,6108	−0,3990	0,2318	—
0,6265	−0,3573	0,2148	0,146
0,6428	−0,3175	0,1980	—
0,6598	−0,2796	0,1815	0,128
0,6776	−0,2438	0,1654	—
0,6961	−0,2100	0,1495	0,110
0,7155	−0,1784	0,1341	—

Expressions (11) and (22), as shown by numerical evaluations, adequately describe the neutron spectrum n(z) in any moderator except hydrogen.

For most practical calculations we can use the Gaussian curve as a simple approximate expression for n(z):

$$n(z)\,dz = \sqrt{\frac{3}{2\pi\eta}}\,e^{-\frac{3}{2\eta}(z-1)^2}\,dz = \\ = -\sqrt{\frac{3}{2\pi\eta}}\,\frac{\bar{v}}{v^2}\,e^{-\frac{3}{2\eta}\left(\frac{\bar{v}}{v}-1\right)^2}\,dv, \qquad (26)$$

where $\bar{v}$ is the average velocity at any given time determined from the condition $z(\bar{v}) = \frac{2l}{\eta \bar{v} t} = 1$.

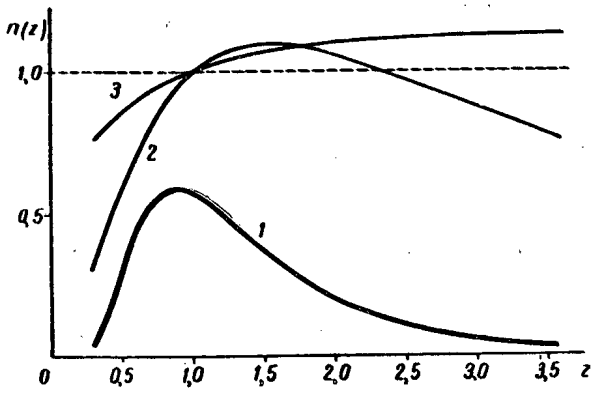

Fig. 2. The distribution functions for neutrons in deuterium (M = 2). 1) Calculated from Equation (11); 2) $e^{-[f_0(z)+\eta f_1(z)]}$; 3) $e^{-\eta f_1(z)}$.

Here, we have only kept the first term in the expansion of the function $f_{-1}(z)$ as a power series in $(z-1)$ [see Equation (23)] and have neglected the contribution from all of the other functions f_i.

TABLE (Continued)

z	$f_{-1}(z)$	$f_0(z)$	$f_1(z)$
0,73576	−0,14912	0,1191	0,092
0,75696	−0,12214	0,1045	—
0,77915	−0,09758	0,0904	0,073
0,79064	−0,08624	—	—
0,80239	−0,07560	0,0768	—
0,81442	−0,06550	—	—
0,82673	−0,05613	0,0639	0,055
0,83934	−0,04742	—	—
0,85225	−0,03941	0,0515	—
0,86546	−0,03210	—	—
0,87900	−0,02551	0,0397	0,036
0,89287	−0,01964	—	—
0,90707	−0,01451	0,0287	—
0,92163	−0,01013	—	—
0,93654	−0,00652	0,0183	0,018
0,95182	−0,00369	—	—
0,96748	−0,00160	0,0088	—
0,98353	−0,00041	—	—
1,00000	−0,00000	0,0000	0,000
1,01688	−0,00042	—	—
1,03418	−0,00169	−0,0079	—
1,05193	−0,00381	—	—
1,07014	−0,00682	−0,0149	−0,018
1,08881	−0,01071	—	—
1,10797	−0,01551	−0,0209	—
1,12763	−0,02122	—	—
1,14781	−0,02788	−0,0259	−0,036
1,16852	−0,03547	—	—
1,18977	−0,04404	−0,0299	—
1,21159	−0,05358	—	—
1,23399	−0,06412	−0,0327	−0,053
1,25700	−0,07566	—	—
1,28062	−0,08823	−0,0343	—
1,30489	−0,10184	—	—
1,32982	−0,11650	−0,0354	−0,070
1,38174	−0,14907	−0,0344	—
1,4366	−0,1860	−0,0321	−0,086
1,4945	−0,2276	−0,0283	—
1,5557	−0,2737	−0,0234	−0,102
1,6205	−0,3247	−0,0167	—
1,6890	−0,3806	−0,0085	−0,117
1,7615	−0,4416	0,0013	—
1,8383	−0,5077	0,0128	−0,131
1,9197	−0,5792	0,0263	—
2,0060	−0,6561	0,0415	−0,144
2,0974	−0,7386	0,0585	—
2,1945	−0,8269	0,0778	−0,156
2,2976	−0,9209	0,0990	—
2,4070	−1,0209	0,1222	−0,167
2,5233	−1,1270	0,1474	—
2,6469	−1,2392	0,1753	−0,176
2,7784	−1,3579	0,2053	—
2,9183	−1,4829	0,2377	−0,183
3,0671	−1,6146	0,2726	—
3,2257	−1,7528	0,3100	−0,189
3,3946	−1,8979	0,3499	—
3,5746	−2,0498	0,3926	−0,194

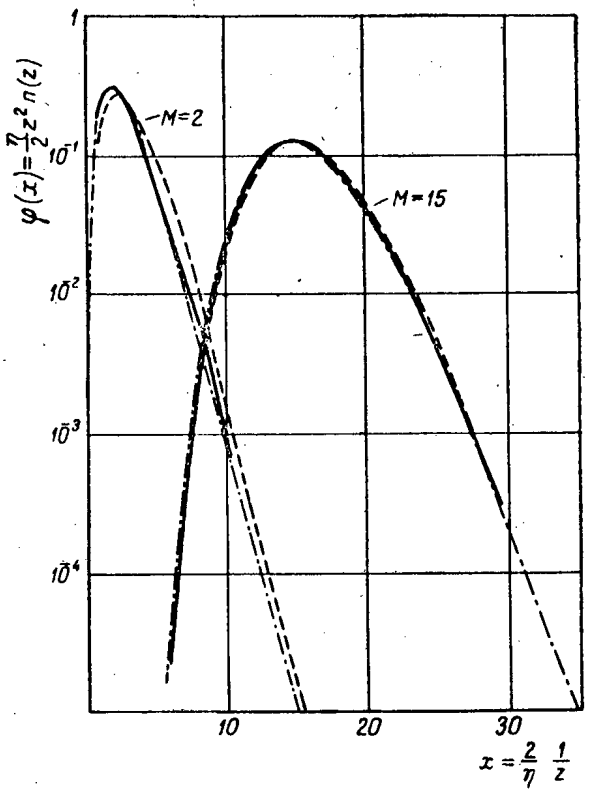

Fig. 3. Comparison of the distribution functions for neutrons in media with M = 2 and M = 15.
——— Author's results; – – – – Marshak's results; – · – · – · – Dardel's results.

The graphs of n(z) calculated from Equation (11) for M = 207.4 (lead) and M = 2 (deuterium) are given in Figs. 1 and 2; for comparison the approximate curve obtained from Equation (26) is also given in Fig. 1. The ratios of the zero and first approximations to the second, i.e., the functions $e^{-[f_0(z)+\eta f_1(z)]}$ and $e^{-\eta f_1(z)}$ (the latter only for M = 2, since in the case of lead the maximum deviation of the quantity $e^{-\eta f_1(z)}$ from unity in the region of z investigated does not exceed 0.07%), are given in the same figures.

In Fig. 3 our results for M = 2 and M = 15 are compared with the results of Marshak's numerical calculations [5] and with those of the more accurate calculations made by Dardel.* As can be seen from the figure, the three functions $f_i(z)$ are completely adequate to describe the neutron distribution even in such a light moderator as deuterium.

* As can be easily verified, the functions of Marshak F(x) and Dardel $\varphi(x)$ are related to n(z) by the expressions

$$F(x)=zn(z)\,\xi/2=x\varphi(x)\,\xi/2,$$

where

$$\xi=1+\frac{\varepsilon}{1-\varepsilon}\ln\varepsilon,\quad x=\frac{2}{\eta}\frac{1}{z}.$$

Let us consider the case when the moderator consists of several types of nuclei. The equation for the total number of neutron collisions per unit time in the energy interval (u, u + du) has the form (for example, see [10])

$$\frac{l}{v}\frac{\partial \Psi(u,t)}{\partial t}+\Psi(u,t)= \\ =\sum_{\alpha}\frac{c_\alpha}{1-\varepsilon_\alpha}\int\limits_{u-u_{M_\alpha}}^{u}e^{-(u-u')}\Psi(u',t)\,du'+ \\ +\delta(u)\,\delta(t), \tag{27}$$

where $\frac{1}{l}=\sum_{\alpha}\frac{1}{l_\alpha}$, $c_\alpha=\frac{l}{l_\alpha}$ and l_α is the mean free path between collisions with nuclei of type α. In the same way as before, we will look for a solution of Equation (27) for large u in the form

$$\left.\begin{aligned}&\Psi_0(u,t)=\frac{\overline{M}+1}{2t}n(z),\\ &z=\frac{\overline{M}+1}{vt}l,\end{aligned}\right\} \tag{28}$$

where $\overline{M}$ is given by the relation

$$\frac{1}{\overline{M}+1}=\sum_{\alpha}\frac{c_\alpha}{M_\alpha+1}. \tag{29}$$

After a simple transformation, we find the following equation for n(z):

$$\left.\begin{aligned}&zn(z)+z^2n'(z)-(\overline{M}+1)\,n(z)+\\ &+2\sum_{\alpha}c_\alpha\frac{\overline{M}+1}{1-\varepsilon_\alpha}\int\limits_{\sqrt{\varepsilon_\alpha}z}^{z}\frac{z'\,dz'}{z^2}n(z')=0,\\ &\int\limits_0^\infty n(z)\,dz=1.\end{aligned}\right\} \tag{30}$$

Following our method (see Appendix), we will look for a solution in the form

$$n(z)=\exp\left\{\frac{\overline{M}+1}{2}f_{-1}(z)+f_0(z)+\right. \\ \left.+\frac{2}{\overline{M}+1}f_1(z)+\ldots\right\}. \tag{31}$$

Then, the recurrence relations (A.11) take the following form:

$$\frac{z^2}{2}f'_{-1}-1+\sum_{\alpha}\frac{c_\alpha}{\beta_\alpha}\int\limits_0^{\beta_\alpha}dx e^{-xzf'_{-1}}=0, \tag{32}$$

$$z^2f'_0+z+\sum_{\alpha}\frac{c_\alpha}{\beta_\alpha}\int\limits_0^{\beta_\alpha}dx e^{-xzf'_{-1}}\{-2xzf'_0+\beta_\alpha+x^2z^2f''_{-1}-2x\}=0, \tag{33}$$

. . . . . .

$$\beta_\alpha=\frac{\overline{M}+1}{M_\alpha+1}. \tag{34}$$

In the general case, the solution of these equations is very complicated and therefore we will restrict ourselves to the case of the most practical interest: when the values of z lie in the region of the maximum of the distribution function, i.e., when f'_{-1} is small. Expanding the integral appearing in Equation (32) into a power series in f'_{-1} and taking into account that

$$\sum_\alpha c_\alpha = 1, \quad \sum_\alpha c_\alpha \beta_\alpha = 1 \tag{35}$$

[the latter relation follows from Equations (29) and (34)], we get

$$\frac{z-1}{2} + \sum_\alpha c_\alpha \frac{\beta_\alpha^2}{3} z f'_{-1} = 0. \tag{36}$$

From this it follows directly that the maximum occurs at z = 1. Near the maximum

$$f_{-1}(z) \approx -\frac{3}{4\sum_\alpha c_\alpha \beta_\alpha^2}(z-1)^2 \tag{37}$$

and

$$n(z) = N_0 e^{-3/4 \frac{\bar{M}+1}{\sum_\alpha c_\alpha \beta_\alpha^2}(z-1)^2} \tag{38}$$

We note that as the result of the identity

$$\sum_\alpha c_\alpha \beta_\alpha^2 \equiv 1 + \sum_\alpha c_\alpha (\beta_\alpha - 1)^2 > 1 \tag{39}$$

the effective average mass $\bar{M}$ which determines the average neutron energy in a moderator consisting of a mixture of nuclei with different masses is always greater than the effective mass $\tilde{M}$ determining the width of the energy distribution:

$$\tilde{M} = \frac{\bar{M}+1}{\sum_\alpha c_\alpha \beta_\alpha^2} - 1. \tag{40}$$

In conclusion the author expresses his deep gratitude to I. M. Gel'fand, V. L. Ginzburg, Iu. A. Gol'fand, I. M. Frank, F. L. Shapiro for valuable discussions and to Z. P. Mukhina for extensive numerical calculations.

APPENDIX

Let us consider the integral equation of the form

$$y(z) = \frac{1}{\eta}\int_{(1-\eta)z}^{z} K(z, z', \eta)\, y(z')\, dz', \tag{A.1}$$

where η is a small quantity and the kernel $K(z, z', \eta)$ is finite as $\eta \to 0$. First of all we note that this equation cannot be solved in the general case by a series expansion of y(z') under the integral sign.* In fact, it

---

* We note that if the expression $\frac{1}{\eta}\int_{(1-\eta)z}^{z} K(z, z', \eta)\, dz'$ is close to unity (this is the case, for example, near the maximum of the neutron distribution function), then the series expansion of y under the integral sign can be used as a method for solving this equation. However, in this case it is not the parameter η but

$$\delta = \frac{1}{\eta}\int_{z(1-\eta)}^{z} K(z, z', \eta)\, dz' - 1.$$

which is small.

$$\frac{1}{\eta}\int_{z(1-\eta)}^{z} K(z, z', \eta)\,dz \neq 1, \tag{A.2}$$

then to the order of magnitude

$$\frac{d^n y}{dz^n} \approx \frac{y}{\eta^n}. \tag{A.3}$$

Thus, the neglected terms will be of the same order of magnitude as those taken into account.

On the other hand, from Equation (A.3) it follows that the function y(z) must have the form

$$y(z) = e^{\frac{1}{\eta}\varphi(z,\ \eta)}, \tag{A.4}$$

where $\varphi(z, \eta)$ is continuous for $\eta \to 0$.

Therefore, expanding $\varphi(z, \eta)$ as a power series in η, we can look for a solution of Equation (A.1) in the form

$$y(z) = e^{\frac{1}{\eta}f_{-1}(z)+f_0(z)+\eta f_1(z)+\ldots}, \tag{A.5}$$

where $f_i(z)$ is independent of η.

Substituting (A.5) into (A.1) and introducing a new variable

$$x = \frac{z-z'}{\eta z}, \tag{A.6}$$

we get

$$\int_0^1 dx\, zK[z,\ z(1-\eta x),\ \eta] \exp\left\{\frac{1}{\eta}f_{-1}[z(1-\eta x)] - \right.$$
$$-\frac{1}{\eta}f_{-1}[z] + f_0[z(1-\eta x)] - f_0[z] + \eta f_1[z(1-\eta x)] -$$
$$\left. -\eta f_1[z] + \ldots\right\} = 1. \tag{A.7}$$

Let us denote the left-hand side of this equation by $J(\eta)$. Then

$$J(\eta) \equiv 1. \tag{A.8}$$

Alternatively, expanding $J(\eta)$ as a power series in η, we get

$$J(0) = 1,\ \left.\frac{\partial J}{\partial \eta}\right|_{\eta=0} = 0,\ \left.\frac{\partial^2 J}{\partial \eta^2}\right|_{\eta=0} = 0\ldots \tag{A.9}$$

Expanding $J(\eta)$ and introducing the quantities

$$\left.\begin{aligned} K_0(z, x) &= \lim_{\eta\to 0} K[z, z(1-\eta x), \eta], \\ a_m(z, x) &= \lim_{\eta\to 0}\frac{1}{m!}\frac{\partial^m}{\partial \eta^m}\ln\{K[z, z(1-\eta x), \eta]\}, \\ z\frac{df_{-1}(z)}{dz} &= t. \end{aligned}\right\} \tag{A.10}$$

we get the following system of algebraic recurrence relations for the first derivative functions $f_i(z)$:

$$\left.\begin{aligned}
&\int_0^1 K_0(z, x)\, e^{-xt}dx = 1,\\
&\int_0^1 K_0(z, x)\, e^{-xt}dx \left[\alpha_1(z, x) + \right.\\
&\qquad \left. + \frac{x^2z^2}{2}\frac{d^2f_{-1}}{dz^2} - xz\frac{df_0}{dz}\right] = 0,\\
&\int_0^1 K_0(z, x)\, e^{-xt}dx \left\{\left[\alpha_1(z, x) + \right.\right.\\
&\quad \left. + \frac{x^2z^2}{2}\frac{d^2f_{-1}}{dz^2} - xz\frac{df_0}{dz}\right]^2 + 2\left[\alpha_2(z,x) - \right.\\
&\quad \left.\left. - \frac{x^3z^3}{6}\frac{d^3f_1}{dz^3} + \frac{x^2z^2}{2}\frac{d^2f_0}{dz^2} - xz\frac{df_1}{dz}\right]\right\} = 0.\\
&\cdots\cdots\cdots\cdots\cdots\cdots
\end{aligned}\right\} \qquad (A.11)$$

The solution of this system, at least numerically, does not present great difficulties.

Let us note that our method can be used for the solution of equations of the general form

$$\sum_{m=0}^{n} \eta^m \varphi_m(z, \eta)\, \frac{d^m y(z)}{dz^m} = \frac{1}{\eta}\int_{z-\eta q_2(z,\eta)}^{z+\eta q_1(z,\eta)} dz' y(z')\, K(z, z', \eta), \qquad (A.12)$$

where $\varphi_m(z, \eta)$ and $q_i(z, \eta)$ are finite for $\eta \to 0$. The method leads to a system of algebraic equations analogous to (A.11) if $n \leq 1$, or to a system of differential equations of order $n-1$ if $n > 1$.

LITERATURE CITED

[1] L. S. Ornstein and G. E. Uhlenbeck, Physica 4, 478 (1937).

[2] O. Olsson, Arkiv fys. 10, 129 (1956).

[3] M. Demeur, A. Gribaumont, and P. Jansens, Bull. cl. . Sci. Acad. roy. Belgique 40, 526 (1954).

[4] G. Placzek, Manhattan Project Report A-25 (Quoted in Reference [5]).

[5] R. E. Marshak, Rev. Mod. Phys. 19, 185 (1947).

[6] G. F. Dardel, Trans. Roy. Inst. Technol. Stockoln 75, 1 (1954); Phys. Rev. 94, 1272 (1954).

[7] R. Walen, Recueil de traveaux de l'Institute de Rechercher sur la Structure de la Matiere, Belgrad, (1952).

[8] L. E. Lazareva, E. L. Feinberg, and F. L. Shapiro, J. Exptl.-Theoret. Phys. (USSR) 29, 381 (1955).

[9] A. A. Bergman, A. I. Isakov, I. D. Murin, F. L. Shapiro, I. V. Shtranikh, and M. V. Kazarnovskii, Physical Research (Reports of the Soviet Delegation at the International Conference on the Peaceful Uses of Atomic Energy) [In Russian] (Izd. AN SSSR, 1955), p. 57.

[10] A. Akhiezer and I. Pomeranchuk, Some Problems in Nuclear Theory [In Russian] (Gostekhizdat, Moscow-Leningrad, 1950), 2nd Edition.

Received November 12, 1957.

INVESTIGATION OF THE STATISTICAL DISTRIBUTION OF SPONTANEOUS U^{238} FISSION ACTS ACCORDING TO THE ENERGIES OF THE TWO FRAGMENTS

B. S. Kovrigin and K. A. Petrzhak

Using an apparatus consisting of a double pulse ionization chamber, two amplifying channels, a coincidence circuit and a two-beam pulsed oscillograph, we measured the kinetic energy of each of the two fragments formed during nuclear fission. 780 cases of spontaneous U^{238} fission and about 4500 cases of U^{235} fission by slow neutrons were recorded. Using these data we plotted the statistical distributions of acts of spontaneous fission and fission with slow neutrons according to the energies of the two fragments. These distributions gave the following curves for the two fission methods: a) the energy spectrum of all fragments and that of light and heavy fragments separately; b) the distribution of acts according to the total kinetic energy of the two nuclear fragments; c) the distribution of fission fragments according to mass; d) the relation of the average total kinetic energy of the two fragments to the ratio of their masses; and e) the relation of the average kinetic energy of light and heavy fragments to their total kinetic energy. The results of the two methods of fission are quite similar. It was found that the total kinetic energy of the two fragments in spontaneous U^{238} fission was, on the average, 4 Mev less than the energy in U^{235} fission by slow neutrons.

In paper [1] the energy spectrum of the fragments from spontaneous U^{238} fission was investigated and compared with the spectrum of the fragments from U^{235} fission by slow neutrons. A qualitative investigation of the energy spectrum of the fragments from spontaneous Cm^{242} fission was carried out in work [2]. In paper [3] the spectra of fragments from spontaneous Pu^{240} fission were compared with those from Pu^{239} fission by slow neutrons, i.e., actually the spectra of fission fragments from the same Pu^{240} nucleus in different energy states. The spectra of fragments from spontaneous fission of heavy nuclei and fission produced by slow neutrons were found to be extremely similar in form.

The method used in these experiments consisted of measuring the energy of one of the fragments from each act of fission using a pulse ionization chamber. This method made it possible to investigate the general form of the energy spectrum of the fragments from spontaneous fission, to determine the most probable energies of light and heavy groups of fragments, and to find the ratio of the heights of the peaks and the ratio of the height of the depression to the height of one of the peaks.

However, in several cases the energy of both fragments has been measured simultaneously [4-9] in studying nuclear fission by slow neutrons, and this makes it possible to obtain much more information on the process of fission from the distribution of fission cases according to the energies of the two fragments.* The purpose of the present work was to apply this method to the investigation of spontaneous U^{238} fission in order to compare directly the distribution of fission acts according to the energies of the two fragments and the results of this distribution with the corresponding ones for U^{235} fission by slow neutrons. Such a comparison could be made using the same sample of natural uranium, as U^{235} and U^{234} contribute little to the rate of spontaneous fission of natural uranium and practically only U^{235} participates in fission by slow neutrons.

* When this article had been sent to press, the authors discovered paper [10] on the use of this method for the comparative study of spontaneous Pu^{242} fission and Pu^{241} fission by thermal neutrons.

Apparatus and Experimental Method

Due to the low probability of spontaneous fission (the rate of spontaneous U^{238} fission is 25 fissions/g·hr [11]) not less than 50 mg of uranium had to be used so as to record 700-1000 acts of spontaneous fission over a period of 2-3 months and thus obtain an acceptable statistical accuracy for the results. In exact measurements of fragment energies, an area density of the layer of not greater than 1% of the range was permitted, i.e., 0.25 mm of air or 0.075 mg/cm^2 of U_3O_8. In order to observe spontaneous fission, we considered an increase of this area density by a factor of 2 as permissible.

The values determined for the total amount of uranium and its area density indicated that the preparation should have a working surface of about 500 cm^2.

In most papers on the simultaneous measurement of the energy of the two fragments, the fissile layer had a thin cellulose nitrate or metal backing. The discrepancies in the fragment spectrum caused by the presence of the backing were considerably reduced by collimating the direction of the fragments. Collimation in our work would have resulted in a large decrease in the rate of counting. We therefore decided to forego collimation and prepare a layer without a backing.

The layer prepared was a plate of U_3O_8 with an area density of about 0.15 mg/cm^2, fixed onto a flat rigid frame with 600 closely arranged holes of 9 mm diameter. The thin plates of U_3O_8 were prepared by cathode sputtering followed by solution of the backing.

The fissile layer acted as the common cathode of a double pulse ionization chamber for fission. The large surface of the preparation required the construction of a chamber whose dimensions were considerably greater than those usually used. The body of the chamber consisted of a section of a 380 mm diameter steel pipe with screwed in steel flanges. The two halves of the double chamber were actually independent and identical pulse chambers.

Both chambers were equipped with grids to shield the collector from positive ions. The chamber was worked out from the theory put forward in paper [12]. The chamber was filled to atmospheric pressure with technical argon, which was constantly purified by being passed through calcium shavings, heated to 300° C. A field strength of 360 v/cm in the cathode – screen space and 1350 v/cm in the screen – collector space provided for saturation and a minimum capture of electrons by the screen.

The measuring equipment consisted of two amplifying channels, a coincidence circuit and a two-beam pulsed oscillograph. A pulse, produced by a fragment, amplified and delayed by 1.5 μsec, was conducted to the vertical plates of one of the oscillograph beams. The undelayed pulse was formed into a standard one and acted upon the coincidence circuit, which triggered the scanning and intensity gate of the oscillograph. The photo plate, after recording the fragments of nuclear fission in the form of two pulses, moved automatically 3-4 mm.

The measuring apparatus had the following characteristics. The amplification of both channels was maintained constant within 5% during the whole period of measurement and the linearity of the amplification within 1% during the operating time. The scanning capacity of the amplifying channels covered an energy of 1.2 Mev. The time of electron collection and, consequently, the time of pulse growth was not greater than 2 μsec. The pulses lasted 20 μsec, the scanning time of the coincidence circuit was 1.5 μsec (the duration of the standard pulses acting on it).

The spontaneous fission was observed without shielding from cosmic rays. At present one may consider it established that the effect of spontaneous fission on natural uranium is approximately two orders greater than the effect of fission by mesons and neutrons of cosmic radiation. U^{235} fission by slow neutrons was observed using a 20-25 cm paraffin shield around the chamber and a neutron source placed within this shield.

Experimental Results

In all, we recorded 780 cases of spontaneous U^{238} fission over a period of 1100 hours operation and about 4500 cases of U^{235} fission by slow neutrons. Combination of the kinetic energies of the fragment pairs for each of these methods of fission gave a statistical distribution of the acts of fission according to the energies of the two fragments.

Figure 1 shows such a distribution for spontaneous U^{238} fission.

The scale of pulse amplitudes according to energy was graduated with α-particles of U^{238} and U^{234}. Papers [13-15] show experimentally that more energy is expended in the formation of one ion pair by a fragment than by an α-particle. However, it was assumed for the graduation that the energies expended in the formation of one ion pair by the fragment and an α-particle are equal. This was done to facilitate the comparison of the experimental results with previous investigations.

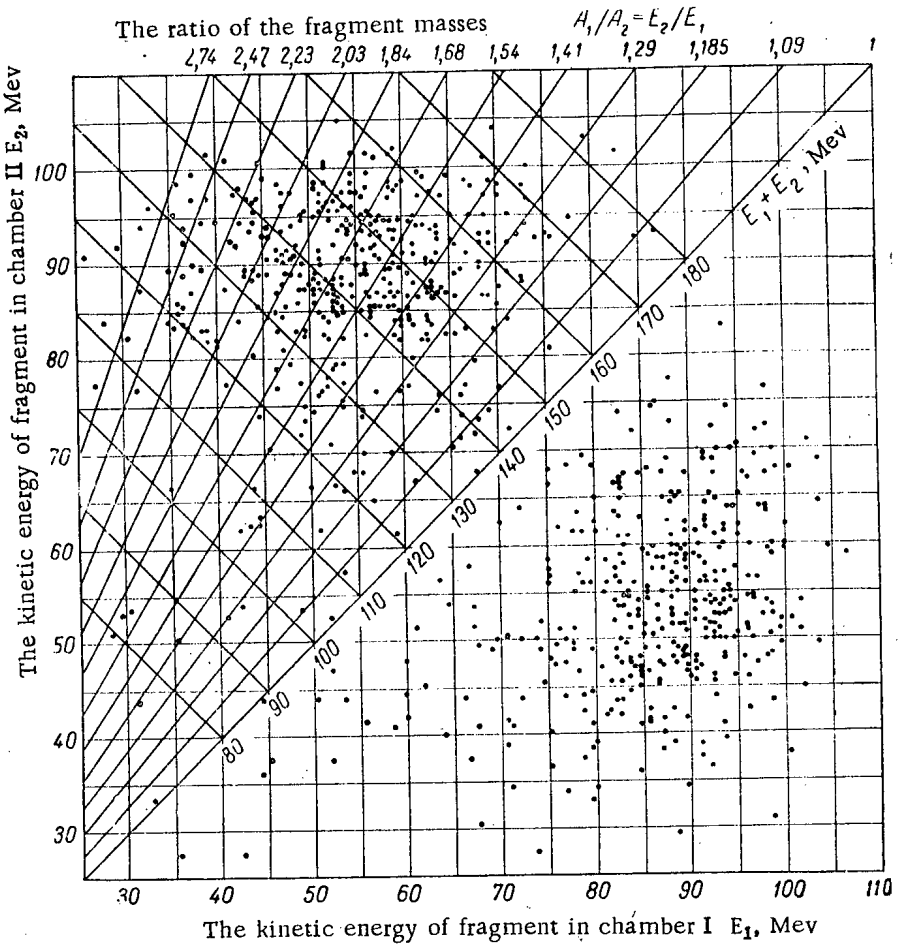

Fig. 1. Statistical distribution of spontaneous U^{238} fission acts according to the energies of the two fragments.
The individual fission acts are represented by points whose Descartes coordinates correspond to the energies of the light and heavy fragments.

The statistical distribution of the fission acts according to the energies of the two fragments gave a series of curves which characterize the two fission methods being compared.

To plot the energy spectra of the fragments (Fig. 2) we first calculated the number of pulses in each energy interval of both coordinate axes and then combined the results for the two axes. The statistical distributions made it possible to resolve the energy spectra into peaks for light and heavy fragments. The peaks, especially those in the case of light fragments, have considerable "tails" in the low energy range. The heavy fragment peaks correspond quite markedly to a Gaussian curve. The characteristics of the energy spectra are given in the table on p. 726.

Figure 3 gives both spectra for a more graphic comparison. Besides certain differences in the form of the spectra, a difference of approximately 2 Mev may be observed in their positions, which is not covered by the limits of error.

The statistical distributions were further analyzed by using the auxiliary coordinate lines $E_1 + E_2 = \text{const}$ and $E_2/E_1 = \text{const}$ (see Fig. 1). According to the law of the conservation of momentum, the ratio of the energies of the

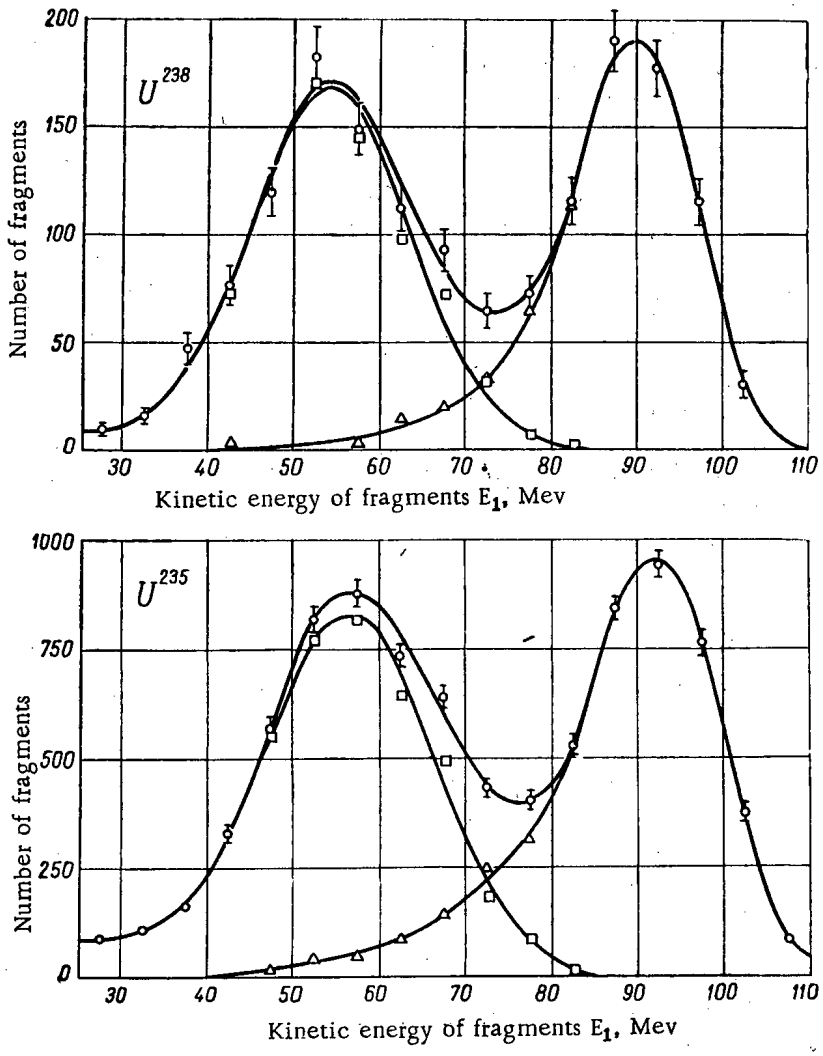

Fig. 2. Energy spectra of fragments from spontaneous U^{238} fission and fragments from U^{235} fission by slow neutrons. △) Data for light fragments; □) data for heavy fragments; ○) data for all fragments.

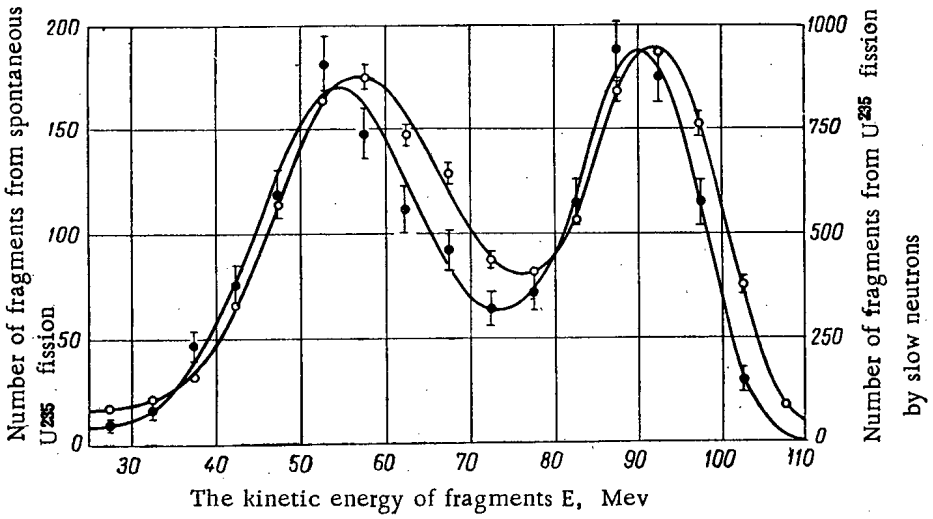

Fig. 3. Comparison of the energy spectra of fragments. ●) Spontaneous U^{238} fission; ○) U^{235} fission by slow neutrons.

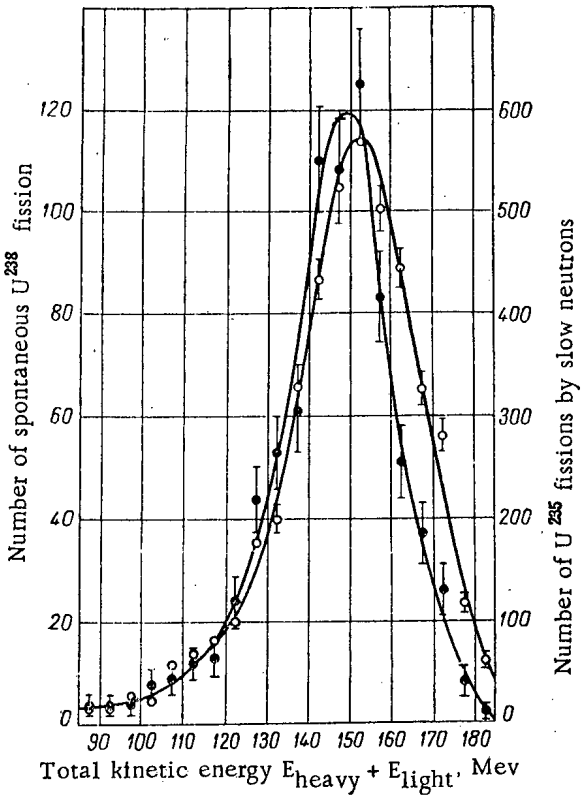

Fig. 4. Distribution of fission acts according to the total kinetic energy of the two fragments. ●) Spontaneous U^{238} fission; ○) U^{235} fission by slow neutrons.

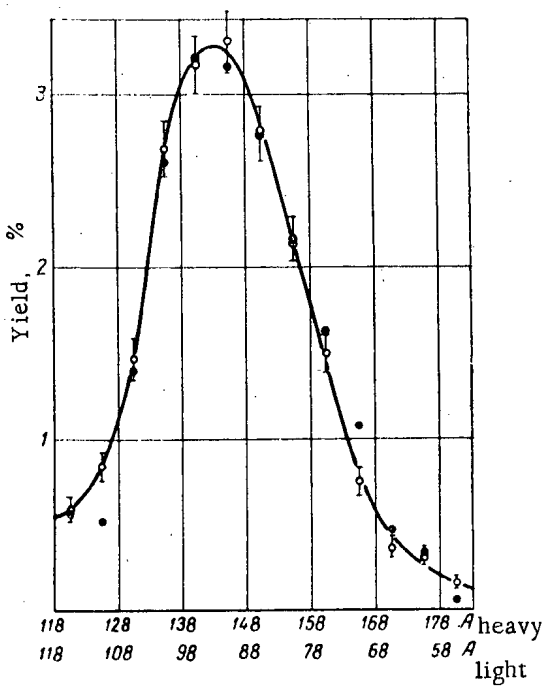

Fig. 5. Distribution of fragments according to mass. ●) Spontaneous U^{238} fission; ○) U^{235} fission by slow neutrons. The mass numbers of light and heavy fragments are plotted along the abscissa, assuming that the mass number of the fissile nucleus equals 236.

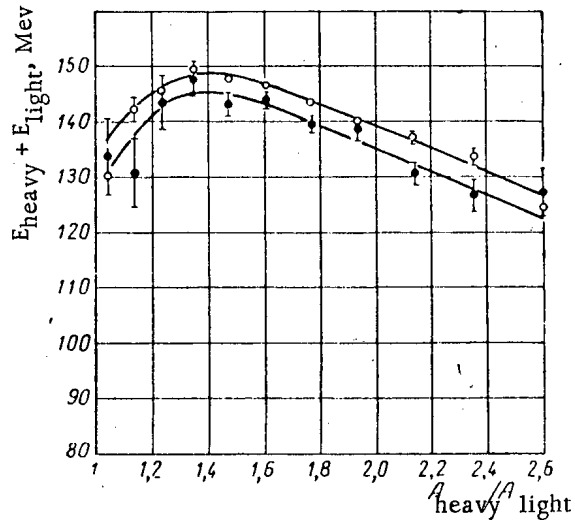

Fig. 6. The relation of the average total kinetic energy of the two fragments to the ratio of the fragments' mass. ●) Spontaneous U^{238} fission; ○) U^{235} fission by slow neutrons.

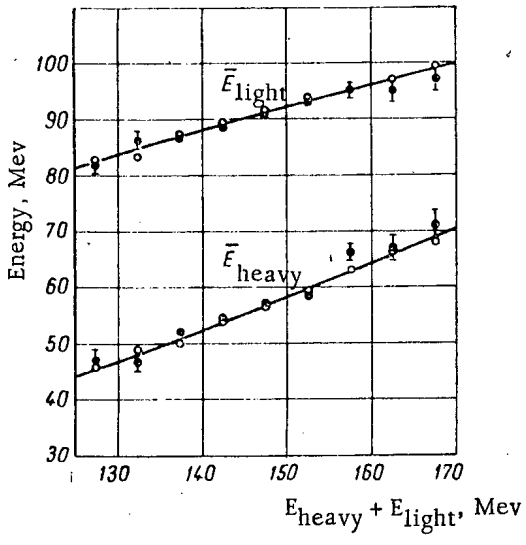

Fig. 7. The relation of the average kinetic energy of light and heavy fragments to the total kinetic energy of the fragments. ●) Spontaneous U^{238} fission; ○) U^{235} fission by slow neutrons.

fragments E_2/E_1 equals the reciprocal ratio of their masses A_1/A_2. For the group of fission cases lying above and to the left of the line $E_2/E_1 = 1$, the symbol E_1 corresponds to the energy of the heavy fragment and may be substituted by E_{heavy}. Similarly, E_2, A_1, and A_2 may be substituted by E_{light}, A_{heavy}, and A_{light}. Figure 4 gives the distribution of acts of fission according to the sum of the kinetic energies of the two fragments in the two cases being compared. The most probable and the average total energies for spontaneous fission were approximately 4 Mev less than those for fission by slow neutrons with a peak half-width 20% less.

TABLE

Characteristics of the Energy Spectra of Fission Fragments

Characteristic	Spontaneous fission		Fission by slow neutrons	
	light fragments	heavy fragments	light fragments	heavy fragments
The most probable energy, Mev	90.0 ± 0.3	54.4 ± 0.4	92.3 ± 0.12	56.6 ± 0.15
The half-width of the peak, Mev	17.5	21.1	19.2	23.5
The ratio of the most probable energies	1.6		1.63	
The ratio of the height of the peak for light fragments to the height of the peak for heavy fragments	1.13		1.15	
The ratio of the height of the depression between the peaks to the height of the peak for light fragments	0.33		0.42	

By summing the acts of fission in the intervals between the coordinate lines $E_2/E_1 = A_1/A_2 = \text{const}$, we obtain the distribution of fragments according to mass (Fig. 5). Within the limits of error, the points of both methods of fission lie on one curve.

The relation of the average total kinetic energy of the two fission fragments to the ratio of the masses of the fragments (Fig. 6) is similar for spontaneous fission and for neutron-produced fission. The average energy of the fragments from spontaneous fission is continually less than the average energy of the fragments from fission by slow neutrons.

Figure 7 gives the curves for the average energy of a group of light and heavy fragments against the total kinetic energy. The average energies of spontaneous fission and of neutron-produced fission increase with an increase in the total energy, but the energy of the light fragment increases more slowly.

Discussion of Results

The statistical distribution according to the energies of the two fragments from spontaneous fission and from fission by slow neutrons has the following characteristics. The probability maxima correspond to unsymmetrical fission; the energies of the light and heavy fragments fluctuate over a considerable range; the energy of one of the nuclear fragments fluctuates over almost as wide a range when the energy of the other fragment is fixed.

Figure 1 includes a number of points that lie in the field of the bisector of the coordinate angle and they could be considered as cases of almost symmetrical fission. There are also points which could denote cases of fission with an extremely low energy of one or both fragments. However, both groups of points should be considered rather as resulting from the energy distribution of the fragments being distorted by energy losses in the actual preparation layer.

The peaks of the light and heavy fragments in the energy spectra of fragments from fission by slow neutrons (Fig. 2) have somewhat greater breadths than those obtained in works [4-9]. The effects of the main sources of

additional broadening were evaluated. Of all the factors which could have caused the broadening of the peaks in our work, the most probable were a variation in the amplification coefficient and the absorption of fragments in the preparation layer. Other causes for broadening (the scanning capacity of the ionization chamber, the scanning capacity of the amplifying channels, errors in measuring the amplitude of the pulses and statistical errors) were approximately the same in works [4-6] as in our experiment. They were less in works [7-9] as apparatus with a greater scanning capacity was used.

The introduction of corrections for the variations in the amplification coefficient would decrease in half-width of the peaks for light and heavy fragments from 19.2 to 15 Mev and 23.5 to 22.6 Mev, respectively. To evaluate the broadening of the peaks due to absorption of fragments in the preparation layer for the peaks of light and heavy fragments taken from paper [4], new distributions according to energy were plotted, taking into account absorption in a preparation layer with an area density of 0.15 mg/cm^2 of U_3O_8. It was found that the additional half-widths acquired by peaks were 3.5 Mev for the group of light fragments and 5.5 Mev for the group of heavy fragments. Taking these values into account, the half-widths of the peaks were found to be 14.5 and 22 Mev. In the calculations, the peaks were assumed to have a Gaussian shape and the partial half-widths were summed according to the law of the addition of random errors. Due to the extremely approximate character of the calculations, the corrected values for the half-widths may be considered as agreeing quite well with the results of other work in which the half-widths of the peaks of light and heavy fragments range from 17 and 22 Mev in earlier work [4], to 12 and 19 Mev in contemporary work [7-9].

It was found that the average total kinetic energy of fragments from spontaneous U^{238} fission was about 4 Mev less than that of U^{235} fission by slow neutrons. This was also confirmed by the results given in paper [1], in which the energy spectrum of fragments from spontaneous U^{238} fission was displaced by about 1.5 Mev toward lower energies in relation to the spectra of U^{235} fragments, although the statistical accuracy was not sufficient for absolute confirmation. It is difficult to draw any conclusions from this difference in energies as different fissile nuclei were compared: U^{238} in its ground state and U^{236} in an excited state. A comparison of the energy characteristics of spontaneous U^{238} fission and those of the photofission of this nucleus at an excitation energy close to that of the fission threshold would have been much more interesting. At the present time the literature does not contain data for such a comparison.

On the mass yield curve (Fig. 5), the graduation of the abscissa in mass numbers of fragments cannot correspond simultaneously to the fission of U^{236} and U^{238} nuclei. The scales for the mass numbers of U^{236} and U^{238} should have been somewhat different. However, the inaccuracy in the graduation of the scale was considerably less than that in the resolving capacity of such a method for determining the mass yield curve. The difference in the distributions according to mass, which could have been caused by the difference in the mass of the fissile nuclei, were covered here by the spread of the curve in both directions as a result of energy losses in the preparation layer. Therefore, the curve shows the presence of fragments with mass numbers greater than 168 and less than 68. The yield of such fragments is zero, as is known from radiochemical investigations. A considerable yield was also observed in the range of symmetrical fission and the possible difference in the yields of fragments from fission by slow neutrons and from spontaneous fission, as detected in paper [16] for Cm^{242}, was completely screened.

The graph of the relation of the average total kinetic energy to the ratio of the fragment masses (see Fig. 6) showed that fission becomes more symmetrical both in the case of spontaneous fission and in the case of fission produced by slow neutrons when the total energy increases. When A_{heavy}/A_{light} tends toward unity, the curves show a fall. This should be considered as due to the fact that in the region of the line $E_2/E_1 = 1$ the statistical distributions according to the energies of the two fragments (see Fig. 1) include mainly fission acts which have a substantial deficiency in total energy due to the considerable loss of energy by the fragments in the preparation layer.

An increase in the symmetry of fission with an increase in the total energy of the fragments may also be seen in Fig. 7, in which the curves of the average energy of light and heavy fragments approach each other when the energy increases. This results in a lower dispersion of energy by the light fragments and in a different width for the peaks of light and heavy fragments in energy spectra in the case of neutron fission and spontaneous fission.

In this work it was found that the statistical distributions of fission acts according to the energies of the two fragments and the consequences of this distribution were quite similar for spontaneous U^{238} fission and U^{235} fission produced by slow neutrons. Of the insignificant differences that exist, the greatest is that the average total kinetic

energy of the two nuclear fragments and the average energy of the light and heavy groups of fragments is about 4 Mev and 2 Mev, respectively, less for spontaneous U^{238} fission than for U^{235} fission by slow neutrons. The results of this work indicate the similarity of the mechanisms of these two methods of fission.

LITERATURE CITED

[1] W. J. Whittenhouse and W. Galbraith, Philos. Mag. 41, 429 (1950).

[2] G. C. Hanna, B. G. Harvey, N. Moss, and P. R. Tunnicliffe, Phys. Rev. 81, 466 (1951).

[3] E. Segre and G. Wiegand, Phys. Rev. 94, 157 (1954).

[4] W. Jentschke and F. Prancl, Z. Physik 119, 696 (1942).

[5] W. Jentschke, Z. Physik 120, 165 (1943).

[6] A. Flammersfeld, P. Jensen, and W. Gentner, Z. Physik 120, 450 (1943).

[7] D. C. Brunton and G. C. Hanna, Canad. J. Res. 28A, 190 (1950).

[8] D. C. Brunton and W. B. Thompson, Canad. J. Res. 28A, 498 (1950).

[9] J. S. Wahl. Phys. Rev. 95, 126 (1954).

[10] A. B. Smith, P. R. Fields, and A. M. Friedman, Phys. Rev. 106, 779 (1957).

[11] E. Segre, Phys. Rev. 86, 21 (1952).

[12] O. Buneman, T. E. Granshou, and J. A. Harvey, Canad. J. Res. 27A, 191 (1949).

[13] R. B. Leachman, Phys. Rev. 83, 17 (1951).

[14] R. B. Lechman, Phys. Rev. 87, 444 (1952).

[15] H. W. Schmitt and R. B. Leachman, Phys. Rev. 102, 183 (1956).

[16] E. P. Steinberg and L. E. Glendenin, Phys. Rev. 95, 431 (1954).

Received July 1, 1957

RECRYSTALLIZATION OF URANIUM BY THE ACTION OF CYCLIC HEAT-TREATMENT

A. A. Bochvar, G. I. Tomson, and N. T. Chebotarev

During cyclic heat-treatment in the temperature range 100-550° C with cycles of 50 second duration, recrystallization resulting in a refinement of the original microstructure occurs in uranium quenched from the γ-phase region, as well as in uranium annealed in the γ-phase and in cast uranium, not subjected to additional deformation. Recrystallization commences at places with maximum distortion of the crystal lattice.

In 1956-1957, papers [1-3] appeared, in which it was stated that polygonization occurs in uranium by the action of cyclic heat-treatment, resulting in the formation of subgrains or the breaking down of the original grains to smaller grains, differing in orientation by a few degrees only.

The present paper describes an investigation of the variation in microstructure of uranium, quenched from the γ-phase, uranium annealed in the γ-phase region and cast uranium in the process of cyclic heat-treatment in the temperature range 100-550° C with cycles of 50 second duration. Our observations show that recrystallization occurs during cyclic heat-treatment, a fact previously mentioned only in paper [4].

Brief Description of the Method

Cyclic heat-treatment of cylindrical uranium specimens, 5 mm in length and 5 mm in diameter, was carried out in an automatic apparatus, with induction heating and with the use of helium as a protective medium against oxidation [5].

Parameters of the cycle:

Upper temperature	540-550° C
Lower temperature	100° C
Mean rate of heating	22 deg/sec
Mean rate of cooling	25 deg/sec
Holding time at upper temperature	12-13 sec

Since the variation in microstructure of uranium with different impurity contents during cyclic heat-treatment had qualitatively the same character, the results of chemical analysis are not given.

The microstructure was revealed by electrolytic polishing in a solution of the following composition:

Glacial acetic acid	1 part
Saturated aqueous solution of chromic anhydride (specific gravity 1.50)	1 part
Water	2 parts

The x-ray photographs of the polished sections were made in RKU-86 cameras using cobalt radiation.

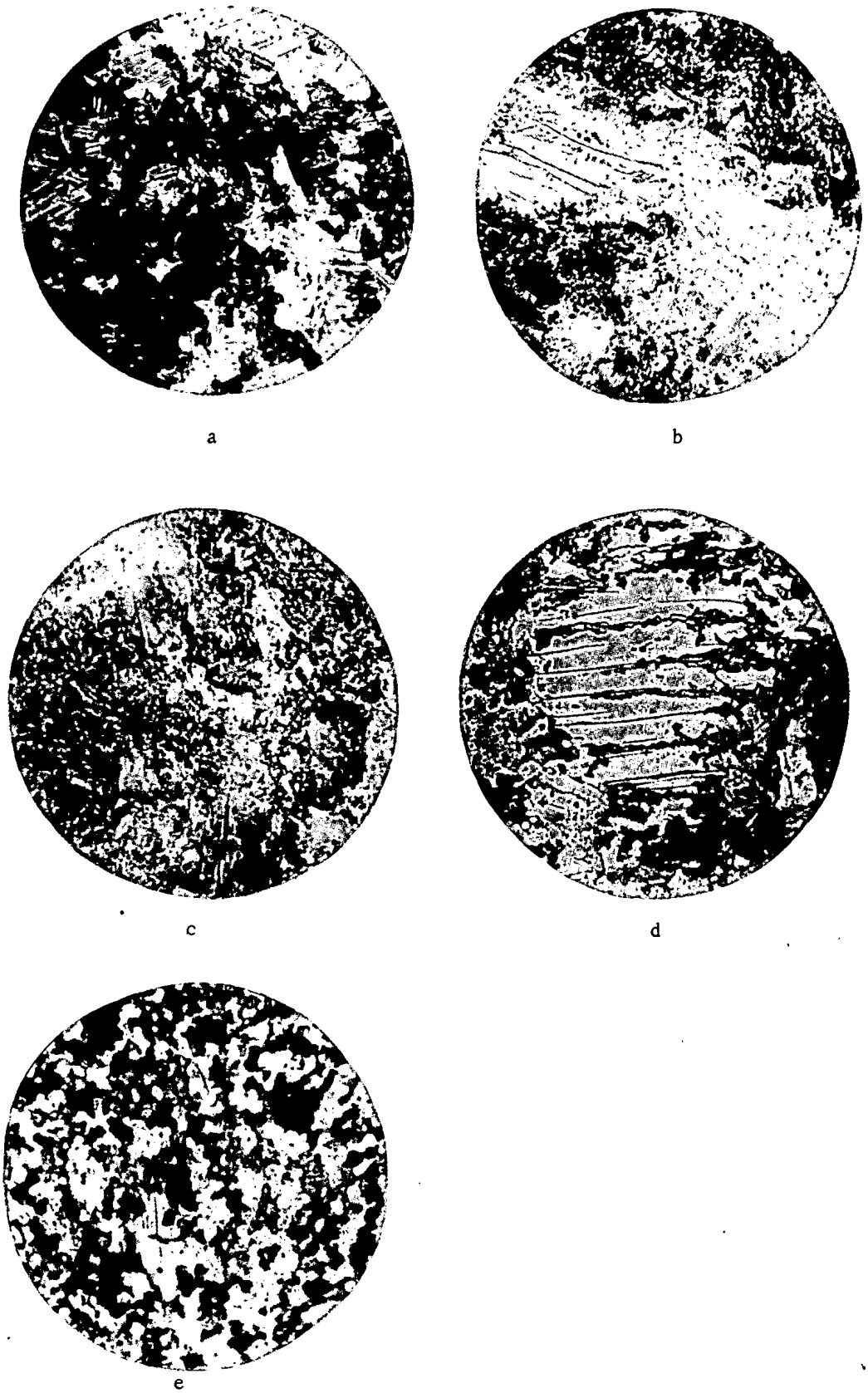

Fig. 1. Variation in microstructure of quenched uranium by the action of cyclic heat-treatment. a) Specimen before cyclic heat-treatment (x 70); b, c) specimen after 450 cycles (x 70); d) specimen after 450 cycles (x 200); e) specimen after 2000 cycles (x 200).

EXPERIMENTAL DATA

Metallographic examination of the specimens before and after cyclic heat-treatment showed that in uranium quenched from the γ-phase region recrystallization occurs by the action of the thermal cycles, resulting in a considerable refinement of the original structure. Figures 1, a-e show the variation in microstructure of quenched uranium with the number of cycles.

For comparison of the data characterizing the effect of cyclic heat-treatment on the microstructure of quenched uranium with the results of corresponding isothermal annealing, a number of quenched specimens were annealed at a temperature of 550° C for 5 hours 30 minutes. This annealing time corresponded to the time at which the specimens remained at a temperature of 540-550° C in the course of 1500 cycles. As will be seen from Fig. 2, showing the same place before and after isothermal annealing * no appreciable change took place in the microstructure.

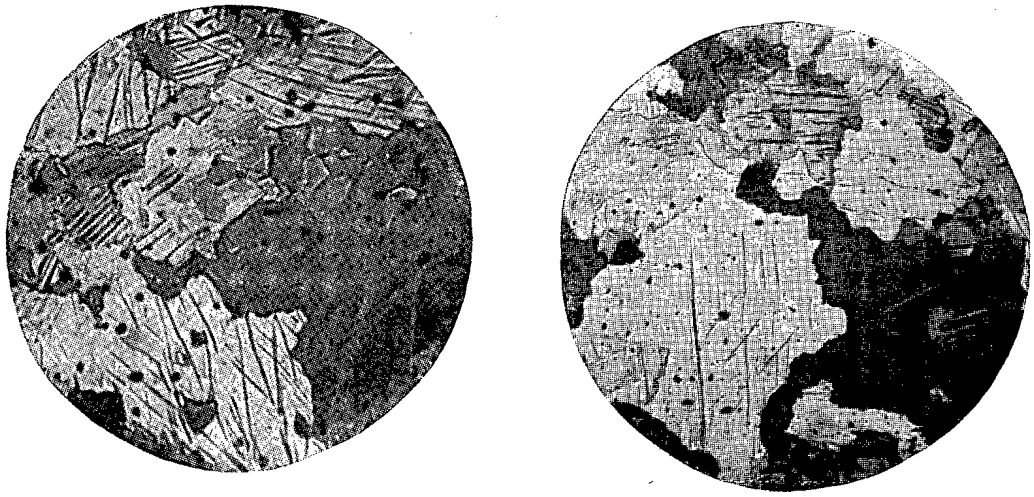

a b

Fig. 2. Microstructure of quenched uranium before and after isothermal annealing at 550° C for 5 hours 30 minutes (× 200). a) Specimen before isothermal annealing; b) specimen after isothermal annealing.

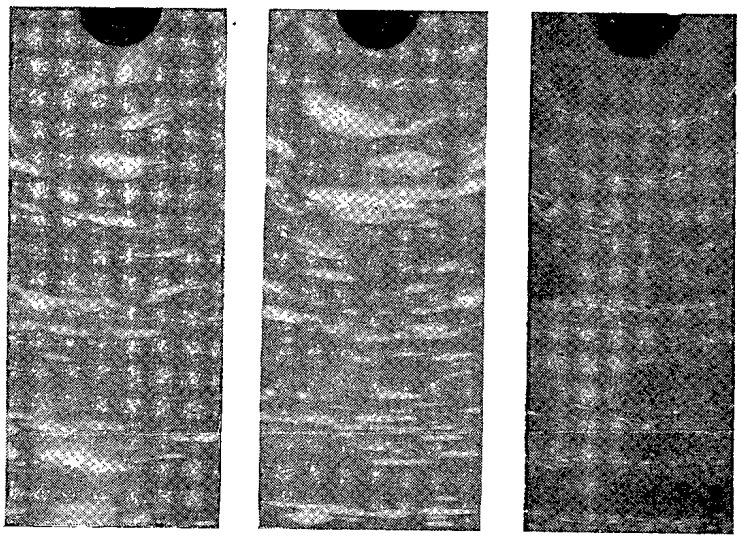

a b c

Fig. 3. X-ray photographs of quenched uranium. a) Initial condition; b) condition after isothermal annealing at 550° C for 6 hr 30 min, c) condition after 1800 cycles in the range 100-550 ° C.

* After isothermal annealing, the specimen underwent additional electropolishing and etching.

Recrystallization of quenched uranium by the action of cyclic heat-treatment is also clearly revealed by the method of x-ray structural analysis. Figure 3 shows x-ray photographs of three specimens of uranium containing approximately 0.1% carbon after a) quenching, b) additional isothermal annealing at 550° C for 6 hr 30 min and c) 1800 cycles.

Comparison of the x-ray photographs shows that the grain size remains practically unaltered after isothermal treatment, whereas there is considerable grain refinement after cyclic heat-treatment.

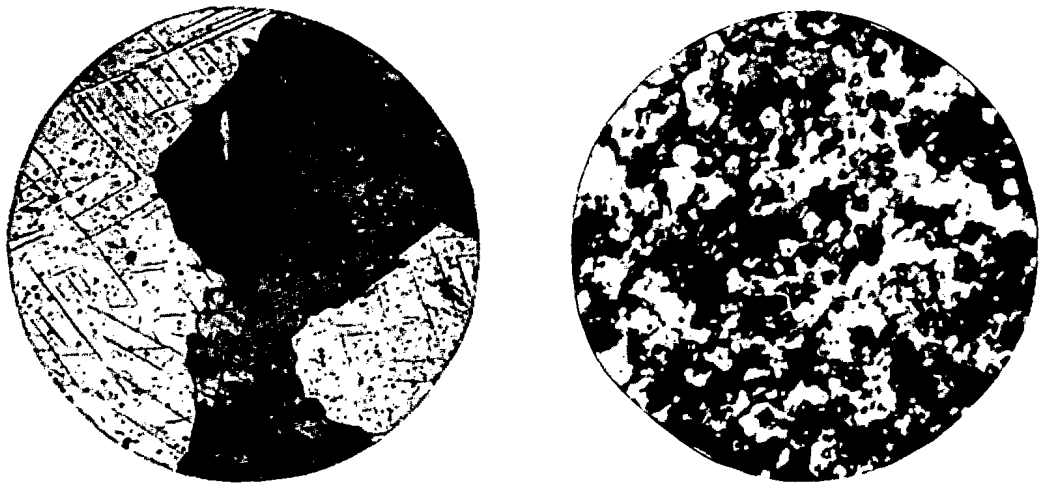

a b

Fig. 4. Variation in microstructure of uranium annealed in the γ-phase by the action of cyclic heat-treatment. a) Specimen before cyclic heat-treatment (x 70); b) specimen after 2000 cycles (x 200).

Uranium annealed in the γ-phase region (annealing temperature 850° C, rate of cooling 1.5 deg/min), likewise recrystallizes by the action of cyclic heat-treatment. Figure 4 shows the microstructure of this uranium before and after cyclic heat-treatment.

The photomicrographs shown in Fig. 5 illustrate the structural changes in cast uranium by the action of cyclic heat-treatment, and show evidence of considerable recrystallization of the uranium.

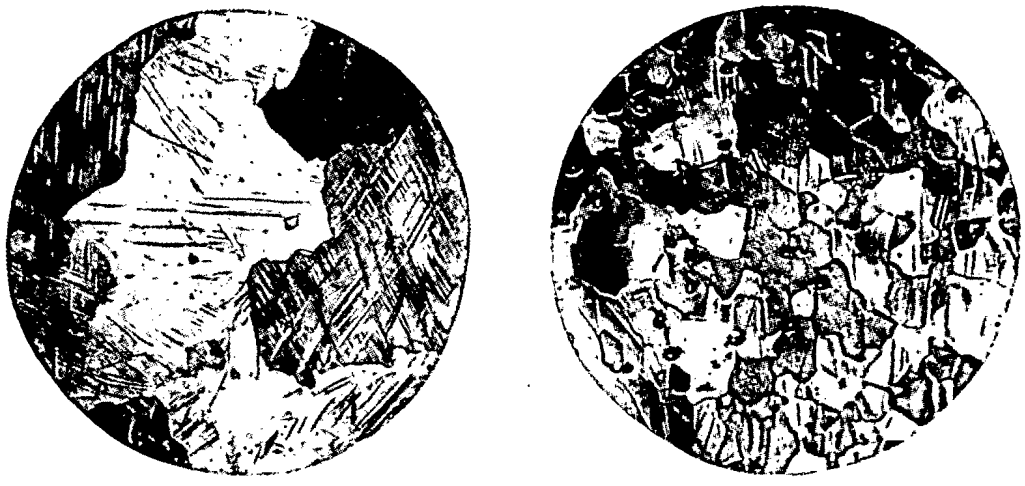

a b

Fig. 5. Variation in microstructure of cast uranium by the action of cyclic heat-treatment. a) Specimen before cyclic heat-treatment (x 70); b) specimen after 1800 cycles (x 200).

Thus, in the conditions specified above, cyclic heat-treatment provides conditions which facilitate the process of recrystallization of uranium quenched or annealed in the γ-phase region and also of cast uranium of different degrees of purity.*

Recrystallization of uranium by the action of thermal cycles commences along the shear twins and lines and also along the grain boundaries (Fig. 1, c, d) that is to say, at the places where the crystal lattice is strongly distorted. This is in agreement with the widely accepted viewpoint of the places of origin of recrystallization centers.

Quenching stresses do not determine the character of the variation in microstructure by the action of cyclic heat-treatment, since the observed character of the variation in microstructure is the same in quenched uranium as in annealed uranium.

The original grain size evidently has some effect on the rate of the recrystallization process by the action of cyclic heat-treatment. Thus, in Fig. 1, c, a large grain in which the recrystallization process has just commenced stands out on a background of fine-grain recrystallized structure. Some reduction in the recrystallization rate was also observed in coarse grain uranium annealed in the γ-phase.

LITERATURE CITED

[1] H. H. Chiswik and L. Kelman, Nuclear Power Metallurgy and the Action of Irradiation on Materials (Papers read by Foreign Scientists at the International Conference on the Peaceful Uses of Atomic Energy) (Metallurgy Press, 1956), p. 612.

[2] F. Foot, Ibid., p. 89.

[3] H. H. Chiswik, Trans. Amer. Soc. Metals 49, 622 (1957).

[4] B. W. Mott and H. R. Haines, J. Inst. Metals 80, 621 (1952).

[5] A. A. Bochvar and G. I. Tomson, J. Atomic Energy (USSR) 2, 6, 520 (1957).**

[6] J. Bloch, Acta Metallurgica 6, (2), 126 (1958).

Received March 18, 1958

* In the article [6], it is pointed out that recrystallization of uranium also occurs by the action of irradiation.
** Original Russian pagination. See C. B. Translation.

TISSUE DOSES OF FAST AND ULTRA-FAST NEUTRONS

M. I. Shal'nov

An investigation has been carried out of depth doses in irradiation of tissue-like dummies (water, paraffin) with broad beams of fast and ultra-fast neutrons generated in the 1.5 meter cyclotron by bombarding a thick beryllium target with deuterons accelerated to 13 Mev (the reaction $Be^9(d, n)B^{10}$) in the six-meter synchrocyclotron by bombarding a thick copper target with deuterons accelerated to 280 Mev (deuteron stripping reaction), and in the six-meter synchrocyclotron by bombarding a beryllium target with protons having an enervy of 480 Mev (proton charge-exchange reaction).

The results of the investigation, when applied to the case of irradiation of tissue with narrow and broad beams of monoenergetic neutrons, permit conclusions to be formed concerning depth doses with any spectrum of neutrons, and make possible the calculation of the mean tissue dose that can be used in comparative radiobiology. Moreover, data on attenuation of the dose of neutrons of various energies in hydrogen-containing media may be of help to the engineer in the construction of shielding.

Experimental and theoretical curves of the variation of the maximal tissue dose with hardness were obtained for broad and narrow neutron beams in the energy interval 0.1-500 Mev. These curves can be used for calibrating dosimeters.

Views are expressed concerning methods of approach to evaluation of the biological effectiveness of nuclear radiations, and to establishing the maximum permissible dose for man.

Tentative values are given for the maximum permissible neutron fluxes for man.

EXPERIMENTAL TECHNIQUES

For a precise determination of tissue doses of fast and ultra-fast neutrons, the depth distribution of absorbed energy was investigated in tissue-like media irradiated at the 1.5 meter cyclotron and the six-meter synchrocyclotron.

In the cyclotron, neutrons were generated by bombardment of a thick beryllium target with deuterons accelerated to 13 Mev ($Be^9(d, n)B^{10}$ reaction). The spectrum of neutrons thus formed has the following characteristics: a considerable fraction of the neutrons have energies from 2.5 to 5 Mev; in the region from 5 to 13 Mev, the number of neutrons per unit interval of energy falls off in proportion to $e^{-0.434E}$ [1]. The mean energy of the neutrons is 5.6 Mev.

The average intensity of the neutron beam at a distance of 100 cm from the target was $2 \cdot 10^{-7}$ neut/cm^2 per sec. The reaction $Be^9(d, n)B^{10}$ is accompanied by γ-radiation having several lines of different intensities in the region of the spectrum from 0.72 to 7 Mev, corresponding to the energy levels of the excited B^{10} nuclei. γ-photons are emitted with energies of 0.72 Mev (approximately 0.7 per neutron) and 5 Mev (approximately 0.97 per neutron) [3].

Irradiation with the cyclotron was carried out in the following manner. The dummy, made in the form of a rectangular parallelepiped 30 x 30 x 42 cm out of paraffin blocks 30 x 30 cm with a thickness of 2 and 5 cm, was placed in the path of the external beam – between the cyclotron chamber and the fixed yoke of the magnet toward which the beam was directed. The neutrons fell on a surface 30 x 30 cm , at right angles to it. Back-scattering of neutrons from the iron yoke of the magnet was important only at large depths within the dummy and was taken into account in analyzing the results of the measurements.

The measurements were conducted with the help of small ionization chambers with condensers, placed in compartments in six blocks, five to a block, each block being at a different depth along the path of the beam. Thus, 30 chambers were exposed at once, permitting readings to be taken in 30 points at six different depths, for one exposure. This insured great accuracy in the measurement of the relative depth doses in each exposure. The materials of the walls of the chambers (bakelite) and the condenser (styroflex) were close to paraffin in hydrogen content, so that the presence of the chambers could not appreciably affect the distribution of neutrons in the dummy. The contribution of the γ-background to ionization was taken into account by the method of differential measurements. For this purpose, aluminum chambers were used alongside the bakelite chambers; these had the same sensitivity to electromagnetic radiation (200 kev and 1.3 Mev) as the bakelite chambers. In the differential method of measurement, the dose resulting from external γ-radiation was excluded, as well as that due to γ-radiation resulting from neutron capture in the paraffin; only the biologically most effective component of the recoil protons and heavy nuclei was considered. The calibration of the bakelite chambers for neutrons was carried out with the help of a Po + Be-source. It has been shown experimentally and theoretically that ionization of 1 cgs unit/cm^3 in an air cavity corresponds to 85 erg/g energy absorbed in hydrogenous material. Thus, the ionization in the bakelite chambers (after allowing for the ionization from γ-background), produced mainly by recoil protons ejected from the walls, could serve as a measure of the absorbed energy of the neutrons at any depth of the irradiated dummy. The ionization current in the chambers was determined from the reduction in the charge on a fixed condenser, using a "Sosno" commercial unit to measure charge.

In experiments on the synchrocyclotron, two neutron spectra were used: the spectrum of the stripping reaction (d, n) in a thick copper target (E_d = 280 Mev) and the charge-exchange spectrum of the reaction (p, n) in a beryllium target (E_p = 480 Mev).

The neutron spectrum of the former reaction is well described by the theory of Serber, and is characterized by maximum neutron emission at the energy $E = E_d/2$.

The mean energy of stripping neutrons was 140 Mev, and of charge-exchange neutrons was approximately 380 Mev.

The neutron flux in the first case was approximately $2 \cdot 10^7$ neutrons/cm^2·sec at 250 μa and a distance of 2 m from the target (along the axis of the beam); in the second case, the flux was about $8 \cdot 10^6$ neutrons/cm^2·sec at the same distance.

Exposure of the dummies was carried out as follows. Cylindrical containers filled with water were situated at a distance of 6-10 m from the target along the axis of the emerging electron beam. With the help of thimble chambers, immersed in water, and made of hydrogen-containing material, ionization measurements were conducted at different depths along the path of the beam. Containers having diameters of 10, 20, and 30 cm and a height of 30 cm were used in different experiments. Similar measurements were carried out in the paraffin dummy described earlier. Holes were drilled in one of the blocks for an ionization chamber. This block, together with the chamber, was placed at various depths along the path of the beam. Thimble chambers and a condenser were also used. The ionization current was measured with the aid of RIP and "Pion" commercial x-ray meters. To monitor the variations of intensity during irradiation, a supplementary instrument with an ionization chamber (monitor) was used, the readings from which supplied corrections that were introduced into the fundamental measurements.

Calibration of the chambers showed that an ionization of 1 cgs unit/cm^3 in air corresponds to the same quantity of absorbed energy as in irradiation with fast neutrons: 85 erg/g.

Depth measurements using wide neutron beams permitted us to estimate the contribution of multiple neutron scattering to the tissue dose (accumulation factor), and to form a definite idea of the distribution of depth tissue doses under these conditions. Tissue doses were expressed in erg/g, referred to a standard flux of 10^6 neutrons/cm^2.

EXPERIMENTAL RESULTS

In Fig. 1, experimental curve 1 represents the depth tissue doses according to the results of measurements in paraffin irradiated from the cyclotron with neutrons having a mean energy of 5.6 Mev. This curve shows the reduction in the tissue dose with depth [see Equation (1)] as a result of neutron absorption by the dummy material and divergence of the beam according to the inverse square law

$$W^*(x) = \frac{BW(0)}{(R+x)^2} e^{-x/L}, \qquad (1)$$

where x is the depth in cm; R is the distance from the target (in this case, 100 cm); L is the relaxation distance in cm (L = 11.6 cm); W(0) is the neutron energy in erg/g, absorbed at the surface with a narrow beam; B is the accumulation factor, taking into account the contribution of multiple neutron scattering.

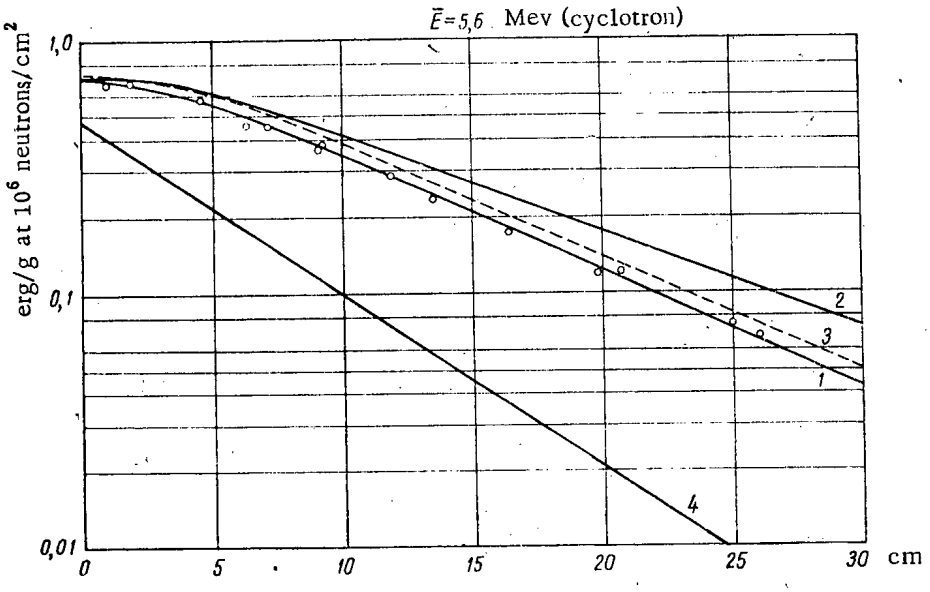

Fig. 1. Experimental and theoretical curves of depth tissue doses for a wide neutron spectrum ($\bar{E}$ = 5.6 Mev).
1) Experimental curve; 2) theoretical curve, on the assumption that R ≫ x = = 30 cm; 3) curve obtained by normalization, according to the spectrum of Tait's theoretical curves; 4) theoretical curve for a narrow beam of wide-spectrum neutrons.

The value of B that satisfies the experimental data is $2.14\,(1-0.3\,e^{-x/3})$. At the surface of the object (where x = 0) B = 1.5; at depths beyond 15 cm, B = 2.14. At large target-to-object distances (R ≫ x), where the divergence of the beam can clearly be neglected, curve 1 (Fig. 1) can be replaced by curve 2, for which the quantity $\frac{W(0)}{(R+x)^2}$ expresses the dose at the surface with a wide parallel beam of neutrons. Tait [4] has investigated the theory of depth tissue doses for wide parallel beams of monoenergetic neutrons in the energy interval from 0.5 to 5 Mev.

The depth doses for wide monoenergetic beams, calculated in Tait's work [4], may be approximated by an expression similar to Formula (1), with $B = 1.58\,(1-0.365\,e^{-x/3})$. By adjusting Tait's theoretical curves for the cyclotron spectrum, we obtained curve 3, which differs slightly from our experimental curve 2. This served as a basis for the choice of an expression satisfying the values of depth tissue doses for wide beams of monoenergetic neutrons:

$$W^*(x) = W(0) \cdot 2{,}37\,(1 - 0{,}365 \cdot e^{-x/3})\, e^{-x/L}, \qquad (2)$$

where W(0) is the dose at the surface for a narrow beam of monoenergetic neutrons (without regard for multiple collisions), which is determined as the product of the incident neutron flux Π times the mean energy of the ionization particles formed as a result of nuclear processes, $\Sigma n_i \sigma_i \overline{E}_i$, where n_i is the number of atoms of some element per cm^3 of tissue, σ_i is its neutron reaction cross section, and $\overline{E}_i$ is the mean energy of the ionizing particle: $W(0) = \Pi \Sigma n_i \sigma_i \overline{E}_i$. When $\Pi = 1$ neutron/cm^2, $W(0) = \Sigma n_i \sigma_i \overline{E}_i$ Mev/cm^3 (or erg/cm^3).

For neutrons of various energies, W(0) has the values cited below:

Neutron energy, Mev	0,5	1	2	5	10	15
$W(0)$ Mev/g at 1 neutron/cm^2 10^{14}	0.1	0.15	0.20	0,30	0,38	0,40

The relaxation length L, for a wide neutron beam in the energy interval 0.5-15 Mev, is given with sufficient accuracy by the relationship $L = l/0.7$, where is the relaxation length for a narrow neutron beam, which in tissue-like media is taken as equal to $2.8 \cdot E^{0.5}$ (E in Mev, l in cm).

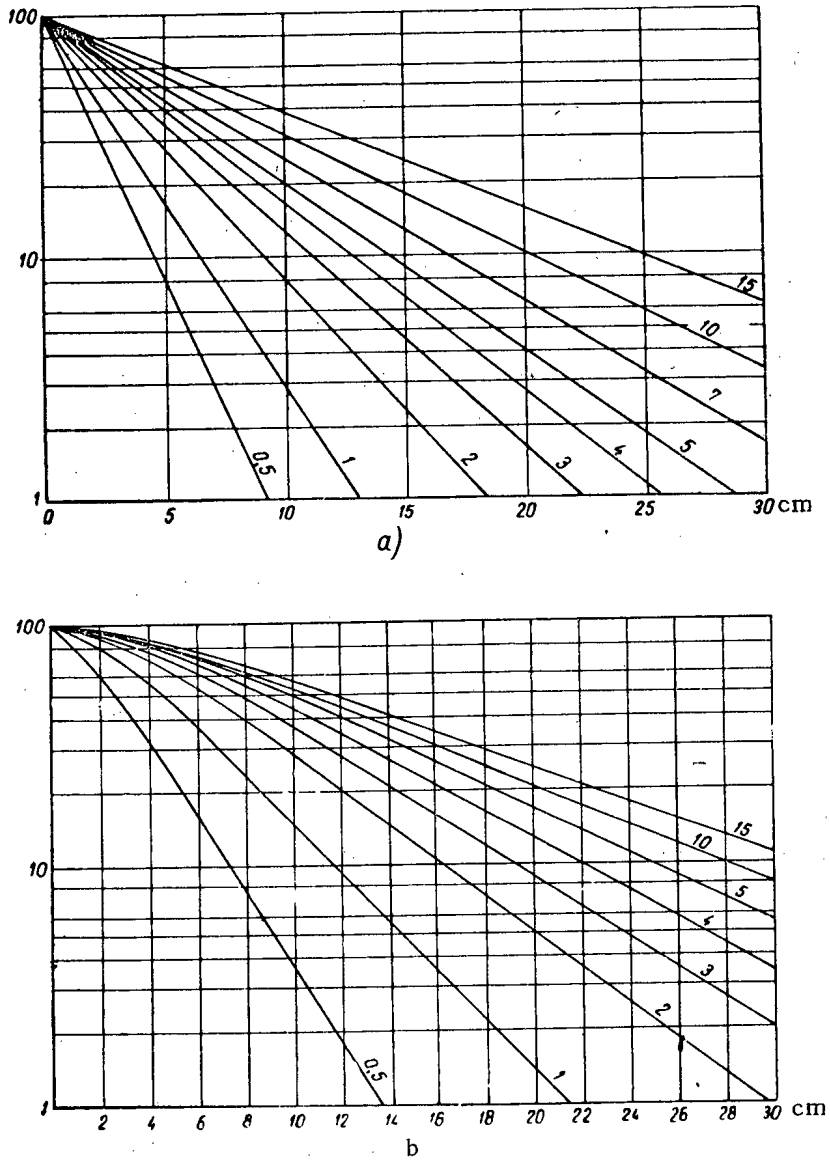

Fig. 2. Depth tissue doses for narrow (a) and wide (b) beams of monoenergetic neutrons with energies from 0.5 to 15 Mev.

The relative depth tissue doses for narrow beams of monoenergetic neutrons, characterized by exponentials, and for wide neutron beams, calculated from Equation (2), make possible the determination of depth tissue doses of neutrons for any spectrum in the interval 0.5-15 Mev (Fig. 2).

For objects having sufficient thickness (e. g., 30 cm, as in our case), the assumption that the accumulation factor B equals 1.5 at the surface may be considered reasonable. The values obtained theoretically [4] and experimentally [5, 6] are close to this value. If we set the narrow-beam surface doses equal to unity, then according to Tait the coefficients of increase for the surface dose for corresponding wide beams of monoenergetic neutrons will be:

Energy, Mev	Coefficient of increase of dose at surface
0.5	1.25
1.0	1.20
2.0	1.15
3.0	1.20
4.0	1.32
5.0	1.25

Experimental curves of the deep distribution of absorbed energy of ultra-fast neutrons having average energies of 140 and 380 Mev are set forth in Fig. 3, a and b.

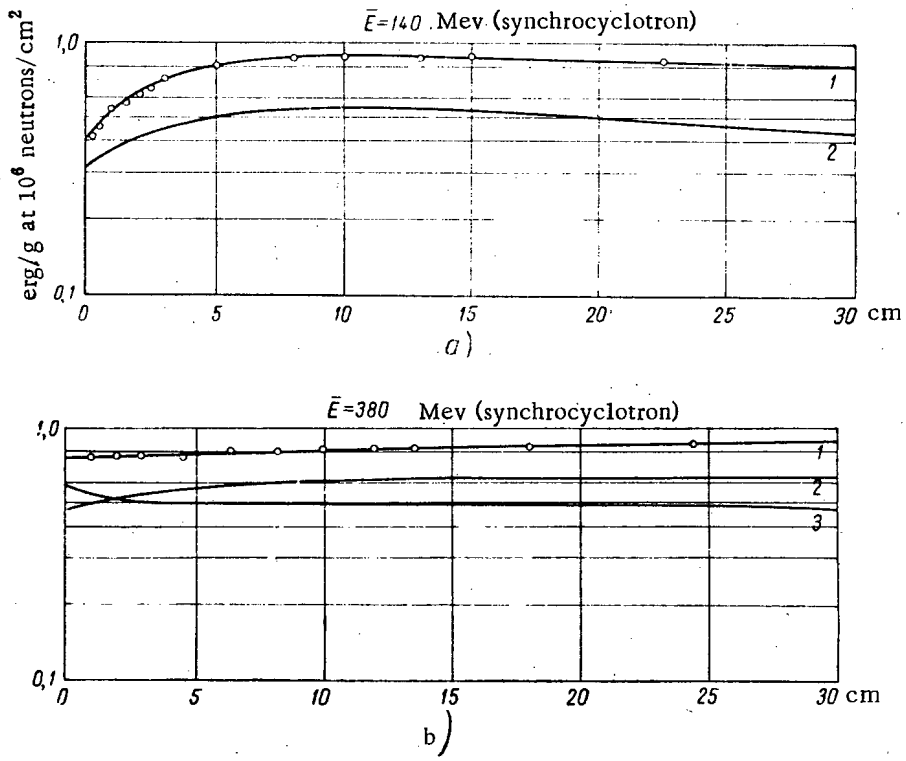

Fig. 3. Experimental (1) and theoretical (2, 3) curves of depth tissue doses of ultra-fast neutrons: a) for deuteron splitting spectrum (E = 140 Mev), b) for proton charge-exchange spectrum (E = 380 Mev).

The results of measurements in water dummies where $\bar{E}$=140 Mev showed that the difference between doses at the surface and at depths up to 10 cm, in dummies of 10, 20, and 30 cm in diameter at the same points (0.25,

0.5, 1.0, 1.5 cm etc.), were not very large, and fell within the experimental error. Therefore, in Fig. 3, a the points of curve 1 up to a depth of 10 cm are for averaged experimental values for these dummies. In measurements with the paraffin dummy, its over-all thickness remained constant and equal to 42 cm.

We may consider the depths of water and paraffin employed to have been sufficiently great that multiple scattering even of ultra-fast neutrons would be effective at surface and depth doses.

In consequence of the fact that exposure was carried out at a great distance from the target (6-10 m), the incident neutron beam can be regarded as parallel. Curves 2 and 3 in Fig. 3, b, lying below curve 1, were obtained on the basis of a calculation of the absorbed energy of recoil protons and protons and deuterons from spallation — which was determined by means of numerical integration (with respect to depth) of Expression (3), taking into consideration: a) relaxation length of neutrons for single collisions with nuclei of tissue atoms, b) spectra of secondary particles, and c) energy losses of particles in the tissue:

$$W_i(x) = W_i \int_0^x e^{-x/l} dx \int_{E_{i\xi}}^{E_{i\max}} \sigma(E_i)\, dE_i d\xi, \qquad (3)$$

where x is the depth in cm from the surface of the dummy; ξ is a depth equal to x — r (r is the range of the particle); l is the relaxation length for single collisions, in cm^{-1}; $\sigma(E_i)$ is a function characteristic of the spectrum of the particles; $E_{i\xi}$ is the energy of particles with the range $r = x - \xi$; $E_{i\max}$ is the maximum energy of particles in the spectrum; and W_i is a normalizing factor.

Information about the spectra $\sigma(E_i)$ of particles from recoil and spallation were obtained by us from data in the literature [7-10]. The energy absorbed at various depths, of recoil C, N, and O nuclei, was calculated as the exponential $W_i e^{-x/l}$, determined only by the relaxation length l of narrow-beam neutrons.

From the results of calculations for narrow beams of neutrons with energies of 40, 90, 220, and 380 Mev, depth dose curves were plotted (Fig. 4), which made it possible, by means of linear interpolation and extrapolation, to extend our conception of depth doses to neutrons of any energy in the interval from 40-500 Mev. First values of the absorbed energy at the maximum were found (Fig. 5, curve 1), after which a family of curves was obtained characterizing the distribution of depth doses as a percent of the maximal dose (Fig. 6). Normalization of the whole family of curves according to the spectra obtained in the experiments and according to the absolute values at the absorption maximum served as a foundation for constructing curves 2 and 3 of Fig. 3. As a criterion of the reliability of the depth doses expressed by these curves, we may take the total and differential profiles of n — p scattering taken for energies of 40, 90, 220, and 380 Mev; n — p scattering has now been studied with great accuracy and makes the largest contribution to the dose (Fig. 4). The fact that the experimental values exceed the theoretical reflects the contribution of multiple scattering of neutrons to the absorbed energy (accumulation factor, equal to 1.5 in this case also).

The agreement of the mean value of the accumulation factor for the dose of ultra-fast incident neutrons in the wide beam with the corresponding value of the factor for fast neutrons with dummies of 30-40 cm thickness is entirely natural. For broad beams of monoenergetic neutrons it was assumed that up to energies of 140 Mev they give a distribution of depth doses somewhat different from the distribution for narrow beams (Fig. 6), but at energies > 140 Mev they give the same distribution as for narrow beams.

On the basis of the constancy of the accumulation factor over the whole energy interval under consideration, for fast and ultra-fast neutrons, a curve of values of maximum doses was plotted for broad neutron beams (curve 2, Fig. 5).

The curve of maximum values of the tissue dose for broad neutron beams can be used in practice for calibrating dosimeters. All instruments for measuring the dose in air in roentgens equivalent physical (REP) must meet the requirement (in the absence of an irradiated object, where neutrons interact only with the material of the instrument) that the instrument have the same variation with hardness in the working interval of neutron energies as the tissue. A second requirement is that the depth doses in the tissue be distributed in the same manner at these energies as under conditions of irradiation with x- or γ-rays. In neutron dosimetry these requirements are substantially met up to 15-20 Mev, i.e., up to those energies at which the maximum tissue dose is produced at the surface of the object. At higher energies, measurement of the neutron dose is best done in absolute units (erg/cm^3).

In calibrating dosimeters from the maximal tissue doses (curve 2, Fig. 5) one must not forget that such a calibration does not meet the requirements of experimental radiobiology. In calibrating dosimeters for measuring irradiation doses to animals, suitable corrections must be introduced.

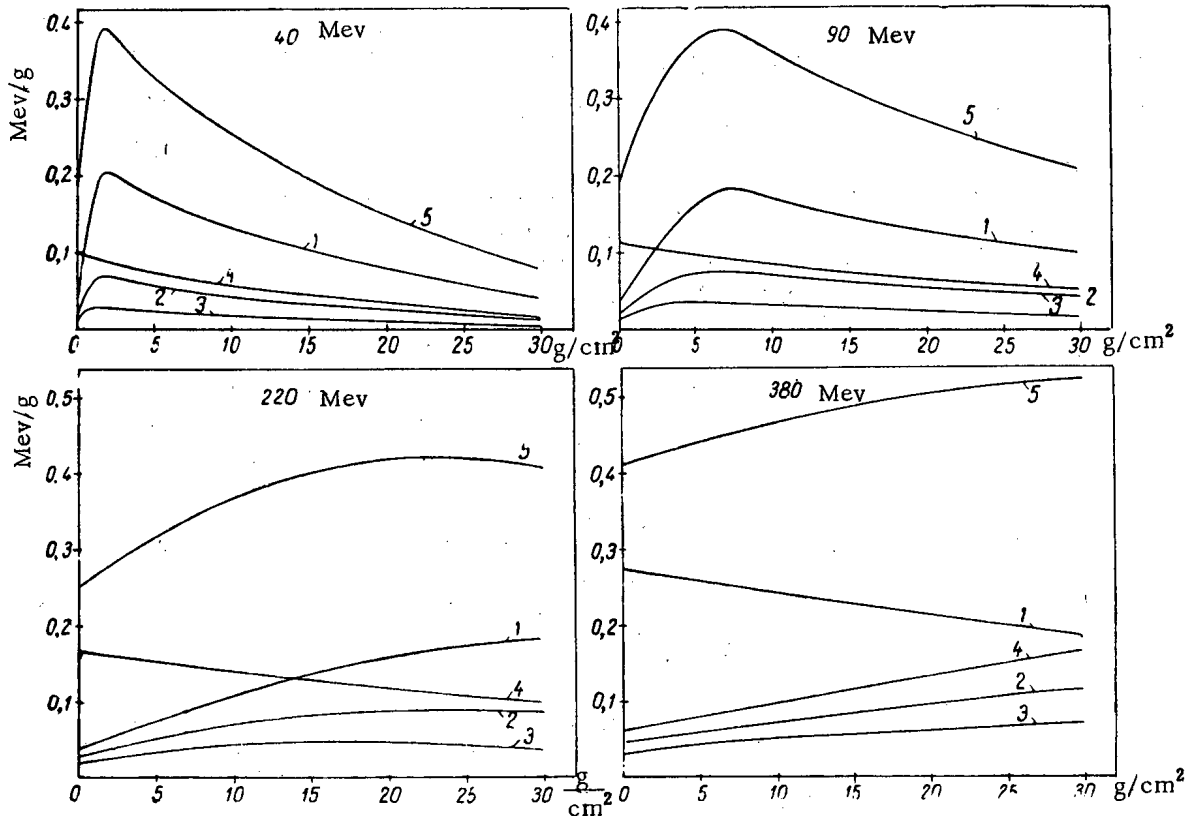

Fig. 4. Depth tissue doses, calculated in absolute units (Mev/g) for narrow beams of monoenergetic neutrons with energies of 40, 90 220, and 380 Mev for unit incident fluxes. 1) Recoil protons; 2) spallation protons (total for C, N, and O nuclei); 3) spallation deuterons (total for the same nuclei) 4) recoil C, N, and O nuclei; 5) cumulative curve of absorbed energy.

To compare the biological action of neutrons with the action of any other form of radiation (e.g., x- or γ-rays) a comparable dosimeter quantity in total-body irradiation is the mean tissue dose, expressed in the same units, best of all in absolute units of absorbed energy (erg/g). The mean tissue dose is defined as the ratio of the total energy absorbed by the object to its mass. Under conditions of different hardness, the mean tissue dose is measured by highly cumbersome methods; study of the depth distribution of absorbed energy in a tissue-like dummy is a necessary step in these measurements.

Let the mean tissue doses of all layers of the object being irradiated be distributed as the values of the function $\overline{W}(x)$. These values may lie close to the distribution curve of depth doses along the axis of the beam, or below the curve (but not above it). In this and other cases, the mean tissue dose can be expressed by the equation

$$\overline{W} = \frac{1}{a}\int_0^a \overline{W}(x)\,dx, \tag{4}$$

where a is the actual or effective thickness of the biological object.

If the values of $\overline{W}(x)$ are close to the depth doses along the axis of the beam, then $\overline{W}(x)$ is replaced by $W^*(x)$ from Equation (2) or from graphs reflecting the same dependence.

The investigation of deep doses of ultra-hard γ-radiation in paraffin at maximal γ-quanta energies of 80, 150, and 250 Mev, generated in the synchrotron, show that the distribution of these doses is almost the same as that from neutrons with energies of 100, 140, and 170 Mev, respectively. In these cases, it is possible to compare

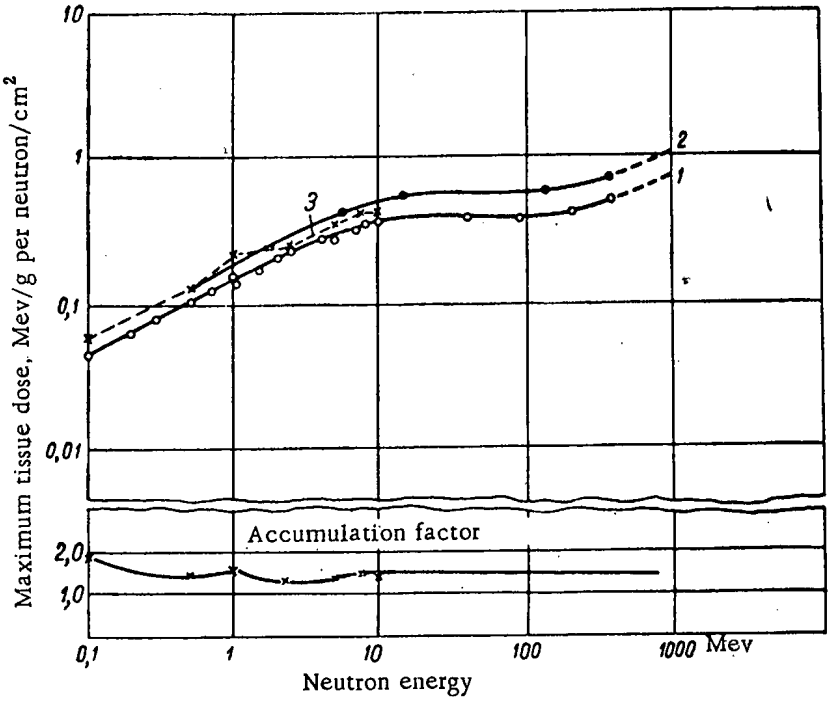

Fig. 5. Dependence of maximum tissue dose on neutron energy (for an object of 30 cm thickness).
1) For a narrow neutron beam; 2) for a broad neutron beam; 3) for a broad neutron beam, according to Snyder [11].

the biological effect of hard bremsstrahlung with that of ultra-fast neutrons on the basis either of maximal or of mean tissue dose. But in the majority of cases, where no such similarity is observed, the mean tissue dose is the sole criterion for comparing the biological effectiveness of radiations.

The Biological Effectiveness of Neutrons and the Maximum Permissible Dose

The following radiobiological data are the main source of our information for establishing the coefficient of relative biological effectiveness (OBE) of one type of radiation in comparison with another:

a) curves of survival of animals as a function of radiation dose of a particular type, where the OBE is defined as the ratio of the LD-50/30 for radiations of two different types;

b) curves of the mean survival time as a function of the dose of a particular type of radiation;

c) reduction of the latent period before the appearance of some biological effect, in chronic irradiation with small doses. In this case the time of appearance of certain remote consequences of irradiation — e.g., cataract or cancer — during the life of the animal can be considered.

The most reliable of these statistically are data concerning the comparative magnitudes of the LD-50/30.

In our experiments on acute irradiation of animals, from a comparison of the LD-50/30 for neutron and x-ray radiation, coefficients of relative biological effectiveness are obtained, equal to 3-4 in the case of neutrons having a mean energy of 5.6 Mev, and about 2 for neutrons of 140 Mev mean energy (Fig. 7). If

coefficients of relative biological effectiveness could be used in establishing the maximum permissible doses for chronic neutron irradiation in man, then an estimate of the maximum permissible intensity of neutron beams could be made directly on the basis of curve 2, Fig. 5. But the experimental coefficients cited above characterize the relative biological effectiveness of neutrons only for cases of single, acute exposure, whereas the maximum permissible dose for man must be defined with regard for the sharp increase in the biological effectiveness of neutrons in the case of chronic exposure to small doses. As the experiments indicate, the consequences of the

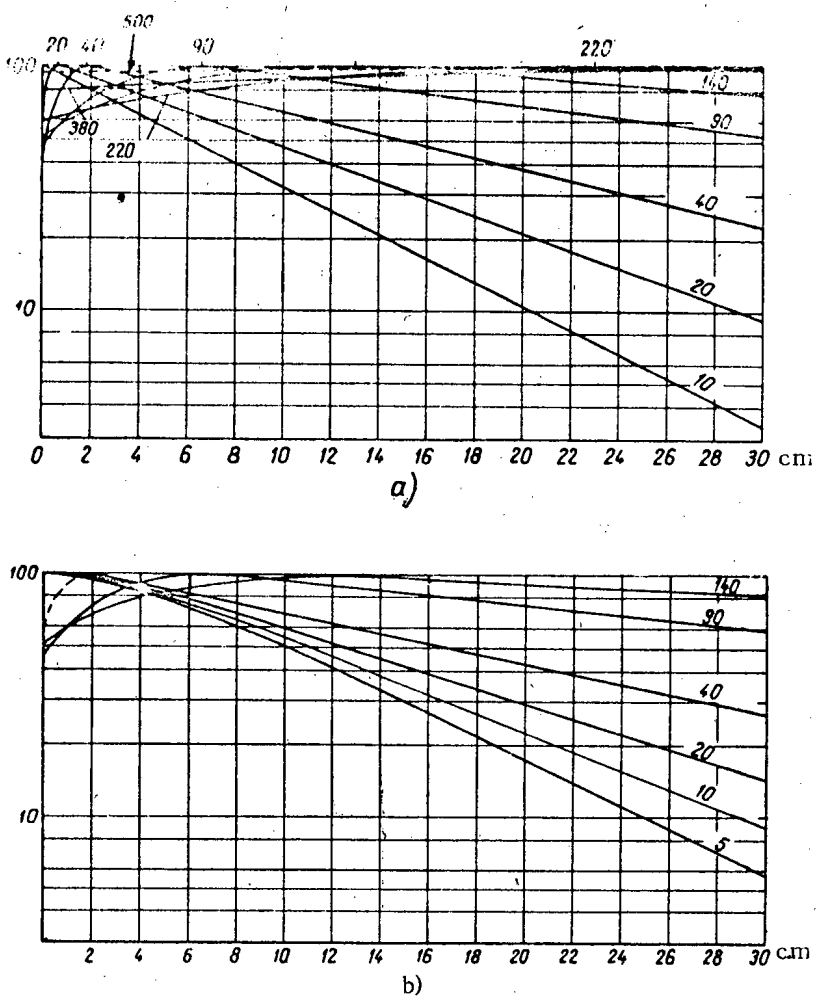

Fig. 6. Depth tissue doses of neutrons (percent of maximum dose): a) for narrow beams; b) for wide beams. (Figures on curves represent neutron energy in Mev.

chronic action of small doses (10-30 REP/day) are more striking than the effects of acute exposures. It is fully possible that the early death of the animals in acute exposures does not permit the development of those symptoms which are observed in chronic irradiation. The increase in the biological effectiveness of neutrons as compared with electromagnetic radiations takes the form of a shortening of the times of appearance of the late effects of irradiation. Thus, for example, at the ordinary level of neutron background (approximately 0.05 REP/day) the symptoms of cataract can be observed in persons working with neutron sources as early as the fifth or sixth year of work.

For the "remote consequences of irradiation" a special criterion of biological effectiveness must be employed, which should be defined not by the ratio of the neutron and x-ray doses that cause the same effect, but by some other mathematical quantity.

In radiation chemistry and in radiobiology, the concepts of "incubation period" and "latent period" are widely used. An adequate mathematical concept is the "expectation time," defined by the probability function

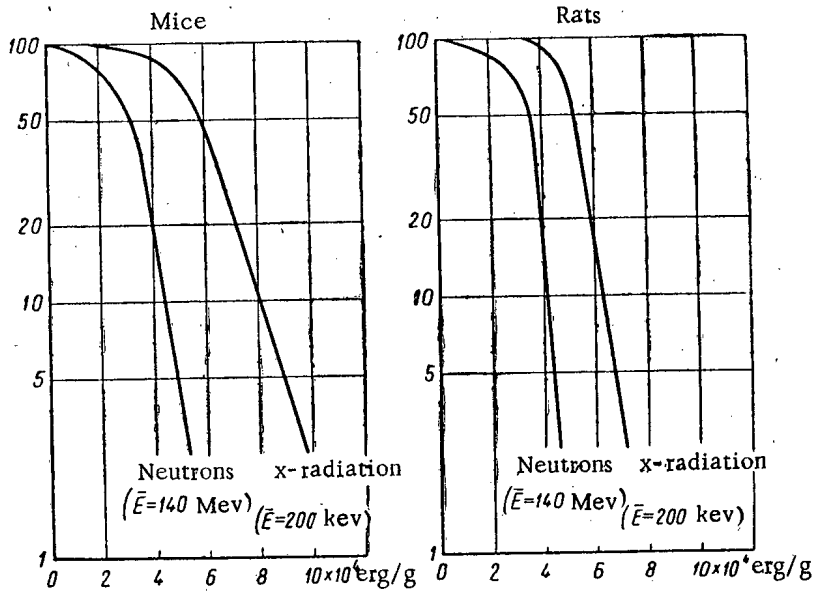

Fig. 7. Survival of animals, as a function of doses of x-radiation and of ultra-fast neutrons.

$t = \tau e^{\epsilon/kT}$, which was very successfully used by Schrödinger [12] to define the expectation time of spontaneous mutations during normal functional activity of an organism. Here τ corresponds to the order of magnitude of the period of molecular fluctuations of the biological system, and ϵ to the energy threshold that must be reached during time t due to thermal motion with the energy kT. For warm-blooded animals (T = 308° K), $\overline{kT} = 0.0267$ ev, $\tau = \frac{1}{\nu} \approx 1.5 \cdot 10^{-13}$ sec. According to Schrödinger, the function $t = \tau e^{\epsilon/kT}$ is a measure of the improbability that an amount of energy equal to ϵ can accumulate by chance in some definite part of the system with a given kT, and the factor τ indicates that although the probability of accumulating the required amount of energy ϵ is very small, it recurs "at each vibration," i.e., about 10^{13} times every second.

Radiation may affect the magnitude of t directly by lowering the energy threshold ϵ for an unfavorable transition, which becomes equal to $\epsilon - \Delta\epsilon$ (where $\Delta\epsilon$ is the radiation energy received by the molecule); or it alters the "characteristic frequency" of the system, i.e., $\frac{1}{\nu} = \tau$, producing disintegration of the molecule; in this case the increase in ν necessitates a reduction in τ.

The use of the probability function of the expectation time to describe the kinetics of radiation sickness in the latent period is entirely natural, since this function characterizes chain-type reactions, and the hypothesis of self-accelerating chain reactions in radiation sickness is currently finding more and more experimental confirmation [13].

Taking all this into account, we may consider that the reduction of the expectation time for unfavorable molecular transitions depends not only on the size of the maximal or mean tissue dose of this or that radiation, but also on the type of radiation. This explains the greater biological effectiveness of the chronic action of heavy charged particles as compared with that of electrons. Since the rate of appearance of the terminal effect of irradiation depends, in our opinion, on the constant action of thermal collisions of molecules, we can expect (other things being equal, e.g., with equal daily doses) that organism to go "out of commission" first in which the radiation energy is localized in processes more profoundly affecting organic structures, and specifically, in reaction with atomic nuclei. Primary physicochemical changes in organic structures under the influence of radiation can take the form, for example, of single rupturings of the most "fragile" intermolecular bonds and of

changes in molecular configurations. Then the frequencies of tautomeric transitions may increase, and the properties of prototropic substances may be altered.* Very little energy is required for these transformations; in comparison with this, the energy released in every ionization (approximately 30 ev) has the effect of the strongest explosion; it is quite possible that a small excitation would be enough to initiate all these transformations. Somewhat more energy is required to bring about stereoisomeric transitions, and still more (on the order of an electron-volt) for threshold isomeric transitions.

These physicochemical changes in living material lead to the distortion of many chemical processes, to a change in the direction of these processes.

Simultaneously with chain ionic transformations and radical tautomerizations, to which radiation imparts an irreversible character, under the influence of a heightened thermal disorder the formation of racemic mixtures goes on in the optically active protoplasm. The protoplasm loses its asymmetry. Substances essential to life, taking part in metabolism — proteins, carbohydrates, lipoids — which characteristically exist in the form of pure optical opposites, suddenly begin to undergo racemization. The formation of a racemic mixture is thermodynamically favorable, since this corresponds to the maximum entropy (disorder).

Continuing on the subject of the terminal effect, in establishing the maximum permissible dose it is necessary to consider not only the effectiveness of the primary event of the reaction, but also the reduction in the expectation time of harmful consequences, which is significantly reduced in neutron irradiation.

But as yet no observations are available of a sort that would make it possible to follow the accumulation of harmful radiation symptoms from generation to generation. So it is common to take an expectation time t equal to the average life span of a single generation. In this case, the biological effectiveness is connected only with the physical properties of the radiation, with the special features of its reaction with the material.

The linear ionization density is taken as the physical factor that determines the biological effectiveness of radiation exposure. In the general case, the biological effectiveness of nuclear particles at equal doses is a complicated function of the beam intensity (I, $cm^{-2} \cdot sec^{-1}$), linear energy losses of the particles (ϑ, erg/cm), and the cross-sectional area of the track (S, cm^2). At higher intensities of radiation ("high background level"), where superposition of the tracks occurs, the track cross section S apparently plays a lesser role. In this case the biological effect is proportional to the product $I\vartheta$, i.e., the intensity of the radiation dose. At a "low background level," ϑ and S appear to play the chief roles. For equal intensities and radiation doses, it can be assumed that the increase in the biological effect will be proportional to a certain quantity, equal to $\sqrt[3]{S\vartheta} = \sqrt[3]{\pi\rho^2\vartheta}$, where ρ is the track radius. The track radius formed in water by Compton- or photoelectrons is considered approximately equal to 15 mμ ($1.5 \cdot 10^{-6}$ cm), i.e., equal to the dimensions of organic molecules. Tracks formed by the heavier particles (protons, α-particles, etc.) have larger radii. For the probability of injuries at equal distances ρ from the axis of the track, the relative effectiveness of two types of radiation can be taken equal to the cube root of the ratio of their linear energy losses, i.e.,

$$\text{OBE} = \eta = \sqrt[3]{\vartheta_1/\vartheta_2}. \tag{5}$$

The energy losses per unit path length in the tissue for various particles can be estimated on the basis of concepts formulated by Rossi [14]. For any particles carrying unit charge and heavier than the electron, if only energy losses due to collisions are considered, the relation between energy and path length of the particle in air is illustrated by the very convenient curve

$$E/mc^2 = f(r/mc^2),$$

where E is the kinetic energy of the particle, mc^2 is the rest energy of the particle, and r is its range in air. For any particle of charge Z, at energies roughly half the rest energy ($E \leq 0.5\ mc^2$), the following relation holds between total path length and energy E:

$$r_i = \frac{0{,}51E_i^{7/4}}{(m_ic^2)\,Z_i^2}, \tag{6}$$

* Prototropic substances are tautomers with migrating protons.

where E_i is the particle energy in Mev, r_i is the particle path length in g/cm^2 of air. This relation is directly confirmed by the experimental data. Here the ranges r_i in g/cm^2 are expressed by E_i in Mev in roughly the same way for tissue-like substances as for air. Consequently, Relation (6) can be extended to tissue with complete justification.

This relation holds for electrons with energies up to 0.25 Mev and for protons with energies up to 500 Mev. For heavier particles it obviously holds at even higher energies.

On the basis of Equation (6), the mean energy losses ϑ per unit path length in the tissue will be given by

$$\vartheta = \frac{E_i}{r_i} = 1{,}96\left(\frac{m_i c^2}{E_i}\right)^{3/4} Z_i^2. \tag{7}$$

Taking Expression (5) for η into account, (7) can be written

$$\eta = \left(\frac{m_i c^2}{m_j c^2}\right)^{1/4}\left(\frac{E_j}{E_i}\right)^{1/4}\left(\frac{Z_i}{Z_j}\right)^{2/3}. \tag{8}$$

Since the choice of the "standard" with which all other forms of radiation are compared is very important for the determination of relative biological effectiveness, and since electromagnetic radiation is usually taken as a "standard," we shall examine the dependence of η on the energy of electrons. Let E_{st} be the energy of the electrons of the "standard," and E be the energy of the electrons in the region below 0.25 Mev, where Formula (6) holds. In this case, $\eta = \left(\frac{E_{st}}{E}\right)^{1/4}$, i.e., η is inversely proportional to the fourth root of the electron energy. In the same energy region ($E \leq 0.25$ Mev), the effectiveness of any other particle in comparison with the electron is equal to $\eta = 6.65\, A^{1/4}\,(E_e/E_i)^{1/4}\, Z_i^{2/3}$. Thus, for example, for the proton ($A = 1$; $Z = 1$) $\eta = 6.65\,(E_e/E_i)^{1/4}$. For a proton and an electron of equal energies, $\eta = 6.65$. The value of η will be greater for heavier particles: for α-particles, 2.24 times as great; for the carbon nucleus, 6 times; for the oxygen nucleus, 8 times.

The energy losses of electrons with energies > 2 Mev obey a more complicated expression than Formula (6). In this region, beginning with 3 Mev, radiative losses are increasing, becoming equal to the ionization losses at an energy of 150 Mev, and at 300 Mev comprising about 75% of the total energy losses of the electrons. The harmful role of cascade processes in tissues has not been investigated, and therefore, in calculating η for the energy region above 150 Mev, especially for large objects (of the order of 30 cm), total energy losses must be considered. For small experimental objects it is reasonable to take only ionization losses into account.

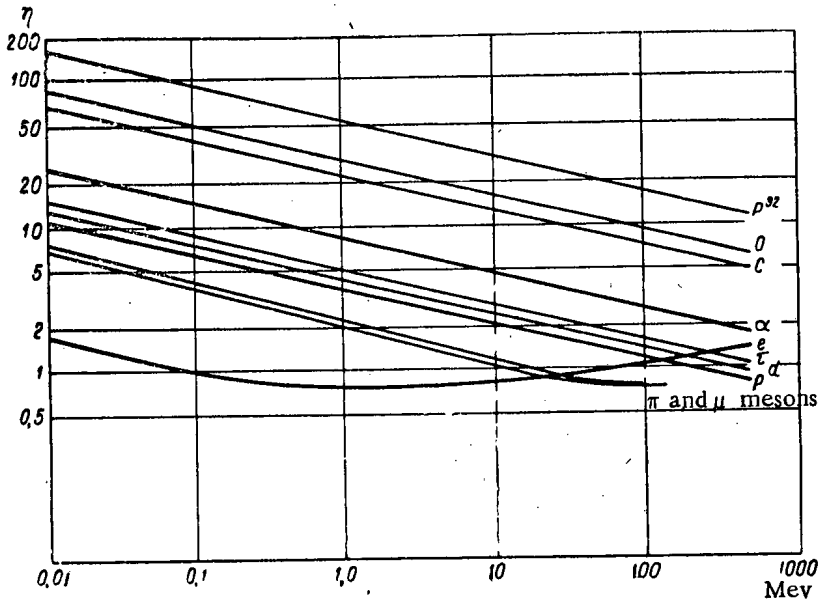

Fig. 8. Biological effectiveness of particles of various energies as compared with electrons with an energy of 100 kev.

In Fig. 8, curves are set forth showing the dependence of η on the energy of particles (electrons, π- and μ- mesons, protons, deuterons, tritons, α-particles, carbon nuclei, oxygen nuclei, and phosphorus nuclei), calculated in relation to a "standard" electromagnetic radiation with an energy of 100 kev, in the energy interval 0.01 - 500 Mev, on the assumption that the harmful action is proportional to $\sqrt[3]{\vartheta}$. The electron curve e shows that at energies above the usual 100 kev, we should expect a reduction in relative biological effectiveness to 0.75 (at energies of 1-2 Mev), and then an increase to 1 (at energies of 50-60 Mev). Values of the relative biological effectiveness of electromagnetic radiation, obtained in experiments at various quantum energies, are in good agreement with calculated values for electrons. Thus, for example, it is observed that the OBE of bremsstrahlung of 20-23.5 Mev energy compared with x-rays having energies of 180-200 kev falls to 0.7-0.8. The OBE of Co^{60} radiation, compared with 200 kev x-rays, is from 0.7 to 0.8, which likewise does not conflict with the following calculated data:

Particle	Theoretical OBE	Statutory OBE
Electron	1	1
π-meson	3.8	–
μ-meson	4.1	–
Proton	6.6	10
Deuteron	7.8	–
Triton	8.6	–
α-particle	14.7	20
Lithium nucleus	19	–
Beryllium nucleus	28	–
Oxygen nucleus	52	–

The calculated OBE values can serve as a basis for the determination of the maximum permissible doses of nuclear radiations of various type and energies, especially in the case of a multicomponent mixture of secondary ionizing particles in neutron work. Thus, for example, for neutrons with a mean energy of 5.6 Mev, when about 90-95% of the dose arises from recoil protons ($\overline{E}_p$ = 2.8 Mev) and 5-10% from recoil C, N, and O nuclei, we may suppose that for the remote consequences, the coefficient of relative biological effectiveness will be of the order of $0.9 \cdot 2.8 + 0.1 \cdot 52 = 7.7$ (compared to x-radiation of 200 kev energy). Experiments on the acute irradiation of dogs yield a coefficient of OBE around 3-4. Similarly, we may expect that the OBE for ultra-fast neutrons will be in the neighborhood of 10-15 (because of the increase in dose, attributable to recoil C, N, and O nuclei), although the comparative study of survival of animals following acute irradiation points to a magnitude of OBE equal to 1.8-2.0 (see Fig. 7).

For maximum permissible neutron fluxes in the energy interval 0.1 - 500 Mev, we assume the coefficient of OBE of neutron radiation compared with x-radiation of 200 kev energy to be equal to 10. Thus, the maximum permissible daily dose is taken equal to 0.005 REP. In calculations, the maximal values of tissue doses (curve 2, Fig. 5) W^*_{max} are used, expressed in Mev/g for 1 neutron/cm^2. First the integral neutron fluxes producing a maximal dose of 1 REP are calculated (1 REP = 93 erg/g = $5.8 \cdot 10^7$ Mev/g). For this, the quantity $5.8 \cdot 10^7$ Mev/g is divided by the appropriate ordinates in curve 2, Fig. 5. Then the result is multiplied by 0.005, to obtain the maximum permissible daily neutron flux. Finally, the maximum permissible neutron flux for a 6-hour work day (42-hour work week) is computed by dividing the maximum permissible daily flux by the duration of a work day in seconds, i.e., by $6 \cdot 3.6 \cdot 10^3 = 2.16 \cdot 10^4$ sec.

The calculated values for the maximum permissible neutron fluxes are represented by the curves in Fig. 9.

There is no reason to expect a reduction of the coefficient of biological effectiveness for high-energy neutrons. Spallation and star formation under bombardment with high-energy nucleons cause the production of particles with a high linear ionization density, and give us occasion to consider the mechanisms by which injuries to organic structures, attributed to individual particles, can become noticeably more frequent. For this reason, it is recommended that the values cited in Fig. 9 be regarded as only a temporary, approximate solution of the problem of the maximum permissible neutron dose. If we take the genetic effect of radiation into consideration, then in calculating the expectation time for harmful mutations it is necessary to take t significantly greater than

the mean time of one man's working in a factory, and perhaps, equal to the lifetime of several generations of men. In this case, the doses quoted must be further reduced several-fold – a conclusion to which radiobiologists have recently inclined.

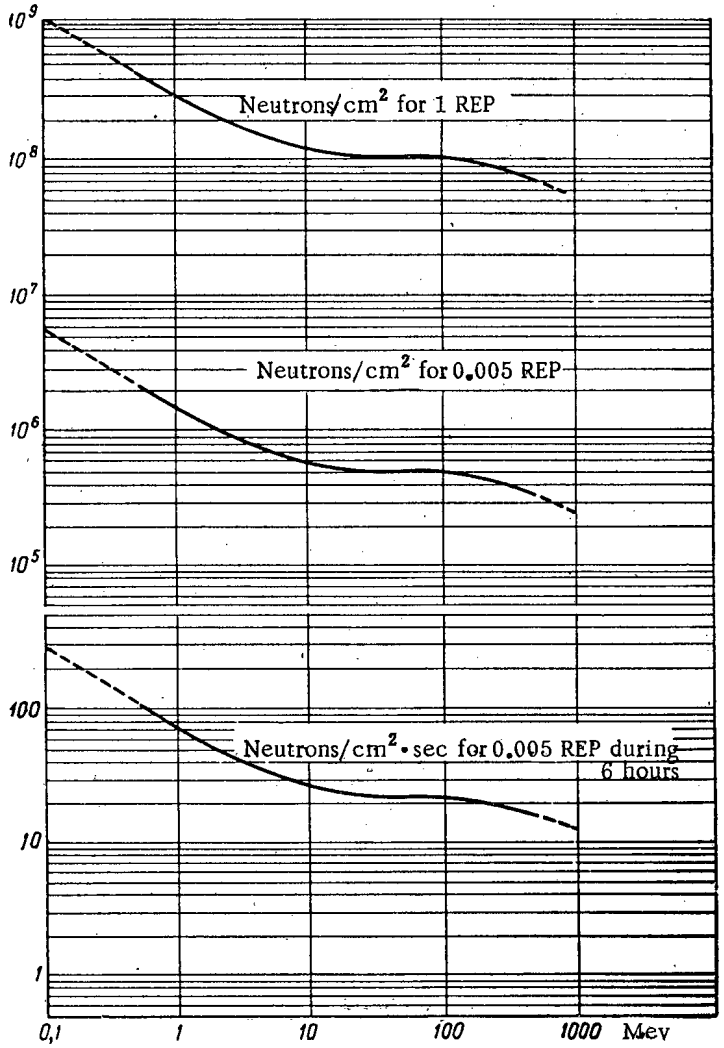

Fig. 9. Number of neutrons per cm^2 producing a maximum tissue dose of 1 and 0.005 REP, and neutron currents in neutrons/cm^2·sec producing a dose of 0.005 REP over a 6-hour work day.
a) Neutrons/cm^2 for 1 REP; b) neutrons/cm^2 for 0.005 REP;
c) neutrons/cm^2·sec for 0.005 REP during 6 hours.

LITERATURE CITED

[1] L. Cohen, Phys. Rev. 81, 184 (1951).

[2] N. A. Vlasov, in the book: Neutrons [In Russian] (Gostekhizdat, 1955).

[3] Coll: Energy Levels of Light Nuclei [In Russian] (Izd. IL, 1952), p. 66.

[4] J. H. Tait, Brit. J. Radiology 23, 269 (1950).

[5] W. A. Mills and G. S. Hurst, Nucleonics 12, 4 (1954).

[6] J. A. Barr and G. S. Hurst, Nucleonics 12, 8 (1954).

[7] J. Hadly, E. Kelly, et al., Phys. Rev. 75, 351 (1949).

[8] G. R. Mott et al., Phys. Rev. 88, 9 (1952).

[9] V. P. Dzhelepov and Iu. M. Kazarinov, Doklady Akad. Nauk SSSR 99, 939 (1954).

[10] V. I. Gol'danskii, Uspekhi Fiz. Nauk XI, 2, 234 (1950).

[11] W. Snyder and J. Neufeld, Brit. J. Radiology 28, 342 (1955).

[12] E. Schrödinger, What Is Life ? (Russian translation), (Izd. IL, 1947).

[13] B. N. Tarusov et al., Coll: Primary Physico-Chemical Processes in Radiation Sickness [In Russian] (Medgiz, 1957), p. 25.

[14] B. Rossi, in the book: High-Energy Particles [In Russian] (Gostekhizdat, 1955).

Received December 23, 1957.

SILICON PHOTOCELLS AS SOLAR-RADIATION CONVERTERS

V. S. Vavilov, G. N. Galkin, and V. M. Malovetskaia

This paper presents the results of investigations into the properties of p-n junctions obtained by the thermal diffusion of phosphorus into p-type silicon. Data are given on the load and spectral characteristics of silicon photocells with p-n junctions, as well as on the operation of these photocells at high intensities of illumination.

One of the methods of obtaining p-n junctions of large area in silicon is the thermal diffusion of admixtures of some elements. In a series of papers devoted to the problem of the direct conversion of solar energy into electrical energy, photoelements are described which were prepared by the diffusion of boron into n-type silicon [1] and of antimony into p-type silicon [2].

p-n junctions obtained by the thermal diffusion of phosphorus from the gaseous stage into p-type silicon were investigated in the present work.*

Volt-Ampere Characteristics

The forward branch of the volt-ampere characteristic of p-n junctions are described by the equation

$$J = J_0 \left[\exp\left(\frac{qU}{AkT}\right) - 1 \right],$$

where J is the current flowing through the junction, U is the potential across the junction, J_0 is the saturation current, q is the electronic charge, and A is a multiplying factor which depends on U.

The resistence of the p-n junctions at the zero point R_0 has a value of about 10^6 ohm. There is no region of "saturation current" on the reverse branch of the characteristic. This branch becomes a straight line whose slope corresponds to a constant resistance of approximately 10^7 ohm. A considerable portion of the forward branch is a straight line (Fig. 1). From the slope of this straight line it is possible to obtain a value for A which is constant over a region of the characteristic. A as a function of the applied potential U is given in Fig. 2.

In real photocells operating at considerable current densities (about 20 μa /cm^2), the resistance in series with the junction should be taken into account in the expression for the volt-ampere characteristic. It is composed of the resistance at the contact on the p-type silicon, the resistance of the thin n-type surface layer, and the volume resistance which is usually small.

The region of the volt-ampere characteristic situated in the 4th quadrant represents the load characteristic.

Load characteristics were obtained for photoelements illuminated by a lamp with a filament temperature of approximately 3100° C and a water filter 1 cm thick. The illumination intensity was chosen so that the value

* The techniques of obtaining p-n junctions by the diffusion of phosphorus into p-type silicon and the manufacture of photoelements were passed on by the authors to the All-Union Scientific Research Institute of Current Sources (VNIIT) and were developed further by A. P. Landsman, A. K. Zaitseva, and A. Ia. Gliberman. Solar batteries made at the VNIIT in 1957 have an efficiency of 5-6%, while individual elements have an efficiency of up to 8%. 14-cell batteries with a working area of about 22 cm^2 produce a voltage of 5.5 v at a current of approximately 20 μa.

of the short-circuit current is the same as for illumination of the photocells by solar radiation with an energy flux of 100 Mw/cm^2. Measurements were made in a vacuum thermostat in temperature intervals of 0 to + 95° C and − 75 to + 90° C with photocells prepared from silicon with a resistivity of 25, 4, and 0.4 ohm·cm. The load characteristics of one of the photocells at temperature of 22, 60, and 94° C are given in Fig. 3. From the graphs it can be seen that the short-circuit current decreases by approximately 10-15% with a decrease in the temperature.

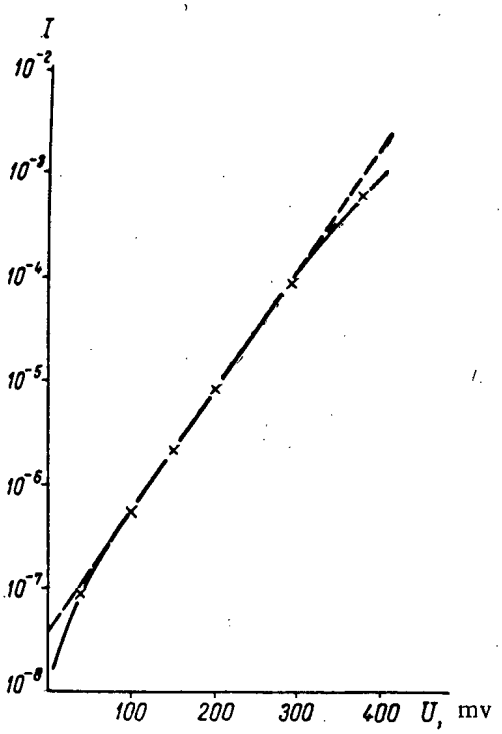

Fig. 1. The forward branch of the volt-ampere characteristic of a nonilluminated silicon photocell.

As the temperature decreases the emf increases considerably, while with increasing temperature the emf falls according to a linear law which is close to the theoretical dependence [3] for the given temperature interval. With an increase in the resistivity of the silicon from which the photocells are made, a fall in the emf and an increase in the slope of the straight line in Fig. 4 are observed.

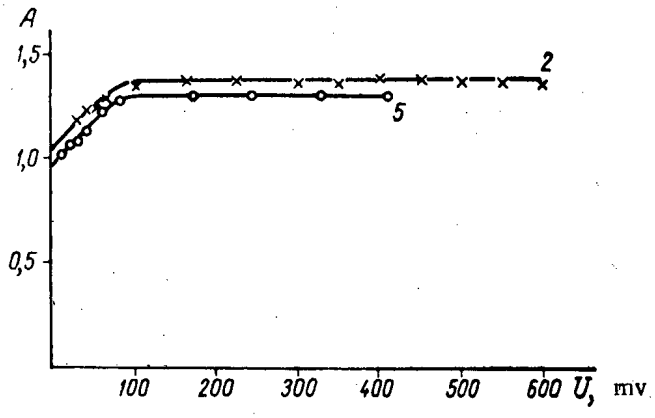

Fig. 2. The dependence of A on U (the numerals on the curves refer to the photocell numbers).

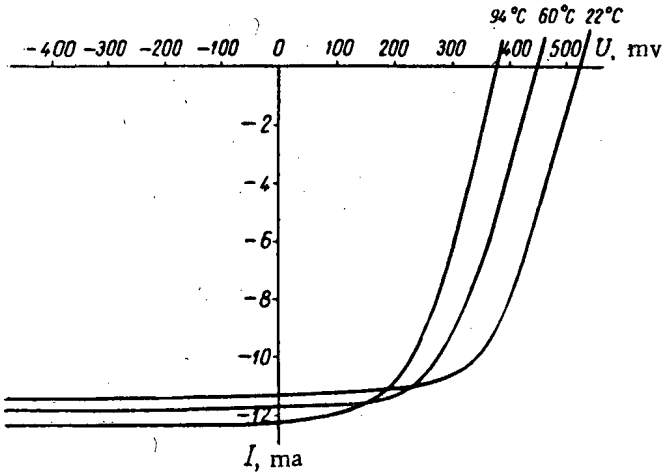

Fig. 3. The volt-ampere characteristics of an illuminated photocell at different temperatures.

From the shape of the load characteristics extrapolated to zero series resistance it follows that for the most favorable construction and for a sufficiently high value of the ratio $J_{s.c.}/J_0$ [4]

$$P \approx 0{,}8 U_0 J_{s.c.}$$

From this it follows that the temperature dependence of the efficiency of the photocells is mainly determined by the temperature dependence of the emf.

Spectral Characteristics

The curves showing the dependence of the collection factor α on the wavelength λ we will call the spectral characteristics of photocells with a p-n junction. The collection factor is the ratio of the carrier flux through the junction when the photocell is short-circuited to the total number of electron-hole pairs generated by light per unit time in the semiconductor.

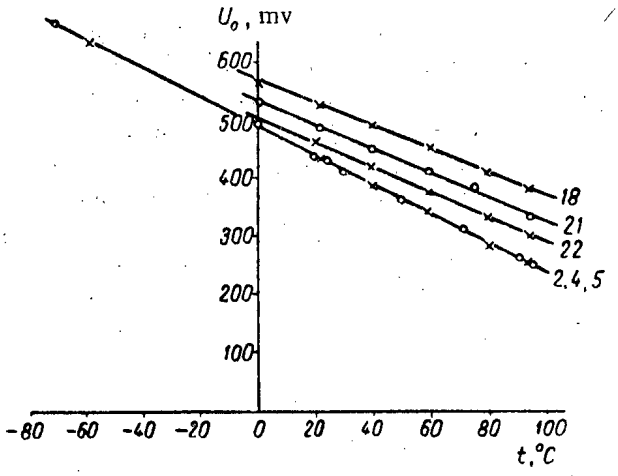

Fig. 4. The dependence of the silicon-photocell emf on the temperature (the numbers on the curves refer to the number of the photocell).

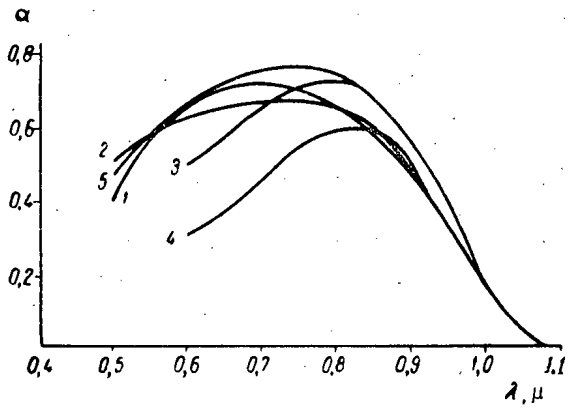

Fig. 5. The spectral characteristics $\alpha(\lambda)$ of photocells with p-n junctions at various depths: 2 μ (curves 1, 2); 9 μ (curve 3), and 15 μ (curve 4). Curve 5) characteristic of the same cell as for curve 1 after the removal of the film which lowers the the coefficient of reflection (the short-circuit current after the removal of the film fell by 21% as the result of an increase of the coefficient of reflection from 12 to 36%).

The spectral characteristics of photocells with p-n junctions at a depth of 2 μ (curves 1, 2, and 5), 9 μ (curve 3), and 15 μ (curve 4) are given in Fig. 5. From the graphs it can be seen that photocells with junctions situated close to the surface have the best spectral characteristics. The true value of the reflection coefficient of the semiconductor surface has to be used in the calculation of the collection factor α. It has been shown that the reflection coefficient of an etched silicon surface falls from 36% at $\lambda = 0.4$ μ to 30% at $\lambda = 1.1$ μ. An unetched silicon surface subjected to phosphorus diffusion from the gaseous phase has a reflection coefficient of about 12% at $\lambda = 0.4 - 0.75$ μ.

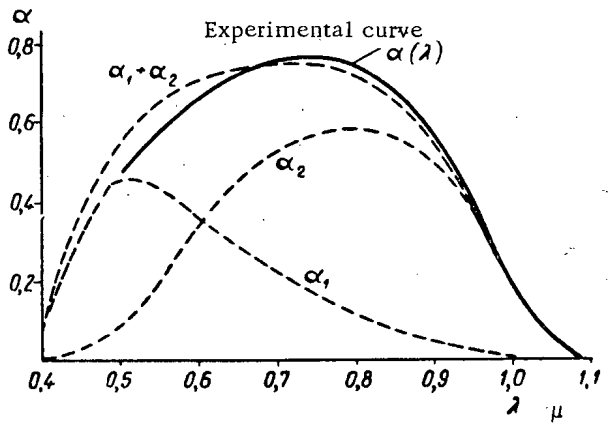

Fig. 6. Comparison of the spectral characteristics of photocells with a p-n junction at a depth $x_s = 2 \cdot 10^{-4}$ cm with the spectral characteristic calculated from the following data: $x_s = 2 \cdot 10^{-4}$ cm, $s = 10^4$ cm/sec, $D = 2$ cm^2/v·sec, $L_s = 2 \cdot 10^{-4}$ cm, $L = 25 \cdot 10^{-4}$ cm; α_1) collection factor for the holes liberated by light in the surface n-type layer; α_2) collection factor for electrons in the p-type region.

The comparison of the curves $\alpha(\lambda)$ for the same cells with a natural transmitting film (curve 1) and without it (curve 5) shows that the film exerts only an insignificant influence on the value of the collection factor, while at the same time it can appreciably (by up to 20%) increase the number of electron-hole pairs produced and consequently raise $J_{s.c.}$ and the efficiency of the photocell.

A general expression for the collection factor when carrier pairs are produced by light on either side of the p-n junction, with surface and volume recombination taken into account, was used for the theoretical interpretation of the spectral characteristics. The latest data on the coefficient of absorption of light in silicon led to the conclusion that when the depth of the junction is less than 2 μ, the absorption of light in the infrared region and, consequently, most of the pair production takes place throughout the bulk of the silicon below the p-n junction. A comparison of the experimental characteristic $\alpha(\lambda)$ for a photocell with a junction at a depth of 2 μ with the characteristic calculated from the equations given in [5] is made in Fig. 6.

The theoretical curve has been calculated by fitting to the experimental one. The depth of the p-n junction, equal to 2 μ, has been calculated from the known features of the diffusion process. The diffusion

length L in p-type silicon lies between the values 20 and 34 μ obtained from independent measurements: the first by a drift method, the second by a diffusion method [6]; the value of the surface-recombination velocity according to our estimates is 10^4 cm/sec ± 50%. The most arbitrary choice made is the value of the diffusion length for carriers in p-type silicon. The diffusion coefficient has been calculated from the data given in the literature on the mobility in highly alloyed silicon [7]. Additional experiments on the determination of the mobility and the diffusion lengths in silicon alloyed with phosphorus will make it possible to predict more accurately the shape of the spectral characteristics and, consequently, also the efficiency of silicon photocells.

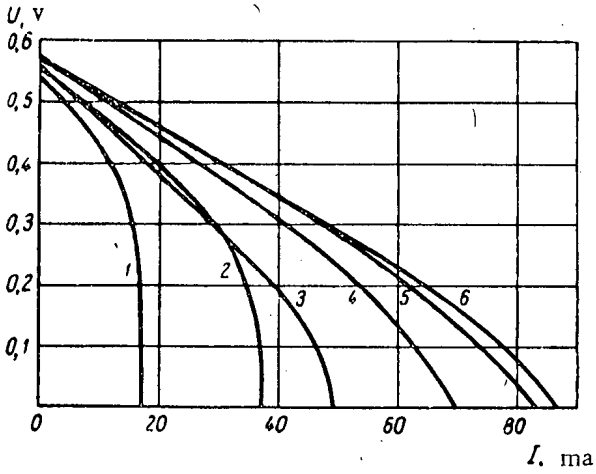

Fig. 7. Load characteristics of a silicon photocell at high illumination intensities. 1) $P_i = 0.1$ w/cm^2; 2) $P_i = 0.2$ w/cm^2; 3) $P_i = 0.3$ w/cm^2; 4) $P_i = 0.38$ w/cm^2; 5) $P_i = 0.53$ w/cm^2; 6) $P_i = 0.7$ w/cm^2.

In view of the high cost of silicon, the question of the concentration of light on to the photocell by means of mirrors or lenses and the increase of the useful power obtained from 1 cm^2 is of considerable interest. Preliminary data on the operation of silicon photocells at a light flux of up to 0.7 w/cm^2 (approximately seven times the value of the solar-energy flux) were obtained in our laboratory by A. V. Spitsyn. A lamp with a water lens, which was also used as a filter, served as the radiation source. The temperature of the filament was maintained within the limits 20 ± 3° C. A series of characteristics of one photocell is given in Fig. 7. As the intensity of the incident radiation increases, the following main features are observed: a) there is a very small increase in the emf; b) $J_{s.c.}$ increases considerably, the increase being linear up to almost 0.5 w/cm^2; c) there is a fall in the efficiency starting from 0.1 w/cm^2 due to the change in the series resistance; d) the series resistance itself decreases, which can be explained by a modulation of the conductivity of the n-type layer.

SUMMARY

The results given lead us to conclude that photocells of p-type silicon with a p-n junction, obtained through the thermal diffusion of phosphorus, can be used as converters of solar-radiation energy.

The following properties of such photocells have been observed:

1. The current in the external circuit is produced by light through the formation of electron-hole pairs both in the n-type region containing phosphorus, as well as in the p-type region below the p-n junction.

2. The diffusion length in the p-type region after the setting-up of the p-n junction falls to 20-35 μ.

3. The surface film formed during the thermal diffusion of phosphorus lowers the reflection coefficient in the most important spectral region from 30-36% to 12-15% and does not appreciably lower the collection factor α, as a result of which the short-circuit current increases by comparison with photocells with an etched front surface.

4. A solar-energy flux of up to 0.5 w/cm^2 can be utilized efficiently with the photocells investigated. When the temperature of the photocells is maintained at 25° C (by the removal of heat), 150 Mw of electric power can be obtained from 1 cm^2 of photocell working surface.

The authors express their thanks to Corresponding Member of the Academy B. M. Vul for constant attention and advice, to V. K. Subashiev for a number of valuable remarks, and also to laboratory associates V. G. Kolotilova, B. Ia. Iurkov, B. D. Kopylovskii, Iu. A. Kolotov, and V. M. Vasin, who in many respects have assisted in the carrying out of the work. Engineer R. Sh. Akchurin and laboratory technicians L. V. Belova, E. M. Divil'kovskaia, and F. M. Sidorov took part in the work.

LITERATURE CITED

[1] D. Chapin, C. Fuller, and G. Pearson, Bell. Lab. Rec. 33, 7, 241 (1955).

[2] Iu. P. Maslakovets, G. B. Dubrovskii, S. A. Poltinnikov, and V. K. Subashiev, J. Tech. Phys. (USSR) 26, 2396 (1956).*

[3] R. Cummerov, Phys. Rev. 95, 1, 16 (1954).

[4] V. K. Subashiev, Semiconductor Solar-Energy Converters [In Russian] (Leningrad House for Scientific and Technical Propaganda, 1956).

[5] W. Pfann and W. Van Roosbroeck, J. Appl. Phys. 25, 1422 (1954).

[6] L. S. Smirnov, J. Tech. Phys. (USSR) 27, 11, 2469 (1957).*

[7] G. Backenstoss, Phys. Rev. 108, 6, 1416 (1957).

Received December 14, 1957.

* Original Russian pagination. See English translation.

RADIOACTIVE CARBON FROM NUCLEAR EXPLOSION AND NONTHRESHOLD BIOLOGICAL EFFECTS

A. D. Sakharov

1. Introduction

When any nuclear weapons are exploded, including the so-called "clean" (fissionless) hydrogen bomb, a very large number of neutrons enter the atmosphere (see Section 2) and they are then captured by atmospheric nitrogen according to the reaction

$$n + N^{14} \longrightarrow p + C^{14}$$

which gives rise to long-lived radioactive C^{14}. This radioactive carbon enters human tissue, where it decays, causing radiation damage, with a dose of $7.5 \cdot 10^{-4}$ r per megaton burst (see Section 3).

I shall make the following assumptions to evaluate the harm to humanity due to the production of radioactive carbon.

1) The human population in the next few thousand years will be thirty billion persons.

2) A dose of 1 r to the reproductive glands leads to hereditary diseases in 10^{-4} cases (see Section 4).

3) Other nonthreshold biological effects triple the number of cases (see Section 4).

The total number of radiocarbon victims from a megaton burst is found, on the above assumptions, to be 6600 persons. This number is spread over a period of the order of 8000 years. According to Leipunskii's data [1], nonthreshold biological effects due to radiostrontium and external radiation due to radiocesium increase the number of cases by a factor of 1.5, the cases occurring in our generation and the one following. The total number of cases due to nuclear tests which have already been performed (50 megaton energy) is estimated at 500,000 persons. This would seem to be a conservative estimate. One cannot eliminate the possibility that the total number of cases is already one million persons and is yearly increased by 200-300 thousand persons.

Continued testing and all attempts to legalize nuclear weapons and testing cannot be reconciled with humanity or international law. Because the so-called "clean" (fissionless) bomb is radioactively harmful, there is absolutely no ground for the propagandistic assertions concerning the particular qualities of this instrument of mass destruction.

2. Neutron Formation in Nuclear Bursts

In an atomic (fission) explosion each act of fission is accompanied by an increase in the number of neutrons by a factor of $\nu - 1$ (where ν is the number of neutrons produced per neutron captured in fission). An insignificant number of the neutrons produced are captured by the surrounding material (with formation of plutonium). We assume that in each act of fission (at 180 Mev) the number of neutrons produced is $\nu - 1 = 1.5$. In military terminology one usually describes the energy of a burst in terms of the equivalent mass of TNT. A burst of 1 megaton TNT equivalent corresponds to the fission of 60 kg of uranium or plutonium, with the emission of $2.25 \cdot 10^{26}$ neutrons.

There are two different types of pure thermonuclear bombs, namely those which use liquid deuterium and those which use the chemical compound of deuterium with the light isotope Li^6. The first of these bombs

produces many more neutrons per unit energy. We shall, however, restrict our considerations to the second, since it would seem that it is just this type of bomb which is at present receiving most attention. The fundamental reactions taking place in this bomb are

$$D + D \rightarrow He^3 + n; \quad (1)$$
$$D + D \rightarrow H^3 + p; \quad (2)$$
$$n + Li^6 \rightarrow He^4 + H^3; \quad (3)$$
$$H^3 + D \rightarrow He^4 + n. \quad (4)$$

The effective probability (that is, the product of the cross section by the rate of reaction) for Reactions (3) and (4) is about one hundred times as great as that for Reactions (1) and (2).

Most of the energy of the burst comes from the "fast" Reactions (3) and (4). These reactions aid each other, and together they leave the total number of neutrons and tritium nuclei invariant. The "slow" Reactions (1) and (2) serve as the initial neutron and tritium sources.

A detailed investigation of the kinetics of the Reactions (1) - (4) shows that when the Li^6 is sufficiently burned out, one cycle of Reactions (3) and (4) leaves about 0.2 neutrons and 0.2 tritium nuclei which arise as a result of (1) and (2). In this cycle 22 Mev of energy is liberated, which means that one neutron is liberated per 110 Mev of burst. This number is very close to the figure $\frac{180 \text{ Mev}}{1.5} = 120$ Mev for an atomic burst.

In a hydrogen bomb surrounded by a uranium shell, a large amount of the energy results from fission of U^{238} by fast neutrons from Reactions (4) and (1). Since, however, the number of neutrons per unit energy is almost the same for a pure atomic and a pure thermonuclear burst, we may say that in this case also we get $2.25 \cdot 10^{26}$ neutrons/megaton.

3. Calculation of the Radiation Dose

We shall use experimental data [2, 3] referring to natural C^{14}. Cosmic rays cause many kinds of nuclear reactions in the upper layers of the atmosphere, and one of the products of these reactions is neutrons at the rate of 2.6-2.4 neutrons/$cm^2 \cdot$sec. After being slowed down, about 95% of these neutrons are captured by atmospheric nitrogen, forming C^{14} according to the reaction

$$(n + N^{14} \longrightarrow p + C^{14}).$$

The half-life of C^{14} is 5570 years. Even in biochemical processes, C^{14} is chemically very similar to stable carbon. During this lifetime the C^{14} concentration reaches equilibrium with the stable carbon of the so-called exchange reservoir, that is, atmospheric carbon in the form of CO_2, carbon in rivers and ocean waters in the form of soluble compounds, and finally carbon in living organisms. For natural C^{14} this concentration has been measured experimentally. In 1 gram of natural carbon of the exchange reservoir there take place 0.25 decays/sec, which corresponds to $6 \cdot 10^{10}$ atoms of C^{14} per $5 \cdot 10^{22}$ atoms of C^{12}. The surface area of the earth is $5 \cdot 10^{18}$ cm^2. We find that the probability for decay of a single C^{14} nucleus formed in the atmosphere per gram of carbon of the exchange reservoir is $\frac{0.25}{2.6 \cdot 5 \cdot 10^{18}} = 2 \cdot 10^{-20}$ per gram.

We shall assume that the geochemical environment of the earth will not change significantly over the next several thousand years. Then the decay probability per gram of carbon which we have obtained for natural C^{14} is good also for carbon nuclei formed at present in nuclear bursts.

This same statement can be phrased in terms of linear equations. Every solution of a set of linear equations (with independent variables x and t) whose right side is q(t) at the point x = 0 can be expressed by a superposition of singular solutions of the following type:

Singular solution
- source $\delta(x)\,\delta(t - t_0)$,
- solution $n(x, \tau)$, $\tau = t - t_0$,

(here n is a Green's function)

$$\text{Superposition} \begin{cases} \text{source} & \delta(x)\, q(t), \\ \text{solution} & N(x, t) = \int_0^\infty q(t-\tau)\, n(x, \tau)\, d\tau \end{cases}$$

In the special case of a steady source q_0 at the point $x = 0$, the solution at $x = x_0$ is

$$N_0(x_0) = q_0 \int_0^\infty n(x_0, \tau)\, d\tau, \quad \text{i.e.,}$$

$$\int n\, d\tau = \frac{N_0}{q_0}.$$

In our case x denotes the coordinates of points in the exchange reservoir, and $x = 0$ denotes the upper layer of the atmosphere; $q_0 = 2.6$ neutrons/cm^2 · sec · $4\pi R^2$; $N_0 = 0.25$ decays/sec · gram; $R = 6.3 \cdot 10^8$ is the radius of the earth; $n(x_0, t - t_0)$ is the number of decays per gram of natural hydrogen per second at the point x_0 at time t divided by the number of C^{14} nuclei produced in the atmosphere at time t_0.

We then obtain $\int n\, dt = 2 \cdot 10^{-20}$ per gram.

For a 1 megaton burst we obtain $2.25 \cdot 10^{26} \cdot 2 \cdot 10^{-20} = 4.5 \cdot 10^6$ decays/megaton · g.

We shall express the radiation dose in roentgens, setting a roentgen approximately equal to a rad which we take as the dose that will produce 100 ergs of ionization energy per gram of tissue.

The maximum energy of C^{14} β-decay is 0.154 Mev, about two-thirds of which is carried away by a neutrino. Thus about 0.05 Mev is liberated in the tissues, or $8 \cdot 10^{-8}$ erg/decay.

Assuming further that carbon makes up about 18% of the weight of the body, we find the total energy liberated per gram of tissue from a 1 megaton bomb to be

$$0.18 \cdot 4.5 \cdot 10^6 \cdot 8 \cdot 10^{-8} = 7.0 \cdot 10^{-2} \text{ erg/g} = 7.5 \cdot 10^{-4} \text{ r}.$$

The data are not as good when we come to the time distribution of the decay, that is, on the form of the function $n(x_0, t)$. Using Anderson's [2] estimate of 8.5 g/cm^2 for the mass in the exchange reservoir, we can assume that within this reservoir equilibrium is attained in a time short compared with the lifetime of C^{14}, and that the C^{14} leaves the reservoir at an insignificant rate. On these assumptions the time dependence of the decay will be an exponential of the form $\exp\left(-\frac{t}{8 \text{ thousand years}}\right)$.

4. Nonthreshold Biological Effects of Radiation

A thermonuclear war involves the potential danger to all of humanity of being subjected to a lethal radiation dose (about 600 r). This danger would not seem to exist in testing nuclear arms, since at the present rate of testing the dose per person is never greater than a roentgen. However, billions of persons are subjected to this dose in addition to the natural background, and will be so subjected (in the case of C^{14}) for several hundreds of generations. The amount of sickness caused by this additional radiation from testing under these conditions is found from the so-called nonthreshold biological effects. The number of cases is proportional to the total dose for all of humanity (that is to the dose in roentgens per person multiplied by the number of persons) independent of the distribution of the radiation over the population or of its time dependence.

The simplest nonthreshold effect of radiation is hereditary [4-6]. The substance which transmits heredity is the gene, a special structure in the chromosomes of cell nuclei. For an irreversible change of a gene (a so-called gene mutation) a single act of ionization is sufficient, so that genetic changes can occur as a result of the weakest radiation doses with a probability which is exactly proportional to the dose.

Each gene is in a certain sense a letter in the biochemical program of the development of an embryo. Therefore a change in one gene may in certain cases (for dominant mutations or accumulation of mutations) lead to very significant hereditary changes.

At the present time human births involve about 2% hereditary diseases (schizophrenia, hemophilia, diabetes, and many others) caused by mutations. The number of actual mutations is less than this, since some people with hereditary diseases reproduce, and a single mutation may give rise to effects over several generations. This does not, however, destroy the proportionality between the number of mutations and the number of hereditary sicknesses. According to presently accepted ideas based on Meller's experiments with mice, 5% of mutations, and therefore also of hereditary sicknesses, results from natural radioactivity (10 r over a human life of sixty years). Collecting all these figures, we obtain the coefficient whichgives the increase of hereditary sickness due to radiation, namely

$$\frac{0.02 \cdot 0.05}{10} = 10^{-4} \text{ per roentgen.}^*$$

The mean human population during the time it takes the C^{14} to decay will probably be about 30 billion persons (about 10 or 11 times greater than at present). This estimate is not incompatible with increases in the earth's productivity as science progresses.

Using this figure, we obtain (for radioactive carbon alone) $3 \cdot 10^{10} \cdot 10^{-4} \cdot 7.5 \cdot 10^{-4} = 2200$ cases of hereditary sickness from a megaton bomb, or 110,000 cases from all the tests already carried out. We are assuming that the tests already performed add up to fifty megatons.

In animal and plant life mutations sometimes give rise to more advanced biological forms. It is conceivable that human mutations (and hereditary sickness) should also be welcomed, since they may be considered a necessary evil in the biological progress of the human race. Actually, however, human nature now changes primarily because of social factors. We are inclined to consider uncontrollable mutations merely as an evil, and experiments with nuclear weapons as being merely an additional cause for the death of tens and hundreds of thousands of persons.

Another example of nonthreshold biological effects of radiation is the possible increase in the amount of cancer [7] and leukemia.

It has been shown experimentally that the cancerogenic effects of various nonradiational cancerogenic substances are additive. There is no reason to believe that the active radicals which arise as a result of ionization will behave in a qualitatively different way. Therefore, the increase in the amount of cancer, or equivalently, the drop in the age at which cancer occurs, will be a linear function of the dose to which humanity is subjected. The total coefficient for all types of cancer and leukemia is taken to be of the same order of magnitude as that for genetic damage, namely $1\text{-}2 \cdot 10^{-4}$ cases/r. Partially verifying this coefficient are data on the frequency of leukemia, a professional disease of radiologists and in some sense related to cancer. The effect of radiation on this disease is easy to study, since it occurs infrequently in nature. A dose of a single roentgen in a year gives rise to additional leukemia fatalities at the rate of $2 \cdot 10^{-6}$, and over a thirty year lifetime this becomes $6 \cdot 10^{-5}$. This coefficient is of the same order of magnitude as that suggested for other forms of cancer.

A possible (though not experimentally proven) nonthreshold effect of radiation is a drop in the immunological reactions of the organism. In all probability premature aging and death is also a nonthreshold effect. The mean life expectancy of medical radiologists (who are subjected to an average dose no greater probably than 1000 r) is five years less than that for the general population. This means that premature death may occur at the rate of 10^{-4} per roentgen.

Further, we should perhaps note that although mutations are not desirable in the human race, for viruses and bacteria they may greatly increase the chance of survival. Examples are the mutation which occurred in diphtheria in the middle of the 19th century and the periodic flu epidemics that affect a large part of the world's population.

* As in the case of Section 3, the use of the expressions for the steady-state natural process gives a proper integral over time, but no information on the decay law for an instantaneous source. Recessive genes may require dozens and even hundreds of generations before they make their presence felt.

It is difficult to evaluate this effect, although it is plausible that it is just as harmful to human health as is the genetic effect.

On the whole, according to our approximate and probably conservative estimate, the loss of human life from all nonthreshold biological effects is at least three times that for the genetic effects alone, which means a rate of about $3 \cdot 10^{-4}$ per roentgen. Summing of all the above effects (without deductions for "vagueness") gives $6 \cdot 10^{-4}$ per roentgen.

Thus the radiocarbon from the tests which have already taken place will affect about 330,000 persons. As is well known, an important factor is the fallout of radioactive strontium and cesium. Using Leipunskii's data [1] we may estimate that the bone damage due to strontium and the external effects of cesium are about 0.5 of the C^{14} effect. For the sake of completeness, we shall give a brief description of the corresponding calculations. If tests are to continue at the present level (that is 10-15 megatons/year) the radioactive strontium concentration in the bones will be about 65 strontium units ($\mu\mu$ C/g of calcium) which means that the radiation dose will be $160 \cdot 10^{-3}$ r per year or $1\text{-}1.5 \cdot 10^{-2}$ r/megaton. This dose causes sickness at about half the rate of the $7.5 \cdot 10^{-4}$ r/megaton for the radiocarbon, since it involves a population of about 2.5 billion people (giving the factor 1/12) and involves only the skeleton, which gives the factor 1/3. The effect of external γ-radiation due to cesium is of the order of 10^{-3} r/megaton, and taking into account the smaller population, this leads to an effect which is about 10% of C^{14} effect. Thus, the total losses from a 1 megaton burst are about 10,000 persons, and the total losses from all nuclear bursts to date are about 500,000. This is a conservative estimate, and if we were to include other radioactive isotopes, other kinds of radioactive damage, and a more complete calculation of all threshold and nonthreshold biological effects we would obtain a larger figure. We cannot exclude the possibility that the total number of victims is already approaching 1 million persons, and that each year continued testing increases this number by 200-300 thousand persons.

What moral and political conclusions can be drawn on the basis of the above figures?

One of the arguments presented by those who maintain the theory that tests are "harmless" is that cosmic rays lead to doses which are greater than those from the tests. This argument forgets that we are adding to the world's toll of human suffering and death, the suffering and death of hundreds of thousands additional victims, including some in neutral countries and in future generations. Two world wars have also added less than 10% to the death rate of the 20th century, but this does not make war a normal phenomenon.

Another argument which is found in the literature of several countries is, in effect, that the progress of civilization and new technological advances have in many other cases led to human suffering. As an example, comparison is often made with automobile accidents. But this analogy is not valid. The automobile raises human living standards and leads to accidents only in individual cases as a result of carelessness on the part of persons who are then legally responsible. The suffering caused by the tests, however, follows immutably from each burst. To the present author it seems that all of the moral implications of this problem lie in the fact that the crime cannot be punished (since it is impossible to prove that any specific human death was caused by radiation) and in the defenselessness of future generations against our acts.

The cessation of tests will lead directly to the saving of the lives of hundreds of thousands of people and will have the more important indirect result of aiding in reducing international tensions and the danger of nuclear war, the fundamental danger of our age.

The author takes this opportunity to express his gratitude to O. I. Leipunskii for valuable discussion.

LITERATURE CITED

[1] O. I. Leipunskii, J. Atomic Energy (USSR) III, 12, 530 (1957).*

[2] E. C. Anderson, Annual Rev. Nucl. Sci. 2, 63 (1953).

[3] W. F. Libby, Radiocarbon Dating, (University of Chicago Press, 1955).

[4] H. J. Muller, Acta radiol. 41, 5 (1954).

[5] N. P. Dubinin, Radiation and Human Heredity [In Russian] (manuscript).

* Original Russian pagination. See C. B. Translation.

[6] S. N. Ardashnikov and N. Shapiro, On the Possible Effect on Man's Heredity of the Increased Radiation Level Due to the Tests of Atomic Armaments [In Russian] (manuscript).

[7] Biological Hazards of Atomic Energy (ed. Glücksmann), (Clarendon Press, Oxford, 1953).

Received July 8, 1958

LETTERS TO THE EDITOR

THE FIRST DISCOVERY OF COFFINITE IN THE USSR

Ia. S. Filipenko

A number of papers published in the U.S.A. [1-5] have reported a newly discovered silicate of uranium, called coffinite $U(SiO_4)_{1-x}(OH)_{4x}$. According to these papers coffinite is found in hydrothermal and sedimentary deposits. Some of the deposits are important economically. The published reports describe chiefly the coffinite from sedimentary deposits. Discoveries of this mineral have not been reported in Soviet literature.

TABLE 1

Comparative Data on Interplanar Distances and on Intensities of Lines of Coffinite and of the Newly Discovered Mineral

Investigated mineral			Coffinite from the Arrowhead mine		
hkl	*d* Å	*I*	*hkl*	*d* Å	*I*
011	4,67	9	011	4,66	strong
200β	3,86	5	—	—	—
200	3,51	10	200	3,47	strong
121	2,184	4	121	2,78	weak
112	2,665	9	112	2,64	moderate
220	2,455	5	220	2,46	very weak
031	2,189	8	031	2,18	weak
013	2,002	7	013	2,01	very weak
321	1,855	3	321	1,841	weak
312	1,813	9	312	1,801	moderate
—	—	—	123	1,787	weak
400	1,742	4	400	—	—
411	1,632	5	411	1,629	very weak
004	1,562	5	—	—	—
—	—	—	420	1,556	very weak
332	1,449	2	332	1,451	»
024	1,430	2	024	1,435	»
431	1,373	3	—	—	—
224	1,319	3	—	—	—
162	1,256	4	—	—	—
044	1,162	5	—	—	—
244	1,104	5	—	—	—
—	1,004	1	—	—	—
552	0,944	4	—	—	—
624	0,900	3	—	—	—
—	0,8813	3	—	—	—

The present note describes a coffinite-type mineral studied by us in 1956. It was found in fractures in granite at depths of 33, 48, and 90 m, occurring in small lenses and nests with irregular form that range from 2-3 to 6-8 cm in long dimension. In all these occurrences the mineral is closely associated with pyrite, galena, and more rarely, chalcopyrite (see Figs. 1 and 2). Small grains of transparent quartz are also commonly found in association. In order of formation, the coffinite preceded the galena.

Megascopically this mineral is brownish black, with a cryptocrystalline structure and an irregular, almost conchoidal fracture. The surface of the mineral is dull. Its streak is brownish black. The hardness is 68-131 kg/mm^2, or 2.9-3.1 on Mohs' scale. The mineral polishes poorly. A bead, fused with NaF, fluoresces clearly in ultraviolet light. Outwardly the mineral resembles hydrated pitchblende; in reflected light it is gray, with yellow-brown internal reflections. Anisotropy is not recognizable; the reflectivity of the mineral is lower than that for sphalerite: R = 5.6- 7.5.

Because the mineral occurs in such small segregations, a pure specimen is very difficult to obtain. In conducting spectral, x-ray, and microchemical studies, we selected approximately 100 mg of comparatively pure mineral from each of two samples.

The x-ray study showed that the mineral in its natural state gives a diffraction picture of a crystalline substance identical to that for the coffinite described in the U.S.A. An analysis was made by the powder method, the exposure being made in unfiltered radiation at a potential of 40 kv and a current strength of 16 amp for 2 hours in a camera with a diameter of 57.3 mm. The

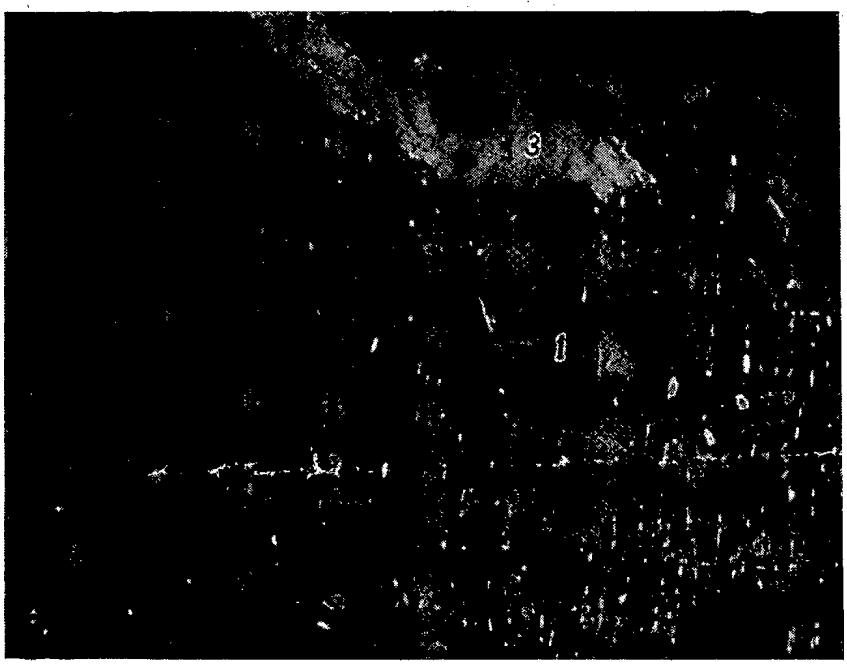

Fig. 1. Coffinite (1) with disseminated grains of quartz (2) and a veinlet of galena (3). Polished section of a sample taken from a depth of 33 m (x 110).

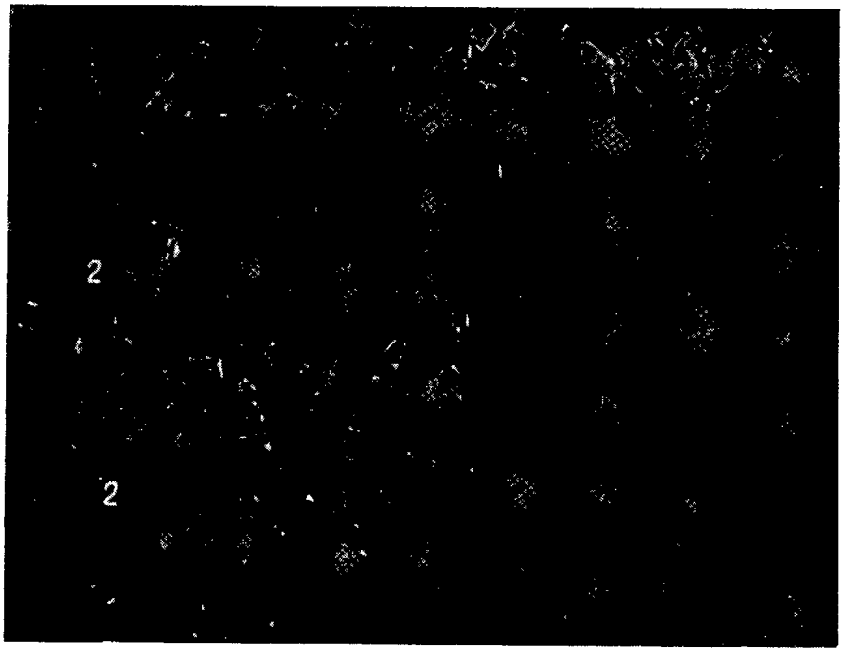

Fig. 2. Inclusions of pyrite (1) in coffinite (2). Polished section of a sample taken from a depth of 48 m (x 110).

film was measured on a comparator with a precision of ± 0.05 mm, and this permitted the interplanar distances to be determined with an accuracy of 0.5% for d from 4 to 2 A and an accuracy of 0.1% for d below 2A.

The intensities of the lines were evaluated visually on a 10-division scale. For precision in the evaluation, a photograph was taken of the samples with an internal standard (NaCl).

The analyses established the fact that the mineral has a crystalline structure like zircon and is in the tetragonal system; after indexing the reflections, the dimensions of the unit cell were determined by a Hull (Hull-Davey) graph: a = 7.01, c = 6.26 ± 0.01 A.

TABLE 2
Results of Spectral Analysis of Coffinite

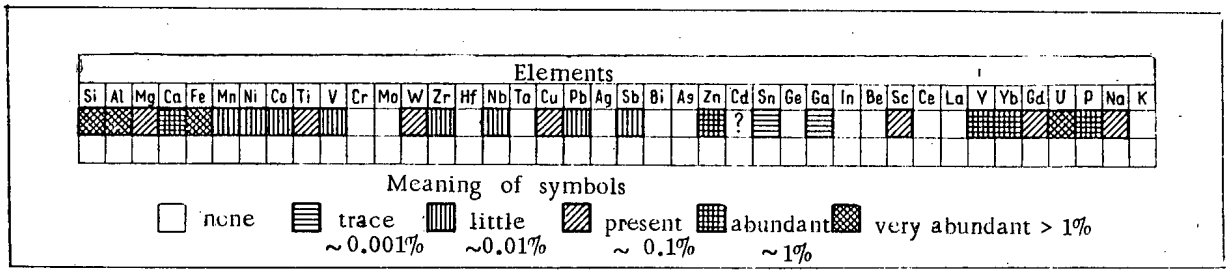

In the papers [1], [2], and [5], coffinite is also described as tetragonal, with a = 6.94 and c = 6.31.

On comparing the results of the x-ray study made by G. A. Sidorenko with the data in the papers [1], [2], and [5], it was discovered that, in the main, the interplanar distances and the line densities agree (see Table 1).

Spectral data are shown in Table 2 and a microchemical analysis, made by V. E. Pankova, is given in Table 3.

TABLE 3
Results of Microchemical Analysis of Coffinite

Depth to mineral occurrence, m \ Oxides	UO_3	UO_2	S	SiO_2	F_2O_3	Al_2O_3	CaO	MgO	Na_2O	$\pm H_2O$	Total
33	17,63	20,05	0,0	23,92	2,51	17,88	1,91	1,34	—	at t=800° C 7,86	99,10
48	9,50	27,66	3,79	31,17	6,34	12,53	1,47	0,94	0,63	at t=1100° C 5,91	99,59

The chemically analyzed material could not be obtained pure, because it was contaminated with pyrite, quartz, iron hydroxides, and, possibly, decomposition products of feldspar (sericite, kaolinite, etc.) inasmuch as the mineral occurs in clay gouge.

This cited material furnishes grounds for considering the investigated mineral to be identical to coffinite.

LITERATURE CITED

[1] A. D. Weeks and M. E. Thompson, U. S. Geol. Surv. Bull. 1009-B, 31 (1954).

[2] L. K. Stieff, T. W. Stern, and A. M. Sherwood, Amer. Mineralogist 41, 9-10, 675 (1956).

[3] R. Zitting et al., Mines Mag. 47, 3, 53 (1957).

[4] E. B. Gross, Econ. Geol. 51, 7, 632 (1956).

[5] C. Frondel, D. Riska, and J. W. Frondel, U. S. Geol. Surv. Bull. 1036-G, 1 (1956).

Received January 21, 1958

THE LIGHT ISOTOPES OF TELLURIUM

M. Ia. Kuznetsova, V. N. Mekhedov,
V. N. Rybakov, and V. A. Khalkin

In the work reported here an attempt has been made to determine the mass numbers and half-value periods of the tellurium isotopes with A < 118 from their daughter products, and also to establish the nature of the radiations from these isotopes.

The light isotopes of tellurium were produced by bombarding metallic antimony by protons from the synchrocyclotron of the Joint Institute of Nuclear Studies. The irradiated target was dissolved in a mixture of hydrochloric and nitric acids, and 10-15 mg of tellurium, selenium, and tin was added to the solution. After the excess nitric acid had been driven off, the selenium and tellurium were precipitated with sulfur dioxide from 3 M HCl. The precipitate was dissolved, and the selenium was driven out by sending HBr through the solution. The tellurium was then precipitated again with sulfur dioxide.

To eliminate radioactive contaminations we used precipitation of $Fe(OH)_3$ from an ammonia solution. The filtrate was acidified with hydrochloric acid, and the tellurium was precipitated again with SO_2, and was finally purified by subliming the metal at 600-800° C in a stream of hydrogen. The condensate was washed out with a few milliliters of concentrated hydrochloric acid containing Br_2. Part of this solution (approximately 0.05 ml), dried on a filter paper, was used for direct measurements of the half-value periods and types of radiation of the light isotopes of tellurium.

The daughter products (isotopes of antimony) were separated from the parent element by extraction in di-isopropyl ether from 8 M HCl containing Br_2.

The extract was washed with 8 M HCl, and the ether was driven off from a 3 M solution of HCl. The tellurium impurity in the resulting preparations did not exceed 0.2%. The separation of the daughter products was carried out for 12 hours at intervals of 1.5 hours. The radioactivity of the preparations was measured with an end-window counter MST-40. To determine the K-capture branching ratio, the radiation of some of the targets was subjected to additional study with a magnetic analyzer [1]. The energy of the positron radiation was determined from the absorption in aluminum.

The measurements gave the following results. The total decay curve of a radioactive preparation of tellurium consists of three components, corresponding to the following half-value periods: approximately 17 days (Te^{121}, K), approximately 6 days (mixture of Te^{118}, K and Te^{119}, K) [2], and, finally, a period approximately 2.5 hours. According to [3] this last period should be assigned to Te^{117}, which emits positrons with energy 2.5 Mev. The analyzer measurements showed, however, that about 75% of the radiation decaying with this period consists of x-rays. Furthermore, the energy of the positrons is somewhat higher (2.7 Mev).

The total decay curve of the antimony isotopes produced in the decay of the light tellurium isotopes also was found to consist of three components. The corresponding half-value periods are: 15 minutes, 2.8 hours, and about 6 days. The last period is in all probability due to slight contaminations (< 0.2%) of the daughter preparation by long-lived isotopes of tellurium. The short half-value periods belong to Sb^{117} (97% K and 3% β^+, $T_{1/2}$ = 2.8 hours) [4] and Sb^{116} (β^+, $T_{1/2}$ = 15 min, $E_{\beta+}$ = 2.4 Mev) [5], [6]* According to our measurements the K-capture branching ratio for Sb^{116} is about 10%.

* The isomer of Sb^{116} with half-value period 60 minutes [7] has not been observed in our work.

From this it follows that the tellurium activity with half-value period 2.5 hours belongs to a mixture of the isotopes Te^{116} and Te^{117}. From the decrease with time of the radioactivity of the daughter products it was found that the half-value periods of Te^{116} and Te^{117} are 2.5 hours and 1.7 hours, respectively.

It was impossible to determine the K-capture branching ratios of the individual tellurium isotopes because of the nearly equal half-value periods and the accumulation of the daughter products. It could be shown, however, that the main type of decay of these isotopes is K-capture. When there are equal amounts of Te^{116} and Te^{117}, 75% of the preparation, apart from that of the daughter products, is in acts of capture of an orbital electron.

LITERATURE CITED

[1] M. Ia. Kuznetsova and V. N. Mekhedov, Izv. AN SSSR, Ser. Fiz. 21, 1020 (1957).

[2] G. Seaborg, I. Perlman, and J. Hollander, Table of Isotopes (Russian Translation) (IL, Moscow, 1956).

[3] R. King, Rev. Mod. Phys. 26, 327 (1954).

[4] C. L. McGinnis, Phys. Rev. 97, 93 (1955).

[5] P. Stähelin and P. Preiswerk, Nuovo cimento 10, 1219 (1953).

[6] A. Aten, I. Manassen, and G. D. De Teyfer, Physica 20, 665 (1954).

[7] P. Stähelin, D. Maeder, and M. Pochou, Z. Physik, 140, 498 (1955).

Received December 11, 1957

MEASUREMENT OF β-ACTIVITY IN AN END COUNTER

N. E. Tsvetaeva and M. N. Brusentsova

The determination of β-activity of samples by measurement with an end counter requires the introduction of a number of corrections which take account of the solid angle, the absorption of the β-radiation in the counter window and the air gap between the counter and the sample, back scattering, self-absorption in the source, etc.

Usually, a general correction is made for the absorption in the counter window and the air [1-3]. When this method is used one adds to the thickness of the window an equivalent thickness for the air gap. The correction is introduced graphically, extrapolating the absorption curve of the β-radiation, or by multiplying the measured quantities by the factor [1, 2]

$$T = 2^{\frac{t_{win} + t_{air}}{d_{1/2}}},$$

where t_{win} is the thickness of the counter window, t_{air} is the width of the air gap, $d_{1/2} = f(E_0)$ is the thickness of the layer in which half of the radiation is absorbed (all quantities are given in mg/cm^2).

The values given in the literature [1, 2, 4] for the thickness of the layer in which half the energy is absorbed as a function of the β-radiation energy, $d_{1/2} = f(E_0)$ differ considerably among themselves (Fig. 1).

The values of $d_{1/2}$ for the nuclides S^{35}, Ca^{45}, Co^{60}, Tl^{204}, RaE, P^{32}, and UX_2 have been measured by absorption of the β-radiation (Fig. 1, Table 1).

The measurements were carried out with a VFL-25 end counter having a mica window 1.1 mg/cm^2 thick with a distance of 3 cm between the sample and the counter window. An aluminum absorber was placed against the counter window. The results were found to be in disagreement with the relation for $d_{1/2} = f(E_0)$ reported

in a paper by Bochkarev et al., [1] and in the book by Gusev [4]. The values for the half-absorption layer are in agreement only for small absorber thicknesses.

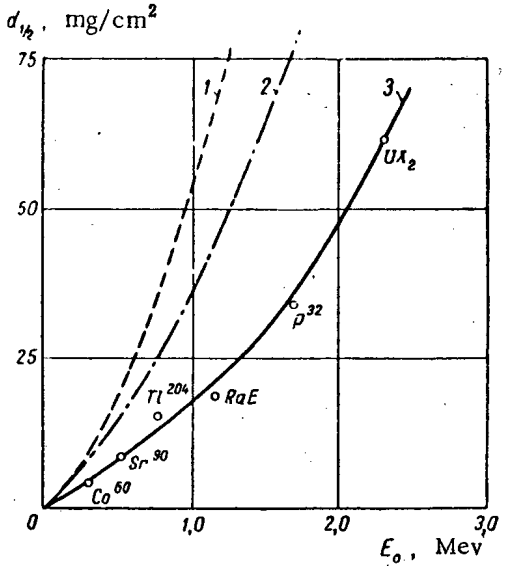

Fig. 1. The function $d_{1/2} = f(E_0)$. 1) Data of Gusev [4]; 2) data of Bochkarev et al., [1]; 3) data of the present work.

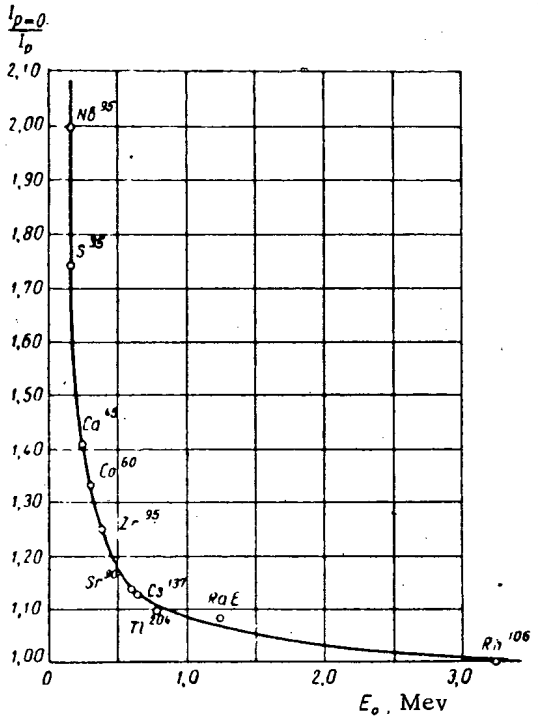

Fig. 2. The correction factor for absorption of β-radiation in air as a function of maximum energy of the β-radiation

$$\frac{I_{p=0}}{I_{p=\text{atm}}} = f(E_0).$$

TABLE 1

Values of $d_{1/2} = f(E_0)$.

Nuclide	Mev	$d_{1/2}$, mg/cm²		
		present data	data of [1]	data of [4] *
S^{35} . . .	0,167	2,8	3	3
Ca^{45} . . .	0,254	3,9	5,5	5,48
Tl^{204} . .	0,765	15,1	25	34,5
Sr^{90} . . .	0,54	8,7*)	15	20
RaE . . .	1,17	19	44	70
P^{32} . . .	1,7	34	77	121

* The layer for half absorption for β-radiation of Sr^{90} was determined from the accumulation of Y^{90}.

TABLE 2

Comparative Data for the Determination of Absolute β-Activity

Nuclide	E_0 Mev	β-activity, decays/min		
		4π-counter	end counter	
			present data	data obtained by usual method of calc.
Co^{60} . . .	0,306	23 700	24 500	36 200
Cs^{137} . . .	0,52	13 148	13 000	16 600
$Sr^{90} \rightarrow Y^{90}$	0,54 2,24	37 480	35 300	40 200

The same approach cannot be used in determining the corrections for the thickness of the counter window and the air gap because the intensity of the β-radiation, all other conditions being equal, will be affected to a great extent by the position of the absorber in the gap between the counter and the sample.

We have determined the correction factors for the absorption of β-radiation in air for Nb^{95}, S^{35}, Ca^{45}, Co^{60}, Zr^{95}, Sr^{90}, Cs^{137}, Tl^{204}, RaE, and Rh^{106} for an air gap 3 cm long (Fig. 2). These measurements were carried out in a vacuum chamber, inside of which was placed the sample being investigated and the VFL-25 counter (in some cases an MST-17 counter was used). The pressure p in the desiccator was varied from 5 to 760 mm Hg.

The corrections which were obtained (Figs. 1 and 2) were used to determine the absolute β-activity of Cs^{137}, $Sr^{90} \rightarrow Y^{90}$, and Co^{60} samples which had first been measured in a 4π-counter. The data are given in Table 2; it follows from this table that the measurements using the end counter agree with the measurements with the 4π-counter to within ± 6%. In Table 2 are also shown results obtained by introducing corrections for absorption in the counter window and in the air by the usual method (from the total thickness of the counter window and the air). At low β-energies these differ considerably from the results obtained with the 4π-counter. For example, in Co^{60} (0.306 Mev) this discrepancy is more than 50%.

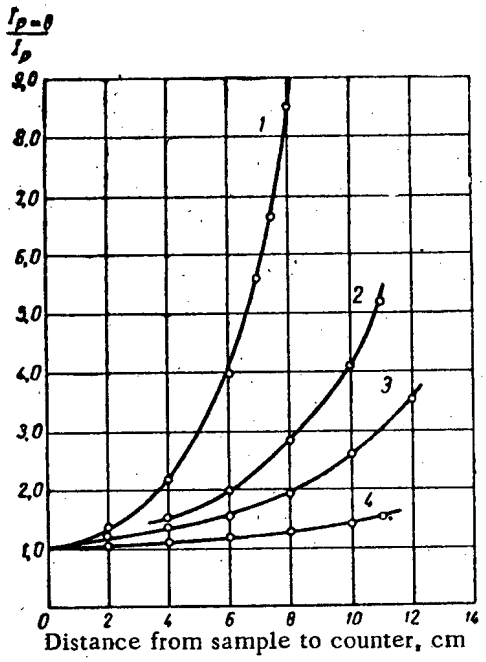

Fig. 3. The correction factor for absorption of of β-radiation in air as a function of the air gap. 1) For S^{35} (0.167 Mev); 2) for Ca^{45} (0.254 Mev); 3) for Co^{60} (0.306 Mev); 4) for Tl^{204} (0.765 Mev).

In Fig. 3 are shown the correction factors for air as a function of the air-layer thickness between 1 and 10 cm for S^{35}, Ca^{45}, Co^{60}, and Tl^{204}. It is apparent from these curves that for soft β-radiation (Ca^{45}, and S^{35}) the correction factor increases sharply as the air gap is increased between the limits indicated above.

The slope of the curves with respect to the abscissa axis falls off as the energy is increased; in Tl^{204} there is a relatively small increase in the correction factor with increasing length of the air gap.

LITERATURE CITED

[1] V. Bochkarev et al., Measurement of the Activity of Data on Beta and Gamma Sources (Academy of Sciences Press, USSR, 1953). *

[2] V. I. Spitsyn et al., Operational Method with Radioactive Indicators (Academy of Sciences, Press, USSR , 1955).*

[3] B. P. Burt, Nucleonics 5, 2, 28 (1949).

[4] N. G. Gusev, Handbook on Radioactive Radiation and Protection (Medgiz, 1956).*

[5] G. Seaborg, I. Perlman, and G. Hollender, Table of Isotopes (IL, 1956). **

Received December 20, 1957

* In Russian.
** Russian translation.

DOSIMETRY NOMOGRAM FOR DETERMINING WORKING TIME IN A MIXED RADIATION FIELD

G. M. Obaturov

In practice, one frequently encounters working conditions in which personnel are exposed to γ-radiation in addition to slow neutrons, fast neutrons, and β-particles; the atmosphere in the operating installation may also be charged by active gases and aerosols. It is also possible for the elements of the installation and clothing to become charged.

In these cases, in computing the permissible working time one must consider, in addition to the γ-radiation, the other types of radiation, the contamination of the air, clothing, and the installation itself.

The author has devised a dosimetry nomogram (see p. 771) for rapid calculation of the permissible working time under conditions in which several harmful agents work simultaneously.

On scale 3 of the dosimetry nomogram are plotted values of the number N for the permissible radiation levels, the contamination of the air by gases and aerosols, the contamination of the installation and clothing.

On scale 2 are plotted values of the function $1/t$; these are plotted in such a way that a permissible level corresponds to a vertically determined value of $1/t$.

The numerical value of $1/t$ is computed from the expression

$$1/t \text{ hours} = 0.125\ N.$$

Along scale 1 is plotted the permissible working time for the conditions which are of interest here. The values of N correspond to definite values of t at points of intersection of the vertical lines with both scales. For example, with N = 20, the permissible working time is 24 min; with N = 80 the permissible working time is 6 min.

Along scale 4 are plotted the values of the γ-fields in microcuries/sec corresponding to permissible level.

On scales 5-7 are plotted the values of fluxes for fast neutrons, slow neutrons and β-particles corresponding to the permissible level determined by a vertical line. The following permissible levels are taken [1]:

γ-radiation	1.8 microcuries/sec
fast neutrons	35 neut/cm^2 · sec
slow neutrons	1100 neut/cm^2 · sec
β-particles	75 particles/cm^2 · sec

The permissible level in gases and aerosols depends on the particular type. In the absence of any shielding against the gases or aerosols, for argon the permissible level is 10^{-8} curies/l, for I^{131} this level is $5 \cdot 10^{-12}$ curies/l, etc. [1].

When a gas protective unit such as the PSh-1, PSh-2, or clothing type LG-1 or LG-2 is used, the permissible level is 10^{-8} curies/l (because of external irradiation by β-particles without taking account of the absorption in the medium, the protective shield, and the jacket) for α-active gases or aerosols. For α-active gases and aerosols (particularly pure α-radiators which do not radiate γ-energy) the permissible level is unlimited when the protection indicated above is used.

In determining the contamination of clothing and the body, the original numbers have been taken as the limiting permissible levels used in the USSR.

In determining the working time with a contaminated piece of equipment, account must be taken of the fact that the clothing itself will become contaminated to the same extent as the equipment; thus, the limiting

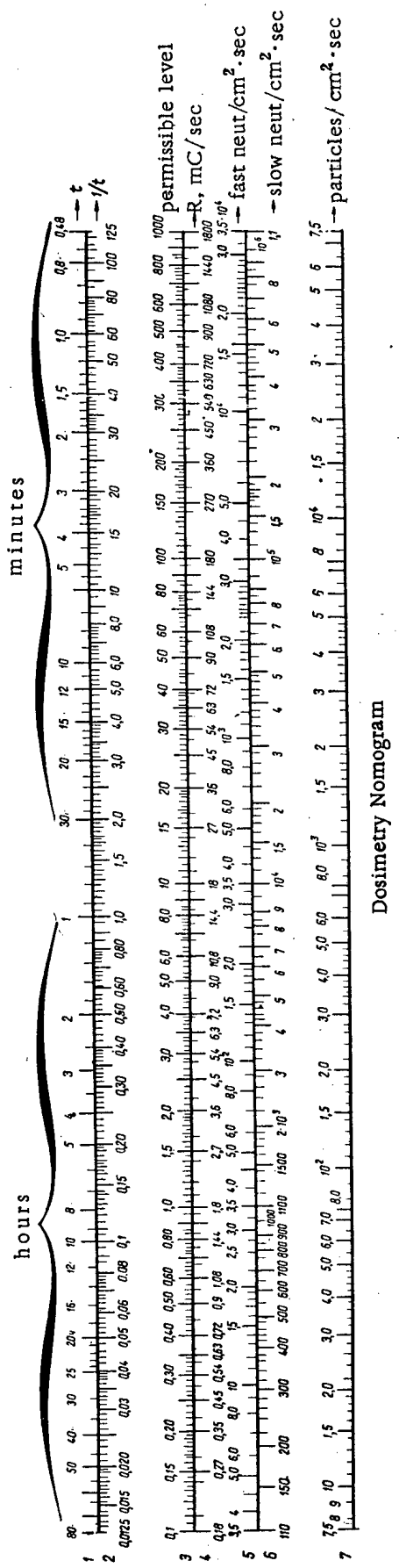

Dosimetry Nomogram

permissible level for contaminated equipment is equal to the limiting permissible level for outer clothing.

The contamination of the equipment is verified by taking smears. If the active meterial is deep in the substance and does not contaminate the clothing, the contamination is taken as zero and one need compute only the flux of β-particles for γ-radiation from the equipment itself.

We now illustrate the use of this dosimetry nomogram.

Suppose that in a given installation the γ-radiation is 20 microcuries/sec, the β-particle flux is 100 particles/$cm^2 \cdot$sec, the fast-neutron flux is 100 neut/$cm^2 \cdot$sec, the contamination of the equipment is twice the permissible level, the contamination of the overalls is 0.5 of the permissible level.

It is required to find the permissible working time in this installation.

Using the nomogram we determine the value of $1/t$ for each factor. The following values are obtained: 1.4, 0.17, 0.36, 0.25, and 0.06. The total is 2.24, which corresponds to a permissible working time of 27 minutes.

A person working in a mixed radiation field receives an actual dose which exceeds the γ-radiation dose.

The total dose, expressed in ber-units is computed from the formula taken from [1]:

$$D = D_\gamma \frac{t_\gamma}{t_{tot}}$$

where D_γ is the dose received in the working time due to γ-radiation which is determined by the individual personnel dosimeter (a film badge type or a KID-1); t_γ is the permissible time computed taking account only of the γ-radiation, t_{tot} is the permissible time computed taking account of all forms of radiation and contamination.

For example, in measuring the radiation and contamination for the purpose of determining the permissible working time in a mixed radiation field we find $t_\gamma = 3$ hours and $t_{tot} = 2$ hours.

After the work a dosimeter of the KID-1 type showed 0.5 of the permissible dose.

Hence the true dose is found to be

$$D = 0.5 \frac{3}{2} = 0.75 \text{ of the permissible dose}$$

The dosimetry nomogram which has been described may be used conveniently for carrying out many types of calculations under different working conditions.

LITERATURE CITED

[1] N. G. Gusev, Handbook on Radioactive Radiation and Protection (Medgiz, 1956).*

Received January 25, 1958.

* In Russian.

SCIENTIFIC AND TECHNICAL NEWS

ON THE PRESENT STATE OF THE PROBLEM OF ACCELERATING ATOMIC PARTICLES

(From the Annual Session of the Academy of Sciences of the USSR)

At the Annual Session of the Academy of Sciences of the USSR, convened in March, 1958, Corresponding Member V. I. Veksler of the Academy of Sciences delivered a speech dealing with the present state of the problem of atomic-particle acceleration. He gave an account of the history of the development of accelerator techniques, and of the difficulties standing in the way of further step-ups in the energy and intensity of beams of charged particles.

The technique of strong beam focusing, proposed by the American scientists Courant, Snyder and Livingston* had opened the way for increasing the maximum energy of accelerated particles only by a factor of several times. In order to obtain beams of high-energy particles with energies in the hundreds and thousands of billions of electron-volts, new accelerating techniques are called for. One of these methods is based on the use of colliding beams of high-energy particles [1]. The process of interaction, as for example, in the collision of two 10-Bev protons moving head-on against each other, matches the effect produced by the bombardment of an immobile proton by a proton of about 200 Bev energy. To enhance the probability of head-on collision between particle beams, the instantaneous values of the current flowing in the accelerators must be raised by 500-1000 times.

We are familiar with the fact that A. A. Kolomenskii, V. A. Petukhov, and M. S. Rabinovich [2] in the Soviet Union suggested, in 1953, magnetic systems using a time-invariant magnetic field, which would facilitate considerably the achieving of increased beam intensity in high-energy particle accelerators. A similar suggestion was voiced somewhat later in the U.S.A. as well (D. W. Kerst, Simon et al.).

V. I. Veksler drew attention to the fact that further research and development work on high-energy particle accelerators using large currents is out of the question unless the collective interaction between particles and studies on processes taking place in plasma are taken into account.

In 1956, the Soviet scientist Ia. B. Fainberg [3] pointed out the possibility of employing a plasma immersed in a magnetic field in particle accelerators. In a linear accelerator coupled to a plasma-filled waveguide, it is possible to combine conditions of phase and space stability which are usually incompatible for a beam of particles.

An intriguing method for making use of plasma in order to obtain high magnetic field strength (in hundreds of kilo-oersteds) has been proposed by the Soviet scientist G. I. Budker [4]. With the aid of this technique, the dimensions and weight of accelerators were considerably reduced.

In the conclusion of his address, V. I. Veksler spent some time on the coherent method of accelerating atomic particles [5]. This technique of particle acceleration involves the use of the interaction of small bunches of charged particles with a stream of high-energy electrons, or the interaction of a bunch of particles at rest with a relativistic bunch of particles of large mass. The interaction between charged, and even quasineutral, bunches and electromagnetic waves may also be used. The magnitude of the accelerating field in the coherent method

* E. D. Courant, M. S. Livingston, and H. S. Snyder, Phys. Rev. 88, 1190 (1952). "The Strong-Focusing Synchrotron, a New High-Energy Accelerator."

is proportional to the number of accelerated particles available. V. I. Veksler considers that, with the aid of the coherent method, it will be possible to proceed to the development of accelerators operating at very high current levels and accelerating to superhigh energies of the order of 10^{12} ev and higher.

LITERATURE CITED

[1] G. K. O'Neill, Phys. Rev. 102, 1418 (1956).

[2] A. A. Kolomenskii, V. A. Petukhov, and M. S. Rabinovich, Symposium: "Some Problems in the Theory of Cyclic Accelerators," (Izvestiia Akad. Nauk SSSR 1955), p. 7.*

[3] K. D. Sinel'nikov, Ia. B. Fainberg, and P. M. Zeidlits, CERN Symposium, Proceedings, 1, 84 (Geneva, 1956).

[4] G. I. Budker, J. Atomic Energy (USSR) 1, 5, 9 (1956).**

[5] V. I. Veksler, J. Atomic Energy (USSR) 2, 5, 427 (1957).**

N. F.

7-Bev AND 12.5-Bev SYNCHROCYCLOTRONS

A communication has already been published, in 1957 [1], on the 7-Bev synchrocyclotron project underway at the National Institute for Research in Nuclear Physics (Britain); some of the details pertaining to the plans for this proton accelerator have been made public since that time [2].

The chamber measures 45 meters in diameter. The weight of the magnet poles is 6000 tons. The building of reinforced concrete which houses the accelerator occupies an area 60 meters across (see Fig. 1). The concrete roof of the structure, with a thickness of 1.35 meter, will be covered over by a layer of earth 3 meters deep. If it is found necessary, the thickness of the earth roof shielding may be doubled. Biological shielding of the personnel will be provided by an earth fill-in and shielding blocks. The basic shielding wall, separating the accelerator site from the measurements pavilion, will be made of concrete 8.4 meters thick, with removable blocks. The measurements pavilion will be surrounded on all sides by earth embankments. Particle beams extracted from the chamber of the accelerator will be absorbed at the terminus of long tunnels hollowed out in the walls of the measurements pavilion. Protective screening against radiation may be installed above the targets. The area set aside for the housing of the remote control apparatus for the accelerator, for measurements gear and preoperational equipment, will occupy 360 m^2.

At the Argonne National Laboratory (U.S.A.), construction of a 12.5-Bev proton synchrocyclotron has been proposed [2, 3]. The cost of the accelerator is estimated at 27 million dollars. Figure 2 gives a view of the arrangement of the basic units of the accelerator.

The synchrocyclotron injector unit will be a 50-Mev linear accelerator. Protons will be introduced into the chamber from the interior of a toroidal magnet. The radius of the orbit will be approximately 29 meters. The duration of an acceleration cycle will be 1 sec. Pulses of particles will be repeated every 4 sec. It is proposed that this accelerator should yield a greater number of particles than any existing or projected accelerator of similar design.

* In Russian.

** Original Russian pagination. See C. B. Translation.

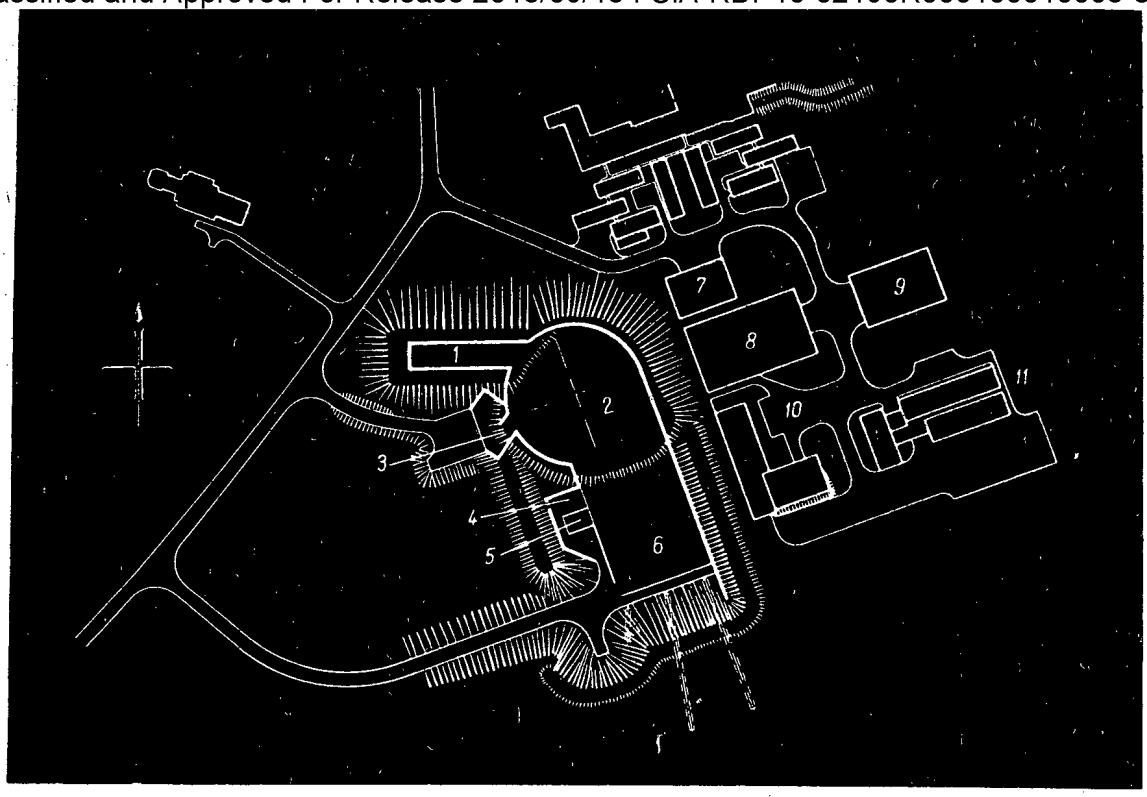

Fig. 1. Diagram showing site of basic components of planned 7-Bev synchrocyclotron (Britain). 1) Injector, 2) accelerator room; 3) measurements cubicle; 4) hydrogen plant; 5) bubble chamber; 6) measurements pavilion; 7) heat-exchanger plant; 8) motor-generators; 9) building for assembly and testing; 10) building for control of accelerator and for preliminary work; 11) administration and laboratory building.

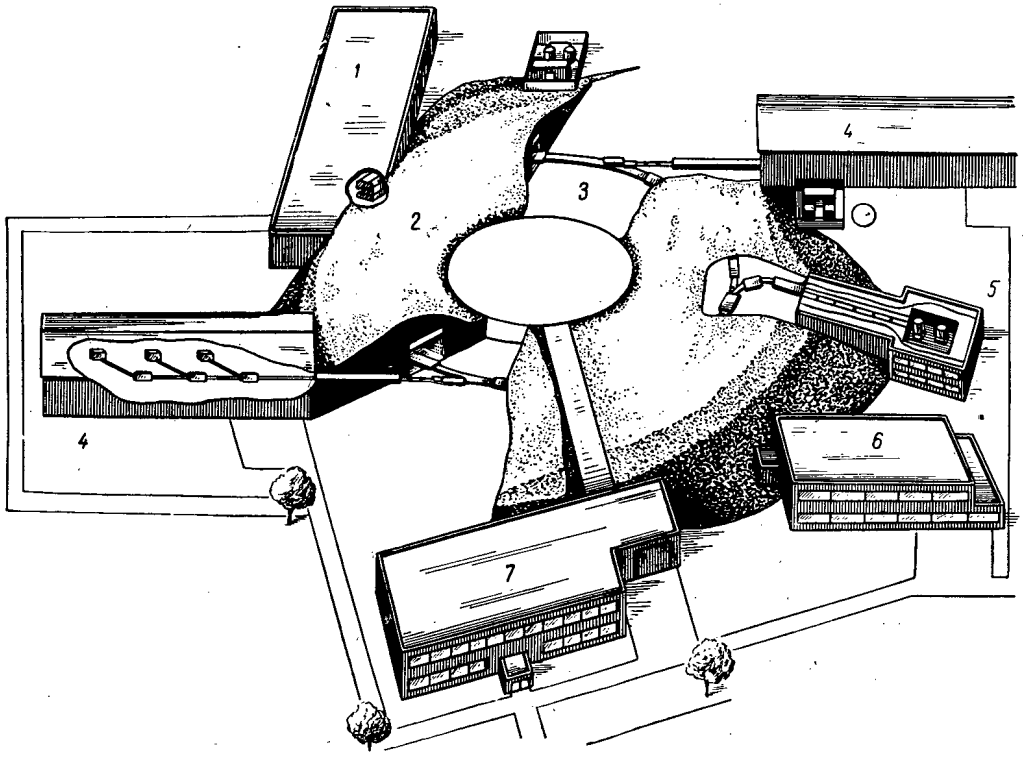

Fig. 2. Diagram showing site of basic components of projected 12.5 Bev synchrocyclotron at Argonne National Laboratory. 1) Building for meson measurements; 2) shielding embankment; 3) toroidal magnet; 4) building for proton measurements; 5) injector; 6) building for housing electrical gear; 7) accelerator control building.

LITERATURE CITED

[1] Nucl. Engineering 2, 18, 401 (1957).

[2] Engineering 185, 4792, 42 (1958).

[3] Engineering 184, 4772, 255 (1958).

N. F.

A SINGLE-DEE CYCLOTRON*

In a conventional cyclotron with two dees, it is not always possible to perform experiments within the accelerating chamber because of space limitations in the area between the dees with their large high-frequency potential. These difficulties are completely eliminated in a cyclotron using a single dee. Instead of the second, a "grounded" frame or dummy dee ["Gegendee"] is installed. The chamber space made available in this manner may be utilized for the placement of measuring probes, ion sources and deflecting systems, while the structural shaping, adjustment and operation of these devices is facilitated to an appreciable degree. In the single-dee cyclotron, the axis of the resonant circuit is directed perpendicular to the accelerating slot between the dee and the grounded frame, with the result that the electric field existing in the slot proves to be symmetric with respect to the center of the slot. As a result of the greater freedom in the choice of the diameters of the stub and tank of the resonant circuit in the single-dee cyclotron, it is possible to achieve a greater stability in the position of the dee in the chamber than is the case with a double-dee cyclotron. The high-frequency power losses are about the same in either case. Consideration should be given, however, to the fact that a single-dee cyclotron has one substantial drawback: the difference in potentials between the dee and frame must be twice the potential difference in a double-dee cyclotron.

All the considerations cited were taken into account in the redesigning of the Heidelberg cyclotron. Since September, 1956, this cyclotron has been operating with a single dee. The figure below shows a cutaway view of the arrangement.

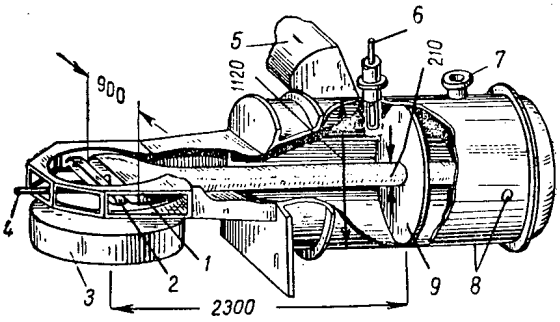

Diagram of chamber and resonant circuit of cyclotron at Heidelberg. 1) Dee; 2) grounded frame ("Gegendee"); 3) pole; 4) ion source; 5) vacuum-pump connection; 6) high-frequency cable; 7) vacuum meter; 8) dee-adjusting device; 9) resonant circuit shorting plate.

The peak energy given to the cyclotron deuterons is 12.9 Mev. The strength of the magnetic field is 16.9 kilo-oersteds. The diameter of the magnet poles measures 101 cm, the pole gap 27.6 cm. The chamber lids are made of soft magnet steel (diameter 100 cm, thickness 6 cm, distance between lids 15 cm). The weight of the magnet is 80 tons, and the available power 54 kw. The magnetic field has 0.01% stability.

The chamber, manufactured from nonmagnetic chrome-nickel steel, has five removable aluminum walls, each 2 cm thick. Deflecting instruments, ion sources and two ports allowing access to measurement probes may be installed on the three forward walls of the chamber. Dee-voltage meters and piping for cooling of the frame may be mounted on the lateral walls. The surfaces of the chamber, along which the high-frequency current flows, are covered with electrolytic copper.

* R. Bock, A. Döhring, J. Fanecke, O. Knecht, L. Köster, H. Maier-Leibnitz, Ch. Schmelzer, and U. Schmidt-Rohr, Zeitschrift für angewandte Physik 10, 2, 49 (1958) "Ein Festfrequenz-Zyklotron mit einem Dee."

The distance between the dee and the chamber coverings is 3.8 cm, while the internal height of the dee at the center is equal to 6 cm, with a height of 4.2 cm at the periphery. The diameter of the tank circuit stub, to which the dee is fastened, measures 21 cm, while the inner diameter of the tank is 112 cm. The position of the dee inside the chamber is controlled with the aid of an adjustment device situated on the shorted end of the resonant circuit. The gross weight of the chamber and resonant circuit is about 3 tons.

The quality factor Q of the resonant system of the cyclotron is closely dependent on the amplitude of the high-frequency voltage and on the state of the vacuum. The rated $Q = 15 \cdot 10^3$. Measurements performed with the aid of a microwave laboratory oscillator (small voltage amplitudes) showed that, at a pressure of 10^{-5} mm Hg, immediately following the shutting off of the cyclotron and after a protracted period of rest, $Q = 3 \cdot 10^3$, while in the range of pressures from 10^{-3} to 76 mm Hg, $Q = 10.8 \cdot 10^3$. At high voltage amplitudes (for measurements in this case, a high-frequency cyclotron oscillator was used), and over the range of pressures from 10^{-5} to 10^{-6} mm Hg, $Q = 10.8 \cdot 10^3$. The lowering of Q at low amplitudes is associated with multiple high-frequency oscillations of the charges formed in response to the ionization of the residual gas. With increased pressure, the mobility of the charges dropped off, and Q increased correspondingly. When the high-frequency field oscillated at large amplitudes, the oscillatory process did not have time to build up, so that the charge was rapidly drawn off to the walls.

The high-frequency oscillator is a seven-stage oscillator. A frequency of 12.8Mc is obtained after the frequency of the driving oscillator is doubled three times. In order to avert the appearance of a glow discharge in the resonant circuit tank at low high-frequency voltages, a steady voltage of 2 kv is applied to the dee and to the stub. For this purpose, the shorting plate in the resonant circuit is made of two parts, separated by a vacuum capacitor of 0.15 μf total capacitance. The change in the grid bias of the high-frequency oscillator second stage may pass rapidly through the danger voltage region of 5-15 kv. After an amplitude of 15 kv is attained, the need for constant voltage is not so pressing. The peak dee voltage value obtained with this cyclotron reaches 100 kv. The dee and the frame are covered with a layer of chromium (25 μ), which protects their surfaces against oxidation and scratches suffered in disassembling the cyclotron, while at the same time reducing the number of high-voltage breakdowns. For protection against protracted discharges, provision is made for a special automated control system shutting off the high-frequency oscillator.

The strength of the magnetic field was measured to an accuracy of 0.01% by an instrument based on the principle of the Hall effect.

The inner annular shims have a width of 8.5 cm and a maximum height of 1.1 cm. Collapse of the field at an end radius of 42.5 cm is about 1.5%. The maximum deviation of the average bounding surface of the magnetic field from the mean geometric plane at a radius of 37-39 cm comes to 0.8 cm. The deviation of the surface at a terminal radius is equal to 0.2 cm. The azimuthal nonhomogeneity of the field is less than 0.1%.

An ion source with a capillary arc and graphite "adapters" is used in the cyclotron. The peak ion current provided by the source is 30 ma, and 0.5 ma at the terminal radius. The energy spread of the beam, as measured by the method of slowing down deuterons in aluminum foils and on the basis of a change in the coloration of LiF crystals, comes to $\pm$ 1%.

The vacuum equipment of the cyclotron consists of an oil diffusion pump (Leybold OT 8000) with a pumping speed of 8000 liters/sec, a booster steam oil pump and two mechanical pumps. The diffusion pump is connected to the tank of the resonant circuit by an exhaust duct measuring 40 cm in diameter. A grid placed across the end cross section of the duct (10 strips of copper foil) eliminates any distortion of the high-frequency field in the circuit tank due to the pumping orifice. The volume to be pumped out is 3 m^3. In 12 hours of pumping after the first operational assembling of the unit, a vacuum of $8 \cdot 10^{-6}$ mm Hg was achieved. A one-hour run-in of the chamber led to an improvement of the vacuum to $5 \cdot 10^{-6}$ mm Hg. The pressure rise with the pump valve closed reaches $5 \cdot 10^{-8}$ mm Hg per sec.

A. B.

A 1-Bev SYNCHROTRON IN ITALY

At the National Laboratory in Frascati (15 km north of Rome), a synchrotron is being built to yield electron energies of 1 Bev [1, 2]. The maximum magnetic flux density at the orbit $B_{max} = 9260$ gauss. The frequency of the alternating current feeding the magnet is 20 cps. The amplitude of the variable component of the flux density and the magnetization vary over a range from 4170 to 4630 gauss. The radius of the fundamental orbit R = 360 cm. The number of rectilinear intervals N = 4. The length of these intervals L = 120.6 cm. The period of revolution of an electron toward the end of an acceleration cycle (v = c) $T = 9.154 \cdot 10^{-8}$ sec. The parameter of the collapse of the magnetic field n = 0.61. The total injection energy $E_i = 2.5$ Mev. The field induction, at the orbit, is $B_i = 22.7$ gauss on injection. Frequency ratio k = 4. Injection frequency $\nu_i = 42.78$ Mc, and, at the end of an acceleration cycle, $\nu_f = 43.70$ Mc. The theoretical value of the modulation index for the frequency is 2.11%.

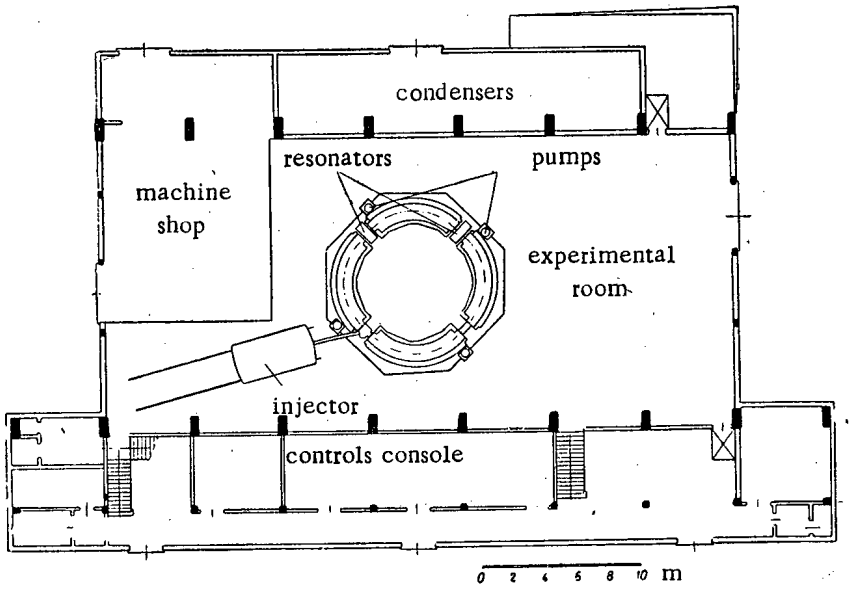

Floor plan of 1-Bev synchrotron installed at the National Laboratory in Frascati. 1) Machine shop; 2) condensers; 3) resonators; 4) pumps; 5) experimental room; 6) injector; 7) controls console.

The gap between the magnet poles is 8.6 cm, the width of the poles 22.7 cm. The weight of iron in the magnet is approximately 93 tons, and the weight of copper is approximately 8-10 tons. ARMCO-DI-MAX silicon steel sheet (0.35 mm thick) was used. Capacitance of the bank of condensers is 3420 μf. An ac generator delivers a power of 510 kva, while a dc generator supplies 315 kw. The sketch shows the ground plan of the synchrotron laboratory and the location of the basic equipment.

LITERATURE CITED

[1] Atomo e Industria 1, 1-2, 9 (1958).

[2] Atomo e Industria 1, 3, 3 (1958).

N. F.

MEASUREMENTS OF THERMAL NEUTRON SPECTRUM IN A SWEDISH D_2O REACTOR R1*

Measurements of the energy distribution of neutrons expelled from nuclear reactors show that no thermal equilibrium is established between the neutrons and the atoms of the moderator in the reactor core lattice. The effective neutron temperature exceeds the moderator temperature by 50-150° C.

In the paper reviewed in the present discussion, the energy distribution of the neutrons emergent from the horizontal channel of the Swedish heavy water reactor R1 were investigated. The arrangement of the experiment is diagrammed in Fig. 1.

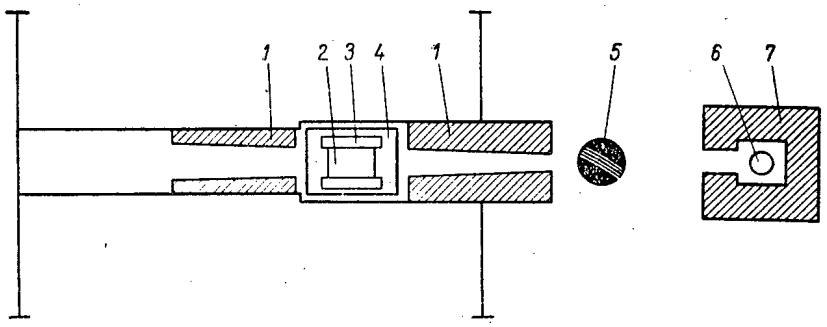

Fig. 1. Experimental arrangement (with beryllium filter inserted). 1) Cast-iron collimators; 2) beryllium filter, 20 × 10 × 10 cm ; 3) cooling jacket filled with liquid nitrogen; 4) evacuated stainless-steel container; 5) mechanical chopper; 6) BF_3 counter measuring 30 mm across; 7) shielding.

Cast-iron collimators shaped a neutron beam with a cross-section area of 10 × 5 cm^2. For the investigation of the "cold" part of the spectrum, a beryllium filter, 20 cm thick, cooled by liquid nitrogen, was inserted into the channel. Analysis of the neutrons was carried out by a velocity delay selector using a slow neutron chopper with curved slits, a boron trifluoride-filled detector and a 100-channel time analyzer.

A flux of neutrons of less than 0.4 ev energy (cadmium cut-off level) at the output of the channel proved to be equal to $3.4 \cdot 10^8$ neutrons/$cm^2 \cdot$sec with the reactor operating at 600 kw power. The cadmium ratio was equal to 65. When the beryllium filter was introduced into the channel, the neutron flux dropped off to $4.4 \cdot 10^6$ neutrons/$cm^2 \cdot$sec.

Correction terms were introduced into the measurements of the neutron spectra for: 1) misreadings in discrete channels of the selector (up to 30%); 2) the epicadmium neutron background (up to 30%); 3) the dependence of the transmission function of the chopper on its speed of rotation (up to 13%); 4) self-screening effect of the counter (up to 100%); 5) absorption and scattering of neutrons in the six-meter-long air gap between the reactor and the counter (up to 50%); 6) absorption and scattering in the 25 mm thick aluminum traversed by the beam. With the aid of the last correction, irregularities in the slope of the neutron energy distribution curve, in the 4.05 to 4.65 A wavelength region (Bragg cut-off wavelengths in aluminum) were eliminated.

Figure 2 shows the distribution measured empirically. The slow-neutron spectrum is given the best fit by the formula

$$dn = \text{const}\, \lambda^{-m} \exp\left(-\frac{\lambda_0}{\lambda}\right)^2 d\lambda, \qquad (1)$$

where m = 4.07 (instead of m = 4 for a Maxwellian distribution), $\lambda_0 = 1.67$ A. The neutron temperature, arrived at with the aid of the constant λ_0, was equal to 341 ± 10° K at a moderator temperature of 298° K.

* K. E. Larsson, R. Stedman, and H. Palevsky, J. Nucl. Energy 6, 3, 222 (1958).

The energy distribution of the neutrons passed through the beryllium filter experiences a sharp discontinuity at the cut-off $\lambda = 3.96$ A. The distribution at $\lambda > 4$ A is described by Formula (1) with the same $\underline{m}$ and λ_0.

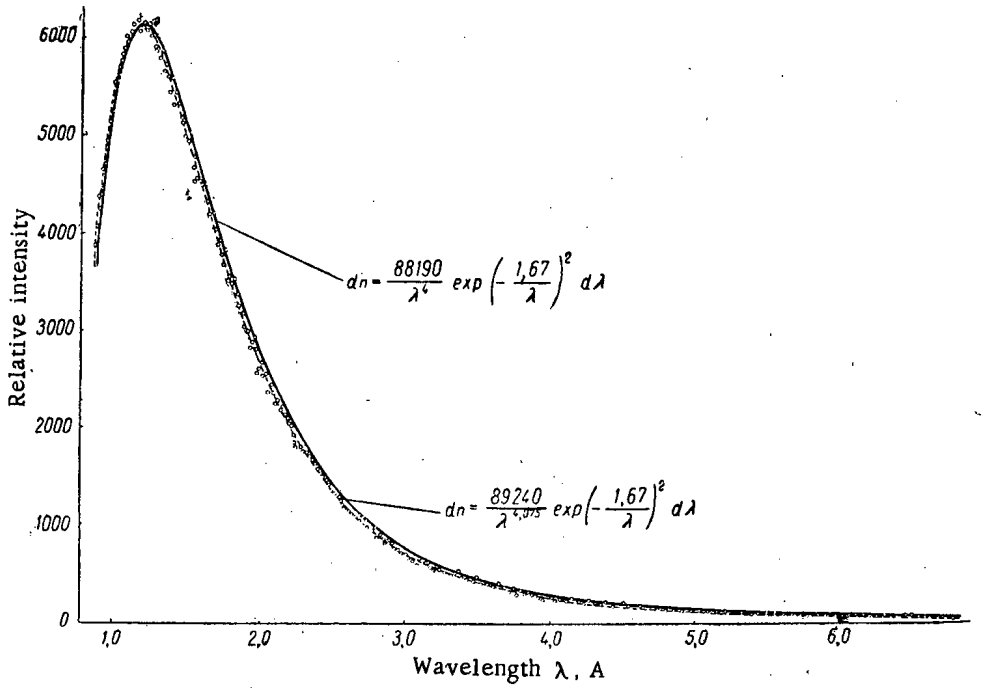

Fig. 2. Energy distribution of neutrons of wavelength $\lambda < 7$ A. The solid line gives the Maxwellian distribution at the same temperature as in the experimental energy distribution.

Integrating this equation over the interval $3.96 \text{ A} < \lambda < \infty$ determines the percentage (5.2%) of cold neutrons passing through the beryllium filter.

P. K.

ENGINEERING TEST REACTOR (ETR)

In September 1957, two years after ground was broken, the Engineering Test Reactor ETR (see Fig. 1) was brought to critical state at the National Reactor Testing Station in Idaho. In October, the reactor was started up for normal operation [1, 4].

The ETR reactor is a more sophisticated version of the well-known MTR reactor. The main purpose of the new reactor is the creation of conditions necessary for full-scale testing of fuel elements, structural materials, coolants, etc. In connection with this task, a large number of experimental channels and loops are provided for in the reactor.

The design of the ETR reactor core is somewhat unconventional. Fuel elements of the same type as employed in MTR, i.e., flat plates 91.4 cm in length, are assembled into a square unit cell of 7.6 × 7.6 cm cross section.

The reactor core contains 49 such unit cells and 16 control rods. The cells and the rods are so arranged that a number of holes are formed in the core, providing access for carrying out experiments (Fig. 2).

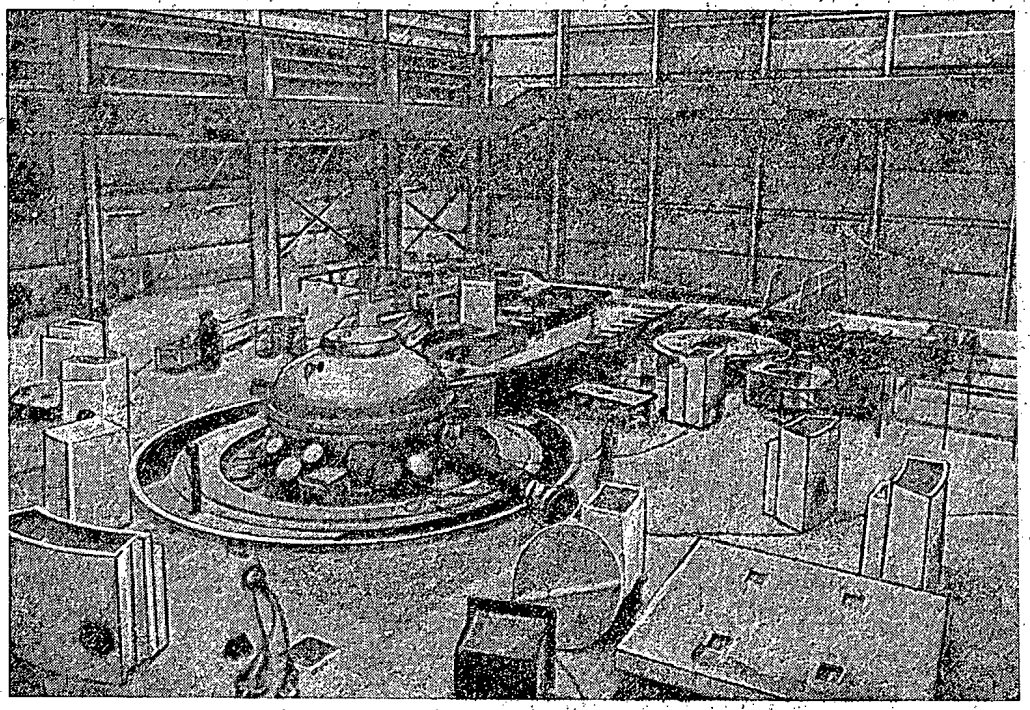

Fig. 1. View of main reactor room. The top shell of the reactor is in view with the upper shielding removed.

Ordinary water is employed as moderator and heat extraction agent in the reactor. The fuel used is enriched uranium. Depending on the number of experiments being performed at one time, the reactor charge fluctuates from 14 to 18 kg U^{235}. For a more uniform variation in reactivity over the course of a run (20 full days), a burnable absorber, boron (1.25 g of boron to each element), is added to the fuel elements.

The core of the pile is surrounded by a beryllium reflector approximately 11.5 cm in thickness. Access holes are formed through the beryllium slabs to facilitate the carrying out of experiments (the holes are capped by removable plugs). Behind the beryllium reflector, there is a water-aluminum reflector, also provided with access holes to facilitate the performance of experiments on core components, while there are openings with removable plugs in the blocks of the aluminum reflector.

Reactor control is carried out by means of 16 control rods, including 12 "gray" [12% reactivity] rods. The absorbing and scattering properties of these rods are the same as that of the fuel elements. The "gray" rods serve to balance and level out slow changes in reactivity. Four "black" rods, capable of absorbing practically all the neutrons impinging on them, are available for scramming the reactor. To maintain the required power levels, two regulating rods are available in the beryllium reflector; rod control is carried out automatically.

The over-all compensating capacities of the rods (in percentage):

12 shim rods	12
4 scram ("black") rods	13.5
2 automatically operated regulating rods	0.3

The automatically operated regulating rods are of boron-modified stainless, with the rod diameter being 44.5 mm. The reactor pressure vessel (Fig. 3) consists of an outer thick-walled shell capable of withstanding the pressure and an inner reactor tank surrounding the core; between them are sandwiched steel thermal-neutron shields.

The pressure vessel is made from carbon steel, and lined on the inside with stainless steel. The diameter of the reactor vessel measures 3.6 meters, the diameter of the inner tank 2.4 meters, and the over-all weight is approximately 75 tons.

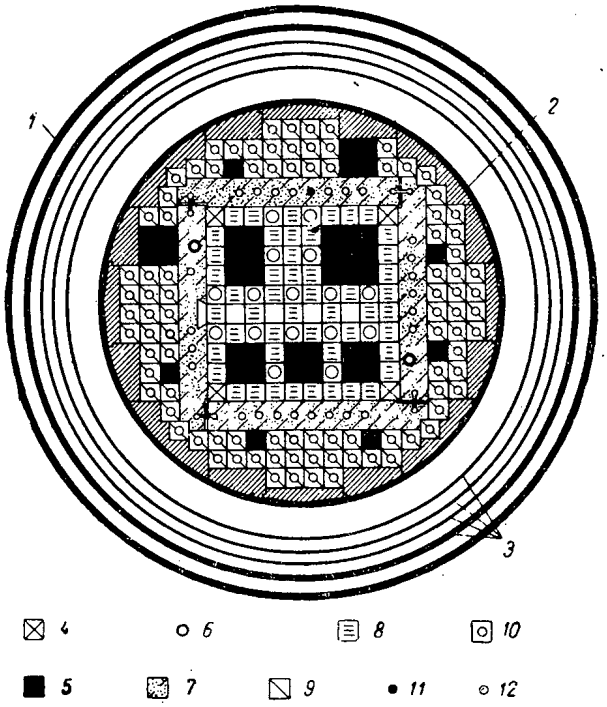

Fig. 2. ETR reactor zone. 1) Reactor pressure vessel; 2) core inner shell; 3) thermal shields; 4) water-aluminum reflector; 5) experimental channel; 6) control rod; 7) beryllium reflector; 8) fuel-element assembly; 9) aluminum reflector; 10) shim rod; 11) source; 12) removable plugs for experimental access holes.

The system of heat extraction from the reactor comprises two loops, with a secondary water system to reject heat from the heat exchanger to a cooling tower. Water is admitted into the reactor through the upper nozzle, is routed downward to cool the fuel elements and the reflector, and then flows upward past the thermal shields and passes out of the reactor via the lower nozzle. The rate of water flow amounts to 10^4 m^3/hr, the temperature of the water at the entrance to the reactor is 43.5° C, the temperature at the exit is 59° C; the maximum temperature at the surface of one of the fuel elements reaches (with a heat flux of approximately $2.7 \cdot 10^6$ kcal/m^2·hr) 138° C. The pressure in the loop is approximately 14 atmospheres.

Biological shielding of the reactor is made from magnetite concrete of 3.5 g/cm^3 density. A thermal shield of lead sheeting, sandwiched between steel jackets, is placed between the reactor and the biological concrete shield.

Basic Characteristics of ETR Reactor

Reactor power	175 Mw
Average heat flux	$1.2 \cdot 10^6$ kcal/m^2·hr
Maximum heat flux	$3.1 \cdot 10^6$ kcal/m^2·hr
Average thermal-neutron flux	$4 \cdot 10^{14}$ neutrons/cm^2·sec
Average fast-neutron flux	$1.5 \cdot 10^{15}$ neutrons/cm^2·sec

Experiment access holes in core, by cross section:

23 × 23 cm	1 hole
23 × 15 cm	1 hole
15 × 15 cm	3 holes
7.6 × 7.6 cm	4 holes

Experimental access holes in reflector, by cross section:

15 × 15 cm	2 channels
7.6 × 7.6 cm	6 channels

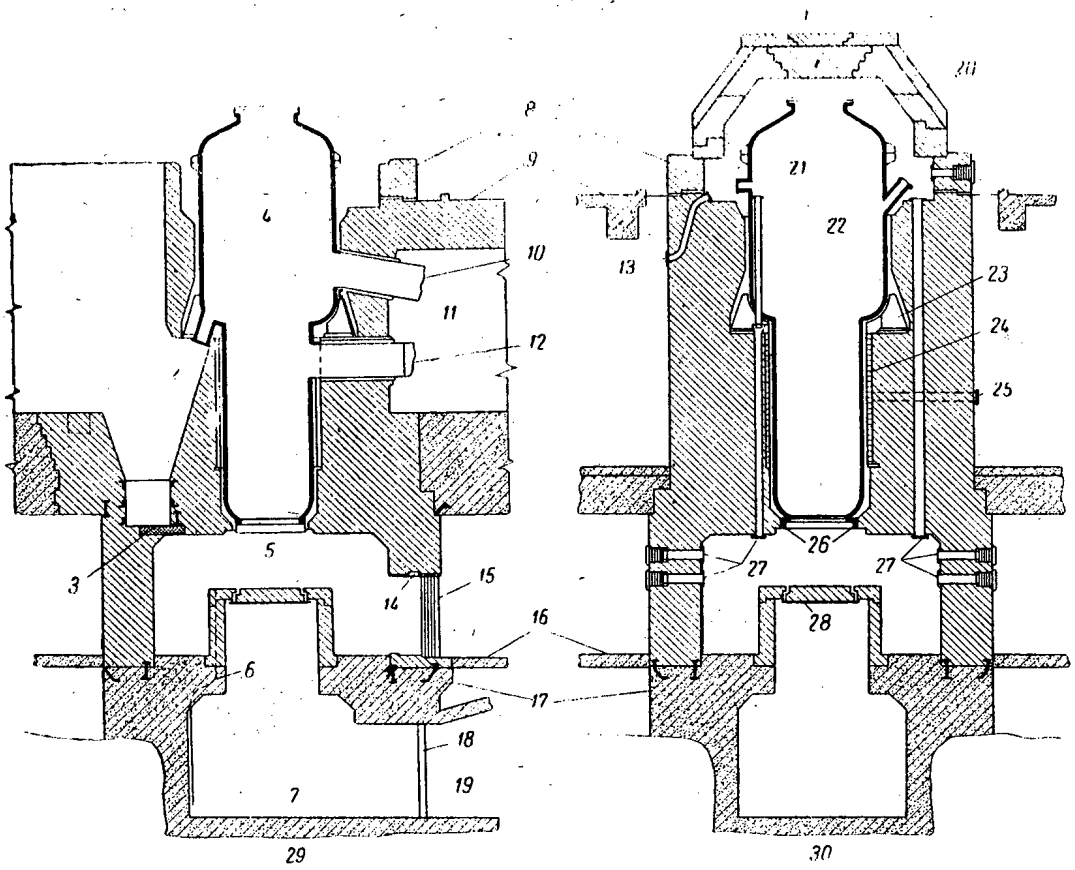

Fig. 3. Schematic cross section of ETR reactor. 1) Reservoir; 2) discharge chute; 3) sheet steel shielding; 4) reactor pressure vessel; 5) subpile room; 6) canopy drainage line; 7) control rod access room; 8) removable shield segments; 9) floor of main room; 10) inlet header; 11) pipe and plumbing tunnel; 12) outlet header; 13) auxiliary access conduit; 14) lead shielding; 15) shielding door, of steel sheet; 16) basement floor; 17) substructure and foundation; 18) door to control rod room; 19) tunnel entrance to control rod access room; 20) reactor top head shield; 21) horizontal nozzle; 22) slanting nozzle; 23) support shoe; 24) outer thermal shield; 25) ionization chamber tube; 26) vessel guide lugs; 27) in-shield sleeves, with plugs (for reactor experiments); 28) control rod mounting plate.

LITERATURE CITED

[1] Nucl. Engineering 2, 20, 476 (1957).

[2] Engineer 5317, 917 (1957).

[3] Engineer 5318, 948 (1957).

[4] Nucleonics 16, 1, 102 (1958).

I. S.

THE AMERICAN BOILING-WATER REACTOR VBWR

The boiling-water reactor VBWR [Vallecitos Boiling-Water Reactor], delivering 30 thousand kw thermal power and 6 thousand kv electric power [1] is the second boiling-water reactor brought to full power (after the EBWR reactor) at the Vallecitos Atomic Laboratory (GE), San Jose, California. Start-up was in October, 1957. The reactor section of the installation (costing some two and a half million dollars) belongs to General Electric Company, while the power plant (costing five hundred seventy two thousand dollars) belongs to the Pacific Gas and Electric Co., whose network is fed by the electric power produced in the plant. The power plant took about 17 months to build [2].

The basic concept behind the structural design of the VBWR is similar to the concept underlying the design of its sister reactor EBWR [3]. Boiling of the water which carries out the function of moderator and coolant takes place in the core inside the pressure vessel. The saturated steam so obtained is admitted directly to the turbine via the separator. The steam condensate from the turbine condenser is recycled to the core for a repeat flash (see Fig. 1) [4].

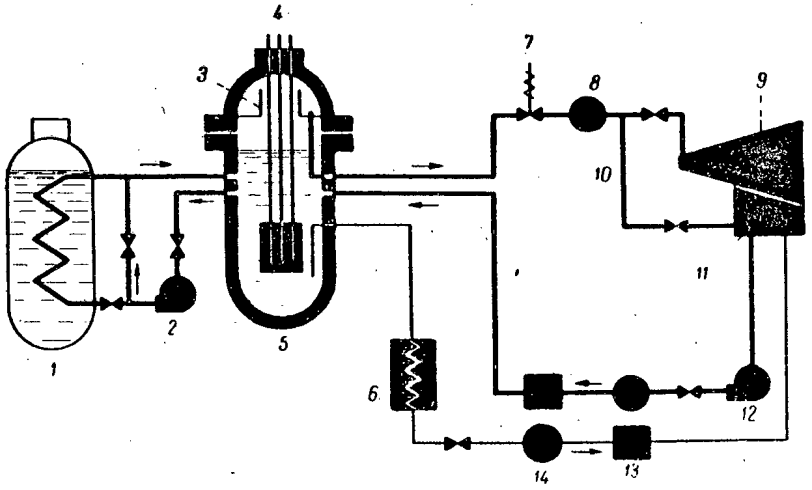

Fig. 1. Schematic diagram of the VBWR reactor installation. 1) Heat exchanger; 2) circulating pump; 3) steam baffle; 4) control rod; 5) reactor; 6) condenser; 7) valve; 8) steam separator; 9) turbine; 10) bypass line; 11) condenser; 12) feeder pump; 13) ion-exchange column; 14) filter.

Two discrete operating conditions are available to the reactor: natural circulation and forced circulation. In the first case, the water brought to a boil in the core is routed upward and then flows downward along the walls of the reactor pressure vessel. In the second case, when the baffle (Fig. 2) is let down, the water is admitted into the pressure vessel by way of the inlet pipes (located above the active section), and then descends along grooves to beneath the baffle, flows further through the core, is boiled and led off through the outlet piping into the circulation loop. Operating under either set of conditions, the steam formed from part of the water leaves the reactor vessel via the outlet steam headers.

The reactor core comprises an ensemble of fuel-element assemblies whose ends are held in position by the stainless steel top and bottom grids (Fig. 3).

The fuel elements are precipitation-hardened flat-plate type elements, with a matrix of 304L stainless containing UO_2 inclusions (particle size varying from 44 to 80 μ).

Each fuel-element assembly in the first charging of the reactor contains 6 individual fuel elements (Fig. 4a). The elements are curved in the longitudinal direction with a radius of curvature of 12.7 cm. Each fuel-element assembly is sandwiched in between stainless steel plates on either side. These plates protrude above the active portion of the fuel-element assembly, thus providing space for the coolant to exit.

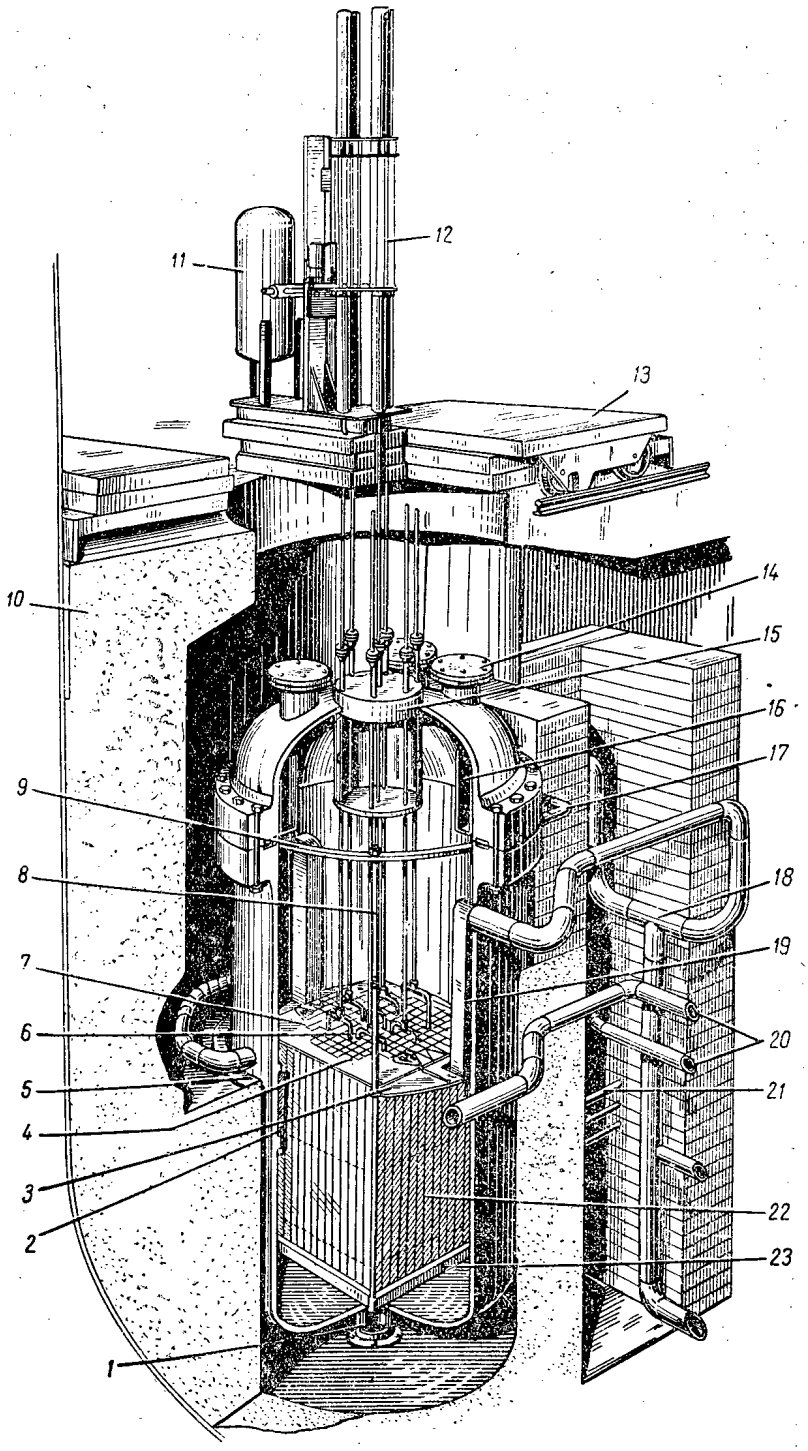

Fig. 2. General view of the reactor. 1) Reactor support; 2) support beam; 3) water baffle; 4) top lattice; 5) reactor foundation; 6) control rod; 7) control-rod holder; 8) core suspension bolt; 9) suspension ring supporting core; 10) concrete shielding; 11) pressurized air flask; 12) control-rod drives; 13) missile shield; 14) access port; 15) control rod shaft guide; 16) steam baffle; 17) steam outlet header; 18) main water manifold; 19) water baffle; 20) plumbing for water cooling circuit; 21) access pipes for measuring devices; 22) reactor core; 23) bottom lattice.

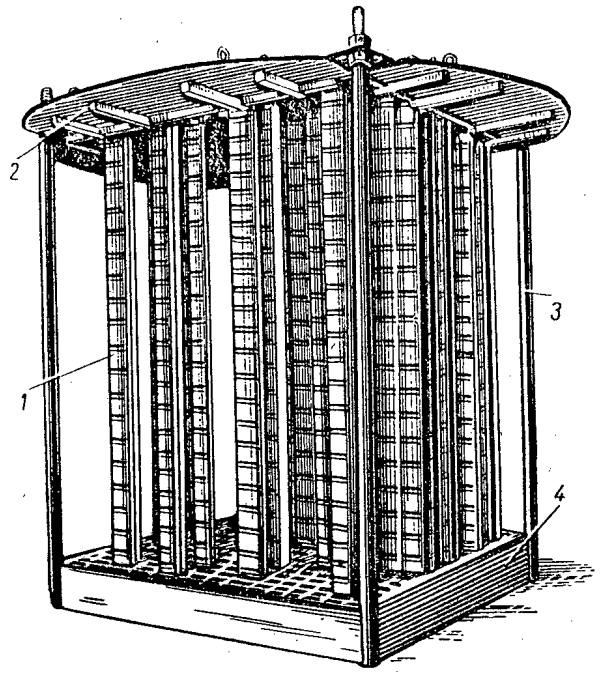

Fig. 3. Reactor zone (with section of fuel-element assembly removed). 1) Fuel-element assembly; 2) upper baffle; 3) fastening rod; 4) lower lattice.

A subsequent charging of the core will contain fuel-element assemblies similar to the assemblies used in the reactor at the Dresden atomic electric power plant (Fig. 4b), which will contain 9 (or 16) tubular fuel elements measuring 13.7 mm across, with fuel in the form of stainless-clad or zirconium-clad UO_2 (2.3% enrichment).

VBWR control rods are B_4C plates clad in stainless steel jackets. In contrast to the EBWR reactor setup, the control-rod drives are here located above the reactor vessel.

Basic Characteristics of VBWR Reactor [2]

Pressure Vessel

Inner height of vessel	~ 5.85 m
Inner diameter	~ 2.1 m
Wall thickness	~ 8.7 cm
Material	carbon steel
Inner lining	
material	304L stainless steel
thickness	3.22 mm
Design pressure	85 atm

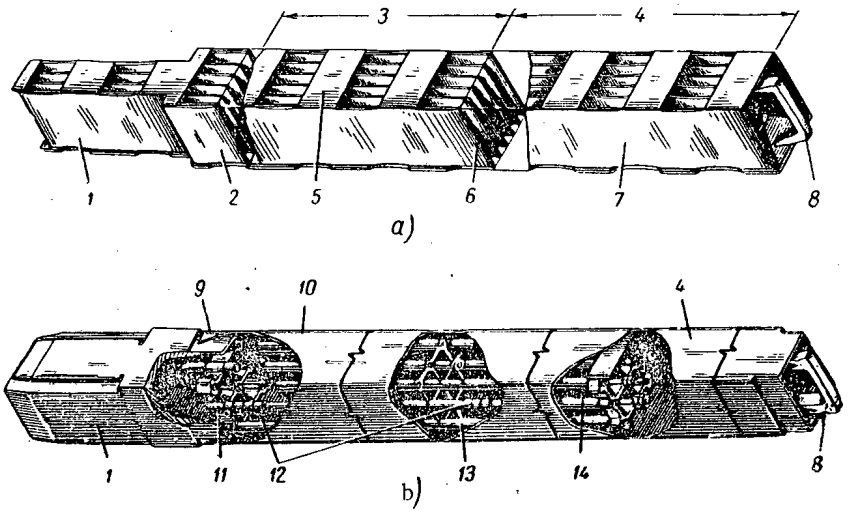

Fig. 4. VBWR reactor fuel-element assemblies. 1) Locating tip; 2) lower steel cladding plates; 3) active section; 4) coolant exit section; 5) side steel plate; 6) laminar fuel element; 7) upper steel cladding; 8) gripping handle; 9) sliding joint; 10) Zircalloy shell; 11) Zircalloy plug; 12) fuel pellets; 13) Zircalloy tubing for fuel element; 14) fuel tube expansion spring.

Core

Shape	cylindrical
Size (diameter, height)	~ 90 • 90 cm
Charge (in U^{235})	23 kg
Composition (by volume)	
water	93%
UO_2	0.25%
stainless steel	6.75%

Control Rods

Number:	
30.4 cm wide	6
14.6 cm wide	1
Efficiency	10% $\frac{\Delta k}{k}$
Withdrawal rate	10.3-31 cm/min
Operating time	0.25 sec
Control-rod positioning accuracy	±1.015 mm

Fuel-element Assemblies

Number	112
Fuel enrichment	> 90%
Number of laminar elements per assembly	6
Size of elements	940 × 75 × 0.635 mm
Composition (by weight):	
UO_2	23%
stainless steel	77%
Temperature of fuel element:	
average	296° C
peak	310° C

Moderator

Material	light water
Thermal flux:	
average	$2 \cdot 10^{13}$ neutrons/$cm^2 \cdot$sec
maximum	$5 \cdot 10^{13}$ neutrons/$cm^2 \cdot$sec
Prompt neutron lifetime	$5 \cdot 10^{-5}$ sec
Temperature coefficient	~ $0.7 \cdot 10^{-5}$ deg^{-1}

Coolant

Material	light water
Volume:	
total	12 m^3
in core	0.52 m^3
Inlet temperature	38° C
Working pressure	70 atm
Exit steam temperature	285° C
Steam flow rate	35.8 m/hr
Coolant flow rate (per 1 kg steam)	50 kg

Thermal stresses

Maximum/average ratio in heat generation:	
axially	1.6
radially	1.3
Heat flux in core:	
average	244 thousand kcal/$m^2 \cdot hr$
maximum	542 thousand kcal/$m^2 \cdot hr$
critical	2170 thousand kcal/$m^2 \cdot hr$

LITERATURE CITED

[1] Atomic Ind. Reporter, 130, 3 (1957).

[2] Nucleonics 16, 2, insert (1957).

[3] J. Atomic Energy (USSR) 3, 9, 266 (1957).*

[4] Nucleonics 15, 7, 56 (1957).

Iu. K.

FLUORIDE FUEL FOR HIGH-TEMPERATURE REACTORS

One of the promising trends in contemporary reactor design is based on the concept of utilizing uranium in the form of compounds, thus opening the way for developing circulating-fuel reactors. A reactor of that type may be exemplified by the homogeneous heavy-water reactor at the Oak Ridge National Laboratory, where the possibilities of designing reactors to operate on circulating nuclear fuel have been under study for quite some time. In this reactor, a slurry of uranyl sulfate in heavy water is employed. However, besides advantages such as the excellent slowing-down power of heavy water and the good solubility of UO_2SO_4 in D_2O, the reactor also exhibits a number of drawbacks: the fuel must be kept under high pressure (in order to obtain high efficiency); an explosive mixture forms during the operating process (necessitating the provision of special recombination chambers).

Another circulating-fuel reactor is the LMFR (liquid metal fuel reactor) at Brookhaven National Laboratory, operating on U-Bi, a uranium-bismuth alloy. Although there are no particular disadvantages inherent in the reactor type referred to above, it has some weak points of its own, due to the danger of the solution solidifying at low temperatures and the low solubility of uranium in bismuth.

The last-mentioned disadvantage may be eliminated by employing a fused mixture of uranium tetrafluoride and thorium with fluorides of the alkali metals, zirconium and beryllium.

Table 1 presents the physical properties of some of the fused fluoride mixtures. Inspection of the table reveals the fact that the specific heat, heat conductivity, viscosity and Prandtl number for the mixtures tabulated and for water are of the same order. The somewhat higher viscosity of the fluorides is offset by their high specific heat. Along with this, fluorine exhibits highly satisfactory nuclear characteristics. The capture cross section of fluorine for thermal neutrons is of the same order as the cross section of beryllium. The mean logarithmic energy loss with one collision is approximately 0.10, which is somewhat lower than for graphite; a system in which slowing down took place only in fluorine would occupy too high a volume, thus necessitating the use of additional

* Original Russian pagination. See C. B. Translation.

moderators. Furthermore, fluorine has an excessively high slowing-down power which would prohibit the use of fluorides in fast reactors.

TABLE 1
Physical Properties of Some Mixtures of Fluoride

Composition (mole %)	Melting point, °C	Density at 700° C, g/cm³	Volume coefficient of expansion, deg⁻¹	Viscosity at 700° C cp	Thermal conductivity cal/sec · cm · deg	Specific heat, cal/g · deg	Prandtl number
53,5NaF—40ZrF_4—6,5UF_4 . .	540	3,27	$3,36 \cdot 10^{-4}$	5,7	0,005	0,24	2,74
71LiF—16BeF_2—12ThF_4—1UF_4	525	3,25	$2,52 \cdot 10^{-4}$	7,1	—	0,37	—
67LiF—30,5BeF_2—2,5UF_4 . .	464	2,10	$1,90 \cdot 10^{-4}$	5,5	—	0,57	—
Water (20° C)	—	—	—	1,00	0,00143	1	7

The slowing-down power of the fused fuel may be improved by addition of beryllium fluoride (BeF_2), although the higher viscosity of such a mixture would set limitations on BeF_2 content to 30 mole percent.

Table 2 cites the slowing-down power and resonance escape probability for several possible mixtures of fluorides. It is clear from the table that the resonance escape probability differs substantially from unity even for an ideal fluoride mixture such as LiF—BeF_2, and drops off sharply with increase in the amount of Li^6 present. With a Li^6 content of higher than 0.1% in the LiF, a homogeneous reactor working on such a mixture will be totally unable to go critical (just as in the case of a homogeneous reactor with a mixture of fluorides of the alkali metals) [3].

TABLE 2
Nuclear Characteristics of Fluorides and Conventional Moderators

Composition (mole %)	Number of Li^6 atoms per one Li^7 atom	Resonance escape probability, energies up to 0.075 ev	Slowing-down power, cm^{-1}
D_2O	—	0,9997	0,18
Graphite	—	0,995	0,07
69 LiF—31 BeF_2	0	0,95	0,038
	0,0001	0,89	
	0,001	0,46	
50 NaF—50 ZrF_4	—	0,58	0,021
46,5 LiF—11,5 NaF—42 KF	0	0,14	0,018
	0,0001	0,13	
	0,001	0,059	

The use of fluorides results in some specific difficulties. Among these are the problem of corrosion, and the need to maintain a rather high temperature for the mixture, whose melting point is in the neighborhood of 500° C. In addition, reactors based on the principle of employing fluorides, when compared, say, to water-cooled reactors, require a higher fuel concentration to reach criticality, all of which leads to relatively low levels of power per kilogram of fuel. This disadvantage is offset, true enough, by the high plant efficiency (as much as 35%) as a result of the high temperature of the circulating fuel [4].

One such reactor operating on fluoride fuel, the ARE (aircraft research reactor), is looked upon as one of the possible prototypes for an aircraft prime mover. It was first described in several reports delivered at a meeting of the American Nuclear Society in June, 1957. This reactor, installed at Oak Ridge National Laboratory, was brought up to criticality on November 3, 1954. The fuel used consisted of a mixture of NaF, ZrF_4, and UF_4, which was pumped in by centrifugal pump action through nickel alloy coils threading the reactor core.

The fuel passed from the reactor to a heat exchanger, where it gave up its heat to an intermediate heat-transfer agent, helium, which transferred the heat, in turn, to water (Fig. 1). Beryllium oxide functioned as both moderator and reflector. The heat generated in the reflector was removed by circulating sodium and added to the water through helium acting as an intermediate heat-transfer agent.

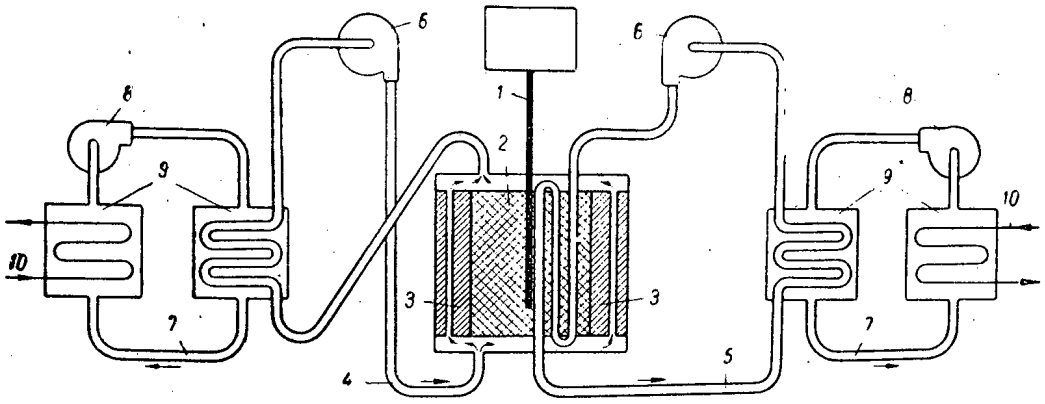

Fig. 1. Schematic diagram of heat flow from reactor. 1) Central control rod; 2) core; 3) reflector; 4) fused sodium as reflector coolant; 5) fused fuel; 6) pump; 7) helium; 8) helium blower; 9) heat exchangers; 10) water.

Reactor control was carried out using a stainless steel rod passing through the center of the core, and also using shim rods and safety rods of boron carbide.

The reactor (see Fig. 2) is a cylinder 85 cm across and 91 cm high; the width of the beryllium reflector is 19 cm. On its outer surface, the core has 48 electric heating units delivering a total power of about 45 kw. The flow speed of the fuel in the core is 1 meter/sec (Reynolds number is 10,000). At rated power, the temperature of the fuel at the entrance to the core was 650° C, while it reached 815° C at the core exit [5].

At first, a mixture of NaF and ZrF_4 was circulated through the reactor; small portions of $2NaF \cdot UF_4$, 93.4% U^{235} enriched, were subsequently added. The reactor went critical at the following composition in the mixture (in mole percent): NaF, 52.8; ZrF_4, 41.0; UF_4, 5.7, corresponding to a content of 0.38 g U^{235} per cubic centimeter of fuel. The critical mass was equal to 14.9 kg U^{235}, the total quantity of U^{235} in the core and in the out-pile loop amounted to about 66 kg [6].

The reactor was in operation 221 hours in all, including 74 hours of operation at full power. Although the reactor design power is 1.5 Mw, it operated successfully even at a level of 2.5 Mw. After developing 96 Mw-hr the reactor was shut down and disassembled.

As was to be expected, the reactor possessed an over-all negative temperature coefficient. In response to rapid changes in fuel temperature, the temperature coefficient due to the change in uranium concentration reached $1.75 \cdot 10^{-4} \frac{\Delta k/k}{^\circ C}$. Slow changes in temperature brought about a positive temperature coefficient for the moderator, while the over-all temperature coefficient was $1.1 \cdot 10^{-4} \frac{\Delta k/k}{^\circ C}$.

It is interesting to take note of the fact that it proved possible to use absorber rods only to establish a mean temperature in the reactor. Control is carried out for the most part with the aid of a change in the flow rate of the helium coolant in the heat exchanger, as a result of which a change is effected in the temperature of the fuel and, in turn, in the concentration of the uranium nuclei at the inlet to the reactor. This leads to a change in the reactivity of the system. Thus, when the rate of flow of the helium is increased, the fuel temperature at the reactor inlet is diminished, while it is increased at the outlet end (the mean temperature in the reactor remains unaltered), with a consequent rise in reactor power. Figure 3 shows the results of one of the experiments illustrating these self-regulating effects [3].

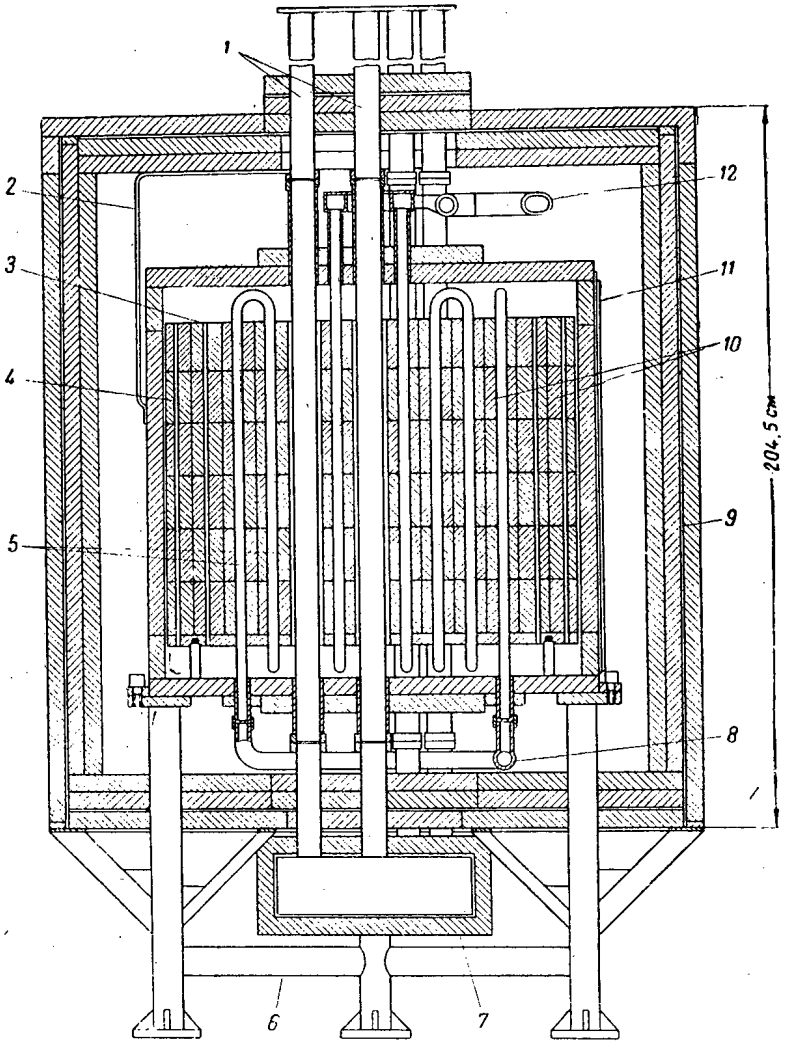

Fig. 2. Vertical cross section through the reactor.
1) Regulating rod assembly and safety rod assembly; 2) thermocouple; 3) core; 4) tubes for the reflector coolant; 5) fuel tubes; 6) support assembly; 7) helium manifold; 8) fuel outlet manifold; 9) thermal shield assembly; 10) beryllium oxide moderator and reflector; 11) heater units; 12) fuel inlet manifold.

As the experiment in operating the ARE reactor has demonstrated, Xe^{135} formation plays a very limited role in poisoning. In the first place, the fuel is in the core only $^1/_4$ of the time of a cycle, which is equivalent, roughtly speaking, to reduction to $^1/_4$ of the mean reactor flux; in the second place, the majority of the neutrons present have energies exceeding the energies of the largest resonance band of Xe^{135}; thirdly, in the process of circulating the fused fuel, Xe^{135} as well as other gaseous fission products are volatilized from the fuel. This

last fact made necessary complete hermetization of the fuel system. This problem was solved satisfactorily for relatively short periods of reactor operation. However, small-scale escape of gaseous products from the surface of the circulating fuel was still taking place, and this sometimes made operation troublesome [3].

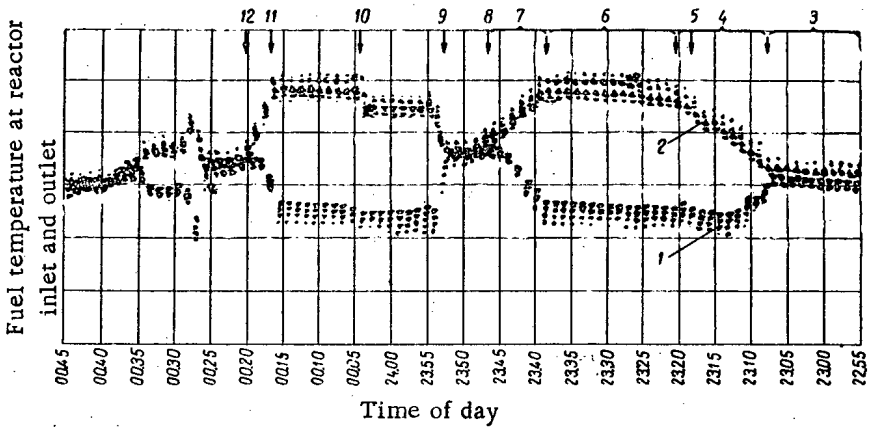

Fig. 3. Temperature of reactor fuel. 1) Inlet fuel temperature; 2) outlet fuel temperature; 3) reactor critical, power 200 kw; 4) slow increase in rpm of fuel-system helium blower unit; 5) liquid-sodium-system helium blower turned on; 6) power 2.5 Mw; 7) fuel-system helium blower rpm reduced to zero; 8) shim rods inserted; 9) fuel-system helium blower turned up to full rpm; 10) regulating rod shifted; 11) fuel-system helium blower turned off; 12) regulating rod inserted (reactor subcritical).

The practical value of the results obtained are not limited to their possible application in atomic-powered aircraft construction. As calculations have shown, the cost of electric power delivered by a 240 Mw atomic-fuel electric power plant with a molten fluoride-fueled reactor does not exceed the cost of electric power produced in conventional electric power plants [4].

LITERATURE CITED

[1] Nucl. Engineering 2, 16, 298 (1957).

[2] Engineering 184, 4783, 604 (1957).

[3] N. K. Ergen et al., Nucl. Sci. Engineering 2, 6, 826 (1957).

[4] R. C. Briant and A. M. Weinberg, ibid., p. 797.

[5] E. S. Bettis et al., ibid., p. 804.

[6] E. S. Bettis et al., ibid., p. 841.

V. A.

EXTRACTION OF URANIUM FROM SPENT NUCLEAR FUEL BY DISSOLVING IN FUSED SALT AND FLUORINATION*

A new process for recovering uranium from irradiated uranium-zirconium fuel elements consists of the following steps. The elements are subjected to hydrofluorination in a melt of $NaF-ZrF_4$ or $NaF-LiF$ salts (650° C). The uranium tetrafluoride forming as a result is fluorinated by plain fluorine to UF_6 (600° C), which is driven off as a gas from the fused salt, along with volatile fluorides of impurity elements and excess of fluorine.

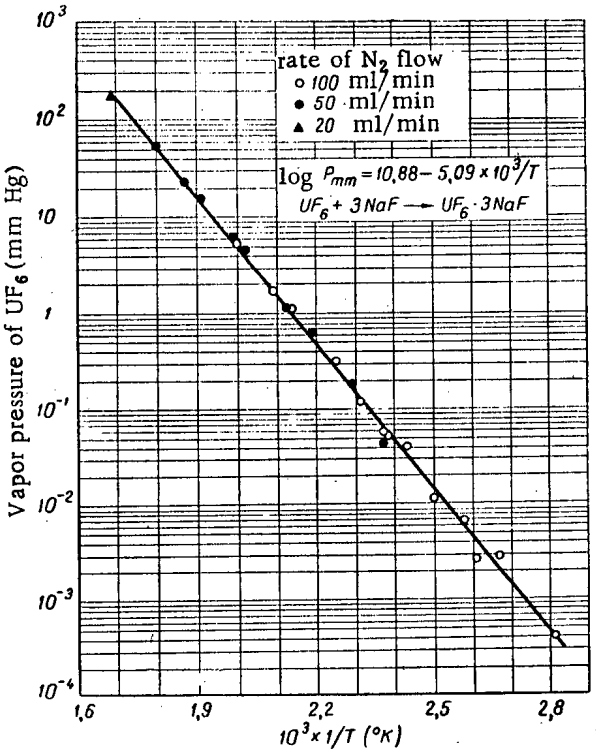

Equilibrium partial pressure of UF_6 above a $UF_6 \cdot 3NaF$ complex, plotted against temperature. (Measurements by the transpiration method).

As a result of the insufficient fluorinating potential of HF, volatilization of the impurity elements is observed only to a slight extent in the hydrofluorination or dissolving of uranium tetrafluoride.

At the fluorination stage, excellent separation of the uranium from nonvolatile fluorides of Cs, Sr, the rare earths and, to a smaller extent, Zr, takes place. Uranium separation from fluorides of Nb and Ru is poor, and is not achieved at all for I, Te, and Mo.

For separation from volatile fission product, UF_6 is adsorbed on a column of granulated NaF at 100° C. The equilibrium curve for $p_{UF_6} = f(T)$ is shown in the accompanying graph. Desorption of the UF_6 is carried out with a flow of F_2 passed through the column at 400° C.

As the gas is filtered and scrubbed, activity is distributed in three parts between U, Ru, and Nb. The bulk of the Ru passes through the first NaF column and is cold-trapped, while the UF_6 and Nb are collected at 100° C. In the UF_6 desorption step, all of the Nb is in essence retained in the first column. The second column serves to eliminate the activity picked up by the flow of UF_6 in the first column

TABLE

Decontamination of Irradiated Uranium in Fluorination and Adsorption on NaF Bed (Cooling time: 120 days)

Process	Decontamination factor						
	by β-radiation	by γ-radiation	Ru	Nb	Zr	Cs, Sr, rare earths	I, Te, Mo
Fluorination	10^2	10^2	10	10	10^3—10^4	$>10^4$	1
Adsorption on NaF bed	$>10^4$	$>10^4$	10^3	10^4	$>10^3$	10^3	unknown
Total	$>10^6$	$>10^6$	10^4	10^5	$>10^7$	$>10^7$	unknown

Recycling through the adsorption-desorption step brings about an over-all decontamination factor greater than 10^6 for the irradiated batches of uranium (see table).

V. P.

* G. J. Cathers, Nucl. Sci. and Engineering 2, 6, 768 (1957). R. P. Milford, Industr. and Engineering Chem. 50, 2, 187 (1958).

ION EXCHANGE BEHAVIOR AND DISSOCIATION CONSTANTS OF EDTA COMPLEXES OF AMERICIUM, CURIUM, AND CALIFORNIUM[1]

A Dowex 50-X12 ion exchange resin in ammonia form was used for the study of the ion exchange equilibria of trivalent americium, curium, and californium. Ethylenediaminetetraacetic acid (EDTA) at 10^{-3} M concentration was employed as the complexing agent. Constancy of the ionic strength of the solution was maintained by 0.1 M NH_4ClO_4. The experiments were carried out under static conditions at a temperature of 25 ± ± 0.02° C over a pH range extending from 2.0 to 3.3.

The experiments established the fact that complexes of the MeY^{-1} type form in the pH range considered, for trivalent actinide elements. In accordance with the equilibrium $MeY^{-1} \rightleftharpoons Me^{+3} + Y^{-4}$, the dissociation constant K_c of this complex is written in the form

$$\frac{[Me^{+3}]\,[Y^{-4}]}{[MeY^{-}]} = K_c.$$

The distribution coefficient K_d for the actinide ion between exchanger and solution may be expressed in the following form:

$$K_d = K_d^0 \frac{1}{1 + \frac{[H_4Y]_t}{\theta K_c}},$$

where K_d^0 is the distribution coefficient for Me^{+3} in the absence of the complex-forming agent, $[H_4Y]_t$ is the total concentration of EDTA in moles/liter, θ is the function of the pH and of the four dissociation constants of EDTA:

$$\theta = 1 + \frac{[H^+]}{K_4} + \frac{[H^+]^2}{K_4K_3} + \frac{[H^+]^3}{K_4K_3K_2} + \frac{[H^+]^4}{K_4K_3K_2K_1}.$$

The following separation factors were obtained:

$$\alpha_1 = \frac{K_d^{Am}}{K_d^{Cm}} = 2{,}04 \pm 0{,}05,$$

$$\alpha_2 = \frac{K_d^{Cm}}{K_d^{Cf}} = 5{,}5 \pm 0{,}1.$$

The dissociation constants for EDTA, obtained in [2], were chosen for computing K_c; K_c then proved to be equal to the following values:

californium . . .	$10^{-19{,}09 \pm 0{,}2}$,
curium	$10^{-18{,}45 \pm 0{,}1}$,
americium	$10^{-18{,}16 \pm 0{,}1}$.

Preliminary experiments performed on the ion exchanger under dynamic conditions demonstrated the fact that EDTA may be used for the separation of the actinide elements.

LITERATURE CITED

[1] J. Fuger, J. Inorg. and Nucl. Chem. 5, 4, 332 (1958).

[2] M. J. Cabell, Analyst 77, 859 (1952).

B. P.

USE OF RADIOACTIVE ISOTOPES IN METALLURGICAL INVESTIGATIONS

Radioactive isotopes are receiving more and more attention in the elaboration of the technology and in the study of ferrous and nonferrous metallurgy at the Metallurgy Institute of the Ural branch of the Academy of Sciences of the USSR.

One of the most widely used isotopes is S^{35}. Research workers' teams from the Steelworking Processes Laboratory of the Ural branch of the USSR Academy of Sciences, from the Ural Institute of Ferrous Metals and the Central Laboratory of the Verkh-Iset metallurgical plant collaborated in studying the desulfurizing of transformer-grade steel in a 14-ton electric furnace. For this purpose, a mechanical mixture of S^{35} and iron in proportions of 150 millicurie to 1 ton of the melt was introduced into the molten metal. Determining the radioactivity of metal and slag samples taken every 5 min, the desulfurizing of the metal in the furnace and in the ladle was studied. Several of the melts were produced in the manner of the routine shop technology, with addition of S^{35} to the metal immediately after the latter had melted down. In addition, in order to shed some light on the desulfurization process, melts were produced at a lowered rate of metal output and with agitation of the vat during the reduction period of the melting process. 8-12 samplings of metal and slag were taken of each experimental melt. The peak activity of the metal (background deducted), was approximately 7.5 times less than the peak activity of a slag sample taken from the ladle. The maximum activity of the metal corresponded to samples taken 5-10 min after S^{35} was introduced, while the minimum activity corresponded to casting samples.

It was found that mixing of the metal with slag as the secondary slag was laid on, and alloying with ferrosilicon, contributed to a more intense desulfurizing, and that slowing down of the rate of output of the metal brought about essentially no change in the distribution of sulfur between metal and slag.

In order to give an explanation of the isotope exchange between metal and slag, addition of S^{35} was made to the slag as the metal was first being soaked in the ladle. Activity measurements of the metal and slag samplings pointed up the fact that, after soaking the transformer metal in the ladle for 20 min or more, the amount of S^{35} transition from slag to metal was negligible, i.e., the rate of isotope exchange was slow under those conditions.

S^{35} was also used for studies of the mechanism of interaction between a number of sulfides with sulfates and sulfur dioxide [1]. It turned out that, in the interaction of CaS with SO_2, sulfide sulfur is completely isolated, and sulfur and oxygen from sulfur dioxide enter into the sulfate then forming. In an analogous interaction between cobalt sulfide and sulfur dioxide, an intermediate reaction takes place with formation of metallic cobalt. For reactions involving interaction between sulfides and sulfates, the use of tagged sulfur made it possible to work out more refined stoichiometric ratios, a problem which was difficult to tackle by conventional techniques.

The mechanism involved in the desulfurizing of pig iron [2] was investigated using Fe^{59} isotope. Industrially pure iron, saturated with carbon, was placed in two compartments of a graphite crucible, above which was situated a common layer of molten slag containing no iron. Fe^{59} and sulfide of nonradioactive iron were added to one of the components. After soaking for an hour at 1600° C, a determination of sulfur content was carried out in the metal taken from the second compartment, and its radioactivity was assayed. The findings so obtained showed that the sulfur passed over into the control alloy in rather high quantities, 1-2 orders of magnitude higher than the iron. It was thus demonstrated that the iron passed over into the slag not in unison with sulfur, but in the form of iron sulfide, or via some other process.

The further development of such techniques, adapted to the study of ores and concentrates of nonferrous metals [3], employing Zn^{65} and Se^{75}, made it possible to drastically reduce the amount of required experiments, to lessen the tediousness and to automate the performing of the experiments. Recourse was had predominantly to zinc sulfate, precipitated by ammonium sulfide from a solution of a mixture of Zn^{65} and ordinary zinc in acid medium. Se^{75} was introduced into a copper concentrate (by the method of isotope exchange) and into synthetic selenides. Se^{75} also replaced sulfur in minerals of the chalcosine and chalcopyrite types. With the aid of Zn^{65}, studies were carried out on the relative rates and completeness of vaporization of the metal as the sulfide was heated in various gaseous media. It was found that sublimation of zinc sulfide took place, starting at 850° C.

Oxidation of the sulfide vapors stepped up the rate of volatilization of zinc sulfide, while oxidation of the solid surface slowed it down. The rate of sublimation also increased in response to reduction of the vapors by wood charcoal, iron, or copper. Despite the low value of the vapor pressure of the sulfide, sublimation reached an appreciable level in the course of the metallurgical processes studied.

Using Se^{75} made it possible to establish the fact that volatilization of selenium in metallurgical operations is favored by oxidative conditions and gets under way at low temperatures. When copper selenide oxidizes in air, heated to 600° C for twenty minutes, for instance, 94% of the selenium present volatilizes out of the compound.

A team working at the Metals Casting Laboratory of the Ural branch of the Academy of Sciences of the USSR used Co^{60} to determine the rate of mixing of charge materials and the smelting level. A cupola measuring 600 mm in diameter was irradiated with gamma radiation from a Co^{60} source (the source was shifted in the vertical plane). The regularities uncovered enabled casting technologists to improve quality control in cupola melting of pig iron.

Co^{60} was also employed for studies of metal distribution between mattes and slags in the nickel industry.

LITERATURE CITED

[1] N. P. Diev,* V. V. Paduchev, and V. V. Toporova, Sbornik trudov Instituta metallurgii ural'skoi filiali Akad. Nauk SSSR 2 (1958).

[2] I. L. Korkiia, O. A. Esin, and V. V. Mikhailov, Doklady Akad. Nauk SSSR 101, 6 (1955).

[3] I. A. Vetrenko, N. P. Diev*, and A. I. Olesova, Sbornik trud. Inst. metallurg. ural'skoi filiali Akad. Nauk SSSR 2 (1958).

N. A. Vatolin and E. A. Vetrenko

DEVELOPMENT OF URANIUM MINING IN CANADA DURING 1957

Data have been published in a number of Canadian periodicals referring to appreciable growth of uranium mining activities in Canada during the year 1957 [1, 2].

These data are furnished in Table 1.

TABLE 1
Canada Uranium Yield During 1956 and 1957

Mining area	1956		1957		% increase over 1956
	U_3O_8 yield tons	% of annual yield	U_3O_8 yield, tons	% of annual yield	
Ontario (Blind River, Bancroft)	408,0	20	3424,1	59	839
Saskatchewan (Gunnar, Ice Bay, etc.)	1251,2	60	1987,5	34	159
Northwest Territories (Great Bear Lake, Marion)	393,3	20	382,5	7	97
	2052,5	100	5794,1	100	280

* Deceased.

The general and notable increase in uranium mining activity in Canada was accompanied by a rather extensive shake-up of the uranium mining industry, with the center of uranium ore mining being shifted from the Athabaska Lake region in Saskatchewan to the neighborhood of Blind River, Ontario. Until 1958, the principal uranium producer in Canada was the Eldorado mine on the shores of Great Bear Lake (Northwest Territories).

This general shift in the uranium mining industry is easily visible from the figures in Table 1, giving the change in the specific weight of particular regions in the over-all uranium yield and tempo of development.

The abrupt jump upward in uranium mining in the Blind River area is due to the launching of six new enterprises during 1957, these six being listed in Table 2.

TABLE 2

Enterprises Entering the Uranium Mining Field During 1957

Mines	Output, thousands tons per day
Algom Uranium Mines (Nordic mine)	3
Consolidated Denison Mines	6
Stanley Uranium Mining Corp.	3
Norsspan Uranium Mines (Nordic mine)	4
Norsspan Uranium Mines (Pynel mine)	3
Can-Met Explorations	3

Thus, the 22,000 ton increase in the amount of ore processed daily was contributed solely by enterprises new on the scene. There was registered, in addition, an increase in productivity over that achieved by enterprises engaged in mining and processing ore in previous years.

In April 1957, in the neighborhood of Bancroft, a uranium ore processing plant was put into operation at the Faraday mine, with an output of 1200 tons of ore daily.

An increase in uranium mining was also recorded (albeit less than in Ontario) in the Athabaska Lake region, largely as a result of the starting up of a new plant at the Lorado site, and also due to an increase in plant productivity at the Gunnar and Ice Bay sites.

There was a modest drop in uranium mining during 1957 for the Northwest Territories mines taken as a whole, in spite of the initiation of the new Rayrock Mines Ltd., with an output of 150 tons daily, working at Lake Marion. This is evidently to be explained by the unfavorable results obtained at the Eldorado and Great Bear Lake mining sites.

Correlation of the data on uranium mining operations in Canada with the data brought out by Johnson [3] on mining in other countries shows that Canada has taken second place among the capitalist countries of the world, being outdistanced only by the United States.

LITERATURE CITED

[1] Canad. Mining and Metallurg. Bull. 549, 2 (1958).

[2] Canad. Mining Journal 79, 2, 90 (1958).

[3] J. C. Johnson, Mines Mag. 11, 23 (1957).

M. K.

USSR. Accredited representatives of the International Atomic Energy Agency visited the Soviet Union during April, 1958, these being: general director of the Agency, S. Cole, assistant to the general director, P. Yolles, and chairman of the council of directors, P. Winkler.

Before his departure from Moscow, Cole held a press conference. In their statements, Cole, Winkler, Yolles, as well as the head of the chief administration board on uses of atomic energy, attached to the Council of Ministers of the USSR, Professor V. S. Emel'ianov, told of the problems and practical work of the agency.

At the conclusion of the interview, Cole answered reporters' questions. In answer to questions directed at him by the representative of the journal "Atomnaia Energiia," Cole stated the agency would begin, in the immediate future, publication of its own press organ, and promised to send information on the work of the agency for publication in our journal.

Australia. The first stage of tests (low-power tests) on the first Australian HIFAR high neutron flux research reactor has been completed. The reactor was built near Sydney, in Lucas Heights.

Austria. Setting up of a research and educational atomic energy center has been proposed for a site 16 km east of Vienna on the grounds of an old aerodrome near Hetzendorf. A 5 Mw tank-type reactor will be installed at the center.

England. At the scientific research atomic center in Harwell, a design has been worked out for a linear electron accelerator operating under a pulsed regime (pulse repetition rate will be 400 cps), making possible a sequential bombardment of two targets by the electron beam produced (Nucl. Instr. 2, 3, 282, 1958). The beam will normally be deflected by an electromagnet to strike the first target, but the electromagnet will be disconnected prior to each eighth pulse, and the beam will then be directed onto the second target. The switching operation is carried out in the interval between pulses. Dimensions of the magnet pole pieces are: length 6 cm, width 1.5 cm. Air gap between poles is 2 cm. The magnetic field strength, at an electron energy of 13.5 Mev, amounts to 1 kilo-oersted (radius of curvature of electron path is 45 cm). Current build-up time in the magnet windings is 1.25 millisec.

England. At Harwell, a design has been worked out for an atomic light bulb operating entirely from the energy of radioactive substances. The bulb has a plastic envelope, and is inner-lined with phosphors. The phosphors glow in response to beta particles emitted by Kr^{85} which fills the bulb. The useful lifetime of the bulb should extend to about 10 years.

England. An atomic clock operating at a rate of error of 3 sec in 300 years has been constructed at the National Physics Laboratory in Teddington (Middlesex).

Afghanistan. Rich uranium deposits have been discovered in a mountainous area in Badakshan province, in northeastern Afghanistan.

Italy. Work begins in the summer of 1958 on construction of an atomic research center at San Pietro a Grado, near Pisa. The center is being built by the University of Pisa, the Naval Academy at Leghorn and by other scientific organizations. A tank-type materials-testing reactor delivering 12-15 Mw power will be installed at the center.

U.S.A. At Yale University, a linear accelerator for heavy ions of elements up to neon became operative. The energy of accelerated nitrogen ions reached 140 Mev. The length of the accelerator is 36 meters. The power consumed at 70 Mc frequency is about 3 Mw. A similar accelerator is in operation at the Radiation Laboratory of the University of California at Berkeley.

U.S.A. Construction work was completed during 1957 on 16 nuclear chain reactors, including 7 power reactors and 9 research and experimental reactors. Construction has begun and is in progress on 59 reactors, of which 35 are power reactors and 24 are research and experimental reactors. Construction of 7 uranium ore reprocessing plants is underway, fuel elements production has been planned by thirteen companies, three companies have completed construction jobs on zirconium processing plants, and two companies have built beryllium processing plants.

U.S.A. At Cambridge, Massachusetts, construction work is in progress on a strong-focusing 6 Bev electron synchrotron for the Massachusetts Institute of Technology and for Harvard University.

U.S.A. The leakproof structure of the cladding on one of the fuel elements ruptured in the experimental boiling-water reactor BORAX-4 at the National Reactor Testing Station in Idaho. Pellets formed from a mixture of uranium and thorium oxide in tubular aluminum sandwiches are used in the reactor. The reason for the failure was apparently a faulty welding job. The accident made it possible to observe the functioning of the reactor with a certain proportion of the fission products still in the loop. The specific power output of the reactor during the experiment was raised to approximately 50 kw/g. The activity of the loop proved to be moderate.

U.S.A. At the Oak Ridge National Laboratory, a homogeneous experimental power-only reactor HRE-2 was started up. Thermal power of the reactor amounts to 5,000 kw. No electric power will be generated during the initial operating period of the reactor.

U.S.A. EBWR, the boiling-water reactor at the Argonne Laboratory, designed for a thermal power of 20 Mw and already operating at a power output of up to 50 Mw, was adjusted to 61.7 Mw power.

U.S.A. At Cornell University, a design has been worked out for a training reactor with two separate cores operating alternately. The first core (10 kw) is intended for use as a neutron source, while the second (10 w) is slated for research in reactor physics.

U.S.A. AEC has allotted $191,000 to Rensselaer Polytechnic Institute for continuation of work on a project studying the possibilities of using uranium oxide-containing fiberglass as a nuclear fuel. It is anticipated that this material will show promise for use in high-temperature reactors.

U.S.A. The seventh conference on hot laboratories and hot laboratory equipment will be convened at Cleveland, Ohio, in April,1959. Reports will be given at the conference on questions associated with the operation of hot laboratories, in particular instrumentation for work with radioactive materials, including questions involving the design, production, use, maintenance, decontamination, redesigning, shielding design and cost of laboratory devices, etc. Abstracts of reports to be proposed for the conference should be directed, prior to September 15, 1958, to the following address: Brookhaven National Laboratory, Upton, New York.

U.S.A. The National Academy of Sciences, the National Research Council and the Society for Radiation Studies are conducting the preparations for the International Congress on Radiation Studies to be held in Burlington, Vermont,from August 10-16, 1958.

U.S.A. At the Livermore Laboratory, the AEC has worked out a new radiation-shielding material, in the form of a slurry of superfine lead particles in paraffin. Use of this material to replace lead and concrete in reactor shielding applications may permit reductions in shielding weight and thickness.

U.S.A. A lead camera has been designed to facilitate discovery of low-activity sources in the presence of a highly radioactive background. This camera may also facilitate obtaining of conventional photographs of radioactive objects which would require exposure of the film in ordinary type cameras. Two types of film are employed in the camera: film of the conventional type and radiation-registering x-ray film. After both films have been developed by superimposing one on the other, the position of the source of radioactivity can be accurately pinpointed. A uranium lens with an aperture diameter of 0.0135 inch is used in the camera. The camera weighs 13 kg.

U.S.A. A cobalt gamma ray facility with a source of up to 100,000 curies has been developed. The unit will be placed below ground. The source will be kept under water. The exposure cell is 3.6 x 3.6 meters in size. Observation of the process by remote viewing is proposed.

U.S.A. RCA has developed a photomultiplier capable of discovering and recording events lasting less than 1×10^{-10} sec. The new device exhibits a resolving power of approximately 10^{-12} sec.

U.S.A. General Electric Company has designed an "electronic transducer" for the direct conversion of thermal, i.e., heat energy into electrical energy. The device consists of two metallic electrodes, separated by a gas at very low pressure, one of the electrodes being maintained at a relatively low temperature, while the other is kept at a temperature in the neighborhood of 1370°. The efficiency of the experimental electronic transducers amounts to approximately 8% for the present.

U.S.A. According to data released by AEC, the amount of radioactive strontium fallout increased by 50 % during 1957. By early 1957, the over-all level of soil contamination by Sr^{90} had reached 11.2 millicurie/ /km^2 in the New York City area. By December, 1957, the total quantity of Sr^{90} fallout in that area amounted to 17 millicurie/km^2. In a communication to the New York Times, published by that paper on April 4, 1958, it was noted that "in no other point on the face of the earth has the level of Sr^{90} come close to the level recorded in New York."

U.S.A. At the Naval Research Laboratory in Washington, a phosphorescent powder (calcium sulfate-manganate) has been developed which is capable of registering infinitesimally small radiation dosages, down to 0.0001 roentgen. The irradiated powder fluoresces (with an intensity proportional to the dose) only when heated and the fluorescence may be studied several hours after the exposure. The novel substance has already won application for dosage monitoring in medical applications of x-rays.

France. EDF-1, a gas-cooled, graphite-moderated reactor operating on natural uranium fuel, is being set up at Chinon (on the Loire). Electric power delivered by the reactor will be 60 Mw, uranium charge will be 120-140 tons. Start-up of the reactor is scheduled for the end of 1959 or early 1960.

France. Starting with 1959, France will be producing about 100 kg of plutonium annually. Pu production will be carried out by the industrial reactors G-2 and G-3, delivering 200 Mw thermal power each, and specially built for Pu production.

Sweden. A separation plant for the electromagnetic separation of isotopes, operated since 1948 by the Nobel Institute of Physics, has been redesigned to give greater resolving power at higher mass numbers (Arkiv for Fysik 13, 13, 145-163, 1958). Resolving power after the plant was remodeled equaled 1400.

Czechoslovakia. An industrial 15 Mev betatron commenced operation toward the end of 1957 (Jaderná Energie 4, 4, 85-92, 1958).

Japan. Japanese specialists returning from Antarctica announced the discovery of pitchblende and pegmatite in an area located 40-80 km to the south of Omgul island.

BIBLIOGRAPHY

E. Teller and A. L. Latter, Our Nuclear Future . . . facts, dangers, and opportunities. Criterion Books, New York, 1958.

This book discusses the principal facts concerning nuclear energy, its peaceful and military utilization, the dangers from radioactivity and the argument in favor of nuclear war and the continuation of atom bomb tests. A list of the chapters will give an idea of the content of the book: I. The Need to Know. II. Atoms. III. Nuclei. IV. The Law of the Radioactive Decay. V. Splitting of the Nucleus. VI. Reactions Between Nuclei. VII. Fission and Chain Reactions. VIII. The Effect of Radiation on Matter. IX. Tests. X. The Radioactive Cloud. XI. From the Soil to Man. XII. The Danger for Individuals. XIII. The Danger for the Race. XIV. The Cobalt Bomb. XV. What About Future Tests? XVI. Can Anything Happen to the Weather? XVII. The Safety of Nuclear Reactors. XVIII. Side-Products of Nuclear Reactors. XIX. The Nuclear Age.

The book aims to convince American citizens of the need for atomic weapons and therefore of the need for continuing the tests. The authors admit that 'the majority of people turn with horror from the question as to how the existence of atomic weapons affects the coexistence of nations' (p. 169). 'The great and universal need for peace creates the desire for disarmament. In the minds of the majority of people a cessation of the tests would be an important step toward disarmament' (p. 139).

Thus in the path of nuclear war and a continuation of the tests there stand the feelings ' . . . of all thinking and honest people on the earth' (p. 139). In order to counteract these feelings and to overcome the resistance of all thinking and honest people on the earth, Teller and Latter have written this book, "Our Nuclear Future". The book contains a review of the physical and biological problems and of the agitation for the continuation of the tests and for a "small" nuclear war (the authors reject a large nuclear war because of the inevitable retaliation).

The chapters of the book which contain a popular scientific account of the principal facts of nuclear physics are written simply, clearly and briefly. Complicated physical matters are explained without a single equation yet with accurate concepts. Recent material is introduced boldly (on nonconservation of parity, on the fission of californium 254 as a source of energy in supernovae, etc.).

The chapters concerning the dangers of radioactivity show the clear slant resulting from the previously noted purpose of the book, which is to convince one of the safety of the tests. This slant led to an uncritical review of the subject of the authors. In speaking of strontium shielding coefficients (Ch. XI), that is, the reduction of the concentration of strontium relative to calcium upon passage from the soil through plants into the human organism, the authors present only cases of a high shielding coefficient in dairy products. This high coefficient results from the action of the root system of plants and especially of the cow's organism; these two "filters" reduce the strontium concentration to 1/10.

The authors do not mention that cereal crops, which lack a "filter," are in a worse position and are contaminated by direct deposition from the air; the ratio of strontium to calcium concentration here can be 10 times greater than in the case of dairy products. In countries which consume a great quantity of grains the amount of strontium which enters the human organism can exceed by one order of magnitude the corresponding amount in countries which consume a large amount of dairy products.*

In characterizing the state of infection of the bones with strontium 90, Teller and Latter give only averaged figures—the average for the population and the average over the entire skeleton. As physicists they should not have neglected fluctuations and the statistical distribution of these quantities.

* Results and interpretation by B. V. Kurchatov.

From an article of the Americal biologists, Kulp, Eckelmann and Schulert [1], it is known that the distribution of persons with respect to their strontium content is not Gaussian and is characterized by a large percentage of great deviations from the mean. In 1.8% of the cases the strontium content of the bones (among adults in the USA) is ten times as large as the mean. Let us remember that 1.8% of the total population of the earth would be 50 million people. It can be said that we can still not be sure of this result since the number of investigated cases is small. Still,this is the only published information about the distribution of strontium content and there is no basis for ignoring it.

There is still another omission in connection with fluctuations. The authors do not take into account the nonuniform distribution of the strontium in the bones. In man strontium collects mainly in the vertebrae, where its concentration is four times greater than the average for the entire skeleton. All countries follow a rule for calculating the permissible level of irradiation from radio-isotopes within the organism from the point of greatest irradiation, the so-called "critical organ," where the greatest concentration of the isotope is found. Thus, if the organism contains iodine, which accumulates in the thyroid gland, we take into account only the irradiation of the thyroid gland although its weight is only 20 g. In the case of strontium the "critical organ" would be the vertebrae rather than the entire skeleton. Furthermore, it is known that strontium in the bones forms pockets so that the standard dose of strontium is customarily increased by a factor of 5.

Thus the level of irradiation given in the book (p. 118) must be increased by a factor of 4 due to the "critical organ" (vertebrae rather than the skeleton) and by a factor of 5 because of pocket formation by strontium, thus by a total factor of 20. For a large portion of the population this level must be increased further by approximately 10 times (according to the statistical distribution). Then the highest level of irradiation of the bones of adults for a large portion of the population is (from the original data of the article by Kulp et al.) 0.08 r/year (instead of the average figure given by Teller and Latter of 0.0003 r/year). These figures are lower than the natural background (0.18 r/year) but are not as negligible as Teller and Latter state.

Only in calculating the average number of illnesses, whose probability is proportional to the average dosage of the bones, can we use the average values of the strontium content, as is done by the authors. They estimate the number of cases of leukemia at 400 per megaton. But this is really the lower limit of the possible number of cases. Other estimates are a few times larger, especially if we take into account the reduction of the strontium shielding coefficient in countries with a cereal diet.

The authors neglect to consider the genetic victims, the number of which must be approximately 4000 per megaton [2]. They also greatly reduce the predictions of contamination, and for a continuation of the tests at the present rate assume an increase of the level of contamination by a factor of 5 (p. 118). A calculation shows [3] that the limit of contamination will be 50 times higher than the present level while the level in 1972 will be 13 times higher. The dosage of the vertebrae in 1972 for a large portion of the population will be 16-60% of the official standard and can be even greater in countries where cereal products predominate in the diet.

Every trained person knows that we cannot permit a large fraction of the population to approach the official acceptable radiation tolerance.

Let us admit that it can be disputed whether the number of victims per megaton is 4000 or 400, whether the level of irradiation of the bones with a continuation of the tests increases by a factor of 50 or 5 and whether the level of irradiation of the bones approaches the official standard or not. Even the obviously exceedingly low estimates of the authors of this book do not justify their conclusion regarding permissibility of the tests, let alone of a small nuclear war.

Teller and Latter compare the number of victims of illnesses associated with the tests with the number of victims of similar illnesses (leukemia and hereditary diseases) resulting from other causes, and find that the number of cases resulting from the tests is considerably lower than from other causes and that they are statistically indistinguishable from other illnesses (p. 170). They compare the reduction of the life span for other reasons of health (smoking, sedentary life, living in a large city, etc.) with an arbitrary estimate of the reduction of the life span from the tests and find that the tests have a considerably smaller effect than the other causes (they . . . are equivalent to the smoking of one cigarette every two months') (p. 124).

Teller and Latter compare the dosage from the tests with the dosage from the natural background and note that the dosage from the tests is smaller than the latter.

Their entire argument can be summed up in a single sentence: There are illnesses and circumstances which lead to a larger number of victims and to a greater reduction of the life span than result from the tests; therefore the tests can be allowed. This is a morality and concept of justice which have nothing in common with what men usually understand. In actuality physicians and society at large regard each cause of the increase of the death rate or detriment to health independently of other causes and attack each cause separately. Using the argument of the authors, physicians could refuse to treat diabetes because there is a more widespread illness – tuberculosis, and the public authorities could refuse to provide a water supply because smoking occurs. Any hospital could refuse to assist patients because the result of the illness would be "statistically indistinguishable" (p. 120).

Teller and Latter state that although radiation can be harmful, it can also be beneficial, because it would be 'more in accord with the ideals of humanity to strive to improve the life of all mankind,' that is, they assume that we may destroy a small number of persons through the action of radioactive fallout in the hope that this effect will be of value to the rest of mankind, and thus essentially propose a medical experiment on people without their consent, which is strictly forbidden by all law.

The entire argument of Teller and Latter is based on a small number of victims of the tests compared with victims of other causes and of natural death. But this small number does not seem small to the victims themselves. The small number of victims is the result of the test explosions, so that each test explosion is a death sentence for a certain number of persons rendered by others who are completely unauthorized to do so.

As soon as scientific data on the danger of the tests had been accumulated, the Soviet government terminated the tests, thus showing that it is a form of society in which morality and justice determine the behavior of the government.

To further "convince" their readers of the permissibility and necessity for the tests, the authors discuss the development of a "clean" bomb, that is, a bomb in which the energy is emitted in thermonuclear reactions rather than through nuclear fission. The reaction products of such a bomb contain almost no fission fragments and in the opinion of the authors it will not present a radioactive danger. The authors declare that it is necessary to conduct tests for the development of a "clean" bomb and when it is ready it will no longer be necessary to fear tests and even war will not result in victims of radioactivity.

The idea of the radioactive safety of a "clean" bomb is a pure contradiction in terms. A "clean" bomb emits several times more neutrons (per unit of energy) than a fission bomb. These neutrons, by reacting with nitrogen nuclei of the atmosphere, form radioactive carbon-14, with a half-life of approximately 5100 years. Calculations show [2, 4] that the total amount of energy from the radioactive decay of carbon-14 produced by a "clean" bomb is three times as large as the total decay energy of cesium-137, strontium-90 and carbon-14 from a fission bomb. At the tolerance limit these energies are equal. An estimate of the number of victims of a "clean" and of an ordinary bomb shows that the results are practically identical.

The difference between a "clean" and an ordinary bomb lies in the time of the appearance of the harmful effects – centuries from the explosion of a fission bomb and thousands of years from the explosion of a "clean" bomb. If it is assumed that our responsibility extends only to the present generation, then "after us the deluge," so that we can forget about far-off consequences of the explosion of a "clean" bomb. Such an argument would be fully in the spirit of the other arguments of the authors which have been discussed above.

It is in the nature of people to be concerned about the future. Only opportunistic arguments would allow illness of the twentieth generation while not allowing illness of the second generation.

Teller and Latter evidently understand the weakness of their argument for convincing readers and finally state: 'There are many specific political and military reasons for not terminating the tests' (p. 145). This is the crux of the matter rather than scientific "proofs" of the permissibility of the tests.

Behind all of this is the policy of certain imperialistic elements in the USA who are preparing to wage an aggressive nuclear war. In order to begin the war the people must be convinced of its necessity. But this is impossible since no real argument can be given. Therefore Teller and Latter begin with postulates to the effect that communistic countries are striving for world domination, that they threaten the security of Americans, that it is impossible to come to an agreement with Russia: 'There are no signs that limited wars are ending. We must prepare effective mobile weapons for such conflicts and this requires the use of nuclear weapons' (p. 170).

A scientist must remain a scientist even when he leaves the field of his specialty. Only then is his opinion of weight and his articles significant. If Teller and Latter had regarded human society as scientists, that is, objectively and with an attempt to find and understand its laws, they would have seen that their "postulates" do not exist and that no one is threatening the USA. They write: '. . . The future is made by people. People are unpredictable. Therefore the future is unpredictable.' Nevertheless, there exists a science of the development of society and the future can be predicted. The laws of the development of society lead to the recognition that all countries must have the same right as the USA to independence and security. Then no atomic bomb and no small or large wars are necessary. It is only necessary to have trade and peaceful rivalry of countries for the improvement of the lives of all their citizens.

Teller and Latter in their book did not mention this alternative for "our nuclear future"; by forsaking the scientific method, they have made their book worthless.

LITERATURE CITED

[1] J. L. Kulp, W. R. Eckelmann, and A. R. Schulert, Science 125, 3241, 219 (1957).

[2] O. I. Leipunskii, J. Atomic Energy (USSR) 3, 12, 530 (1957).*

[3] O. I. Leipunskii, J. Atomic Energy (USSR) 4, 1, 63 (1958).*

[4] A. D. Sakharov, J. Atomic Energy (USSR) 4, 6, 576 (1958).*

O. I. Leipunskii

* Original Russian pagination. See C. B. Translation.

THE POLISH JOURNAL "NUKLEONIKA" (NUCLEONICS)

(A Review)

Beginning in the second half of 1956 there has been published in Poland the scientific and technical journal "Nukleonika," which is the organ of the Committee on the Peaceful Uses of Atomic Energy of the Polish Academy of Sciences. While the first few issues of the journal contained principally translations of articles from foreign scientific journals, later original articles began to predominate, which were written by Polish specialists, although the 1957 issues contained articles by well-known foreign scientists who had visited Poland: D. I. Blokhintsev (USSR), E. Brode (Austria), J. Cockcroft (England), F. Perrin (France) and others.

Among the articles by Polish specialists* which were published in 1957 we must mention "The basic problems of nuclear power" (V. Frankovskii), "The role of fast-neutron plutonium reactors in the development of nuclear power" and "Utilization of plutonium dioxide as nuclear fuel" (M. Taube), "Fast-neutron spectrometry" (D. O'Connor), "The production of Geiger-Mueller counters in Poland" (A. Ianikovskii), "Radiochemical laboratories" (R. Gvuzd), "A review of deactivation methods in radiochemical laboratories" (I. Seika), "The production of radioactive isotopes in Poland" (R. Pleevskii), "The use of radiochemical methods in the investigation of nuclear reactions" (S. Sekerskii), "Methods of determining traces of impurities in reactor materials" (I. Minchevskii), "Accelerators" (V. Zykh), "A spherical pistol-type manipulator" (V. Nei), etc.

In 1958 the journal has devoted much more space than previously to articles on reactor design. These include, for example: "A plan for the development of nuclear power in Poland" (P. Novatskii), "The first nuclear reactor in Poland" (Iu. Aleksandrovich and P. Shul'ts), "Work on the designing of a second Polish research reactor" (K. Koval'skaia), "Reactor graphite" (A. Grossman). In 1958 the journal is conducting a discussion of methods of developing nuclear power in Poland.

Of original articles by Polish authors on other questions we may mention "On the refining of Polish uranium ore" (T. Adamskii), "The effect of nuclear radiation on semiconductors" (G. Rzhevuskii), "Chemical shielding from ionizing radiation" (A. Dantsevich), "On some reaction mechanisms of hot atoms" (I. Kampbell).

Review articles periodically discuss the problems and state of development of the utilization of atomic energy in different countries. Each issue of the journal contains material on recent developments of nuclear technology as well as current news. "Nukleonika" can now rightly be regarded as one of the leading scientific and technical journals of Poland. The intense development of work on the utilization of atomic energy in the country will make this journal even more important.

M. T.

* The names of Polish scientists appear here as transliterated from the Russian – Publisher

RECENT LITERATURE *

Books and Collections of Articles

Reactor design. The list of translated books on nuclear technology which have been published recently in the Soviet Union now contains two new titles. The Foreign Language Press (IIL) has now translated into Russian and published the monographs of two outstanding American specialists "The Control of Nuclear Reactors and Power Plants" by M. Schulz, 1957 (460 pp., 17 r. 60 kop) and "Shielding of Nuclear Reactors" by T. Rockwell, 1958 (337 pp., 26 r. 40 kop).

The first book contains 11 chapters. At the beginning there is a brief resume of the physical basis of the operations and kinetics of a reactor. Then there is an examination of the automatic regulation of reactors and nuclear power plants, the mechanisms of a reactor control system, the start-up systems, operation at rated power level and shut-down. Much attention is devoted to the problems of models of reactor processes and loops for the removal and utilization of heat. Finally, a description is given of radiation detectors which are used for control of reactors.

The second book is a handbook with wide coverage of all the problems associated with the designing and planning of the shielding of nuclear power reactors. The book contains 10 chapters. The first few chapters discuss the fundamental methods of solving shielding problems and give the basic concepts, definitions and units for measurements of radiation. The following chapters cover the shielding of the reactor core, radioactive heat generation in the shielding, the activation of coolants and the shielding of heat-transfer loops. Considerable space is devoted to shielding materials and the geometry of radiation sources. A special chapter is devoted to the least fully developed question of the influence of irregularities on shielding (gaps, cavities in tubing, etc.). The book contains rich factual material in the form of tables, graphs and nomograms. Although the book does not treat all problems fully, it is a useful aid for the designers of reactor shielding.

A large number of American specialists in the various fields participated in the writing of both books. Therefore, they reflect contemporary achievements and the state of reactor technology. Since Soviet readers as a whole have not thus far had literature of this kind available, these two books will to a considerable degree fill the gaps which exist. For specialists these books can serve as useful reference works.

Problems of nuclear power. Collections of translations and reviews of foreign periodical literature, No. 1, 1958, IIL, 106 pp., 8 r. 40 kop.

The section on Power Plants and Layouts contains translations of the articles "Thermal problems of atomic power stations" from Combustion 28, 8, 51 (1957); 28, 12, 51 (1957) and "A boiling-water reactor with an intermediate heat exchanger" from Nucl. Power 2, 17, 369 (1957).

The section Designs and Materials contains translations of the articles "Heat exchangers for atomic power plants" from Heat Eng. 32, 2, 30 (1957), "The utilization of organic compounds as moderators and coolants in nuclear reactors" from Atomkernenergie 5, 176 (1957) and "Magnetic jack—a new control drive mechanism" from Nucleonics 15, 6, 118 (1957).

The section Transfer Processes contains translations of the articles "Chemical problems in the use of gas coolants" Nucl. Eng. 2, 17, 321 (1957), "Activity transport in sodium-cooled systems" from Nucleonics 15, 2, 58 (1957), "The selection of a coolant for a high-temperature reactor" from Nucl. Power 2, 17, 381 (1957), "The problem of corrosion caused by water at high temperatures in nuclear reactors" from Atomkernenergie 6, 207 (1957); 7, 248 (1957), "The water system of pressurized water reactors (PWR)" from Engineers Soc. of Western Pennsylvania, Proc. Seventeenth Annual Water Conference, October, 1956.

* The titles of non-Russian works appear here as translated from the Russian. The wording may therefore differ from that of the originals. — Publisher.

The section Nuclear Power News contains translations of the articles "Fuel elements of the Calder Hall power plant" from Nucl. Power 2, 17, 394 (1957), "Tubes for heat exchangers" from Nucl. Power 2, 18, (1957), "A discussion of fuel elements" from J. Brit. Nucl. Energy Conf. 2, 3 (1957).

Methods of determining the radioactive elements in ores. Gosgeoltekhizdat, 1958, 70 pp. 2 r. 20 kop. A collection to the chemical determination of radioactive elements in minerals and rocks. Working instructions for the various methods are given.

Science News. Radiobiology. Biological Effects of Ionizing Radiation, Vol. 1, A. M. Kuzin, Ed., Academy of Sciences Press, 1957, 436 pp. 19 r. This book is a critical review of articles on radiobiology from 1935 to 1955, which form a very extensive literature both at home and abroad.

Shielding of Personnel against Ionizing Radiation. Translated from English by L. B. Prokhorova, IIL, 1958, 182 pp. 7 r. 80 kop. This book provides information regarding infections due to radiation, tolerances and the methods of shielding personnel.

Lebedinskii, A. V., The Effects of Ionizing Radiation on the Living Organism, "Znanie" Press, 1957, 56 pp., 1 r. 20 kop. This pamphlet is devoted to one of the most important problems of modern science — the effects of various forms of ionizing radiation (x-rays; alpha, beta, and gamma rays; neutron flux) on the living organism.

Mikhailov, V. A., The Physical Foundations of the Production of Atomic Energy, 2nd revised and enlarged edition, Voenizdat, 1958, 176 pp., 2 r. 75 kop. This is a popular presentation of the physical foundations of the production and utilization of atomic energy for both peaceful and military purposes.

Articles in Journals

Agranat, V. Z., On the accumulation of radioactive polonium (Po^{210}) in aqueous forms, Meditsinskaia radiologiia 3, 1 (1958).

Breslavets, L. P., Radioactive emissions in agriculture, Priroda 3 (1958).

Vol'doberg, D. B. et al., Atomic energy. (A general review of foreign countries for 1956-1957). Power production abroad. Supplement to the journal "Eleketricheskie stantsii".

Gell-Mann, M. and Rosenbaum, E., Elementary particles, Uspekhi fiz. nauk 64, 2 (1958) [Russian translation].

Graevskii, E. Ia. and Zinov'eva, E. G., On the possibility of altering the radiosensitivity of cells by means of fluorochromes, Doklady Akad. Nauk SSSR 118, 3 (1958).*

Grik, B. et al., Extraction of uranium from phosphoric acid, Khimia i khim. tekhnol. (condensed translation from foreign period. lit) 2 (1958).

Denisov, N. G., On the resonant absorption of electromagnetic waves by an inhomogeneous plasma (letter to editor), J. Exp. Theoret. Phys. 34, 2 (1958).**

Zakutinskii, D. I. Problems in the toxicology of radioactive substances, Meditsinskaia radiologiia 3, 1 (1958).

Kovalev, V. P., Measurement of the fission-neutron spectra of U^{233}, U^{235}, and Pu^{239} from 50 to 700 kev (letter to editor), J. Exp. Theoret. Phys. (USSR) 34, 2 (1958).**

Kosta, L., Separation of Th^{234} from uranyl nitrate, Khimia i khim. tekhnol. (Condensed translation from foreign period. lit.) 2 (1958).

Kuznetsov, E. V., Bubble chambers, Uspekhi fiz. nauk 64, 2 (1958).

Kuz'minov, B. D. and Smirenkin, G. N., Systematics of the average number of prompt fission neutrons ν (letter to editor), J. Exp. Theoret. Phys. (USSR) 34, 2 (1958). **

* See C. B. Translation.

** See English Translation.

Marei, A. N. et al., On the transfer of radioactive strontium from open reservoirs to the human organism, Meditsinskaia radiologiia 3, 3 (1958).

Perlin, I. L. et al., Compression of beryllium, zirconium, uranium, and thorium (from the literature), Tsvetnye metal. 2 (1958).

Pik-Pichak, G. A., Fission of rotating nuclei, J. Exp. Theoret. Phys. (USSR) 34, 2 (1958).*

Pipperd, D. et al., Separation of tetravalent berkelium by extraction with solvents, Khimia i khim. tekhnol. (condensed translation from foreign period. lit.) 2 (1958).

Protopopov, A. N. and Shiriaev, B. M., Investigation of gamma rays accompanying the fission of U^{235} by neutrons from 2.8 to 14.7 Mev, J. Exp. Theoret. Phys. (USSR) 34, 2 (1958).*

Sinel'nikov, K. D. et al., Separation of isotopes in unsteady molecular flow, J. Exp. Theoret. Phys. (USSR) 34, 2 (1958).*

Stepanov, V. G. et al., On rotating plasma (letter to editor), J. Exp. Theoret. Phys. (USSR) 34, 2 (1958).*

Tarantin, N. I. et al., Mass distribution of fission products from the irradiation of gold and uranium with nitrogen ions, J. Exp. Theoret. Phys. (USSR) 34, 2 (1958).*

Anderson, O. A. et al., Phys. Rev. 109, 2, 612 (1958). Neutron production in linear deuterium pinches.

Barton, G. B. et al., Ind. Eng. Chem. 50, 2, 212 (1958). Recovering fission products (cesium).

Bengston, J., Nucl. Sci. Eng. 3, 1, 71 (1958). Self-shielding of neutrons in a simple two-dimensional lattice.

Bernstein, I. B., Phys. Rev. 109, 1, 10 (1958). Waves in plasma in a magnetic field.

Blaise, S. et al., J. phys. radium 19, 1, 66 (1958). Measurement of the average number of neutrons emitted in U^{238} fission by 14.2 Mev neutrons.

Bochinski, J. et al., Ind. Eng. Chem. 50, 2, 157 (1958). Separation of monazite rare earths by solvent extraction.

Bock, R. et al., Z. angew. Phys. 10, 2, 49 (1958). A single-dee constant-frequency cyclotron.

Bolt, R. O. and Carroll, J. G., Ind. Eng. Chem. 50, 2, 22 (1958). Radiolysis and radiolytic oxidation of oils.

Burger, L. L. and McClanahan, Ind. Eng. Chem. 50, 2, 153 (1958). Gamma radiolysis of tributyl phosphate and its diluent systems.

Butler, J. W. and Grotenhuis, Nucl. Sci. Eng. 3, 1, 47 (1958). Activity decay of fission products in reactor cycling.

Chiotti, P. and Shoemaker, Ind. Eng. Chem. 50, 2, 137 (1958). Pyrometallurgic separation of uranium from thorium.

Codding, J. W. et al., Ind. Eng. Chem. 50, 2, 145 (1958). Tributylphosphate - hydrocarbon systems.

Cox, R. P. et al., Ind. Eng. Chem. 50, 2, 141 (1958). Separating hafnium from zirconium (solvent extraction with tributyl phosphate).

Davis, M. V., Nucl. Sci. Eng. 3, 1, 107 (1958). Temperature coefficient for fuel elements with U^{235}.

Dio, W. H. and Schopper, E., Nucl. Phys. 6, 2, 175 (1958). Temperature dependence of the diffusion coefficient and the diffusion length of thermal neutrons in water.

Diven, B. C. et al., Phys. Rev. 109, 1, 144 (1958). Capture to fission ratios for fast neutrons in U^{235}.

Dykstra, J. et al., Ind. Eng. Chem. 50, 2, 161 (1958). Solvent extraction system for enriched uranium.

* See English Translation.

Dykstra, J. et al., Ind. Eng. Chem. 50, 2, 181 (1958). A 25-pound-per-hour fluorine plant.

Edwards, S. F., Phil. Mag. 3, 27, 302 (1958). Correlations in the charge density of a classical plasma.

Evans, J. B. et al., Ind. Eng. Chem. 50, 2, 192 (1958). Chemical effects of nuclear transformations.

Foley, D. D. and Filbert, R. B. Jr., Ind. Eng. Chem. 50, 2, 144 (1958). Purifying thorium nitrate by solvent extraction (with tributyl phosphate).

Fuger, J., J. Nucl. Inorg. Chem. 5, 4, 338 (1958). Ion-exchange behavior and dissociation constants of Am, Cu, and Cf combined with ethylenediaminetetraacetic acid.

Fulmer, C. B. and Cohen, B. L., Phys. Rev. 109, 1, 94 (1958). Equilibrium charges of fission fragments in gases.

Gallagher, T. L., Nucl. Sci. Eng. 3, 1, 110 (1958). Self-shielding in detectors made of food wrappings.

Goodman, E. I., Ind. Eng. Chem. 50, 2, 210 (1958). A radio tracer for studying sewage distribution.

Greer, A. H. et al., Ind. Eng. Chem. 50, 2, 166 (1958). A new ion-exchange resin for uranium recovery.

Henry, A. F., Nucl. Sci. Eng. 3, 1, 52 (1958). Application of reactor kinetics to the analysis of experiments.

Hotten, B. W. and Carroll, J. G., Ind. Eng. Chem. 50, 2, 217 (1958). Radiation damage in lubricating greases.

Hubbs, J. C. et al., Phys. Rev. 109, 2, 390 (1958). Hfs measurements on Pu^{239}.

Huizenga, J. R., Phys. Rev. 109, 2, 484 (1958). Correlation of competition between neutron emission and fission.

Hull, D. E., Ind. Eng. Chem. 50, 2, 199 (1958). (Measurement of the velocity of flow with radioactive tracers). Total-count technique in the refinery.

Hurwitz, H. and Nelkin, M. S., Nucl. Sci. Eng. 3, 1, 1 (1958). Thermal neutron spectrum in a diffusive medium.

Kasten, P. R. and Aven, R. E., Ind. Eng. Chem. 50, 2, 171 (1958). Fuel costs in batch and continuous-processed homogeneous reactors.

King, W. H. Jr., Ind. Eng. Chem. 50, 2, 201 (1958). Radioisotopes in petroleum refining.

Lonati, R. et al., Nuovo cimento 7, 2, 133 (1958). Investigation of very weak alpha-radioactivity.

Magnac-Valette, D. et al., J. phys. radium 19, 1, 88 (1958). A 340-kev accelerator for investigating reactions induced by tritons.

Margenau, H., Phys. Rev. 109, 1, 6 (1958). Conductivity of plasmas to microwaves.

McMurray, H. L. et al., Nucl. Sci. Eng. 3, 1, 38 (1958). Estimation of the length of runs of reactors with small cores.

Milford, R. P., Ind. Eng. Chem. 50, 2, 187 (1958). Engineering design of Oak Ridge fluoride volatility pilot plant.

Moore, J. A., Phys. Rev. 109, 2, 417 (1958). Resonance scattering of slow neutrons in In.

Mueller, R. H., Ind. Eng. Chem. 50, 2, 205 (1958). Interaction of beta rays with matter.

Osborn, R. K., Nucl. Sci. Eng. 3, 1, 29 (1958). Some properties of the thermal-neutron scattering probability.

Ranftl, J. W., Ind. Eng. Chem. 50, 2, 196 (1958). Using electrons in chemical processing.

Rosenbluth, M. N. and Kaufman, A. N. Phys. Rev. 109, 1, 1 (1958). Plasma diffusion in a magnetic field.

Strickler, T. D. et al., Nucl. Sci. Eng. 3, 1, 11 (1958). Fast-neutron scattering in thick plates.

Vavalides, S. P. et al., Ind. Eng. Chem. 50, 2, 178 (1958). High-capacity long-life fluorine cell.

Werner, F. G. and Wheeler, J. A., Phys. Rev. 109, 1, 126 (1958). Superheavy nuclei.

SIGNIFICANCE OF ABBREVIATIONS MOST FREQUENTLY ENCOUNTERED IN SOVIET PHYSICS PERIODICALS

AN SSSR	*Academy of Sciences, USSR*
FIAN	*Physics Institute, Academy of Sciences USSR*
GITI	*State Scientific and Technical Press*
GITTL	*State Press for Technical and Theoretical Literature*
GOI	*State Optical Institute*
GONTI	*State United Scientific and Technical Press*
Gosenergoizdat	*State Power Press*
Gosfizkhimizdat	*State Physical Chemistry Press*
Gozkhimizdat	*State Chemistry Press*
GOST	*All-Union State Standard*
Goztekhizdat	*State Technical Press*
GTTI	*State Technical and Theoretical Press*
GUPIAE	*State Office for Utilization of Atomic Energy*
IF KhI	*Institute of Physical Chemistry Research*
IFP	*Institute of Physical Problems*
IL	*Foreign Literature Press*
IPF	*Institute of Applied Physics*
IPM	*Institute of Applied Mathematics*
IREA	*Institute of Chemical Reagents*
ISN (Izd. Sov. Nauk)	*Soviet Science Press*
I YaP	*Institute of Nuclear Studies*
Izd	*Press (publishing house)*
KISO	*Solar Research Commission*
LETI	*Leningrad Electrotechnical Institute*
LFTI	*Leningrad Institute of Physics and Technology*
LIM	*Leningrad Institute of Metals*
LITMiO	*Leningrad Institute of Precision Instruments and Optics*
Mashgiz	*State Scientific-Technical Press for Machine Construction Literature*
MATI	*Moscow Aviation Technology Institute*
MGU	*Moscow State University*
Metallurgizdat	*Metallurgy Press*
MOPI	*Moscow Regional Institute of Physics*
NIAFIZ	*Scientific Research Association for Physics*
NIFI	*Scientific Research Institute of Physics*
NIIMM	*Scientific Research Institute of Mathematics and Mechanics*
NII ZVUKSZAPIOI	*Scientific Research Institute of Sound Recording*
NIKFI	*Scientific Institute of Motion Picture Photography*
OIYaI	*Joint Institute of Nuclear Studies*
ONTI	*United Scientific and Technical Press*
OTI	*Division of Technical Information*
OTN	*Division of Technical Science*
RIAN	*Radium Institute, Academy of Sciences of the USSR*
SPB	*All-Union Special Planning Office*
Stroiizdat	*Construction Press*
URALFTI	*Ural Institute of Physics and Technology*

NOTE: Abbreviations not on this list and not explained in the translation have been transliterated, no further information about their significance being available to us.—*Publisher.*

recent Russian research
—in complete English translation

A Supplement to "HELIUM"

BY *E. M. LIFSHITS*
AND *E. L. ANDRONIKASHVILI*

THIS NOTABLE volume consists of two supplementary chapters, by these outstanding Soviet physicists, which were added to the Russian translation of W. H. Keesom's classic book "HELIUM."

The first chapter, by Lifshits, is a concise resume of the Landau theory of superfluidity *(quantization of the motion of a liquid; superfluidity of Helium II; macroscopic hydrodynamics of Helium II)*. The second chapter reports in considerable detail the experimental work conducted by Peter Kapitza and E. L. Andronikashvili in this field *(motion of Helium II due to the influx of heat; the two forms of motion in Helium II; viscosity of the normal component; reversibility of hydro-thermal processes and the thermo-mechanical effect; critical velocities; heat transport in slits and capillaries; heat transport in free Helium II; second sound; films; impurities)*.

Recent experiments on the superfluidity of helium make A SUPPLEMENT TO "HELIUM" of major interest to all researchers in low temperature physics.

cloth bound • 175 pages • $7.50

CB translations are by bilingual scientists, and include all photographic, diagrammatic and tabular material integral with the text.

Complete Table of Contents

SUPERFLUIDITY (THEORY)

QUANTIZATION OF THE MOTION OF A LIQUID

Helium II—a quantum liquid • energy spectrum of a quantum liquid • energy spectrum of an almost-ideal Bose-Einstein gas • calculation of the thermodynamic properties of Helium II

SUPERFLUIDITY OF HELIUM II

superfluidity of Helium II at absolute zero • Helium II at temperatures above absolute zero • calculation of the ratio ρ_n/ρ • heat transport in Helium II • mechano-caloric effect in Helium II • effect of impurity atoms in Helium II

MACROSCOPIC HYDRODYNAMICS OF HELIUM II

system of hydrodynamic equations for Helium II • hydrodynamic equations for an incompressible liquid • propagation of sound in Helium II • radiation of sound in Helium II • effect of impurities on the propagation of second sound in Helium II • scattering of light in Helium II • viscosity of Helium II • the Tisza theory of Helium II

SUPERFLUIDITY (EXPERIMENTAL DATA)

MOTION OF HELIUM II DUE TO THE INFLUX OF HEAT

introduction • heat transport in Helium II moving in a capillary • nature of the jet and the jet profile • reaction of the jet • heat transport in free Helium II—radiometer effect • discussion of the results—heat transport mechanism in Helium II

THE TWO FORMS OF MOTION IN HELIUM II

formulation of the problem • description of the experiment • results of the experiment • discussion of the results

VISCOSITY OF THE NORMAL COMPONENT

the notion of viscosity in Helium II • critique of the earlier experiments • determination of viscosity from experiments in which two forms of motion are observed • determination of the viscosity of the normal component from experiments with heavy disks • determination of the viscosity of the normal component from experiments on heat transport in slits • discussion of the results

REVERSIBILITY OF HYDRO-THERMAL PROCESSES AND THE THERMO-MECHANICAL EFFECT

heat content of Helium II • thermo-mechanical effect and reversibility of hydro-thermal processes • new method of obtaining low temperatures • thermo-mechanical effect and the viscosity of the superfluid component • discussion of the results

CRITICAL VELOCITIES

critical velocities and wall films • critical velocities in thin slits and capillaries • critical velocities in wide slits • discussion of the results

HEAT TRANSPORT IN SLITS AND CAPILLARIES

general remarks • apparatus • wide slits • narrow slits • discussion of results

HEAT TRANSPORT IN FREE HELIUM II

introduction • optical observations of the heat transport process • temperature distribution close to a heat disseminating surface • discussion of results

SECOND SOUND

introduction • generation of second sound by the thermal method • filtration method • conversion of second sound to first sound • second sound under conditions of high pressure • discussion of results

FILMS

film thickness • vapor pressure above the film • thermo-mechanical and mechano-caloric effects in films • motion of a film without gravitational forces • momentum of the film • problem of film formation from the gas phase

IMPURITIES

behavior of colloids in Helium II • the He^3 isotope • separation of helium isotopes by cyrogenic techniques • distribution of the He^3 isotope between two phases of the solvent • discussion of results • other properties of a solution of He^3 in He^4 • separation of helium isotopes by the thermal diffusion method

(c/b)

CONSULTANTS BUREAU, INC.
227 WEST 17TH STREET, NEW YORK 11, N. Y.